Phase Relationships for Molecular Salts

A thesis submitted to the University of Manchester for the degree of Doctor of Philosophy in the Faculty of Engineering and Physical Sciences

Claire Cooke

2010

The School of Chemical Engineering and Analytical Sciences

TABLE OF CONTENTS

TABLE OF FIGURES

TABLE OF TABLES

ABSTRACT

The University of Manchester

Claire Louise Cooke

Submitted for the degree of Doctor of Philosophy

Phase Relationships for Molecular Salts

Submitted December 2010

The pharmaceutical industry has for many years been interested in the formation of salts as a means of controlling the chemical/physical properties of API (active pharmaceutical ingredient) molecules. While current interest in cocrystals has led to study of their formation and phase behaviour, comparatively little data is available for salts. This work aims to come some way to redress that balance. Initial studies focussed on a single base manually ground with a number of acids (leading on from previous solution work). Salt formation was noted in a significant number of cases. The work was followed by two more detailed and contrasting case studies. These case studies are ephedrine with pimelic acid and benzoic acid.

Both mono- and di-basic salts of ephedrine and pimelic acid were formed both by grinding and solution methods. Binary and aqueous ternary phase diagrams were measured to allow assessment of pure phase regions. The ideality of the systems was assessed and, while the binary phase diagram showed some relatively ideal regions, the ternary system appeared highly non-ideal.

Effects on the shape and size of phase regions have been considered, especially the role ionisation plays in the ternary non-ideality. Using fundamental equations solubility has been determined as a function of pH and compared to experimental data. The pH value has also been calculated using concentrations of acid and base along the experimental liquidus of the ternary phase diagram and comparisons made with measured pH values. From these comparisons it was determined that the non-ideality and shape of the liquidus in the ephedrine/pimelic acid/water ternary phase diagram is not solely due to ionisation of the components.

Some major issues that may arise in attempted salt formation studies are discussed in relation to the ephedrine and benzoic acid system. Aqueous salt formation was not successful; therefore reasons for this failure are discussed. It is concluded that while the ternary phase behaviour of a salt should be considered, it does not mean the ionisation behaviour (and hence the speciation diagram) should be ignored. These two sources of information should be assessed in conjunction with one another in order to gain the most accurate insight into a system.

DECLARATION

No portion of the work referred to in this thesis has been submitted in support of any other application for another degree of qualification at this or any other university or institute of learning.

.....

Claire Cooke

COPYRIGHT STATEMENT

ACKNOWLEDGEMENTS

Firstly I would like to thank my academic supervisor Professor Roger Davey for all his help, guidance and encouragement over the last three years, especially during the writing up process when he has provided feedback on a very tight timeline. Also, significant thanks must go to my industrial supervisor Dr. Simon Black for his helpful discussions, ideas and the industrial perspective he provided.

I would like to thank Helen Jones for her help with the solubility/pH calculations and use of the Solver function in Excel, Kevin Day and Steph Brown for their help and guidance when using the AstraZeneca IR microscope. Thanks to both Dr. Robin Pritchard and Dr. Chris Muryn, who have performed the crystallography shown in this thesis and to Dr. Colin Seaton for completing the final details on some of the crystal structures. Thanks to Geoff Dent for his help and advice with the spectroscopy used in this work. Thank you to James Clayton for his help with the reaction mechanism.

Thank you to the SCI, BACG, BCA and UKRC4SET for funding allowing me to attend hugely helpful conferences in Maastrict, Toronto and Singapore during my PhD. Thanks to the EPSRC and AstraZeneca for funding this work.

To the whole CCI group, past and present, a big thank you for all the help, discussion and debate during my time in the office. Ladies (and Kev), the tea breaks have kept me sane!

Last, but certainly not least, to Phill, thank you for loving me and putting up with me through my many, many years of education. Does this prove I know something about science?

1. LITERATURE REVIEW

1.1 BACKGROUND

1.1.1 PHARMACEUTICAL SALTS

For all pharmaceutical companies the physical state of a novel drug is of vital importance in the drug's progression to market. There are three physical states in which a compound can exist, solids, liquids and gases[1]. Very few pharmaceutical products are gaseous (with some exceptions including asthma inhalers) and only a small amount liquid (including cough medicines and intravenous anaesthetics), due to storage and analysis issues with both[2]. The vast majority of pharmaceutical products are in a solid form, leading to the situation where solid formulation is a key step in a drug's normal route to market[3]. Solids can be sub-categorised as either amorphous or crystalline, with crystalline samples exhibiting long-range order and amorphous samples not[4]. Amorphous solids raise issues in pharmaceutical research due to the possibility that they are non-homogeneous, making accurate dosages difficult. Overall amorphous solids are less stable due to their lack of long-range order, meaning they are more soluble, and also more hygroscopic. Crystalline solids are generally more stable, meaning they are easier to formulate and can be more easily analysed[2]. This means the majority of pharmaceutical products are crystalline solids.

The development of new crystalline solid drugs for the market requires a form with good bioavailability, processability, solubility and physical stability. This usually requires the formation of a salt in order to give the optimum bio and physiochemical properties. By forming a salt, the physical properties of the drug (listed above) can be adapted to make the most suitable formulation. The importance of choosing the 'correct' salt for each application is outlined in a published review[5]. Despite this importance, the selection of salt forms still remains a difficult, semi-empirical choice[6]. Factors influencing the choice of salt form are not just physical, but also financial. The cost of raw materials (such as the acid to act as the counter-ion and solvents) and percentage yield of the salt from crystallisation are major considerations[5]. Extensive studies are carried out by

pharmaceutical companies to ensure they market the most effective salt form; meaning a more educated method of salt selection (or essentially a method of property prediction) would have greater financial and time saving benefits. Any new understanding of how salts form, transform, melt or dissolve can aid this field. The example of Sertraline can be used to show the sheer volume of experiments sometimes undertaken, with over three thousand experiments used to yield a total of eighteen crystalline salts[7].

Crystallisation from solution is the most common method of producing salts. Crystallisation from solution also has disadvantages. The conditions under which a solid is crystallised can affect the physical properties of the salt[4]. These conditions include temperature, solvent and agitation speed and they can affect the size, morphology, purity and polymorphic form of the crystals[8]. One of the most important physical characteristics of a resulting molecular salt form is the solubility. For most pharmaceutical compounds, sufficiently high water solubility is important. Although most organics are poorly water soluble, the formation of their salts leads to the drug substance being ionised and becoming more soluble[2]. In solid drug forms, such as tablets, dissolution rate in gastrointestinal (GI) conditions is a key factor in how effective the drug is within the body, as it dictates the speed at which the drug will enter the bloodstream (if at all). Although GI solubility is measured at a significantly lower pH than that of water, the higher dissolution rate of a salt has been attributed to its higher solubility in the aqueous diffusion layer surrounding the solid[9].

1.1.2 EPHEDRINE

Within this work the pharmaceutical base considered is (1R, 2S)-2-methylamino-1-phenylpropan-1-ol, more commonly known as (1R, 2S)-(-)-Ephedrine (hereafter "ephedrine"). Ephedrine is an optically active amine with two chiral centres, shown in Figure 1. Also available is (1S, 2R)-(-)-Ephedrine, the opposing enantiomer[10]. Much work has also been published on the enantiomers (1S, 2S)-(+)-Ephedrine and (1R, 2R)-(-)-Ephedrine, or (+) or (-) pseudoephedrine respectively, as they are more commonly known[11]. (+)-pseudoephedrine has melting point of 120 °C, well above that of ephedrine worked with here which melts at 36 °C[12].

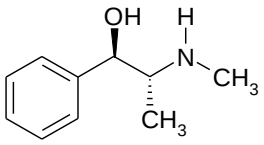

FIGURE 1- THE STRUCTURE OF (1R, 2S)-(-)-EPHEDRINE

Ephedrine is a sympathomimetic drug, meaning it is a substance that mimics the effect of the sympathetic nervous system. It is most commonly used in the pharmaceutical industry as a decongestant[13], appetite suppressant[14], concentration aid[15] and is also used as a treatment for hypertension caused by anaesthesia[16]. It also trades on the black market as it can be used as an effective precursor for amphetamines[17]. There are strict guidelines governing its sale both here in the UK and in the US[18, 19]. Much literature has been published on one particular salt of ephedrine, that of ephedrine hydrochloride[20-23]. Due to the liquid nature of the hydrochloric acid used to make this salt, it was not considered in this study. The aim of many HCl papers was to investigate the quality of resolution via diastereomeric salt formation. Previously published work by Collier *et al*[24] and Black *et al*[25] formed salts with ephedrine and a range of acids. They attempted to produce salts using equimolar amounts of the acid and the base in known volumes of solvent under conditions leading to supersaturation (either heating followed by cooling, or evaporation). It was then determined by a range of different analyses such as differential scanning calorimetry (DSC), powder X-ray diffraction (pXRD) and infra-red spectroscopy (IR), whether a salt had been formed. Crystal structures were also determined using single crystal XRD whenever possible. The aim in the Black *et al* paper was to assess patterns of salt formation by studying thermodynamic effects.

1.1.2.1 EPHEDRINE HEMIHYDRATE

Ephedrine readily hydrates in air to form ephedrine hemihydrate. The physical properties of the hemihydrate are very similar to that of anhydrous ephedrine (i.e. melting points and solubility) and the crystal structure has been previously determined and published. The use of the hemihydrate or anhydrous sample will be discussed as and when required in the context of specific examples and experiments.

1.1.3 THIS PROJECT

In this thesis the solubility, melting behaviour and other physical properties of salts and their respective component acids and bases will be discussed and compared to some of the work done by Collier *et al*[24] and Black *et al*[25]. Formation of salts from grinding and contact, as well as crystallisation from a solvent, will be investigated and the respective merits and problems considered. The mechanism of formation for this technique will also be studied and discussed. A number of salts will be taken forward as case studies and investigated in more detail, considering and comparing solution and solid state formation and how this affects the physical properties. Finally, as the ionisation of components is an important consideration when forming salts, it will be investigated in a range of different environments and with respect to a number of different terms.

1.2 CRYSTALLISATION

1.2.1 THEORY

A crystal is an ordered three dimensional molecular array formed by the coming together of molecules, ions or atoms in a fluid. Due to the reproducibility of the crystal assembly and the discriminating power of their surfaces only allowing molecules of a similar scale to attach, they are highly effective in their ability to separate. Crystallisation is widely used across many industries as a purification technique, with the selective surface of a crystal growing with the deposition of only the desired molecules, leaving unwanted by-products in solution[4, 26].

Crystallisation can occur either by suspension or solidification processes. Suspension processes occur from solution, while solidification processes occur when working with a melt (liquid above its melting point)[4, 26]. Suspension processes are the most common technique used in this work, and although some experiments were undertaken using molten samples, their crystallisation from a molten phase is not studied. In this thesis focus will be placed upon the theories governing suspension processes.

There are three basic steps in the formation of a crystalline solid from a solution. The first is the formation of a supersaturated solution, followed by nucleation and finally further growth.

1.2.2 SUPERSATURATION

Supersaturated solutions are commonly formed by one of two methods, referred to as 'cooling' and 'evaporation'. 'Cooling' involves dissolving the solid into a heated solvent and then lowering the temperature. As the solution is cooled the solubility decreases causing the solution to become supersaturated. Evaporation involves dissolving the solid in solvent at a fixed temperature and allowing the solvent to evaporate, reducing the volume of solvent the solid is dissolved in and increasing the concentration of the solute. Both these methods cause the solid to exceed its solubility, hence leading to the term 'supersaturation'. The methods can be more clearly understood using a hypothetical solubility curve[4, 26, 27].

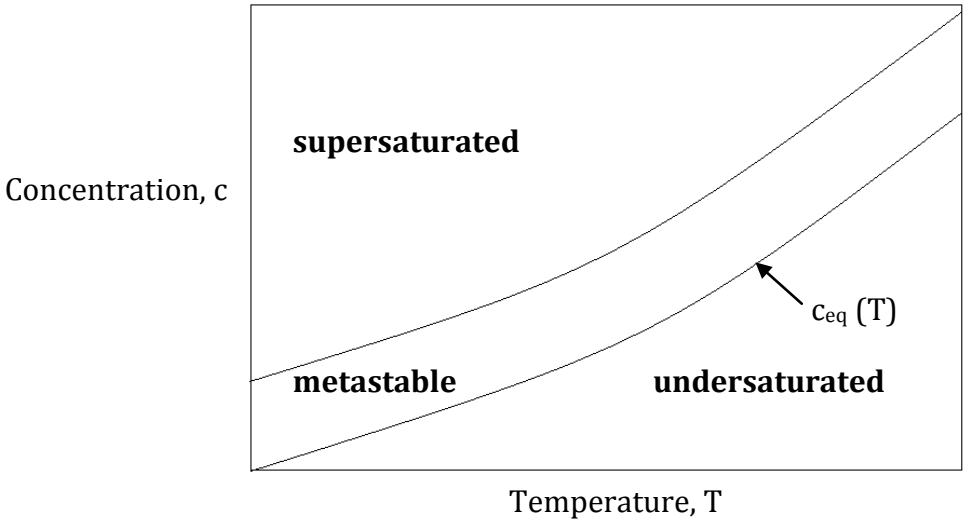

FIGURE 2- SOLUBILITY/SUPERSOLUBILITY DIAGRAM

Figure 2 shows a hypothetical solubility curve, $c_{eq}(T)$. If a solution has a composition below this line it is said to be undersaturated, causing any crystals present in solution to dissolve. If the composition of the solution lies above this line it is supersaturated, as the volume of solute dissolved is above the equilibrium saturation value. The metastable zone, also labelled in Figure 2, is the region of low

supersaturation where, although existing crystals will grow, it is not easy for new ones to nucleate. The region of the phase diagram above the metastable zone is the labile zone, and here spontaneous nucleation is found to occur.

Supersaturation, σ, can be expressed by comparing actual and equilibrium compositions, and in thermodynamic terms can be defined as the difference in chemical potential between a molecule in an equilibrium state, μ_{eq}, and a molecule in its supersaturated state, μ_{ss}. Therefore,

$$\sigma = (\mu_{ss} - \mu_{eq}) / kT \qquad \text{EQUATION 1:1}$$

where k is the Boltzmann constant for the nuclei population and T is the temperature of the system in Kelvin. This can be reduced to give the supersaturation in terms of composition for an ideal solution (a non-ideal solution would include an activity term)

$$\sigma = \ln(\chi_{ss} / \chi_{eq}) \qquad \text{EQUATION 1:2}$$

where χ_{ss} is the composition of the supersaturated solution (equal to the actual amount of solid dissolved) and χ_{eq} is the composition of the saturated solution (equal to the solubility at equilibrium at temperature T)[4, 26, 27].

1.2.3 NUCLEATION AND CRYSTALLISATION

The second stage in the crystallisation process is the formation of crystal nuclei from the supersaturated solution. This is termed nucleation and for this to occur the solution must contain a number of minute solid bodies, nuclei or seeds. On the phase change from fluid to solid state, solute molecules will not all end up in the same chemical environment, as some will be internally bound in a crystal as it forms (interior) and others will become part of the surface. These clusters of molecules (crystals) continue to grow, with more molecules adding to the surfaces. The number of interior molecules increases. The number of molecules in a stable crystal nucleus may vary from ten to several thousand. In the interior all available interactions are satisfied (z_b in Figure 3), whilst on the outside they are not, hence encouraging further growth. Before the nuclei reach maturity (or their critical size)

they are unstable and may redissolve into the solution (critical nuclei are discussed in more detail below)[4, 26].

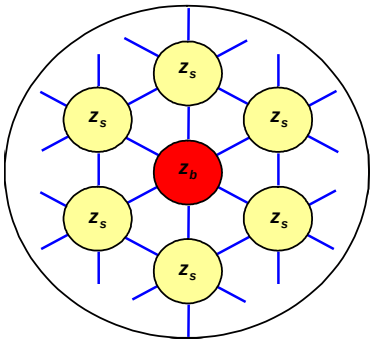

FIGURE 3- MOLECULAR CLUSTERING DURING NUCLEATION

To quantify the phase change occurring upon nucleation a cluster composed of z molecules must be considered where z_b are within the bulk solid and z_s are surface molecules. Using these terms the free energy of the cluster g_z can be written thus,

$$g_z = z_b g_b + z_s g_s \qquad \text{EQUATION 1:3}$$

or

$$g_z = (z_b + z_s) g_b + (g_s - g_b) z_s \qquad \text{EQUATION 1:4}$$

By including the interfacial tension γ between the cluster and the solution the equation becomes,

$$\gamma = (g_s - g_b) z_s / A \qquad \text{EQUATION 1:5}$$

hence,

$$g_z = z g_b + \gamma A \qquad \text{EQUATION 1:6}$$

For a spherical cluster of molecules,

$$A \propto z^{2/3} \qquad \text{EQUATION 1:7}$$

If this is rewritten in terms of chemical potentials the free energy of the cluster can be determined,

$$g_z = z\mu_b + \beta\gamma z^{2/3} \qquad \text{EQUATION 1:8}$$

where β is an area shape factor and μ_b is the chemical potential of a bulk molecule[4, 26, 27].

Nucleation continues until eventually the deposition of further molecules causes a decrease in free energy, as shown in Figure 4. Before the nucleus reaches this critical size, z_c, the only way of decreasing the free energy is dissolution. Clusters of this size are called critical nuclei. This free energy change is calculated by writing the nucleation event as a quasi equilibrium between monomers and the crystal clusters:

$$zA \Leftrightarrow A_z \qquad \text{EQUATION 1:9}$$

so the free energy change (ΔG) per mole of A_z nucleated is

$$\Delta G = g_z - z\mu \qquad \text{EQUATION 1:10}$$

with μ being the chemical potential of monomers. From thermodynamics

$$\mu = \mu^0 + kT\ln x_{eq} \qquad \text{EQUATION 1:11}$$

therefore the equation becomes

$$\Delta G = (z\mu_b + \beta\gamma z^{2/3}) - z(\mu^0 + kT\ln x_{ss}) \qquad \text{EQUATION 1:12}$$

For a saturated solution

$$x = x_{eq} \qquad \text{EQUATION 1:13}$$

and hence

$$\mu_b = \mu^0 + kT\ln x_{eq} \qquad \text{EQUATION 1:14}$$

so this equation becomes,

$$\Delta G = -zkT\ln(x_{ss} / \ln_{eq}) + \beta\gamma z^{2/3} \qquad \text{EQUATION 1:15}$$

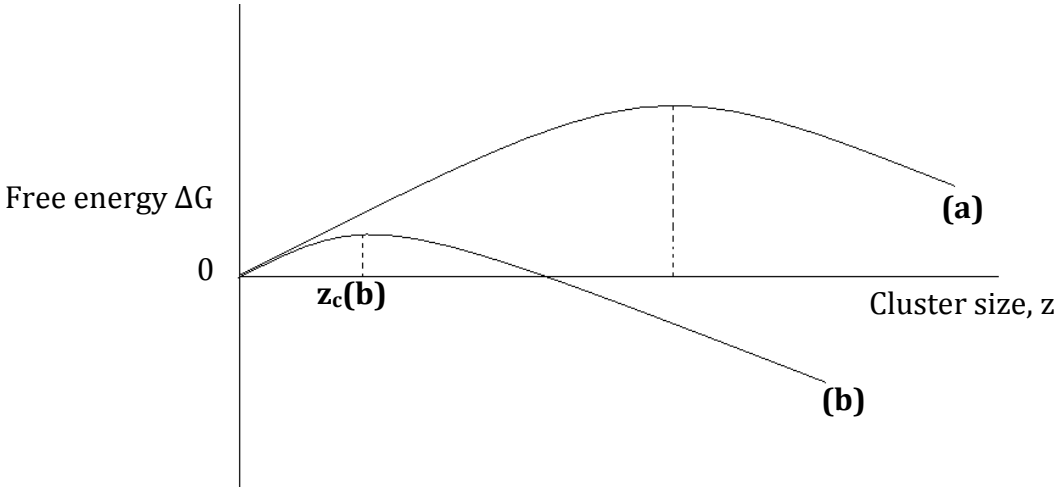

FIGURE 4- THE FREE ENERGY CHANGE AS A FUNCTION OF CLUSTER SIZE AND SUPERSATURATION. CURVE (A) AT LOW SUPERSATURATION AND CURVE (B) AT HIGH SUPERSATURATION[26].

From Figure 4 it is clear that as the supersaturation increases (curve (a) shows low supersaturation and (b) shows high supersaturation), the height of the free energy barrier, ΔG, and the value of the critical size (z_c) decrease. The more supersaturated a solution, the greater the chance of nucleation being spontaneous[26].

1.2.4 NUCLEATION RATE

The rate of nucleation is defined as the rate clusters grow through the critical size (z_c) to become crystals. To write the rate equation an assumption must be made that aggregation is a stepwise process with nuclei A having a critical size z_c as defined previously. The overall reaction can be written

$$z_c A \rightarrow A_c \qquad \text{EQUATION 1:16}$$

From this the equilibrium constant can be defined as,

$$K_z = [A]^{z_c} / [A_c] \qquad \text{EQUATION 1:17}$$

it can also be defined in terms of free energies thus

$$\ln K_z = -\Delta G_c / RT \qquad \text{EQUATION 1:18}$$

The concentration of critical nuclei can be related to the activation free energy for nucleation by

$$[A_c] = [A]^{z_c} \exp(-\Delta G_c / RT) \qquad \text{EQUATION 1:19}$$

Davey[26] then continued this to calculate the relationship between nucleation and supersaturation giving the equation

$$J = A\exp(-B\gamma^3 / T^3\sigma^2) \qquad \text{EQUATION 1:20}$$

where J is the nucleation rate (the number of nuclei formed per unit time per unit volume), A and B are constants, γ is the interfacial surface tension, T is the temperature and σ is the supersaturation. This equation was originally derived by Max Volmer in 1939[28] and can be graphically represented by plotting nucleation rate as a function of supersaturation (Figure 5). From this relationship it can be seen that supersaturation is only an expression of the free energy available to overcome the interfacial tension of a surface. The interfacial tension is overcome at a critical supersaturation level, σ_c, resulting in a huge increase in nucleation rate[4, 26, 27].

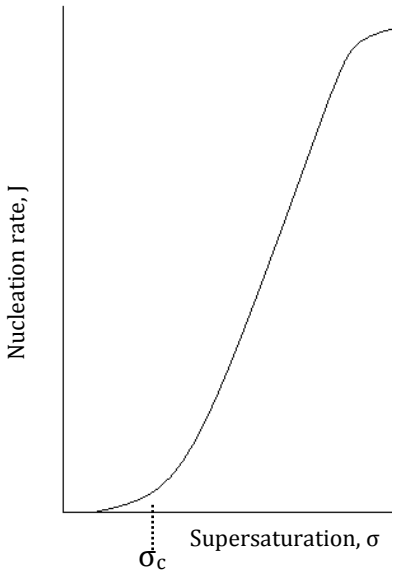

FIGURE 5- THE RATE OF NUCLEATION AS A FUNCTION OF SUPERSATURATION[26].

1.3 AMORPHOUS MATERIALS

As described in Section 1.1.1 crystalline materials are solids displaying long-range order. In contrast amorphous materials are solids displaying no long-range order and share many structural characteristics of a liquid state[29], or some have said a supercooled liquid[30]. As mentioned in Section 1.1.1 amorphous states are less desirable from a pharmaceutical perspective due to their lack of stability. Amorphous states are only kinetically stable and are a higher energy state than the crystalline form in terms of enthalpy, entropy and volume[29, 31, 32]. This high energy leads to enhanced solubility, dissolution rate and often reactivity[33]. The benefits provided by these improved properties may be great enough that solutions to stability issues are investigated further and the amorphous drug progressed to market. Over 25 amorphous drugs have been marketed[34].

1.4 GENERAL DEFINITIONS

Both salts and cocrystals are multicomponent crystals composed of a single homogeneous phase, which can be formed by the crystallisation methods described in Section 1.2.3. The definition of these two systems is under dispute due to issues with what has been termed 'a salt-cocrystal continuum'[35,36]. For the purpose of the rest of this project, both are independently defined.

1.4.1 COCRYSTALS

Cocrystals have only in recent years become an area of intensive research, despite their existence being known since the late 19th century[36]. This resurgence is due to the interest from pharmaceutical companies looking for an alternative to the traditional salts for drug delivery. The definition of a cocrystal is hotly debated and much literature is devoted to its definition[35, 37-39]. This debate will not be discussed further within the scope of this thesis. Within this project a cocrystal is defined as a multi component crystal showing no proton transfer between the components[35].

1.4.2 SALTS

As is discussed in Section 1.1.1, salts have been of interest to pharmaceutical companies for many years, aiding in the manipulation of drug properties. The differences (if any) between salts and cocrystals is widely debated. Salts are defined within this thesis as multi component systems where proton transfer has occurred between the components[35].

1.4.3 POLYMORPHS

In the study of crystallisation, polymorphism is always a subject that should be considered, as the transformation from one polymorph to another can seriously affect the physical properties of a solid. A standard definition is 'a substance capable of crystallising in different, non solvated, crystalline forms'[4]. At the outset of this work a number of the acids planned for use in experimental work were already known to be polymorphic. Ephedrine is not polymorphic and, from previously published work, none of the known salts appear to be either.

1.5 THE PHASE RULE AND PHASE DIAGRAMS

The use of the phase rule and phase diagrams can greatly aid the development of crystallisation processes. Simple measurements of solubility and heats and temperatures of melting can give important data on the phases crystallising, and process yields can be determined relatively quickly and easily[26]. A phase diagram constructed from a range of temperature, pressure and concentration measurements can be used to give a complete picture of the behaviour of a system[4]. Phase diagrams can be plotted with relative ease for one, two (binary) or three (ternary) components.

1.5.1 THE PHASE RULE

The phase rule, as originally stated by Gibbs[40], relates the number of phases, components and degrees of freedom of a system in heterogeneous equilibrium. It assumes that the only variables are temperature (T), pressure (P) and composition (x)[41]. A phase is defined as a homogeneous, physically distinct and mechanically

separable part of a system, e.g. gases, pure liquids (melts), solids and solutions. The presence of solutions in this list suggests the phases do not need to be chemically homogeneous. Equilibrium is defined as the state of rest of the system where T, P and x remain constant for an infinite time. A change to any of these variables will shift the equilibrium[26, 42].

In 1876 Gibbs showed the relationship between the number of phases, P, the number of components, C, and the degrees of freedom, F, can be defined thus

$$P + F = C + 2 \qquad \text{EQUATION 1:21}$$

where the number of degrees of freedom is the number of variables (temperature, pressure and composition) that must be fixed to ensure an equilibrium state. This is the phase rule[26].

For a one component system the calculation reads,

$$F = 1 + 2 - 3 = 0 \qquad \text{EQUATION 1:22}$$

where three phases are present, giving no degrees of freedom, hence showing that equilibrium can only exist at one temperature and pressure. If there are two phases (a liquid and a vapour, a liquid and a solid, or a solid and a vapour) present, then the system is said to be multivariant. This means if the temperature is set arbitrarily the equilibrium pressure exerted by the two phases will be a function of this temperature. Points representing a two phase system will be along lines in the diagram.

Three phase systems (solid, liquid and vapour) are described as invariant. Neither temperature nor pressure can be fixed arbitrarily. Equilibrium between the three states can only exist at one value of temperature and pressure, called the triple point. One component systems can be represented on a two dimensional phase diagram, plotting pressure as ordinate and temperature as abscissa (Figure 6)[26, 41, 43].

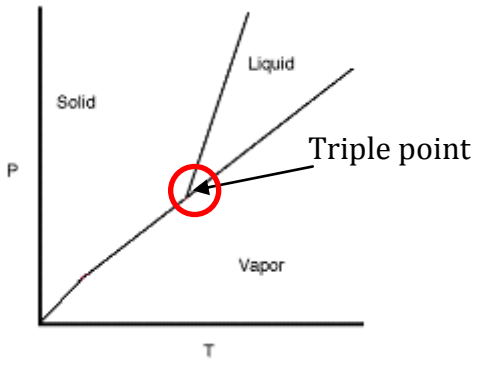

FIGURE 6-ONE COMPONENT PHASE DIAGRAM SHOWING THREE PHASES AND THE TRIPLE POINT

In a two component system with three phases there is one degree of freedom. This means altering a variable defined above would alter the equilibrium state. The phase rule is used in a qualitative way in the definition of equilibrium states. By measuring data on the relation between these variables, the phases can be represented on a two dimensional phase diagram which will be discussed in more detail in Section 1.5.3 [26, 41-43].

1.5.2 RAOULT'S LAW AND IDEAL SOLUTIONS

Raoult's Law states that the mole fraction of solute A, x_A, is equal to the ratio of the partial vapour pressure of A in liquid B (p_A) to its vapour pressure as a pure liquid (p_A^*)[44]. As a system mixes, neither component experiences a change in chemical environment. A system that obeys this law is said to behave ideally.

$$x_A = \frac{p_A}{p_A^*} \qquad \text{EQUATION 1:23}$$

If the solubility of a solid is greater than the ideal it is referred to as a negative deviation from ideality. If the solubility is less than ideal there is a positive deviation.

1.5.2.1 THE IDEALITY OF EPHEDRINE

The ideality of ephedrine (as described in Section 1.1.2) in water has been discussed previously by Black *et al*[25]. Ephedrine was found to behave in a highly non-ideal manner with an ideal solubility of 47.7 mol/L, 137 times the actual

solubility of only 0.34 mol/L in water. This non-ideality is thought to be due to the difficulty in solvating the phenyl ring of the structure in water.

1.5.3 BINARY PHASE DIAGRAMS

In a system containing two components, A and B, a phase diagram can be plotted by measuring the solubility curve of the components i.e. one of the components is the solvent and the other is the solute. In an extended phase diagram the terms solvent and solute are irrelevant. To construct a phase diagram for a binary system a range of AB mixtures must be made and their melting points, the point B just dissolves, or the point A just crystallizes must be measured. Figure 7 is a generic diagram of this type for two components forming a eutectic mixture. This type of diagram assumes the two components are immiscible[26, 42].

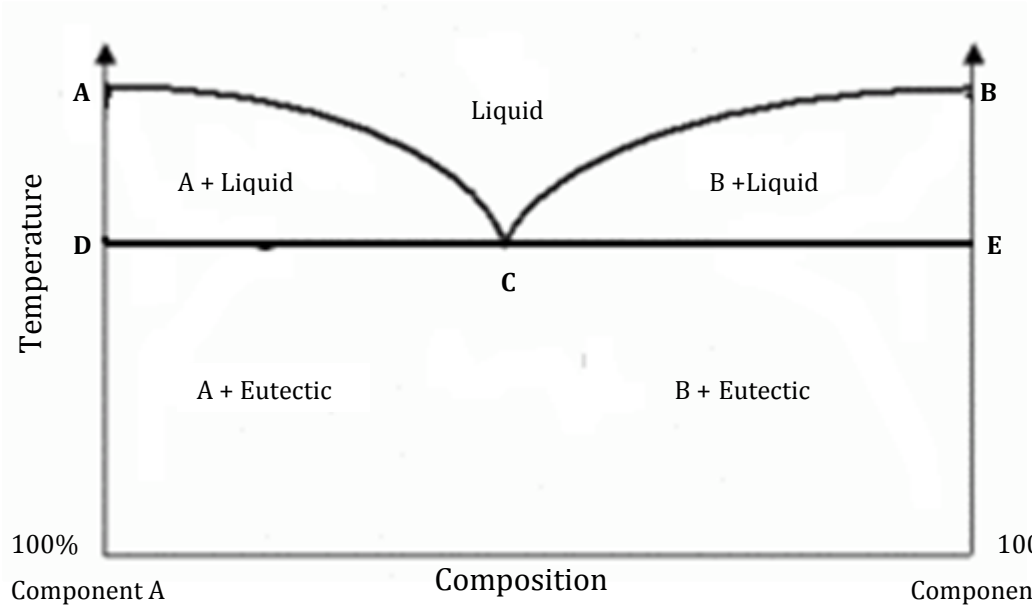

FIGURE 7- EUTECTIC BINARY (TWO COMPONENT) PHASE DIAGRAM FOR A EUTECTIC MIXTURE[26]

In Figure 7 line AC corresponds to the melting of A into B, with pure A in equilibrium with A/B liquid. Line BC corresponds to the melting of B into A, with pure B in equilibrium with A/B liquid. C is the intersection of the two curves, called the eutectic point, and it is at this point the solution is in equilibrium with both components A and B. At the eutectic point the system has the eutectic composition

at the eutectic temperature. The line ACB is referred to as the liquidus, due to it giving the equilibrium composition of the liquid phases. Line ADCEB is the solidus as it gives the equilibrium composition of the solid. As well as an eutectic there are two other types of binary systems, solid solutions and compound forming systems (including cocrystals and salts), as shown in Figure 8.

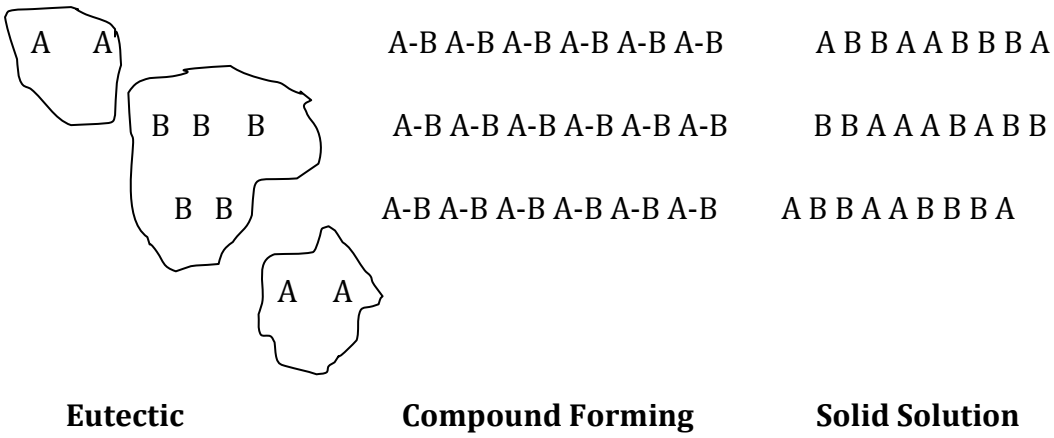

FIGURE 8- TYPES OF BINARY MIXTURES

1.5.3.1 CALCULATING BINARY PHASE DIAGRAMS USING THE IDEAL SOLUBILITY EQUATION

The crystallisation/melting curves of pure components in contact with the liquid phase (where all the components are completely miscible in the liquid phase and immiscible in the solid phase) can be calculated using the Schröder-Van Laar (ideal solubility) equation, which taking into account the effect of temperature on ΔH_f, (the enthalpy of fusion) gives,

$$-\ln x^l \gamma^l = \frac{\Delta H_f}{R}\left(\frac{1}{T_f}-\frac{1}{T}\right)+\frac{\Delta_f C_p}{R}\left(\ln\frac{T}{T_f}+1-\frac{T}{T_f}\right) \quad \text{EQUATION 1:24}$$

where T_f is the temperature of fusion, γ^l is the activity coefficient of the substance at temperature T and mole fraction x. The molar heat capacity taken at constant pressure for the melting temperature T is defined as $\Delta_f Cp^0$. The activity

coefficient is assumed to be one in the case of ideal systems. In their 1981 book Jacques *et al*[42] demonstrate that the second term is generally negligible relative to the first term and it is often neglected. It is also uncommon for heat capacities to be known, especially for new products. This leaves the commonly recognised Schröder-Van Laar equation[42].

$$-\ln x = \frac{\Delta H_f}{R}\left[\frac{1}{T_f} - \frac{1}{T}\right] \qquad \text{EQUATION 1:25}$$

Ideal solutions are ones which have interactions between solute and solvent molecules identical to the mean of the solute-solute interactions and solvent-solvent interactions. They are accepted to be unlikely to exist, however can provide a useful reference condition. Using known heats of melting, and temperatures of melting, the ideal solubility can be predicted and plotted on a phase diagram[4]. The resulting melting temperatures are then plotted for both components at a range of mole fractions, with them crossing at the eutectic. This forms a theoretical binary phase diagram as shown in Figure 9[4, 43, 45].

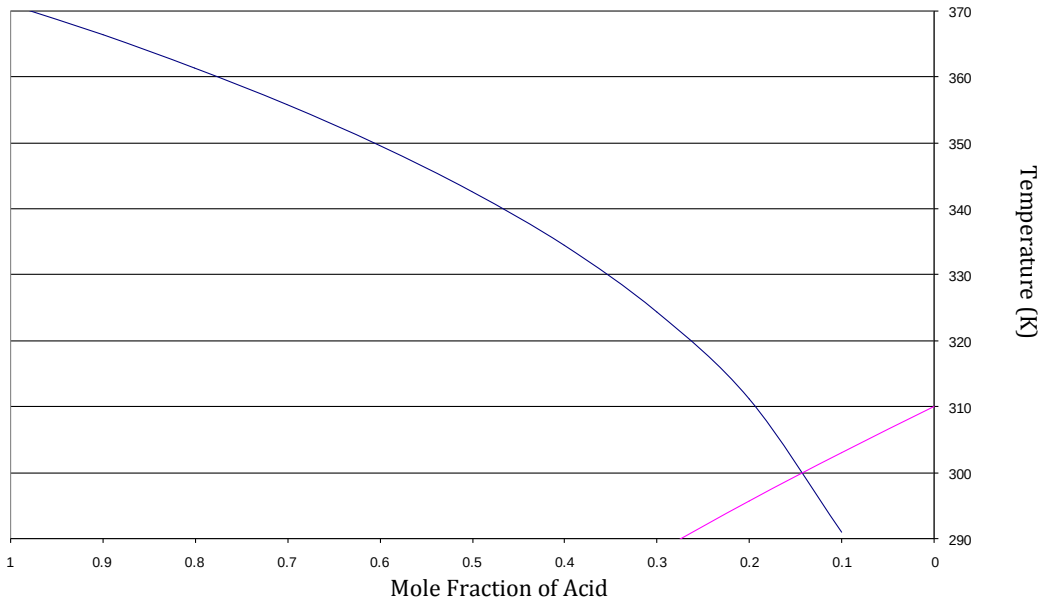

FIGURE 9- THEORETICAL BINARY PHASE DIAGRAM FOR EPHEDRINE AND GLUTARIC ACID, PLOTTED USING THE IDEAL SOLUBILITY EQUATION

The intersection of the curves gives the ideal eutectic composition and temperature. Above the point of intersection the liquid phase would be expected to

form. If this point is below room temperature the contacted powders would be expected to form a liquid without any heating.

1.5.3.2 BINARY PHASE DIAGRAMS FOR COMPOUND FORMING SYSTEMS

Compound forming systems include salts and cocrystals and have slightly more complicated binary phase diagrams (Figure 10) than eutectic mixtures. In Figure 10 the line AC describes the effect of composition on the melting temperature of A, BD describes the effect of composition on the melting temperature of B and CD via E describes the effect of composition on the melting temperature of the salt. The full curve ACEDB is the liquidus, as described in Section 1.5.3. Points C and D are the eutectics of the system. If the composition of the salt equals E then the salt melts congruently, if it does not equal E it melts incongruently.

The Prigogine-Defay equation is used to describe the congruent melting curve of a salt. It is specific to 1:1 salts and can be derived from a more general equation published by Rastogi[46]. For a salt with a congruent melting point (as in Figure 10) the following reaction is taking place[47],

$$A + B \Leftrightarrow AB \rightarrow AB_{(solid)} \qquad \text{REACTION 1-1}$$

If there is a mixture of x_1 moles of A and x_2 moles of B, then $x_1 + x_2 = 1$. Also it can be assumed that x moles of AB are formed so,

$$X_{AB}\,(\text{MOLE FRACTION OF AB}) = x/(1-x) \qquad \text{EQUATION 1:26}$$

$$X_{A}\,(\text{MOLE FRACTION OF A}) = (x_1 - x)/(1-x) \qquad \text{EQUATION 1:27}$$

$$X_{B}\,(\text{MOLE FRACTION OF B}) = (x_2 - x)/(1-x) \qquad \text{EQUATION 1:28}$$

The equilibrium constant, K, can be calculated for the reversible section of the reaction and is given by,

$$K = \frac{x_{AB}}{x_A x_B} \qquad \text{EQUATION 1:29}$$

for an ideal system. At equilibrium the chemical potentials of AB in the liquid and solid states must equal the sum of the chemical potentials of A and B, as defined by Gibbs,

$$\mu_{AB}{}^{s} = \mu_{AB}{}^{l} = \mu_{A}{}^{l} + \mu_{B}{}^{l} \qquad \text{EQUATION 1:30}$$

where $\mu_{AB}{}^{s}$ is the chemical potential of the salt in the solid phase and $\mu_{AB}{}^{l}, \mu_{A}{}^{l}$ and $\mu_{B}{}^{l}$ are the chemical potentials of AB, A and B in the liquid phase. K, defined above, can be related to ΔH , the heat of formation in the liquid phase thus,

$$\Delta G = -RT \ln K \qquad \text{EQUATION 1:31}$$

where ΔG is the Gibbs energy. The change in Gibbs energy is also defined by,

$$\Delta G = \Delta H - T\Delta S \qquad \text{EQUATION 1:32}$$

Where ΔS is the change in entropy and T is the temperature. If these two equations for Gibbs energy are combined,

$$\ln K = \frac{-\Delta H}{RT} + \frac{\Delta S}{R} \qquad \text{EQUATION 1:33}$$

Taking the derivative of this equation,

$$\frac{d \ln K}{dT} = \frac{\Delta H}{RT^{2}} \qquad \text{EQUATION 1:34}$$

and by combining this with the equation defined for K above,

$$\frac{d \ln x_{AB}}{dT} - \frac{d \ln x_{A}}{dT} - \frac{d \ln x_{B}}{dT} = \frac{\Delta H}{RT^{2}} \qquad \text{EQUATION 1:35}$$

At equilibrium conditions for an ideal system this becomes,

$$\frac{d}{dT} \ln[x^{l}{}_{A}(T) x^{l}{}_{B}(T)] = \frac{\Delta_{f} H}{RT^{2}} \qquad \text{EQUATION 1:36}$$

and by integrating,

$$\frac{\Delta_{f} H}{R}\left(\frac{1}{T} - \frac{1}{T_{c}}\right) = -\ln(x_{A}{}^{l})(x_{B}{}^{l}) + \ln(x_{A}{}^{l})_{c}(x_{B}{}^{l})_{c} \qquad \text{EQUATION 1:37}$$

where T_c is the congruent melting temperature of the salt and $(x^l{}_A)$ and $(x^l{}_B)$ are the mole fractions of the salt components in the liquid phase. The subscript *c* denotes the mole fractions of the components in the molten phase of the salt (0.5 for each component in a 1:1 salt). Setting these values to 0.5 gives,

$$\frac{\Delta_f H}{R}\left(\frac{1}{T}-\frac{1}{T_c}\right) = -\ln\left(x_A{}^l\right)\left(x_B{}^l\right) + \ln\frac{1}{4} \qquad \text{EQUATION 1:38}$$

This system can be expressed in one component by making $x_B{}^l = 1 - x_A{}^l$ so,

$$\frac{\Delta_f H}{R}\left(\frac{1}{T}-\frac{1}{T_c}\right) = -\ln x_A{}^l\left(1-x_A{}^l\right) + \ln\frac{1}{4} \qquad \text{EQUATION 1:39}$$

Rearrangement of this equation gives the Prigogine-Defay equation,

$$\ln 4x(1-x) = \frac{\Delta_f H}{R}\left(\frac{1}{T}-\frac{1}{T_c}\right) \qquad \text{EQUATION 1:40}$$

This equation defines the curve in binary phase diagrams for compound forming systems in a 1:1 molar ratio (curve CED in Figure 10)[47].

The 1:1 salt composition (for a salt with congruent melting) is represented by a dashed line in Figure 10. In reality these diagrams can be skewed with some regions much larger, and others much smaller. Determination of the composition of the two components needed to form a salt at a given temperature is possible from the diagram (Figure 10).

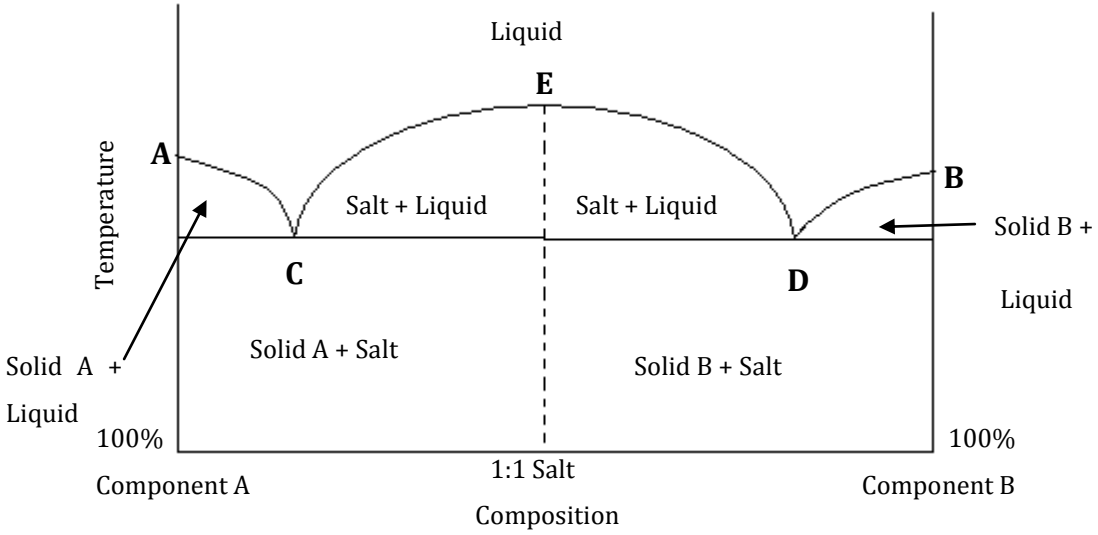

FIGURE 10- BINARY PHASE DIAGRAM FOR A SALT WITH A CONGRUENT MELTING POINT[41]

The binary phase diagrams for solid solutions are not covered in this project but further information can be found in books by Davey and Garside[26] and Jacques *et al*[42].

Multi-component systems may include a salt of a ratio other than 1:1. The ideal solubility equations must be adapted to account for this. To do this Rastogi's equations[46, 48] must be used where n is the ratio of one component divided by the other e.g. for a 1:1 salt, (1/1=1) n=1 and for a 2:1 salt (2/1=2) n=2.

$$\ln(1-x)+n\ln(x)=-\frac{L_c}{T}+\frac{L_c}{T_c}+n\ln n-(n+1)\ln(n+1) \qquad \text{EQUATION 1:41}$$

$$\ln(1-x)+n\ln(x)-n\ln n+(n+1)\ln(n+1)=-\frac{L_c}{T}+\frac{L_c}{T_c} \qquad \text{EQUATION 1:42}$$

$$\ln\frac{(1-x)x^n(n+1)^{(n+1)}}{n^n}=\left(\frac{L_c}{T_c}-\frac{L_c}{T}\right) \qquad \text{EQUATION 1:43}$$

Where

$$L_c=\frac{\Delta_f H}{R} \qquad \text{EQUATION 1:44}$$

Therefore if n=1

$$\ln \frac{(1-x)x2^2}{1} = \left(\frac{L_c}{T_c} - \frac{L_c}{T} \right)$$

$$\ln 4(1-x)x = \left(\frac{L_c}{T_c} - \frac{L_c}{T} \right)$$

Rearrangement of this solution for n=1 gives the Prigogine-Defay equation, given as Equation 1:40.

If n=2

$$\ln \frac{(1-x)x^2 3^3}{4} = \frac{\Delta_f H}{R} \left(\frac{1}{T} - \frac{1}{T_c} \right)$$

$$\ln \frac{27}{4}(1-x)x^2 = \frac{\Delta_f H}{R} \left(\frac{1}{T} - \frac{1}{T_c} \right) \qquad \text{EQUATION 1:45}$$

Using Equations 1:44 and 1:45 the curves for a salt of any ratio can be calculated by changing the values for n and dividing the enthalpy of fusion by the number of molecules present.

There are a large number of published papers showing experimentally determined binary phase diagrams. Some are for enantiomeric systems[49-51], some for cocrystals[52-54] and there is a lack of literature concerning salts. As mentioned previously salts are commonly used in the pharmaceutical industry. As they are not as 'new' to science as cocrystals, they appear to have been somewhat over looked in terms of phase diagrams. This work will aim to remedy this.

For enantiomeric systems the determination of a binary phase diagram is simplified as it will always be symmetrical. The behaviour of one enantiomer will always be identical to the other. The shape of binary phase diagrams for salt and cocrystal systems can either show congruent or incongruent melting depending upon the interactions between components. A greater amount of interaction would be expected in a salt system due to the influence of ionisation.

1.5.4 TERNARY PHASE DIAGRAMS

Using the phase rule defined in Section 1.5.1, it is known that in a three component system with three phases, there are two degrees of freedom and this can be graphically represented on a ternary phase diagram. The two degrees of freedom represented in these systems are composition and temperature[4, 42].

A system containing three components needs to be represented on a three dimensional diagram and triangular prisms (either equilateral or right angled) are used. Usually only a slice of this three dimensional shape is studied, representing the phase diagram of three components at a single temperature (shown by the triangular plane T_0 in Figure 11). This is an isothermal slice.

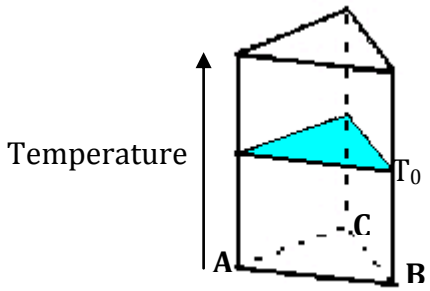

FIGURE 11- GRAPHICAL REPRESENTATION OF A TERNARY PHASE DIAGRAM

Composed of three pure components, A, B and C the isothermal slice can be used to determine the composition of any other point, in the case of Figure 12 labelled m. This is done by drawing lines parallel to the three axes (AB, AC and BC) straight through the point. Each side is taken as unity and the mole fractions/percentages are given by the distance along the sides of the triangle. The composition is then determined by reading the point each line intersects the axes, in Figure 12 the composition would read 25% A, 50% B and 25% C. To construct the diagram all the solubilities must be known at the same temperature. The compositions can either be measured as solubilities in mole fraction or weight percent.

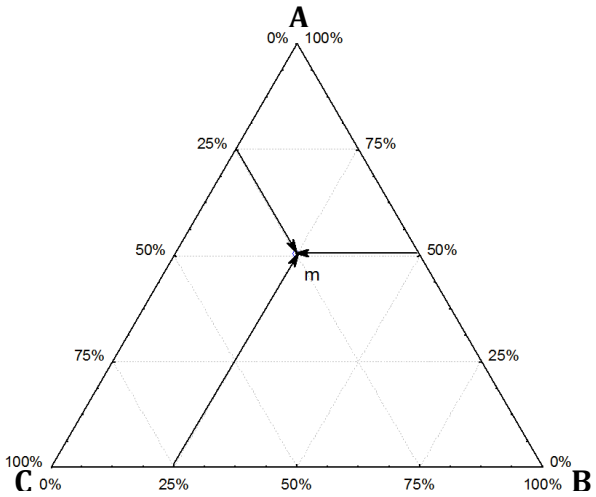

FIGURE 12- THE DETERMINATION OF THE COMPOSITION OF A POINT ON A TERNARY PHASE DIAGRAM-AN ISOTHERMAL SLICE[42]

From ternary phase diagrams a more calculated approach to growing a salt or cocrystal can be used. Instead of using a 1:1 ratio of moles of acid to moles of base, which has sometimes been used in the literature[24, 25], using a ternary phase diagram can provide a more accurate method of selecting the correct ratio of components to ensure pure salt, and not either solid component, crystallises out. This can be done for racemic mixtures, including salts, shown in Figure 13.

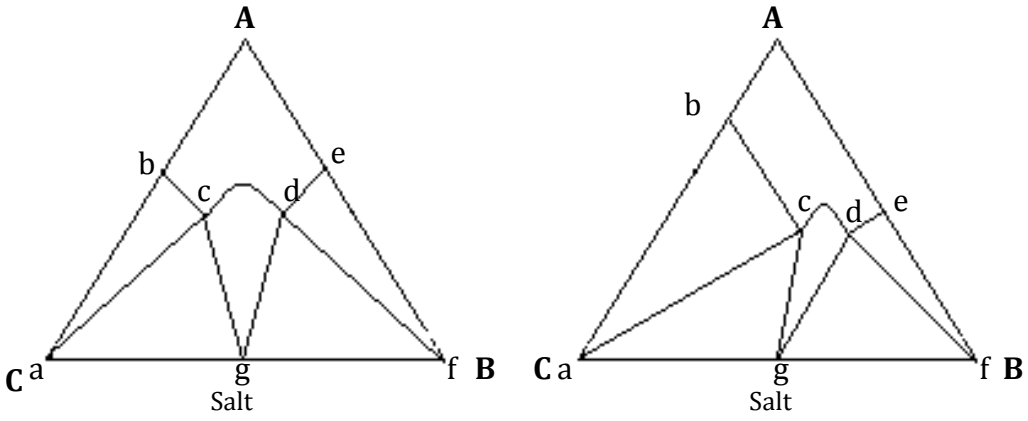

FIGURE 13- TERNARY PHASE DIAGRAMS (SOLUBILITY ISOTHERMS) FOR SALTS[42]

Areas acg and dfg in both diagrams are eutectic areas where a mixture of solid phases will be obtained. In the region abc it is possible to crystallise pure C, in the region cdg it is possible to crystallise the pure salt and in region def it is possible to crystallise pure B.

Publications showing experimentally determined ternary phase diagrams are more prolific in papers about cocrystal[52, 53, 55-57] or chiral[49, 51, 58, 59] systems, than for those concerning salts. For chiral systems the diagrams are significantly easier to determine as the diagram will always be congruent and only one side has to be measured for the full diagram to be determined. The ternary phase diagrams for cocrystal or salt systems may be congruent or incongruent, depending upon the formation of multicomponent crystals of different stoichiometries or skewed solubilities of the constituent components. It is suspected that salt systems will show a greater deviation from the ideal due to the effects of ionisation. In this thesis investigation will be undertaken in order to go some way to remedy this.

1.6 MULTICOMPONENT CRYSTAL FORMATION BY CONTACT AND GRINDING

Literature on the formation of multicomponent crystals by the contacting of solid components, or by grinding the solid components together, is scarce (for salts), in comparison to publications focussing upon crystallisation from solvents. Crystal growth from solution is discussed in Section 1.2 of this project. In this section cocrystals and salts (defined in Section 1.4.1 and 1.4.2 respectively) will be discussed, due to the overlap between these areas of literature and increased discussion on grinding relating to cocrystal formation rather than salts.

Interestingly, despite a lack of literature on grinding, the technique was being utilised as early as the mid 19th century[36, 60]. In these early publications a pestle and mortar is used to initiate a reaction between the components, sometimes with a small amount of solvent added. This is an early example of what is now commonly termed liquid-assisted grinding[61-63]. In these papers the distinction between salt and cocrystal is vague as is also the case in some modern papers[64].

In more modern literature, mechanical milling has been used to facilitate the formation of amorphous salts of formulated drug products to increase the dissolution rate and hence the bioavailability[65]. Salts and cocrystals have been formed both by neat grinding and by liquid assisted grinding, as was described in the early literature, with grinding often still done by hand using a pestle and

mortar, or now alternatively mechanically using a mill[52, 63, 64, 66, 67]. Grinding, and even solvent drop grinding, are seen as environmentally friendly alternatives to solution methods due to the lack of solvents used[68, 69]. This also reduces costs as the safe disposal of solvents to meet government guidelines is no longer needed.

Little work has been published concerned with understanding the mechanism of grinding induced syntheses. In the most comprehensive review of this subject, Friščić *et al*[70] conclude that the mechanism of neat grinding cannot be described by a single mechanism, but rather there are several mechanisms the reaction may proceed via. The recognised mechanisms include molecular diffusion (vapour phase)[71], cocrystallisation mediated by an amorphous phase[72] and eutectic formation (metastable liquid)[52]. In all three of these mechanisms there is an intermediate bulk phase with improved mobility and higher molecular energy over the crystalline material. The three mechanisms are discussed in detail with more literary examples.

In 1962 Rastogi *et al*[73] published a short note suggesting that solid state reaction between naphthalene and picric acid occurs via a vapour diffusion method. The components were contacted in a capillary and maintained at a temperature below the eutectic. The initial contact position was noted and as a colour change occurred upon product formation, the position of reaction was noted. It was concluded that the naphthalene diffused through the product layer, while the acid did not. No discussion was included on the composition of the product, therefore assessment of whether a salt or cocrystal formed is not possible. In 1963 a continuation of this work was published[71] and it was concluded that two solids with sufficiently high vapour pressures would form a product upon contact.

Kuroda *et al*[74] co-milled and mixed benzoquinone with diol crystals of different melting temperatures. Again this was determined to be proceeding by a diffusion method. Of the two structurally related phenols tested in this publication, one reacted much more quickly than the other. It was concluded that this was due to a more extensive hydrogen bonding network in the less reactive diol. In these reactions the role of mechanochemical grinding was to expose fresh surfaces and mix the reactants, allowing the reaction to go to completion. This was especially

true for the less reactive phenol, where the grinding was believed to have aided in overcoming strong intermolecular forces.

A 2003 paper by Kaupp[75] discusses how molecules must migrate for this mechanism to occur. The new product formation rate must be sufficiently high and the new crystal must disintegrate to allow new surfaces to become exposed. The author hypothesises that the exposure of these new surfaces may be facilitated by grinding, providing reasoning to the success of this technique.

Nguyen *et al*[72] used Terehertz radiation to probe the formation of a cocrystal by mechanochemical grinding of phenazine and mesaconic acid. Partial cocrystal formation was reported after 30 minutes. The reaction was then reported to go to completion after the sample was allowed to stand for a number of days. The authors felt this was due to both particle size effects and partial amorphisation of the sample. When SEM was undertaken it was observed that the particle size had not changed. The authors concluded that aging of the sample allows crystallisation of the amorphous phase. This was reinforced by further grinding of the sample producing a lower cocrystal yield. This suggests that the grinding is causing the amorphisation. The mechanism of cocrystal formation is crystallisation from an amorphous phase.

Chadwick *et al*[52] considered the possibility of the mechanism being dependent upon the presence of a submerged eutectic by studying the system benzophenone/diphenylamine. These two components were already known to form a cocrystal under solid-state grinding at ambient temperatures. It was discovered that a metastable binary eutectic exists, which has a eutectic temperature lying below the melting point of any of the known solid phases. The temperature of this eutectic point was estimated by extending the melting point curves of the pure components (illustrated as a phase diagram, described above in Section 1.5.1). The position of this hypothetical eutectic was then proved experimentally[52].

Other papers discuss solid-solid reactions including salt and cocrystal formations. Many publications do not give a clear hypothesis of the mechanism this is

proceeding via, however for these works there are other research aims achieved[76, 77].

Ephedrine has been shown to form its racemic compound by placing the two racemates diametrically in a petri dish. This paper deduces that formation of this compound occurs due to the high vapour pressure of ephedrine, however the vapour pressure of ephedrine is not measured[78]. If the same effect is noted to occur it may suggest another mechanism of salt formation by contact or grinding.

1.6.1 VAPOUR PRESSURE

Equilibrium vapour pressure can be defined as the pressure when a condensed phase is in equilibrium with its own vapour. Vapour pressure increases with temperature as molecules have been provided with sufficient energy to leave the liquid[79]. The liquid vapour boundary is shown on a plot of vapour pressure against temperature (Figure 6).

1.7 SALT SOLUBILITY

1.7.1 THEORY

The dissolution of a salt involves the breaking of interionic bonds in the solid, separation of solvent molecules to accommodate the solute, and the formation of new interactions between the solvent and the solute. The intermolecular bonds in the salt will include ionic interactions and may also include van der Waals forces and hydrogen bonding. In a salt there is an ionic attraction between the acidic and basic components. This attractive force, F, is expressed by Coulomb's Law,

$$F = q^{+}.q^{-} / D.d^{2} \qquad \text{EQUATION 1:46}$$

where q^+ and q^- are the electric charges on the ions, D is the dielectric constant of the surrounding medium (where D = 1 in a vacuum), and d is the distance between the ions. When a salt dissolves in polar solvents, such as water, the ion-dipole interaction is dominant and so the salt is hydrated. This is due to the ion being surrounded by as many water molecules as possible[2]. This effect causes the increased solubility of salts over their unionized constituents and deviation from

the 'ideal' situation (defined in Section 1.5.2). This is one of the properties that make salt formation desirable for pharmaceutical companies[80].

1.7.2 THERMODYNAMICS

For dissolution to occur, a decrease in Gibbs energy must take place as Gibbs energy (G) is a chemical potential which is minimized when a system reaches equilibrium. The equation for the change in Gibbs energy (ΔG) is,

$$\Delta G = \Delta H - T\Delta S \qquad \text{EQUATION 1:47}$$

To increase the solubility, ΔG must be made negative[45]. This means making ΔH negative (or more negative), making ΔS positive (or more positive) or increasing the temperature. As entropy can be defined as the degree of disorder in a system it can be stated that dissolution is an entropy driven process. The disorder of the system increases as the regular structure of a salt is broken and the component ions are free to move in solution.

Solubility of a solid also depends upon the activity coefficient of the solute (a function of the intermolecular forces between solvent and solute), the fugacity (*f*) of the standard state to which the activity refers and on the fugacity of the pure solid. For the solute:

$$f_{\text{(PURE SOLID)}} = f_{\text{(SOLUTE IN LIQUID SOLUTION)}} \qquad \text{EQUATION 1:48}$$

or

$$f_{\text{(PURE SOLID)}} = \gamma x f^{0} \qquad \text{EQUATION 1:49}$$

where *f* is the fugacity, *x* is the solubility as a mole fraction, γ is the activity coefficient in the liquid phase and f^0 is the standard state fugacity referred to by the activity coefficient. Solubility is dependent on both fugacity and the activity[45].

When salts enter the solvent and are dissociated the reaction can be written thus:

$$A_m B_n \leftrightarrow mA^{n+} + nB^{m-} \qquad \text{REACTION 1-2}$$

with the solubility product, K_{sp}, given by:

$$K_{sp} = [A]^m[B]^n \qquad \text{EQUATION 1:50}$$

The solubility product holds when a solid ionic salt is in equilibrium with the solution containing its ions, or in other words when the solution is saturated. When the solid phase is pure its activity is unity and can be neglected[81]. For salts which are only sparingly soluble the solubility can be more accurately determined using conductivity measurements. This will not be explored in this project. Literature is available on the subject[4, 82, 83].

1.7.2.1 SOLUBILITY PRODUCT, pH AND SOLUBILITY

A practical use for the equations discussed above is the calculation of the K_{sp} value of a solid if the pH is measured alongside its solubility, as discussed by Jones *et al* in the 2005 paper[8]. This calculation is detailed below using some fundamental thermodynamic equations.

$K_{HA} = [H^+][A^-]/[HA]$ EQUATION 1:51

$K_{BH} = [B][H^+]/[BH^+]$ EQUATION 1:52

$K_{sp} = [BH^+][A^-]$ EQUATION 1:53

$pH=-Log[H^+]$ EQUATION 1:54

$\text{Solubility of base} = [BH^+]+[B]=[BH^+]\{1+K_{BH}/[H^+]\}$ EQUATION 1:55

$\text{Solubility of acid} = [A^-]+[HA] = [A^-]\{1+[H^+]/K_{HA}\}$ EQUATION 1:56

$\text{Solubility of the salt} = [BH^+][A^-]\{1+[H^+]/K_{HA}\}\{1+K_{BH}/[H^+]\}$ EQUATION 1:57

By combining Equations 1:53 and 1.57, the salt solubility in terms of K_{sp} can be determined (Equation 1:58) and the K_{sp} can then be solved with only one solubility measurement (as long as the pH is known) by iteration.

$\text{Solubility of salt} = K_{sp}\{1+[H^+]/K_{HA}\}\{1+K_{BH}/[H^+]\}$ EQUATION 1:58

In the 1978 paper Chowhan[84] determined the pH-solubility profile for naproxen and other carboxylic acids with a range of metal cations. Here the pH was altered by one of two methods. The first involved using dilute hydrochloric acid, dilute sodium hydroxide or dilute potassium hydroxide (depending on the salt being formed). The second involved the addition of the salt, followed by pH adjustment carried out using small quantities of dilute HCl or NaOH. The theoretical pH-solubility profiles were also calculated and compared to the experimental results, as will be undertaken in this work. In this publication the correlation between theoretical and experimental data is very good.

In 1984 Streng *et al*[85] showed that a pH-solubility profile is defined by the K_{sp}, pK_a and the uncharged species solubility. In 1985[86] the group determined the solubility of a zwitterionic compound as a function of pH and temperature. Using this data they went on to calculate the K_{sp}, intrinsic solubility of the uncharged species and a range of thermodynamic properties as a function of temperature. They determined that as temperature is increased the pK_as of a compound decrease. Over the same temperature increase the authors also noted an increase in the solubility of the uncharged species.

Li *et al*[87] published their 1998 paper with the aim of assessing why pH and complexation work better when used together to improve solubility than they do independently. The authors conclude that the combined improvement is due to the 25 times greater solubility of the ionised drug to the unionised drug. Hence upon complexation the ionised complex is 6 times more soluble than the unionised complex. This provides an explanation as to why salt systems are favoured for drug delivery by pharmaceutical companies.

1.8 SUMMARY

Within this section the theory behind the processes investigated in this work is laid out alongside the earlier examples of literature for these fields and a range of up-to-the minute publications. General definitions of terms that will be used extensively throughout this thesis, such as salt, cocrystal and polymorph, are defined to aid the reader.

1.9 REFERENCES

1. Atkins, P. W. in The Elements of Physical Chemistry (Oxford University Press, Oxford, 2003).
2. Stahl, H. P. & Wermuth, C. G. Handbook of Pharmaceutical Salts-Properties, Selection, and Use (Wiley-VCH, 2002).
3. Brittain, H. G. Physical Characterization of Pharmaceutical Salts (ed. Brittain, H. G.) (Marcel Dekker Inc., 1995).
4. Mullin, J. Crystallization (Butterworth-Heinemann, Oxford, U.K., 1993).
5. Berge, S. M., Bighley, L. D. & Monkhouse, D. C. Pharmaceutical Salts. Journal of Pharmaceutical Sciences 66, 1-19 (1977).
6. Gould, P. L. Salt Selection for Basic Drugs. International Journal of Pharmaceutics 33, 201-217 (1986).
7. Remenar, J. F. et al. Salt Selection and Simultaneous Polymorphism Assessment via High-Throughput Crystallization: The Case of Sertraline. Organic Process Research and Development 7, 990-996 (2003).
8. Jones, H. P., Davey, R. J. & Cox, B. G. Crystallization of a Salt of a Weak Organic Acid and Base: Solubility Relations, Supersaturation Control and Polymorphic Behaviour. Journal of Physical Chemistry 109, 5273-5278 (2005).
9. Nelson, E. Comparative Dissolution Rates of Weak Acids and their Sodium Salts. Journal of the American Pharmaceutical Association (Science Edition) 47, 297-299 (1958).
10. Portoghese, P. S. Stereochemical Studies on Medicinal Agents. IV. Conformational Analysis of Ephedrine Isomers and Related Compounds. Journal of Medicinal Chemistry 10, 1057-1063 (1967).
11. Duddu, S. P., Khin-Khin, A., Grant, D. J. W. & Suryanarayanan, R. A Novel X-Ray Powder Diffractometric Method for Studying the Reaction between Pseudoephedrine Enantiomers. Journal of Pharmaceutical Sciences 86, 340-345 (1997).
12. Butz, P. et al. in Lasers for Science Facility Programme (Physical and Theoretical Chemistry Laboratory, Oxford University, Oxford, 2000/2001).

13. Charlton, S. T., Davis, S. S. & Illium, L. Evaluation of Effect of Ephedrine on the Transport of Drugs from the Nasal Cavity to the Systemic Circulation and the Central Nervous System. Journal of Drug Targeting 15, 370-377 (2007).
14. Zheng, J., DiLorenzo, D. J., McLaughlin, L., Roberts, A. T. & Greenway, F. L. Stimulation of Sympathetic Innervation in the Upper Gastrointestinal Tract as a Treatment for Obesity. Medical Hypotheses 72, 706-710 (2009).
15. Magkos, F. & Kavouras, S. A. Caffeine and Ephedrine: Physiological, Metabolic and Performance-Enhancing Effects. Sports Medicine 34, 871-889 (2004).
16. Chua, S. S. & Benrimoj, S. I. Non-Prescription Sympathomimetic Agents and Hypertension. Medical Toxicology and Adverse Drug Experience 3, 387-417 (1988).
17. Lynch, J. & House, M. A. Cardiovascular Effects of Methamphetamine. Journal of Cardiovascular Nursing 6, 12-18 (1992).
18. (Medicines and Healthcare products regulatory agency, 2009).
19. Drug Enforcement Administration (DEA), J. (ed. DEA) 4973-3982 (Federal Register, 2010).
20. Bergin, R. Refinement of the Structure of (-)-Ephedrine Hydrochloride. Acta Crystallographica Section B: Structural Science B27, 381-386 (1971).
21. Erk, N. Assay of Ephedrine Hydrochloride and Theophylline in Pharmaceutical Formulations by Differential-derivative Spectroscopy. Journal of Pharmaceutical and Biomedical Analysis 23, 255-261 (2000).
22. Phillips, D. C. The Crystal and Molecular Structures of Ephedrine Hydrochloride. Acta Crystallographica 7, 159-165 (1954).
23. Florey, K. Analytical Profiles of a Drug Substance (Academic Press, Inc., London, 1986).
24. Collier, E. A., Davey, R. J., Black, S. N. & Roberts, R. J. 17 Salts of Ephedrine: Crystal Structures and Packing Analysis. Acta Crystallographica, Section B: Structural Science B62, 498-505 (2006).
25. Black, S. N., Collier, E. A., Davey, R. J. & Roberts, R. J. Structure, Solubility, Screening, and Synthesis of Molecular Salts. Journal of Pharmaceutical Sciences 96, 1053-1068 (2007).

26. Davey, R. J. & Garside, J. From Molecules to Crystallizers (Oxford University Press Inc., New York, 2000).
27. Hartman, P. Crystal Growth: An Introduction (eds. Bardsley, W., Hurle, D. T. J. & Mullin, J. B.) (North-Holland Publishing Company, Amsterdam, 1973).
28. Volmer, M. Kinetik der Phasenbildung (Steinkopff, Dresden, 1939).
29. Hancock, B. C. & Zografi, G. Characteristics and Significance of th Amorphous State in Pharmaceutical Systems. Journal of Pharmaceutical Sciences 86, 1-12 (1997).
30. Cheng, Y.-T. & Johnson, W. L. Disordered Materials- A Survey of Amorphous Solids. Science 235, 997-1002 (1987).
31. Yu, L. Amorphous Pharmaceutical Solids: Preparation, Characterisation and Stabilisation. Advanced Drug Delivery Reviews 48, 27-42 (2001).
32. Patterson, J. E. et al. The Influence of Thermal and Mechanical Preparative Techniqueson the Amorphous State of Four Poorly Soluble Compounds. Journal of Pharmaceutical Sciences 94, 1988-2012 (2005).
33. Craig, D. Q. M., Royall, P. G., Kett, V. L. & Hopton, M. L. The Relevance of the Amorphous State to Pharmaceutical Dosage Forms: Glassy Drugs and Freeze Dried Systems. International Journal of Pharmaceutics 179, 179-207 (1999).
34. Hancock, B. C. Disordered Drug Delivery: Destiny, Dynamics and the Deborah Number. Journal of Pharmacy and Pharmacology 54, 737-746 (2002).
35. Childs, S. L., Stahly, G. P. & Park, A. The Salt-Cocrystal Continuum: The Influence of Crystal Structure on Ionization State. Molecular Pharmaceutics 4, 323-338 (2007).
36. Ling, A. R. & Baker, J. L. Halogen Derivatives of Quinone. Part III Derivatives of Quinhydrone. Journal of the Chemical Society, Transactions 63, 1314-1327 (1893).
37. Lara-Ochoa, F. & Espinosa-Perez, G. Cocrystal Definitions. Supramolecular Chemistry 19, 553-557 (2007).
38. Rodriguez-Hornedo, N. Cocrystals: Molecular Design of Pharmaceutical Materials. Molecular Pharmaceutics 4, 299-300 (2007).

39. Aakeroy, C. B., Fasulo, M. E. & Desper, J. Cocrystal or Salt: Does It Really Matter? Molecular Pharmaceutics 4, 317-322 (2007).
40. Gibbs, J. W. Collected Works (Longmans, 1928).
41. Ricci, J. E. The Phase Rule and Heterogeneous Equilibrium (Dover Publications, Inc., New York, 1966).
42. Jacques, J., Collet, A. & Wilen, S. H. Enantiomers, Racemates and Resolutions (Wiley-Interscience, New York, 1981).
43. Prigogine, I. & Defay, R. Chemical Thermodynamics (Longmans Green and Co, London, New York, Toronto, 1954).
44. Atkins, P. W. in The Elements of Physical Chemistry 118 (Oxford University Press, Oxford, 2003).
45. Prausnitz, J. M., Lichtenthaler, R. N. & Gomes de Azevedo, E. Molecular Thermodynamics of Fluid-Phase Equilibria (Prentica-Hall inc, Englewood Cliffs, N.J., 1986).
46. Rastogi, R. P. Thermodynamics of Phase Equilibria and Phase Diagrams. Journal of Chemical Education 41, 443-448 (1964).
47. Chadwick, K. in School of Chemical Engineering and Analytical Science 260 (The University of Manchester, Manchester, 2008).
48. Tabora, J. E. et al. Identification and Characterization of an Anomalous Racemate. Fluid Phase Equilibria 258, 140-147 (2007).
49. Tamagawa, R. E., Miranda, E. A., Santana, C. C. & Guilietti, M. Determination of the Binary and Ternary Phase Diagrams of R(+)-/S(−)-Ketamine Using Differential Scanning Calorimetry. Journal of Chemical Engineering Data 54, 16-21 (2009).
50. Srisanga, S. & Ter Horst, J. H. Racemic Compound, Conglomerate, or Solid Solution: Phase Diagram Screening of Chiral Compounds. Crystal Growth and Design 10, 1808-1812 (2010).
51. Lorenz, H. & Seidel-Morgenstern. Binary and Ternary Phase Diagrams of Two Enantiomers in Solvent Systems. Thermochimica Acta 382, 129-142 (2002).
52. Chadwick, K., Davey, R. J. & Cross, W. How Does Grinding Produce Co-crystals? Insights from the Case of Benzophenone and Diphenylamine. Chemical Communications 9, 732-734 (2007).

53. Guo, K., Sadiq, G., Seaton, C., Davey, R. & Yin, Q. Co-Crystallisation in the Caffeine/ Maleic Acid System: Lessons from Phase Equilibria. Crystal Growth and Design 10, 268-273 (2010).
54. He, Q., Rohani, S., Zhu, J. & Gomaa, H. Sertraline Racemate and Enantiomer: Solid-State Characterization Binary Phase Diagram, and Crystal Structures. Crystal Growth and Design 10, 1633-1645 (2010).
55. Chiarella, R. A., Davey, R. J. & Peterson, M. L. Making Co-crystals- The Utility of Ternary Phase Diagrams. Crystal Growth and Design 7, 1223-1225 (2007).
56. Jayasankar, A., Sreenivas Reddy, L., Bethune, S. J. & Rodriguez-Hornedo, N. Role of Cocrystal and Solution Chemistry on the Formation and Stability of Cocrystals with Different Stoichiometry. Crystal Growth and Design 9, 889-897 (2009).
57. Chadwick, K., Davey, R., Sadiq, G., Cross, W. & Pritchard, R. The Utility of a Ternary Phase Diagram in the Discovery of New Co-crystal Forms. CrystEngComm 11, 412-414 (2009).
58. Codan, L., Mazzotti, M. & Babler, M. U. Phase Diagram of a Chiral Substance Exhibiting Oiling Out in Cyclohexane. Crystal Growth and Design 10, 4005-4013 (2010).
59. Tulashie, S. K., Lorenz, H., Malwade, C. R. & Seidel-Morgenstern, A. Ternary Solubility Phase Diagrams of Mandelic Acid and N-Methylephedrine in Chiral Solvents with Different Carbon Chain Lengths. Crystal Growth and Design 10, 4023-4029 (2010).
60. Wöhler, F. Untersuchung über das Narcotin und seine Zersetzungsproducte. Annalen der Physik 51, 532-543 (1844).
61. Adams, C. J., Colquhoun, H. M., Crawford, P. C., Lusi, M. & Orpen, A. G. Solid-State Interconversions of Coordination Networks and Hydrogen Bonded Salts. Angewandte Chemie. International edition in English 46, 1124-1128 (2007).
62. Myz, S. A. et al. Synthesis of Co-crystals of Meloxicam with Carboxylic Acids by Grinding. Mendeleev Communications 19, 272-274 (2009).

63. Trask, A. V., Haynes, D. A., Motherwell, W. D. S. & Jones, W. Screening for Crystalline Salts via Mechanochemistry. Chemical Communications 51, 51-53 (2006).
64. Huang, K.-S., Britton, D., Etter, M. C. & Byrn, S. R. A Novel Class of Phenol-Pyridine Co-crystals for Second Harmonic Generation. Journal of Material Chemistry 7, 713-720 (1997).
65. Gupta, M. K., Vanwert, A. & Bogner, R. H. Formation of Physically Stable Amorphous Drugs by Milling with Neusilin. Journal of Pharmaceutical Sciences 92, 536-551 (2003).
66. Braga, D., Rubini, K. & Maini, L. Transition from a charge-opposed (+)N-H-N(+) inter-cation hydrogen bonded form of the salt [HN(CH2CH2)3N][OOC-(HC=CH)COOH] to the more traditional charge-assisted (+)N-H-O(-) cation-anion hydrogen bonded pseudo-polymorph upon hydration. CrystEngComm 6, 236-238 (2004).
67. Haynes, D. A., Weng, Z. F., Jones, W. & Motherwell, W. D. S. The Crystal Structures of Three Novel Lutidinium Pamoate Salts. CrystEngComm 11, 254-260 (2009).
68. Trask, A. V., Motherwell, W. D. S. & Jones, W. Solvent Drop Grinding:Green Polymorph Control of Cocrystallisation. Chemical Communications, 890-891 (2004).
69. Trask, A. V. & Jones, W. Crystal Engineering of Organic Cocrystals by The Solid-State Grinding Approach. Topics in Current Chemistry 254, 41-70 (2005).
70. Friscic, T. & Jones, W. Recent Advances in Understanding the Mechanism for Cocrystal Formation via Grinding. Crystal Growth and Design 9, 1621-1637 (2009).
71. Rastogi, R. P., Bassi, P. S. & Chadha, L. S. Mechanism of the Reaction Between Hydrocarbons and Picric Acid in the Solid State. Journal of Physical Chemistry 67, 2569-2573 (1963).
72. Nguyen, K. L., Friscic, T., Day, G. M., Gladden, L. F. & Jones, W. Terahertz Time-Domain Spectroscopy and the Quantitative Monitoring of Mechanochemical Cocrystal Formation. Nature Materials 6, 206-209 (2007).

73. Rastogi, R. P., Bassi, P. S. & Chadha, L. S. Kinetics of Reaction Between Naphthalene and Picric Acid in the Solid State. Journal of Physical Chemistry 66, 2707-2708 (1962).
74. Kuroda, R., Higashiguchi, K., Hasebe, S. & Imai, Y. Crystal to Crystal Transformation in the Solid State. CrystEngComm 6, 463-468 (2004).
75. Kaupp, G. Solid-state Molecular Syntheses: Complete reactions Without Auxiliaries Based on the new Solid-state Mechanism. CrystEngComm 5, 117-133 (2003).
76. Kaupp, G. Waste-free Large-scale Syntheses Without Auxiliaries for Sustainable Production Omitting Purifying Workup. CrystEngComm 8, 794-804 (2006).
77. Karki, S., Friscic, T. & Jones, W. Control and Interconversion of Cocrystal Stoichiometry in Grinding: Stepwise Mechanism for the Formation of a Hydrogen-Bonded Cocrystal. CrystEngComm 11, 470-481 (2009).
78. Duddu, S. P. & Grant, D. J. W. Formation of the Racemic Compound of Ephedrine Base from a Physical Mixture of Its Enantiomers in the Solid, Liquid, Solution, or Vapor State. Pharmaceutical Research 9, 1083-1091 (1992).
79. Atkins, P. W. in The Elements of Physcial Chemistry 99 (Oxford University Press, Oxford, 2003).
80. Yazdanian, M., Briggs, K., Jankovsky, C. & Hawi, A. The 'High Solubility' Definition of the Current FDA Guidance on Biopharmaceutical Classification System may be too Strict for Acidic Drugs. Pharmaceutical Research 21, 293-299 (2004).
81. Butler, J. N. & Cogley, D. R. Ionic Equilibrium- Solubility and pH Calculations (John Wiley and Sons, inc, New York, Chichester, Weinheim, Brisbane, Singapore, Toronto, 1998).
82. Findlay, A. Findlay's practical physical chemistry (ed. Levitt, B. P.) (Longman, Harlow, 1973).
83. Matthews, G. P. Experimental physical chemistry (Clarendon, Oxford, 1985).
84. Chowhan, Z. T. pH-Solubility Profiles of Organic Carboxylic Acids and Their Salts. Journal of Pharmaceutical Sciences 67, 1257-1260 (1978).

85. Streng, W. H., Hsi, S. K., Helms, P. E. & Tan, H. G. H. General Treatment of pH-Solubility Profiles of Weak Acids and Bases and the Effects of Different Acids on the Solubility of a Weak Base. Journal of Pharmaceutical Sciences 73, 1679-1684 (1984).

86. Streng, W. H. & Tan, H. G. H. General Treatment of pH Solubility Profiles of Weak Acids and Bases. II. Evaluation of Thermodynamic Parameters from the Temperature Dependence of Solubility Profiles Applied to a Zwitter Ionic Compound. International Journal of Pharmaceutics 25, 135-145 (1985).

87. Li, P., Tabibi, S. E. & Yalkowsky, S. H. Combined Effect of Complexation and pH on Solubilization. Journal of Pharmaceutical Sciences 87, 1535-1537 (1998).

2 EXPERIMENTAL METHODS AND TECHNIQUES

2.1 INTRODUCTION

Within this chapter the general methods used in the experimental portion of this thesis are explained. The wide range of analytical techniques used is also detailed.

2.2 CRYSTALLISATION AND SOLUBILITY

The crystallisation of salts is a major part of this project; therefore the technique used is described here. The solubility of salts and their components were also investigated and the method used described.

2.2.1 SALT FORMATION FROM SOLUTION

2.2.1.1 APPARATUS

A 50 ml jacketed vessel was used for performing all crystallisation experiments. Jacketed vessels can provide a uniform temperature as they are connected to a water bath, from which the temperature can be controlled. A magnetic stirrer was used to agitate the sample. The vessel was also stoppered, providing a method of inhibiting evaporation.

2.2.1.2 CRYSTALLISATION OF SALTS

The formation of salts is dependent upon the ionic equilibria between the component acids and bases in their solutions. In this project the base was always ephedrine (as defined in Section 1.1.2) forming a salt with a range of acidic counter-ions. To form a salt the secondary amine group in ephedrine (structure shown in Section 1.1.2) is protonated, going from NH to the cation NH_2^+ ([BH^+] in Figure 14). The proton is donated by the acid counter-ion, leaving an anion ([A-] in Figure 14). The pK_a refers to how acidic a specified hydrogen atom is within a structure (how readily it donates a proton), hence it indicates the pH region in which ionisation of both components will occur. It is commonly regarded as a

general rule that the formation of a salt requires an acidic pK_a at least two pK_a units lower than the pK_a of the base[1]. It is generally accepted that a pK_a difference of less than two will produce a cocrystal[2] (for definitions of salts and cocrystals please refer to Section 1.4). Theoretically, salt formation will result when both components are at the maximum mole fraction[3]. This information can be visually represented on a distribution or speciation diagram. A generic diagram of ephedrine in water with known aqueous pK_a values is shown in Figure 14. In the speciation diagram the points where the two species concentrations (for either acid or base) cross is the pK_a value. In Figure 14 salt formation would be expected to occur between pH values of 4 and 8, where both component ions are at the maximum mole fraction.

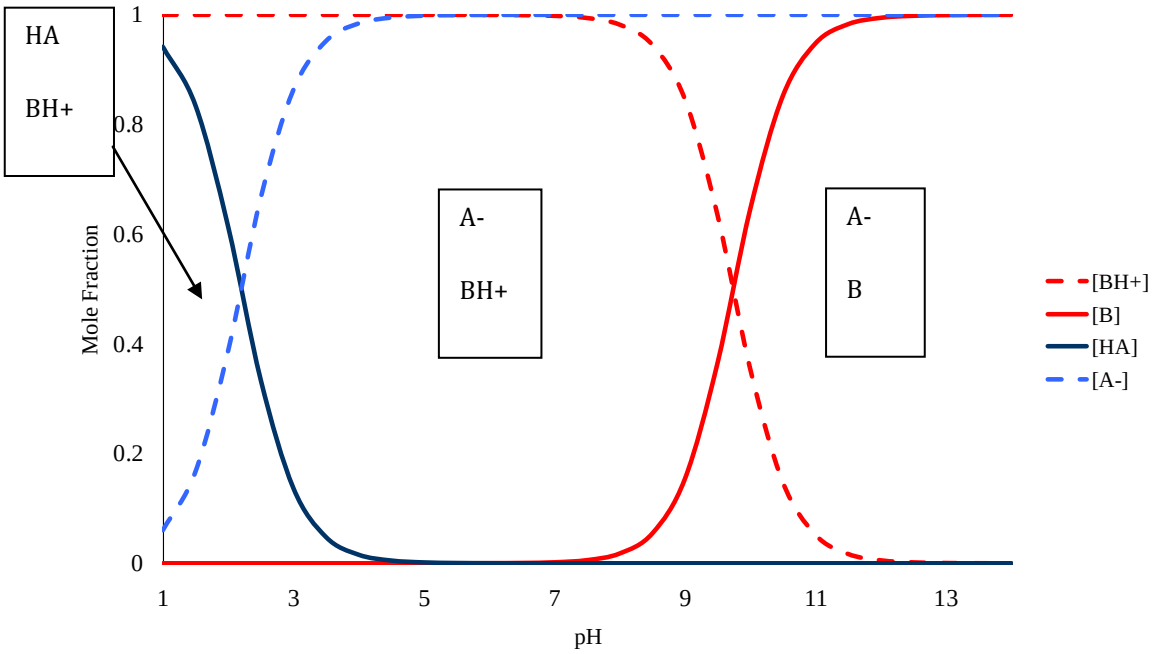

FIGURE 14-DISTRIBUTION DIAGRAM FOR EPHEDRINE AND A GENERIC ACID. THE REGIONS WHERE PARTICULAR IONS ARE PRESENT ARE LABELLED.

Previous research into these systems found most acids fit this basic rule of salt formation with ephedrine, due to the high aqueous pKa value of ephedrine (9.74)[3, 4]. In a previous study by Collier *et al*[4], salts were formed using equimolar amounts of acid and base; however for this project the ratio of acid to base was calculated by an alternative approach.

A ternary screening method was used to try and minimize the number of experiments required to determine whether it would be possible to form a salt between ephedrine and an acid in water. The first step was to measure the solubilities of the acid and ephedrine separately in the solvent. These data were then plotted onto a ternary phase diagram (diagram 1 in Figure 15). The ideal solubility lines for the acid and ephedrine, assuming the system forms a eutectic mixture (not a salt), were then extrapolated. This was in order to determine the eutectic composition at 25 °C (as shown in diagram 2 in Figure 15). The ideal solubility lines run parallel to the side of the triangle due to the assumption that species do not interact in solution. A ternary composition was then chosen just below this ideal eutectic (shown in diagram 3 in Figure 15) and a slurry allowed to form. The slurry was left to stir for 3 days in order to reach equilibrium. The solid was recovered and analysed to determine the species present. Working in this region increases the chance of finding a salt for systems where the solubility of one component is much higher than the other. If the two components of a system have similar solubilities this method will be approximately equivalent to working at an equimolar ratio.

If both components are observed in the solid filtered from the slurry then the acid and ephedrine cannot form a salt in water. If a new product forms, further assessment of the rest of the phase diagram and determination of the region of salt formation is undertaken. A table showing the calculation used for this screening method is shown as Table 1.

TABLE 1- THE EXPERIMENTAL SOLUBILITIES OF SOLIDS A AND B IN SOLVENT S USED TO PLOT THE IDEAL TERNAY PHASE DIAGRAM

	A	B	S
Saturated solution of A	x	0	100-x
Saturated solution of B	0	y	100-y
Eutectic	x	y	100-(x+y)

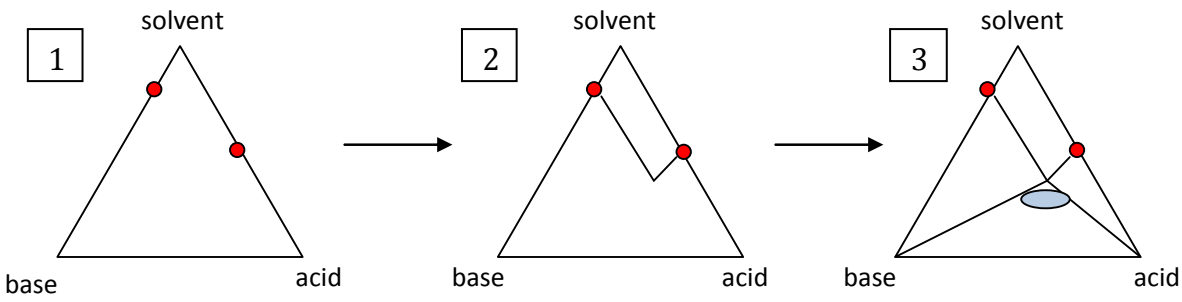

FIGURE 15- THE THREE STAGES OF CONSTRUCTION OF A TERNARY PHASE DIAGRAM FOR A TERNARY SCREENING METHOD

2.2.2 SOLUBILITY

Previously the solubility of a large range of ephedrine salts have been determined by Collier[4, 5]. However, within the same study the solubility of the acids used as counter ions were not investigated. Many different solubility values have been published for some of the acids (adipic, maleic, malonic etc.), while others have virtually none (glycolic, glutaric, pimelic etc.). The acid solubilities were therefore all determined at 25 °C using a classic gravimetric method to ensure consistency.

To determine the solubilities of the acidic components a thermostatted jacketed vessel, as described in Section 2.2.1.1, was used. The sample of acid was added to distilled water and held at 25 °C with stirring overnight. This allowed the slurry to reach equilibrium. The pH of the solution was then measured using a pH meter which had been calibrated using solutions of pH 4 and 7. A sample of the pure solution was removed using a syringe and dispensed into a pre-weighed Petri dish. The dish and solution were then weighed together. The solvent was allowed to evaporate and the sample and dish weighed again. The weight percent of solute was calculated thus,

watch glass – dry sample = solvent evaporated

(solvent evaporated / solution weight) x 100 = weight percent of solvent

100 – weight percent of solvent = weight percent of solute

The recrystallised acids were analysed using DSC and pXRD to ensure they had not changed form e.g. to a different polymorph or hydrate.

The solubility of ephedrine had previously been recorded; however this experiment was also repeated to ensure consistency.

2.2.3 DETERMINATION OF A TERNARY PHASE DIAGRAM

To determine a ternary phase diagram experimentally there are a number of stages for a general compound forming system. These are detailed in steps 1-3 below[6].

1. The solid phases present in the systems should be known, either from previous experimental work, crystal structures on the CSD or by a new solid phase screen. If a new solid phase screen is required, different compositions across a ternary system (Figure 16) should be made and allowed to equilibrate for several days. The solid present should then be analysed.

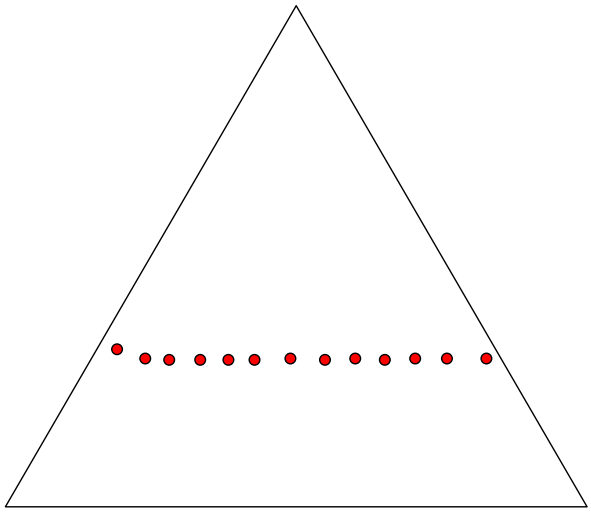

FIGURE 16- SCREENING SPOTS (RED) SELECTED ON A TERNARY PHASE DIAGRAM IN ORDER TO ASSESS THE SOLID PHASES FORMED IN SOLUTION

2. To approximate the phase boundaries, a wider range of compositions should be slurried (than in step 1) and then analysed by the same solid phase screening method.
3. From these solid phase screens the liquidus lines of the phases can be determined using the solubility (using a gravimetric method, as described in Section 2.2.2). The composition of the solid phase, starting composition and mass % solvent in the liquid phase is then known. The lever rule can be used to determine the ternary composition of the liquid phase, provided the

point is within a single solid phase region. Table 2 shows the data required in order for the lever rule to be used and yellow shading shows the unknowns.

TABLE 2- SHOWING THE KNOWN (UNSHADED) AND UNKNOWN (SHADED YELLOW) COMPOSITIONS OF A TERNARY SYSTEM

Starting Composition	x_A^i	x_B^i	x_C^i
Solid Phase	x_A^s	x_B^s	x_C^s
Liquid Phase	$\boldsymbol{x_A^l}$	$\boldsymbol{x_B^l}$	x_C^l

This calculation varies depending upon whether work is undertaken within a one or two component solid phase region (i.e. a salt). The equations for both are given below.

For a single component solid phase

$$\frac{x_C^i}{x_B^i} = \frac{x_C^l}{x_B^l} \qquad \text{EQUATION 2:1}$$

For a two component solid phase

$$x_{AB}^l = x_{AB}^i - (x_{AB}^s \times (x_C^l - x_C^i)) \qquad \text{EQUATION 2:2}$$

Examples of these equations in use can be studied in Section 4.1.5.

2.2.4 DETERMINATION OF A BINARY PHASE DIAGRAM

In order to determine an experimental binary phase diagram for this project DSC was utilised. The technical theory behind DSC is given in Section 2.4.3.2. The use of this technique for the determination of binary phase diagrams is well established[7, 8]. A range of stoichiometric ratios of the acidic and basic components were weighed into DSC pans. Traditionally the DSC would be run with a temperature profile consisting of a heating phase, a cooling phase and another heating phase. The initial heating phase melts the sample. The cooling phase causes recrystallisation, and then the final heating phase should give two endothermic peaks which can be used to plot the phase diagram. The first peak is the eutectic

melt and the second is the liquidus of the salt. Using a heat/cool cycle allows confidence in the homogeneity of the system. If this is not completed, more than the desired two endotherms may be present in the DSC trace.

2.2.5 MATERIALS

The materials used in this investigation were based upon those used in the paper by Collier *et al*[4] and Collier's thesis[5]. The other acids included for investigation in this study that were not used in the Collier et al paper[4] (oxalic, glutaric, pimelic and suberic acids) were initially chosen in order to establish patterns in the solubilities of the dicarboxylic acids. All materials were sourced directly from Sigma-Aldrich and used as received. As solubility of the acidic counter-ions was initially a major concern of this project, only solid acids were selected for investigation and a complete list is given in Table 3.

TABLE 3- LIST OF ACIDS USED

Group	**Acid**
Carboxylic acids	Benzoic
	Salicylic
Dicarboxylic	Adipic
	Fumaric
	Glutaric
	Maleic
	Malonic
	Oxalic
	Pimelic
	Suberic
	Succinic
Hydroxy acids	Citric
	Glycolic
	L-(-)-malic
	L-(+)-tartaric

The basic component in all the salts was (1R, 2S)-(-)-Ephedrine, also purchased from Sigma-Aldrich with the production of appropriate licences. Ephedrine readily

hydrates to the hemihydrate in air. This led to experiments being carried out with an equal mixture of anhydrous and hemihydrate forms (determined by pXRD). Experiments were carried out to check the effect of the water present at a number of points throughout this work and will be discussed as and when appropriate. The most notable points are the effect on binary phase diagram determination (Section 4.3.2) and ternary phase diagram determination (Section 4.5.2).

2.3 SOLID STATE SALT FORMATION

The acids used for the solid state salt formation were the same as those used for the solution crystallisations and solubility studies and given in Table 3.

2.3.1 GRINDING

The initial method used to form salts by grinding was later adapted for certain systems depending upon information gathered. Any adaptations are described in the appropriate chapters as and when deemed necessary. Initially an equimolar amount of acid and base were ground together using a pestle and mortar for 15 minutes with no solvent present.

Salts formation was confirmed using a range of analytical techniques. These were powder X-ray diffraction (pXRD), Infra-red spectroscopy (IR) and Differential Scanning Calorimetry (DSC). Detailed descriptions of these techniques, including experimental set up, analysis and some theory, can be found in Section 2.4 below.

Grinding using a mechanical milling machine was also undertaken, however due to the cohesive nature of the salts, the samples became stuck in the sample holders. This technique was therefore not pursued further and will not be discussed within this work. The samples most likely became stuck due to the amorphisation caused by the grinding[9-13].

2.3.2 CONTACT

On a microscope slide single crystals of two components were contacted and reaction observed using a microscope. Confirmation of salt formation was difficult as the samples were neither single crystals nor powder and pure components

could be observed to have remained. PXRD proved the most effective method, provided accurate sample positioning in the beam was used. Powder contacting was also conducted to assess whether reaction may be observed on a larger scale.

2.4 ANALYTICAL TECHNIQUES

A wide range of analytical techniques were used to determine the total or partial formation of salts and also the purity of components. Some of the techniques can also be used to monitor the progress of a reaction, or investigate some effect on the sample.

2.4.1 FOURIER TRANSFORM INFRA-RED (FTIR)

Infrared is a vibrational spectroscopy technique, as it provides information on the molecular vibrations occurring within a molecule[14].

2.4.1.1 THEORY[14, 15]

The vibrations within molecules are commonly represented using 'ball and spring' models, with atoms as balls and the chemical bonds between them as springs with no mass, as shown for a diatomic model in Figure 17, where m_1 and m_2 are the masses of the atoms.

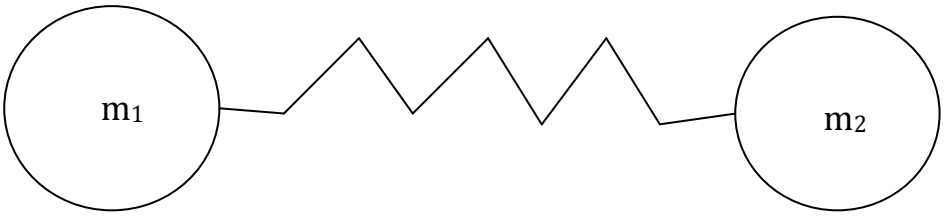

FIGURE 17- THE BALL AND SPRING MODEL FOR A DIATOMIC MOLECULE

Hooke's law, with respect to this diatomic molecule, can be written thus,

$$F = -kx \qquad \text{EQUATION 2:3}$$

where F is the restorative force of the string, k is the force constant of the spring and x is the displacement of the atoms from their equilibrium position. The motion resulting from this equation is a simple harmonic, and hence based on these

assumptions the ball and spring model is a simple harmonic oscillator. The frequency of these vibrations, v_0, can be calculated in terms of classical mechanics to give

$$v_0 = \frac{1}{2\Pi}\sqrt{\frac{k}{m}} \qquad \text{EQUATION 2:4}$$

where m is the reduced mass, given by

$$m = \frac{m_1 m_2}{m_1 + m_2} \qquad \text{EQUATION 2:5}$$

In vibrational spectroscopy the units most commonly used are wavenumbers, $\tilde{\nu}$, which are defined as the number of waves in one centimetre and are given by the relationships,

$$\tilde{\nu} = \frac{1}{\lambda} = \frac{\nu_0}{c} \qquad \text{EQUATION 2:6}$$

where λ is the wavelength and c is the velocity of light. In the equation for frequency, v_0 given above, the only variables are the reduced mass and the force constant. This means prediction can be made of which chemical bonds will have the highest frequency vibrations. Bonds with a large reduced mass will vibrate more slowly than those with a smaller reduced mass. Bonds with a larger force constant (stronger bonds) will have a higher vibrational frequency. Provided v_0 lies in the infrared region of the electromagnetic spectrum, vibrational transitions absorb and generate infrared radiation.

Quantum mechanics defines the quantized vibrational energy levels of a harmonic oscillator, E_{vib}, according to the following,

$$E_{vib} = h\nu_0(n + \frac{1}{2}) = \frac{h}{2\Pi}\sqrt{\frac{k}{m}}(n + \frac{1}{2}) \qquad \text{EQUATION 2:7}$$

where h is Planck's constant and n is the vibrational quantum number with values of 0, 1, 2, 3 etc. Quantization occurs due to boundary conditions defined by the Schrödinger equation, which is not discussed further in this project, however is

covered by all quantum mechanics textbooks[16-18]. The ground state ($n=0$) is called the zero point energy and is defined by,

$$E_{vib,0} = \frac{1}{2} h\nu_0 \qquad \text{EQUATION 2:8}$$

So far the vibrations of molecules in a vibrating atom have been considered as harmonic, which makes the mathematics significantly easier. However, it is really anharmonic vibrations that are taking place. In anharmonic motion the restorative force is no longer proportional to the initial displacement. The energy levels of an anharmonic oscillator are given by the equation,

$$E_{vib} = h\nu_0[(n+\frac{1}{2}) - x_a(n+\frac{1}{2})^2] \qquad \text{EQUATION 2:9}$$

where x_a is the anharmonicity constant. These energy levels converge as they increase; therefore at high excitations the energy levels are closer together.

Polyatomic molecules can be considered as a system of coupled anharmonic oscillators. Assuming there are N atomic nuclei in the molecule there will be $3N$ degrees of freedom of motion for all the atoms. If the pure translations and rotations of the molecule are subtracted $(3N-6)$ vibrational degrees of freedom in a non-linear molecule and $(3N-5)$ vibrational degrees of freedom in a linear molecule are left. Modes of vibration and rotation are not discussed in this project, but there is much literature on the subject[15].

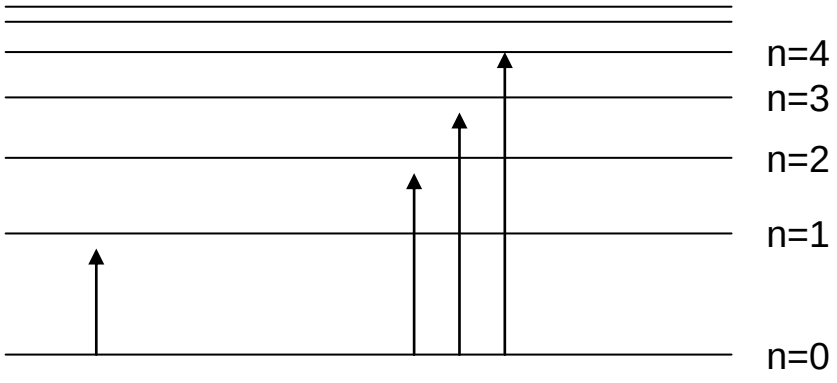

FIGURE 18- THE ENERGY LEVELS OF AN ANHARMONIC OSCILLATOR

Vibrations and rotations require the absorption of energy, inducing transitions between vibrational energy levels (as defined above and shown in Figure 18). If the transition is from $n = 0$ to $n = 1$ it is referred to as a fundamental transition. These fundamental transitions provide the most intense bands in the mid-infrared spectrum (range between 4000-400 cm^{-1}). Due to anharmonicity, transitions from the ground state ($n = 0$) to higher excited states ($n = 2,3,4\ldots$) are also possible and are called overtones. Overtones give weak absorption bands around twice the wavenumber of the corresponding fundamental transition.

In the measurement of an infrared (IR) spectrum a sample is exposed to a range of infrared frequencies, resulting in some being absorbed for molecular rotations and vibrations (as described above). A detector can then indicate which frequencies pass through the compound with little or no loss and which are strongly absorbed. The amount of each frequency passing through the sample is measured as the percentage transmittance. A percentage of 100 meaning none of that frequency is absorbed. In reality a small percentage is usually lost, leaving a maximum possible transmittance of around 95 %. In this work spectra are presented in absorbance to aid clarity in discussions.

2.4.1.2 SOLID STATE FTIR

In this project a Fourier Transform Infrared Spectrometer was used, as opposed to a standard spectrometer. The energy source passes through an interferometer, instead of a monochrometer as used in standard IR spectrometers, and onto the sample. In each scan all source radiation gets to the sample, hence improving the signal to noise ratio of the system. In an interferometer the light passes through a beam splitter, sending the light in two directions, 90° to one another. One of these beams goes to a moving mirror (varying the beams path length), while the other goes to a stationary mirror then back to the beam splitter (maintaining a set path length). As the path lengths of the beams are now different, they recombine to give constructive and destructive interference. This is an interferogram. This recombined beam then passes through the sample, which absorbs all the characteristic wavelengths of its spectrum (as discussed in Section 2.4.1.1), removing them from the interferogram. A laser beam is used to provide a

reference for the instrument operation. A Fourier transformation converts intensity versus time into intensity versus frequency[19-21].

The spectrometer used in this work was a ThermoNicolet Avatar 360 ESP with an Attenuated Total Reflection (ATR) attachment (Smart Golden Gate), integrated with Nicolet's OMNIC software. The ATR attachment allows both solid and liquid samples to be studied. IR radiation is directed onto the sample and passed through it. Initially a background spectrum (no sample) is collected and subtracted from each sample spectrum. A Specac Heated Golden Gate Controller can also be attached to this instrument to assess the effects of melting and recrystallisation events on a sample as temperature is increased and decreased. By using this attachment the effect of temperature on polymorphic changes or salt formation can be assessed. In this thesis samples were analysed between 400 cm^{-1} and 4000 cm^{-1}.

2.4.1.3 SOLUTION FTIR

A Mettler Toledo ReactIR 4000 FTIR probe was used to assess the ionisation of salt systems in the solution phase. The infrared probe was inserted into solutions a number of times as evaporative crystallisation occurred in the system. The data were then collected and analysed using Mettler Toledo iCIR version 4.0.636.0. Samples were analysed from 650 cm^{-1} to 4000 cm^{-1}.

2.4.1.4 IR MICROSCOPY

IR microscopy was undertaken at AstraZeneca's Macclesfield site. The instrument used is a Thermo Continuum FTIR microscope linked to a Thermo Nexus FTIR spectrometer. The spectra are analysed using Nicolet's OMNIC software. The microscope was used in reflectance mode and only provides spectra if the samples are very thin or molten, otherwise spectra obtained are merely noise. Samples were analysed between 600 cm^{-1} and 4000 cm^{-1}.

2.4.1.5 INTERPRETATION

To interpret IR spectra the position of the absorption bands is interrogated. The region 4000-1500 cm^{-1} is known as the functional group region and the region 1500-400 cm^{-1} is known as the fingerprint region. The functional group region

contains peaks characteristic of specific types of bonds, therefore allowing the determination of the presence of certain functional groups. The fingerprint region is usually very complicated, arising from deformations of the molecule. Peaks in this region may be due to molecular symmetry or combination bands (due to multiple bonds deforming simultaneously). Hydrogen bonding effects can also be seen in this region.

In the assessment of salt formation using carboxylic acids, FTIR is a very useful technique. The absorption due to the stretch of the carbonyl bond has a characteristically high intensity in this technique, as is shown in Figure 19 and highlighted in Figure 20. IR can only observe the anti-symmetric stretch, present in both monomeric and dimeric carboxylic acids. Therefore, whether the pure acid forms a dimer in its crystal structure or not, the technique can analyse it[22]. In the acid it displays a peak somewhere between 1675 and 1725 cm^{-1}. For the salt, the peak due to the corresponding carboxylate bond presents at a significantly lower wavenumber, further into the fingerprint region[23].

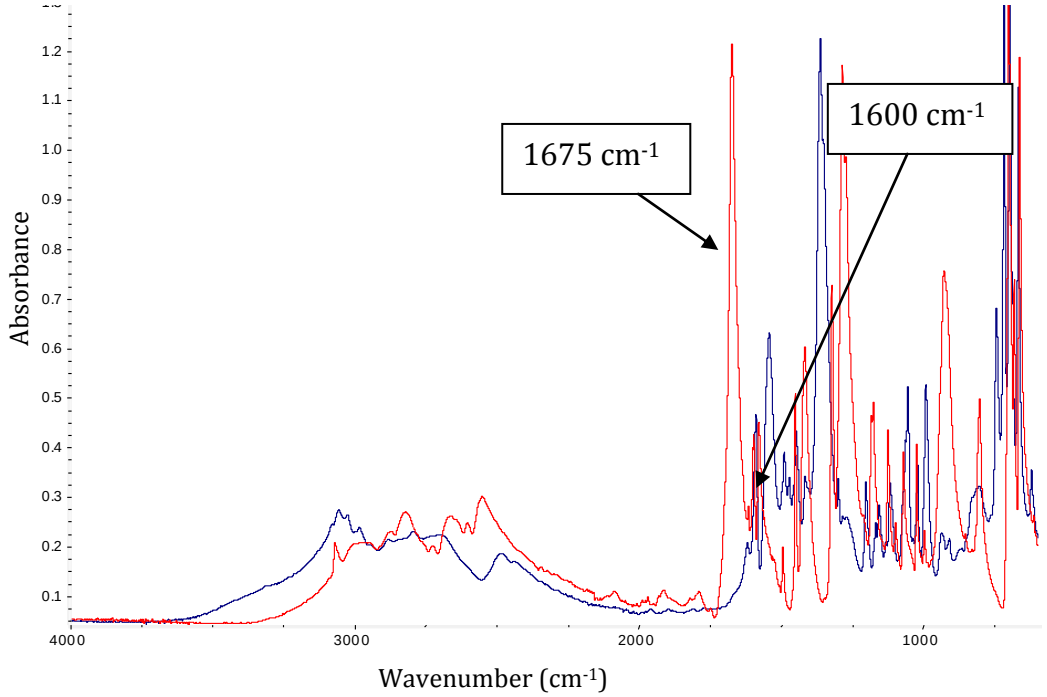

FIGURE 19- FULL SPECTRA OF BENZOIC ACID (RED) AND THE CORRESPONDING EPHEDRINE SALT (BLUE)

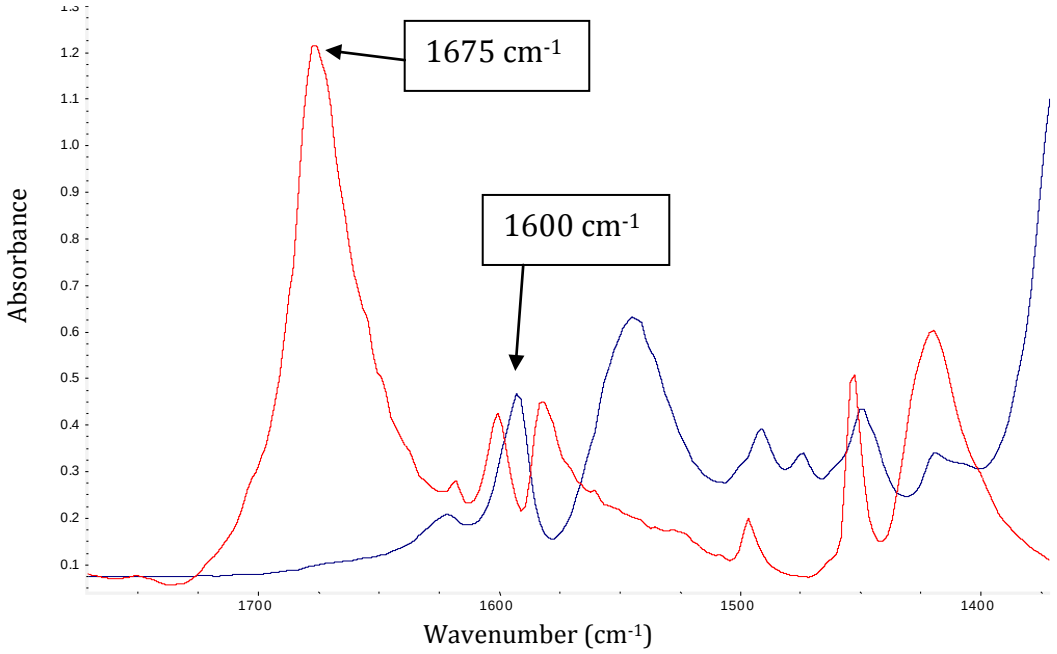

FIGURE 20- CARBONYL REGION OF A MONO CARBOXYLIC ACID (BENZOIC ACID- RED) AND THE CORRESPONDING EPHEDRINE SALT (BLUE)

The spectra in Figure 20 show the peak due to the carbonyl of carboxylic acids clearly shift from an absorption at ~1675 cm^{-1} in its unionised form (red) to a band with a lower value of ~1600 cm^{-1} in an ionised salt (blue). This shift is used extensively in all IR techniques within this thesis to assess whether salt formation has occurred.

2.4.2 X-RAY DIFFRACTION (XRD)

The theory behind X-ray diffraction techniques is vast and well established. Much literature has been published on this topic, so only a brief background will be given here. More information can be found in a range of texts[24-28].

X-rays, discovered in 1895 by W.C. Röntgen, travel in straight lines, like light. Röntgen made the major discovery that the power of objects to absorb these rays was only dependent upon the kind of atoms in the absorbing screen. Hence, thick piles of paper absorb very little, but thin sheets of some metals were very absorbing. Less than 20 years later, in 1912, the first account of X-ray diffraction

was published by Bragg, after it was realised that X-rays were of a shorter length than the interatomic differences in a crystal (usually a few Ångstroms). When this distance is similar, interference of the scattered wavelengths can occur. Interference between wavelengths can cause reinforcement in one direction while in other directions wavelengths can destroy one another. Consequently X-ray diffraction can be used to determine information about atomic positions in crystals[24, 26, 29].

A diffractometer is an instrument for measuring the intensities of diffracted beams individually by counting the number of X-ray photons that arrive at a suitably positioned detector[26]. Within this project this is done for both single crystals and powders.

2.4.2.1 X-RAY GENERATION

If a stream of high energy electrons is allowed to hit a sheet of metal, an electron will be ejected from an inner orbital of the metal atom. To replace this electron, another electron drops down from a higher energy level and X-rays are emitted. X-ray emission also occurs when electrons hit the metal target and is called background radiation, or Bremsstrahlung[29]. Diffraction experiments require a single wavelength of X-ray radiation, usually produced by a graphite monochromator.

2.4.2.2 BRAGG'S LAW[24]

If atoms are taken as points in a lattice plane, a diagram can be drawn in two dimensions (Figure 21) to represent the diffraction of a beam by a single crystal. A beam which is scattered by point A will travel a fixed distance, while a beam scattered by point B will travel an extra distance, $2l$. This is called the path difference and is dependent upon the distance between the lattice planes, d_{hkl}, and the angle of incidence of the X-ray beam, θ. This path difference must be a whole number of wavelengths for constructive interference, and hence a maxima in diffracted X-rays, to occur. The Bragg equation can be used when the number of wavelengths path difference, n, is a whole number and relates the X-ray wavelength, λ, to the lattice spacing, d, thus

$$\text{PATH DIFFERENCE} = 2l = 2.d\sin\theta = n\lambda \qquad \text{EQUATION 2:10}$$

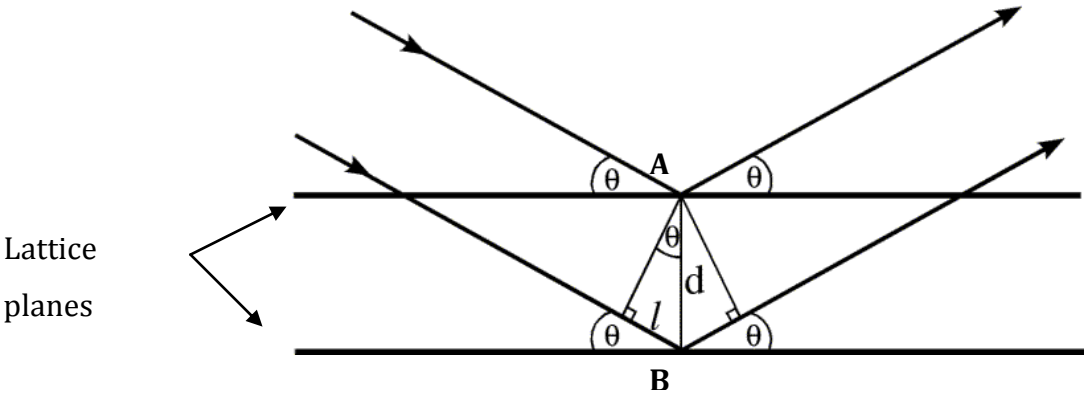

FIGURE 21- DIFFRACTION OF X-RAYS BY A SET OF LATTICE PLANES[26]

2.4.2.3 SINGLE CRYSTAL

Single crystal X-ray diffraction (sXRD) is used to determine the absolute structure of crystals.

2.4.2.3.1 THEORY

SXRD occurs by the process shown in Section 2.4.2.1, only in three dimensions. In a real crystal the lattice points are the regular array of atoms. From the diffraction pattern the position of these atoms can be determined, due to the information contained on atomic distances, atom types and electron densities.

2.4.2.3.2 APPARATUS

To perform XRD suitable crystals must be grown and separated. They must be single and have no smaller crystalline particles attached to the surface. In this project the structures were determined using the Oxford XCalibur 2 diffractometer and the Bruker SMART CCD diffractometer. The selected crystal is mounted on the goniometer head using inert oil and a glass fibre. Once on the diffractometer a cryostream 'freezes' the crystal in position. As there are many different planes in a crystal there are many different angles a reflection can occur at. Once unit cell dimensions are determined by the computer, angular settings can be adjusted

(both the crystal and the detector can move) to observe any peak in the diffraction pattern[15].

2.4.2.4 POWDERS

Powder X-ray diffraction (pXRD) is used to identify the crystal structure of a powdered sample. The pXRD pattern is unique for each compound, and by cross referencing with simulated powder patterns from the CSD (see Section 2.4.7.1) the powder can be 'fingerprinted'. For the purposes of this project this means it can be determined whether a salt has completely formed, or if some pure component is still present. Powder patterns simulated from single crystal data are identical to experimentally determined powder patterns, except for their much increased intensity. This decrease in intensity in a powder pattern is due to the orientation of the crystals. Crystals may also have what is referred to as 'preferred orientation'. For example, for plate-like crystals, preferred orientation means peaks due to those planes parallel to the large faces will have a much greater intensity than those which are perpendicular to these faces. This can lead to some peaks being abnormally large in powder patterns. Therefore peak intensities are, including in this work, often ignored and only the peak positions assessed. More peaks can be observed in simulated powder patterns than experimentally determined powder patterns as more reflections are available. Ideally samples are ground before analysis by pXRD, however in this work this was not always possible. Reasons for this will be discussed as and when they arise.

2.4.2.4.1 THEORY

For pXRD the theory is similar to that of sXRD, but the diffraction is now occurring from thousands of tiny crystals. These will be randomly oriented in many directions, unlike one relatively large crystal[29]. The X-rays are diffracted into a cone shape for each lattice spacing which, on a two dimensional detector, shows as a ring (Figure 22).

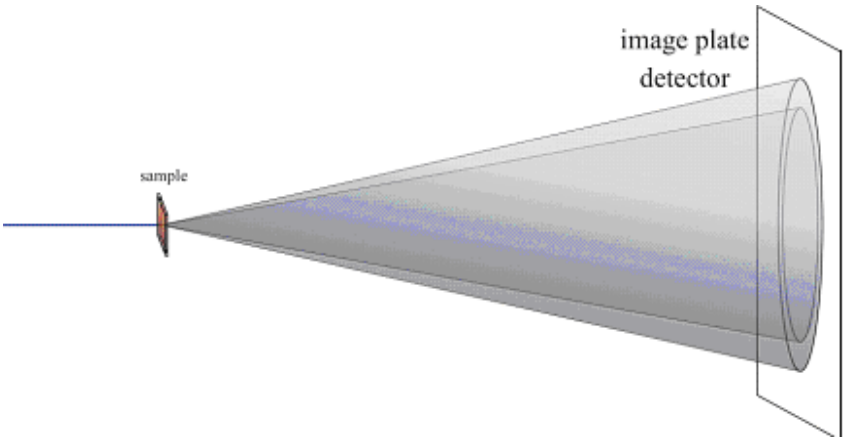

FIGURE 22- A POWDER DIFFRACTION EXPERIMENT IN TWO DIMENSIONS

The diffraction angle, 2θ, for each diffraction cone is calculated then plotted against intensity in a two dimensional plot (Figure 23).

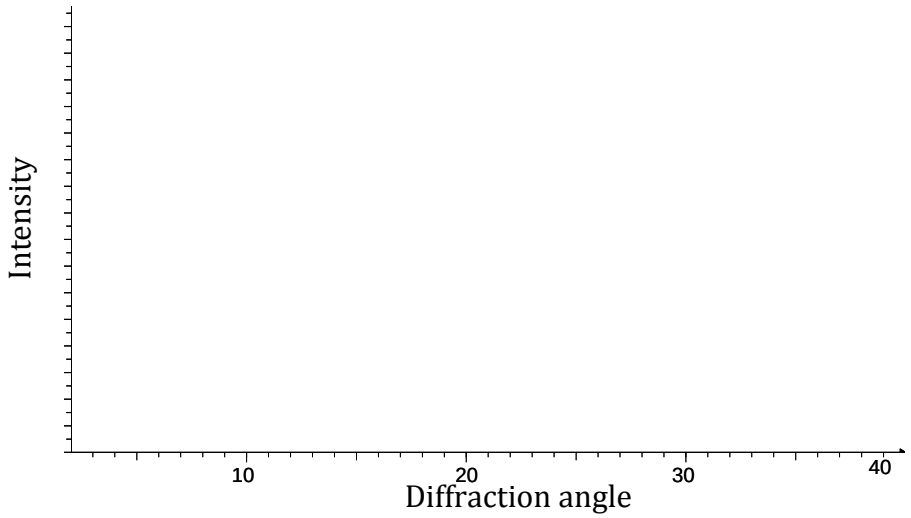

FIGURE 23- XRPD PATTERN IN TWO DIMENSIONS

2.4.2.4.2 APPARATUS

To record powder patterns the Rigaku miniflex benchtop XRD system was used. Samples were ground using a pestle and mortar whenever possible and placed on a sample holder. The X-ray pattern was then recorded between 5° and 40° 2θ using a step size of 0.03°. A scan speed of 1.5° per minute was routinely used. On occasion different parameters were used. These are discussed as and when necessary.

2.4.3 DIFFERENTIAL SCANNING CALORIMETRY (DSC)

Differential scanning calorimetry (DSC) is a technique that measures the change in the energy of materials. It is routinely used to determine the purity of samples, their melting temperatures and their enthalpies of fusion[15]. DSC can be used for a wide range of purposes which will not be covered in this project, however literature is available[30, 31].

2.4.3.1 THEORY

This technique is used to measure the heat transferred to or from a sample during a chemical reaction or phase change at a constant temperature[15]. The difference in the amount of heat required to heat a sample and a reference to a constant temperature is measured.

2.4.3.2 APPARATUS AND SOFTWARE

The DSC system used for this project was the Mettler DSC 30.

For this system samples must be placed in 40µl, shallow aluminium pans, compressed with sealed, pierced lids to ensure good contact between the sample, pan and heating plate. The sample pan is placed in the furnace along with an empty reference pan. Both pans are heated symmetrically at a predetermined heating rate to a preset temperature, all controlled by an attached computer (Figure 24). The system can similarly cool the sample due to the attachment of a liquid nitrogen source. Cycles of heating and cooling can be programmed to determine a complete thermal data set for a sample.

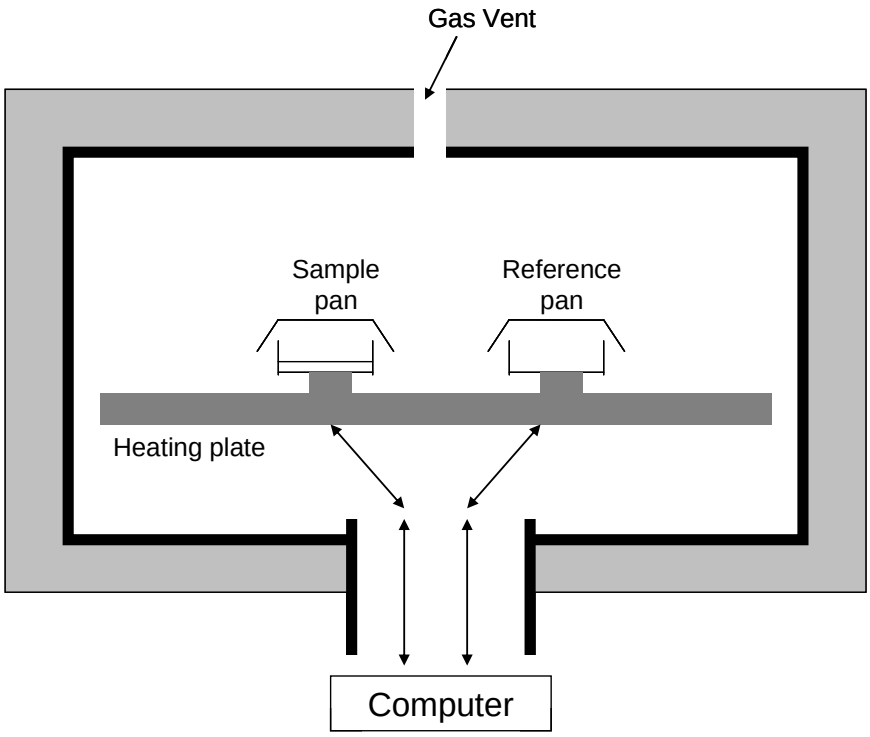

FIGURE 24-SCHEMATIC OF DSC

The results obtained from DSC analysis show the differential rate of heating plotted against temperature. From the peaks and troughs in the plot it can be determined whether heat is being absorbed by the system (an endothermic transition such as melting) or is being evolved by the system (an exothermic transition such as crystallisation). The melting of a sample is an endothermic transition, and by using the onset of this peak in DSC, temperature of melting, T_m, can be determined. Integration of this peak, followed by multiplication by the samples molecular mass, gives the enthalpy of fusion, ΔH_f. The enthalpy of fusion is defined as the amount of energy required to melt the sample, as it is the difference between the enthalpy of the solid and liquid states. If a sample is polymorphic, or impure, extra peaks may be present. The shape of the peak can be used to indicate the crystallinity of a sample, as highly stable crystalline materials give sharp peaks and less stable crystalline forms (or amorphous samples) give broad peaks[32].

A range of different heating and cooling rates were used throughout this project, depending on the data required. For the determination of enthalpies of fusion and melting temperatures a heating rate of 5 °C per minute was used to ensure accurate data was gained. For quick identification of solid phases in slurries a rate of 10 °C per minute was used. It quickly became apparent that ephedrine and the corresponding salts do not recrystallise in the small DSC pans. Therefore, a cooling cycle was deemed unnecessary.

DSC has also been used in the calculation of binary phase diagrams by determining the melting points of binary mixtures with differing stoichiometries. Two examples of this were published by Guarrera *et al*, hydroquinone with bis (N, N-diethyl) terephthalamide and bis (N, N-dimethyl) terephthalamide[8]. The method used is discussed in more detail in Section 2.2.4.

2.4.4 OPTICAL MICROSCOPY

An optical microscope was used to take images of the crystals grown for this project. Some experiments were also carried out on the microscope system enabling reactions to be visually monitored.

2.4.4.1 APPARATUS

The microscope used was the Zeiss Axioplan 2. A Linkam hot stage was used on the microscope to both heat and cool samples. To seal the system in the case of hygroscopic systems, a small plastic ring was glued to a microscope slide and another slide could then be placed on top, sealing the system.

2.4.5 GRAVIMETRIC VAPOUR SORPTION (GVS)

Using this technique the vapour sorption properties of solids can be assessed using precise environmental control. As the temperature and percentage relative humidity (% RH) are varied, the difference in weight between the sample pan (S) and empty reference pan (R) is measured by the balance. From this moisture sorption/desorption of the sample can be monitored. This technique allows the assessment of how hygroscopic a sample is i.e. its susceptibility to water uptake or loss. In the pharmaceutical industry hygroscopicity is an important parameter in

the selection of a salt form for a new drug. It is represented by the % mass increase at 80% RH, as is shown in Table 4[1]. The system used was manufactured by Surface Measurement Systems and experiments were controlled using *DVSWin software v.2.17*.

TABLE 4- DEFINITIONS OF HYGROSCOPICITY[1]

% mass increase at 80 %RH	**Definition**
Less than 0.2%	Non-hygroscopic
0.2-2.0%	Slightly hygroscopic
2.0-15.0%	Hygroscopic
Greater than 15%	Deliquescent

2.4.6 SOFTWARE AND DATABASES

2.4.6.1 CAMBRIDGE STRUCTURAL DATABASE (VERSION 5.31-NOVEMBER 2009)

The Cambridge Crystallographic Database Centre (CCDC) contains the structures of thousands of organic and organometallic compounds[33]. The CSD (Cambridge Structural Database) was searched using ConQuest (version 1.12), a search engine developed by the CCDC. Searches can be undertaken by chemical name, formula, 2D structure, journal citation or reference number. From these data entries previously published work can be assessed, the crystal structures can be studied and the 2-dimensional XRD patterns simulated (both when transferred to Mercury (see Section 2.4.6.2 below)). The structures on the database can also be searched and studied to assess any similarities and differences between structures and look for trends and patterns.

2.4.6.2 MERCURY (VERSION 2.3)

As is described in Section 2.4.6.1, Mercury is used for the 3D visualisation of crystal structures stored on the CSD[34]. XRD patterns can be simulated from the structures and viewed in 2-dimensions. Structures can be viewed in 3D then overlaid, rotated, highlighted or molecules deleted in order to view another aspect of the structure more clearly. This program can also be used for molecular modelling; however this was not employed in this work.

2.4.6.3 STATISTICA (VERSION 6.1)

Statistica is a mathematical program produced by StatSoft Ltd. and was used in the plotting of ternary phase diagrams for this project. Again this program contains much of functionality not used in this thesis.

2.5 SUMMARY

This section summarises the experimental techniques, apparatus and methodologies used in the course of this work. The various methods (both solid and solution state) employed in the formation of salts are discussed, as are the analytical techniques used in their analysis and identification.

2.6 REFERENCES

1. Stahl, H. P. & Wermuth, C. G. Handbook of Pharmaceutical Salts-Properties, Selection, and Use (Wiley-VCH, 2002).
2. Stevens, J. S., Byard, S. J., Muryn, C. A. & Schroeder, S. L. M. Identification of Protonation State by XPS, Solid-State NMR, and DFT: Characterization of the Nature of a New Theophylline Complex by Experimental and Computational Methods. Journal of Physical Chemistry B published ASAP (2010).
3. Florey, K. Analytical Profiles of a Drug Substance (Academic Press, Inc., London, 1986).
4. Collier, E. A., Davey, R. J., Black, S. N. & Roberts, R. J. 17 Salts of Ephedrine: Crystal Structures and Packing Analysis. Acta Crystallographica, Section B: Structural Science B62, 498-505 (2006).
5. Collier, E. A. in Department of Chemical Engineering 179 (The Univeristy of Manchester Institute of Science and Technology, Manchester, 2004).
6. Chadwick, K. in School of Chemical Engineering and Analytical Science 260 (The University of Manchester, Manchester, 2008).
7. Davey, R. (ed. Hilton, A.) Fax concerning work on Melt Equilibria-DSC Scans (Blackley, Manchester, 1994).
8. Guarrera, D., Taylor, L. D. & Warner, J. C. Molecular Self Assembly in the Solid State- The Combined Use of Solid-State NMR and Differential Scanning

Calorimetry for the Determination of Phase Constitution. Chemistry of Materials 6, 1293-1296 (1994).

9. Bahl, D. & Bogner, R. H. Amorphization of Indomethacin by Co-Grinding with Neusilin US2: Amorphization Kinetics, Physical Stability and Mechanism. Pharmaceutical Research 23, 2317-2325 (2006).
10. Bruneel, E., Verbist, K., Fiermans, L. & Hoste, S. Amorphization During Mechanical Grinding of Bi-Pb-Sr-Ca-Cu-O Ceramic Superconductors. Applied Superconductivity 4, 357-364 (1996).
11. Ikeya, T. & Senna, M. Amorphizationand Phase Transformation of Niobium Pentoxide by Fine Grinding. Journal of Material Science 22, 2497-2502 (1987).
12. Willart, J. F. & Deshamps, M. Solid State Amorphization of Pharmaceuticals. Molecular Pharmaceutics 5, 905-920 (2008).
13. Vucelic, D., Simic, D., Kovacevic, O., Dojcinovic, M. & Mitrovic, M. The Effects of Grinding on the Physiochemical Characteristics of White Sepiolite from Golesh. Journal of Serbian Chemical Society 67, 197-211 (2002).
14. Wartewig, S. IR and Raman Spectroscopy: Fundamental Processing (Wiley-VCH GmbH & Co. KGaA, Weinheim, 2003).
15. Atkins, P. W. Physical Chemistry (Oxford University Press, 1994).
16. Sakurai, J. J. in Modern Quantum Mechanics (Addison-Wesley, Reading, Wokingham, 1994).
17. Shankar, R. in Principles of Quantum Mechanics (Plenum Press, New York, London, 1994).
18. Zettili, N. in Quantum Mechanics: Concepts and Applications (Wiley, Chichester, 2001).
19. Brisdon, A. K. Inorganic Spectroscopy Methods (Oxford Chemistry Press, Oxford, 1998).
20. Stuart, B. Modern Infrared Spectroscopy (Wiley, New York, 1996).
21. Williams, D. H. & Fleming, I. Spectroscopic Methods in Organic Chemistry (McGraw and Hill Inc., 1989).
22. Vanderhoff, P. A., Lanancette, R. A. & Thompson, H. W. An Effecient Screen for Determining Solid-State Hydrogen-Bonding Patterns in Carboxylic Acids. Journal of Organic Chemistry 55, 1696 (1990).

23. Bellamy, L. J. in The Infrared Spectra of Complex Molecules (Chapman and Hall, London and New York, 1980).
24. Bragg, L. The Development of X-ray Analysis (G. Bell and Sons Ltd., London, 1975).
25. Cullity, B. D. Elements of X-Ray Diffraction (Addison-Wesley, Reading (Mass.), London, 1978).
26. Dunitz, J. D. X-Ray Analysis and the Structure of Organic Molecules (Verlag Helvetica Chimica Acta, Basel, 1995).
27. Warren, B. E. X-Ray Diffraction (Dover, New York, 1990).
28. Nuffield, E. W. X-Ray Diffraction Methods (Wiley, New York, London, 1966).
29. Weller, M. Inorganic Materials Chemistry (Oxford University Press, Oxford, 1994).
30. Hohne, G. W. H., Hemminger, W. F. & Flammersheim, H.-J. Differential Scanning Calorimetry (Springer, Berlin, 2003).
31. Brown, M. E. & Gallagher, P. K. in Handbook of Thermal Analysis and Calorimetry (Elsevier Science, Amsterdam, 2008).
32. Brittain, H. G. Physical Characterization of Pharmaceutical Salts (ed. Brittain, H. G.) (Marcel Dekker Inc., 1995).
33. Allen, F. H. & Taylor, R. Librarians, Crystal Structures and Drug Design. Chemical Communications, 5135-5140 (2005).
34. Allen, F. H. & Taylor, R. Research Applications of the Cambridge Structural Database. Chemical Society Reviews 33, 463-475 (2004).
35. www.accelrys.com/products/materials-studio/. (Accessed on 09/11/2010).

3 SOLID STATE METHODS IN THE FORMATION OF EPHEDRINE SALTS

3.1 INTRODUCTION

Papers have previously been published documenting how multi-component compounds can be formed by merely grinding the components together. As mentioned in the literature review, greater focus has previously been placed upon cocrystals than salts[1-6]. In fact there is a lack of literature published on salts formed by grinding, with a few published exceptions[7, 8].

Chadwick *et al*[1] published a cocrystal paper offering an explanation of the underlying theory governing why formation may occur. The conclusions drawn suggest that an underlying metastable eutectic phase, with a melting point well below that of any of the known solid phases (and the ambient temperature), leads to the formation of a liquid phase. From this liquid phase the stable cocrystal could be observed to nucleate. This publication also demonstrated the contact of two pure components (as both powders and single crystals), removing the factors of heat and pressure associated with grinding.

Rastogi *et al*[5, 9] also published papers discussing the formation of cocrystals by diffusion. If this mechanism occurs, product formation should be observed without grinding. Grinding may result in more complete product formation due to increased surface area available for reaction.

Nguyen *et al*[6] concluded that solid-solid reactions can occur via an amorphous phase, from which the product crystallises. This means over grinding would cause the sample to become more amorphous and not actually speed up formation of the crystalline product. Samples that are already crystalline immediately after the initial grind, or those that remain amorphous, do not form via this method.

Over the next three chapters attempts are made to determine whether salt formation by grinding is governed by one of the phenomena discussed above, as cocrystals are, or controlled by other physical effects.

3.2 GRINDING

3.2.1 METHOD

Equimolar amounts of the acid and base were ground together in a pestle and mortar for five minutes. The samples were analysed using pXRD, DSC and FTIR.

In initial work studies were completed using identical ratios, but varied grinding times. Grinding was carried out for both 5 and 30 minutes in a pestle and mortar using ephedrine and benzoic acid. The products formed were analysed using pXRD and FTIR (Figure 25 and Figure 26 respectively). It was concluded that a grind time of thirty minutes was needed to ensure the pure components had sufficiently reacted.

In Figure 25 it is apparent that peaks due to the pure components are still present in both samples. These peaks are much more intense in the sample ground for the shorter time. New peaks (suggesting a new product) are more clearly apparent in the sample that had undergone a longer grind time. A negative implication of a longer grind time is the increased amorphisation of the sample, demonstrated by the increased broadening of the peaks.

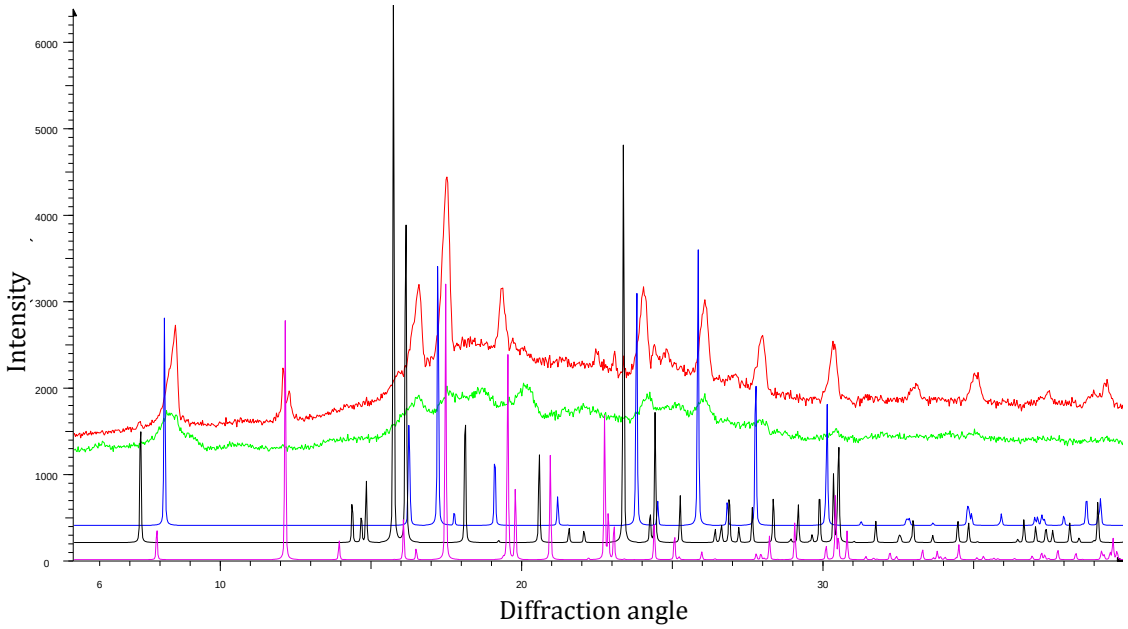

FIGURE 25- COMPARISON OF THE TIME A SAMPLE IS GROUND USING PXRD. ANHYDROUS EPHEDRINE (PINK), EPHEDRINE HEMIHYDRATE (BLACK), BENZOIC ACID (BLUE), SAMPLE OF EPHEDRINE AND BENZOIC ACID GROUND FOR 5 MINUTES (RED) AND SAMPLE OF EPHEDRINE AND BENZOIC ACID GROUND FOR 30 MINUTES (GREEN)

The improvement in product formation after a longer grind time was confirmed using FTIR. From the spectra shown in Figure 26 the carbonyl can be seen to have only partially shifted from the unionised position (1681 cm^{-1}) to the ionised position (1600 cm^{-1}) after 5 minutes (red). The shift is complete after 30 minutes grinding (green).

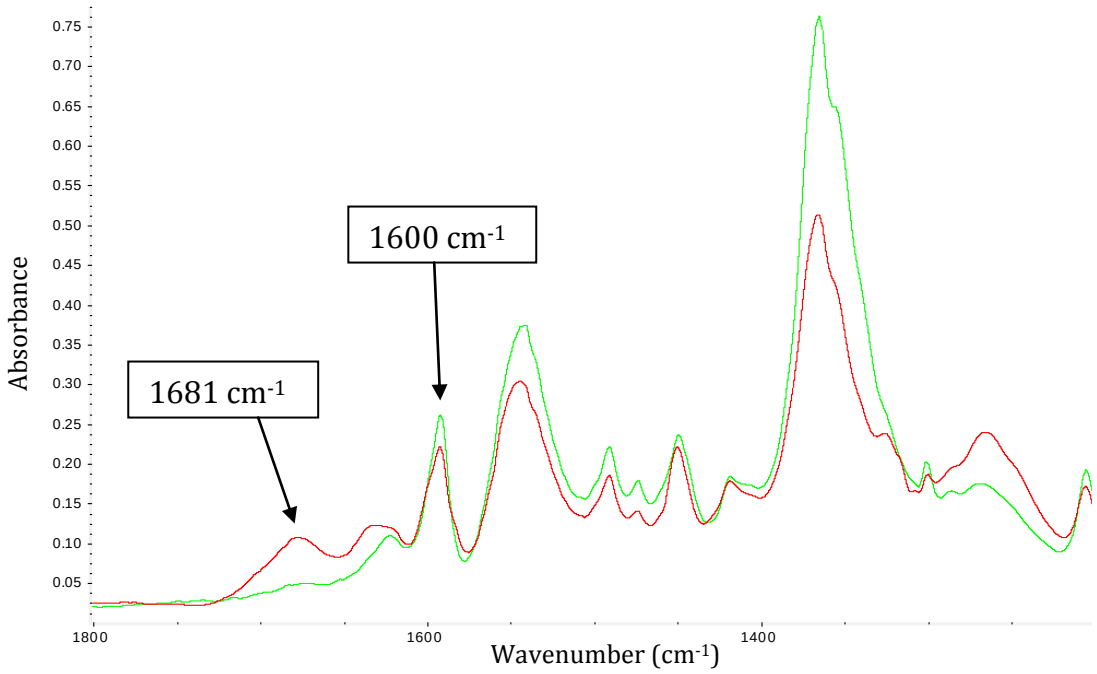

FIGURE 26- COMPARISON OF SAMPLES GROUND FOR DIFFERENT TIMES ANALYSED USING FTIR. SAMPLE OF EPHEDRINE AND BENZOIC ACID GROUND FOR 5 MINUTES (RED) AND SAMPLE OF EPHEDRINE AND BENZOIC ACID GROUND FOR 30 MINUTES (GREEN).

The range of acids used in this study was chosen for a number of reasons. Previously work on salt formation using ephedrine has been published by Collier *et al*[10] from the more comprehensive 2005 thesis[11]. Therefore, it was decided that the acids used in this previous publication would provide a starting point, as many crystal structures had already been determined. The previous determination of a crystal structure makes fingerprinting using pXRD much easier. Some acids were removed from the list as they were liquids. It was felt this defeated the main objectives of the study as one component would be dissolving in the other. Other acids were removed due to their high toxicity. More dicarboxylic acids were added with the initial aim of comparing the properties of salts of these related acids. The

physical properties of the acids used as salt co-formers with ephedrine are given in Table 5.

The chemicals used were sourced directly from Sigma-Aldrich and were used as provided.

TABLE 5- PHYSICAL DATA FOR ACIDS USED IN GRINDING EXPERIMENTS. MELTING POINTS, ENTHALPIES AND SOLUBILITY EXPERIMENTALLY DETERMINED

Acid	**Melting Point/ °C**	**Enthalpy of fusion/ kJmol^{-1}**	**Solubility 25 °C/ weight %**	**Chemical Formula**	**Class of Acid**	**pKa**
Adipic acid	151	40.27	2.35	$(CH_2)_4(CO_2H)_2$	Dicarboxylic	4.42, 5.41[12]
Benzoic acid	122	16.69	0.27	$C_6H_5CO_2H$	Carboxylic	4.2[13]
Fumaric acid	298	46.39[14]	0.74	$CO_2HCH=CHCO_2H$	Dicarboxylic	3.02, 4.38[12]
Glutaric acid	97	26.93	59.89	$(CH_2)_3(CO_2H)_2$	Dicarboxylic	4.34, 5.42[12]
Glycolic acid	78	27.82	81.24	CH_2OHCO_2H	Hydroxy	3.82[13]
DL-Malic Acid	130	63.16[14]	80.17	$CH_2CHOH(CO_2H)_2$	Hydroxy	3.4, 5.13[13]
Maleic acid	141	45.10[14]	44.68	$CO_2HCH=CHCO_2H$	Dicarboxylic	1.93, 6.58[13]
Malonic acid	135	24.11	60.96	$CH_2(CO_2H)_2$	Dicarboxylic	2.83, 5.69[12]
Oxalic acid	101	46.80[14]	14.20	$(CO_2H)_2$	Dicarboxylic	1.2, 4.2[13]
Pimelic acid	104	31.78	4.65	$(CH_2)_5(CO_2H)_2$	Dicarboxylic	4.48, 5.42[12]
Suberic acid	141	41.78	Barely soluble	$(CH_2)_6(CO_2H)_2$	Dicarboxylic	4.52, 5.40[12]
Succinic acid	188	36.02	7.71	$(CH_2)_2(CO_2H)_2$	Dicarboxylic	4.19, 5.48[12]

Tartaric acid	171	?	62.72	$C_2(OH)_2(CO_2H)_2$	Hydroxy	2.89, 4.40[13]

*Referenced enthalpies of fusion used where experimental data was not accurate enough due to sampling issues or instrument error.

3.2.2 GRINDING RESULTS

The results of the grinding experiments are shown below in Table 6. For those samples without a previously determined crystal structure there is no fingerprint available for comparison to identify the suspected salt. This scenario accounts for seven of the 13 acid systems. To determine salt formation the production of a new pXRD pattern (unlike any of the components), a shift in the carbonyl peak (from nearly 1700 cm^{-1} to around 1600 cm^{-1}) in the FTIR spectrum and a new melting temperature in the DSC trace are relied upon. This combination is at least partially apparent for six of the seven.

Of the three anhydrous salts previously known (with full crystal structures published) all show at least partial salt formation. The salt formation was usually determined to be partial due a number of endotherms present in the DSC traces and remaining pXRD peaks common to the pure components. Only the glycolate salt was deemed to be pure by all three analytical techniques.

From CSD searches the other salts in the table had only been previously formed as either hydrates, amorphous salts or disordered crystals. Therefore full structures of anhydrous salts were not available on the CSD. These were treated in the same way as those with no previous salt formation attempted. The results from this group were mixed, with two suspected amorphous salts (benzoic and malonic), a non-reaction (maleic) and some uncertainty in the other results.

One example is given in detail below, ephedrine and glycolic acid. Displayed are the pXRD pattern (Figure 27), FTIR spectrum (Figure 28) and the DSC trace (Figure 29) of the ground sample. From the pXRD (Figure 27) it can be clearly observed that the ground sample (red) matches the simulated salt spectrum (blue) rather than either of the pure components. The FTIR spectrum (Figure 28) of the ground sample (red) shows a clear shift of the carbonyl from that of the pure acid

(blue). The DSC (Figure 29) shows a single sharp peak confirming the purity of the ground sample.

As mentioned in Sections 1.1.2.1 and 2.2.5 ephedrine readily hydrates to ephedrine hemihydrate. The samples used were roughly an equimolar mix of the hydrated and anhydrous forms (determined by pXRD). This may have had an effect on the grinding experiments with a quarter of a mole of water present for every mole of ephedrine. With the determination of binary phase diagrams this will be investigated further. In the grinding experiments performed here the presence of water may have affected the results as it may have acted like a solvent drop in liquid assisted grinding experiments. This is a well published technique for facilitating solid state cocrystal formation[8, 15, 16]. This will not be further considered until individual case studies are investigated in further chapters.

All other patterns, spectra and traces are provided in the appendix with the exceptions of pimelic acid and benzoic acid which are covered in Chapters 4 and 5 respectively.

TABLE 6- TABLE SHOWING WHETHER SALTS HAVE FORMED BY SOLVENT FREE GRINDING USING PXRD, FTIR AND DSC

Acid	**Salt Previously Known**	**Salt formed**	**pXRD**	**FTIR**	**DSC**
Adipic acid	Yes	Yes (partially)	Crystalline, pXRD matches simulated XRD for ephedrine adipate. Some other peaks due to pure components.	Mono-salt formed. COOH band to two COO^- and a remaining COOH peak. Characteristic of monoprotonated dicarboxylic acid.	Peak at 37 °C due to ephedrine. Two peaks at 89 °C and 103 °C indicate a phase change and a melt. Crystalline.
Benzoic acid	Yes (amorphous)	Maybe*	Mostly amorphous.	Mono-salt formed.	Two small broad peaks at 65 °C

			Peaks remaining from pure components.	COOH band to COO^-.	and 91 °C = some amorphous behaviour and possible phase change of new product.
Fumaric acid	No	Yes (partially)	Crystalline, unique peaks present. Some remaining from pure components.	Mono-salt formed. COOH band to two COO^- and a remaining COOH peak. Characteristic of monoprotonated dicarboxylic acid.	Numerous sharp peaks. 1st @ 28 °C due to remaining ephedrine, 2nd @ 67 °C and 3rd @ 113 °C, new compound and maybe a phase change. Broad peak at 210 °C due to decomposition.
Glutaric acid	No	Maybe* (partially)	Crystalline, unique peaks present. Some remaining from pure components.	Mono-salt formed. COOH band to two COO^- and a remaining COOH peak. Characteristic of monoprotonated dicarboxylic acid.	Two sharp peaks @ 36 °C (ephedrine remaining) and @ 74 °C (new compound). Broad peak at 171 °C due to decomposition.
Glycolic acid	Yes	Yes	Crystalline, pXRD matches simulated XRD for ephedrine glycolate.	Mono-salt formed. COOH bands to COO^-.	Single sharp peak at 102 °C = crystalline phase, stable.
Maleic acid	Yes (monohydrate)	No	Crystalline. No new, unique peaks.	COOH and NH still present.	Peak at 30 °C due to ephedrine. Other peaks not well defined.

Malic Acid	Yes	Yes, some ephedrine remaining	Crystalline, pXRD matches simulated XRD for ephedrine malate.	Mono-salt formed. COOH band to two COO^- and a remaining COOH peak. Characteristic of monoprotonated dicarboxylic acid.	2 sharp peaks = crystalline. 1st @ 30 °C due to ephedrine, 2nd @ 115 °C = new phase. Broad peak starting @ 140 °C = decomposition.
Malonic acid	Yes (hemimalonate)	Yes (amorphous)	No peaks = amorphous.	Mono-salt formed. COOH band to two COO^- and a remaining COOH peak. Characteristic of monoprotonated dicarboxylic acid.	Single broad peak @ 159 °C = amorphous phase.
Oxalic acid	No	No	Crystalline. No new, unique peaks.	COOH still present.	Sharp peak @ 176 °C. 2 broad peaks @ 228 °C and 275 °C (decomposition).
Pimelic acid	No	Maybe*	Crystalline, unique peaks present.	Mono-salt formed. COOH band to two COO^- and a remaining COOH peak. Characteristic of monoprotonated dicarboxylic acid.	Single sharp peak at 132 °C = crystalline phase, stable at a higher temperature than any component.
Suberic acid	No	Maybe* (partially)	Crystalline, possibly some unique peaks present. Many remaining	Mono-salt formed. COOH band to two COO^- and a remaining COOH peak. Characteristic of	Multiple peaks. 1st @ 37 °C due to ephedrine remaining. Other peaks are small, broad and therefore not

			from pure components.	monoprotonated dicarboxylic acid.	assignable. Possible new phases.
Succinic acid	Yes (not on CCD as disordered structure)	Maybe* (partially)	Crystalline. No new, unique peaks.	Possible mono-salt formed. COOH band may have shifted as COO^- formed.	2 sharp peaks @ 35 °C and @ 110 °C due to ephedrine and potential new phase. Decomposition peak @ 222 °C.
Tartaric acid	Yes (monohydrate and hemitartrate trihydrate)	No	Crystalline. No new, unique peaks.	COOH band gone, COO^- not present either. Spectrum dominated by ephedrine.	Single, sharp peak @ 37 °C due to ephedrine.

*salt formation appears likely, however no known single crystal structure to use as a fingerprint.

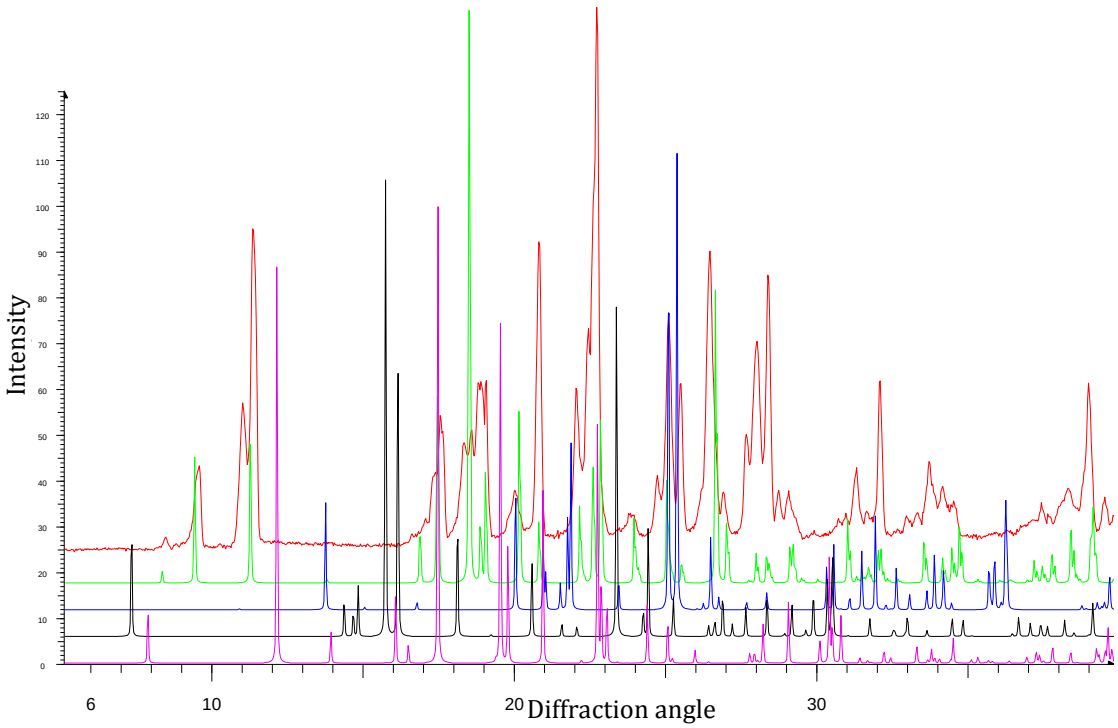

FIGURE 27- PXRD PATTERNS OF ANHYDROUS EPHEDRINE (PINK), EPHEDRINE HEMIHYDRATE (BLACK), GLYCOLIC ACID (BLUE), SIMULATED EPHEDRINE GLYCOLATE SALT (GREEN) AND GROUND EPHEDRINE AND GLYCOLIC ACID SAMPLE (RED)

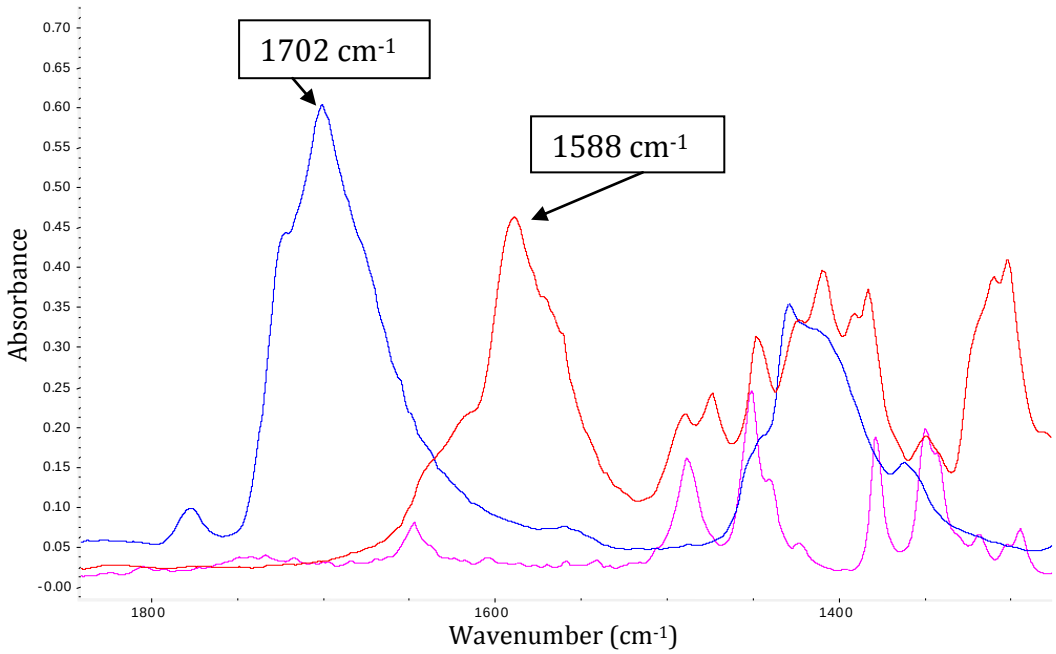

FIGURE 28- FTIR SPECTRA OF EPHEDRINE (PINK), GLYCOLIC ACID (BLUE) AND GROUND EPHEDRINE AND GLYCOLIC ACID SAMPLE (RED) SHOWING THE CARBONYL REGION. THE CARBONYL BANDS FOR THE GLYCOLIC ACID AND SALT ARE HIGHLIGHTED

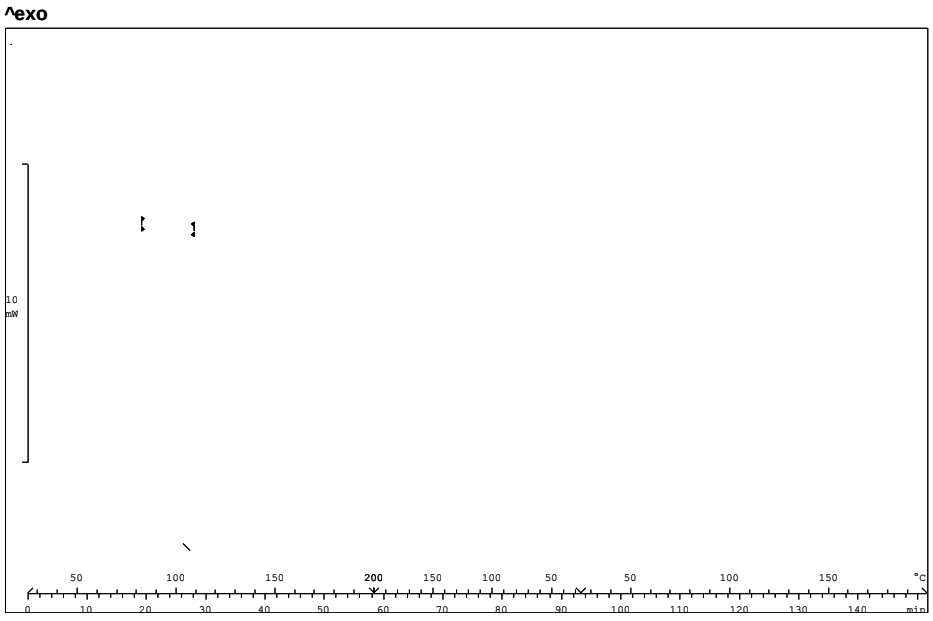

FIGURE 29- DSC OF GROUND EPHEDRINE AND GLYCOLIC ACID SAMPLE SHOWING HEATING TO 200 °C, COOLING TO 30 °C AND HEATING AGAIN TO 200 °C

3.3 THEORETICAL BINARY PHASE DIAGRAMS

The 2008 paper by Chadwick *et al*[1] discusses a method of assessing multicomponent crystal formation by the contacting of single crystals on a hotstage microscope to assess whether salt formation occurs. It also discusses contacting powders under ambient conditions. Three acid/base systems used in the grinding experiments in Section 3.2.2 were chosen for this further analysis. Glycolic acid and ephedrine showed the most complete salt formation, hence was taken for further study. Benzoic acid and ephedrine showed salt formation with some amorphous character (from pXRD). This system raised the question, 'by not grinding the components can crystalline salt formation be achieved?' Ephedrine and pimelic acid also showed a good prospect for salt formation by contact and was a previously unexplored system. It was suspected that the formation of these salts by grinding was due to eutectic points submerged below room temperature. The salts would therefore form upon contact or grinding. Grinding may also induce salt formation at lower temperatures due to the mechanical action (with associated heat and pressure) of milling.

The binary phase diagram for ephedrine and glycolic acid (Figure 30) has a theoretical eutectic point at just below 297.5 K (24 °C). If salt formation in the system proceeds via Chadwick's method it would be expected to occur without the aid of grinding.

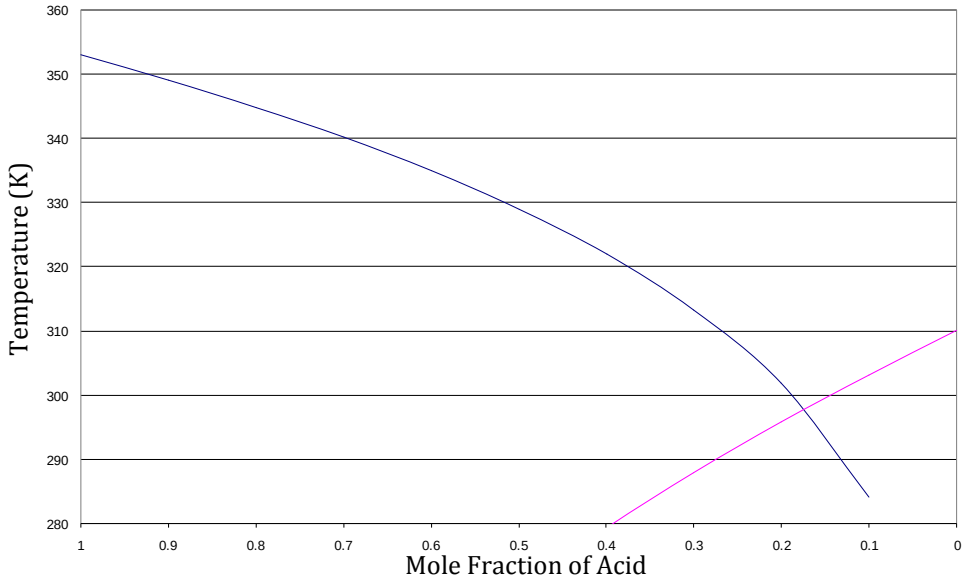

FIGURE 30- IDEAL BINARY PHASE DIAGRAM OF EPHEDRINE AND GLYCOLIC ACID

The binary phase diagram for ephedrine and benzoic acid (Figure 31) has a theoretical eutectic at just below 297 K (23.5 °C). If the reaction proceeds via Chadwick's method it would be expected for salt formation to occur in this system without the aid of grinding.

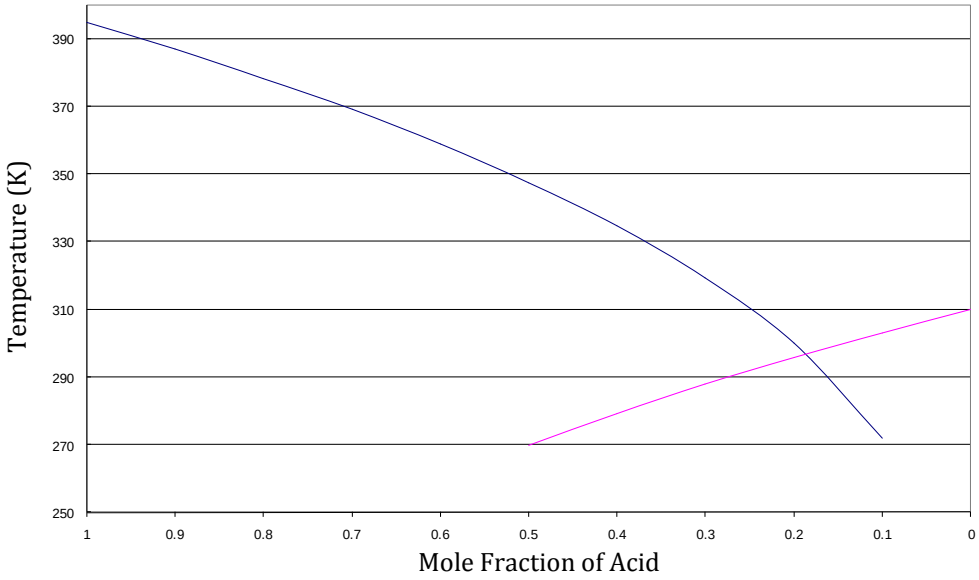

FIGURE 31- IDEAL BINARY PHASE DIAGRAM OF EPHEDRINE AND BENZOIC ACID

The binary phase diagram for ephedrine and pimelic acid (Figure 32) has a theoretical eutectic point just below 304.5 K (31 °C). According to Chadwick's method this system appears less likely to form a salt without the aid of grinding or heating to above this temperature.

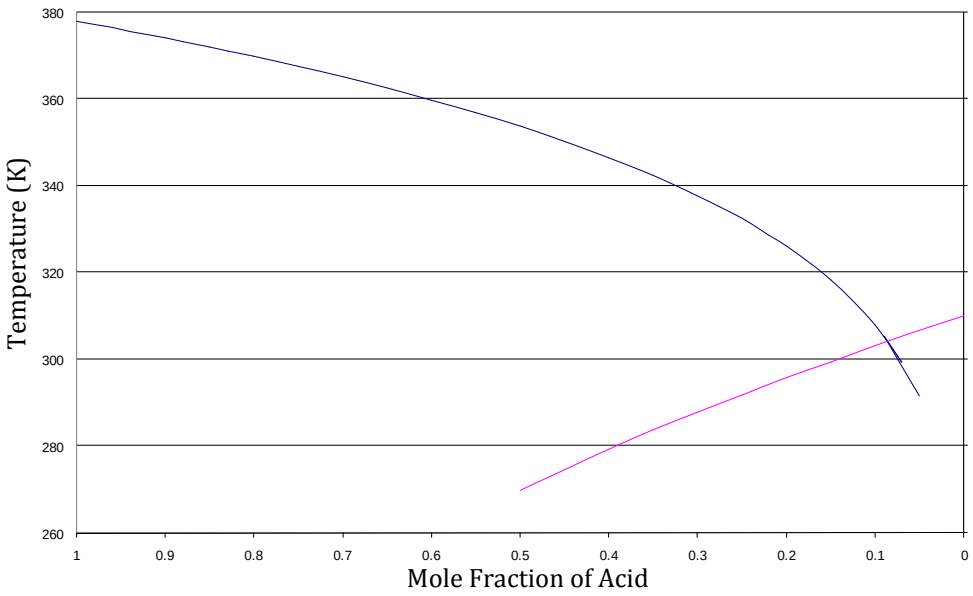

FIGURE 32- IDEAL BINARY PHASE DIAGRAM OF EPHEDRINE AND PIMELIC ACID

3.4 CONTACT

To assess experimentally whether the theoretical binary phase diagrams calculated and displayed above are accurate at predicting salt formation by contact, experiments were conducted on two different scales. This method also allowed assessment of potential salt formation by diffusion. Assessment of salt formation was made by eye using either a microscope with attached camera or on a larger scale simply a camera.

3.4.1 METHODS

3.4.1.1 SINGLE CRYSTAL CONTACTING

Single crystals of the two components were grown from solution where possible. Pimelic acid forms as rectangular flat crystals from water, while ephedrine and benzoic acid form as long thin needles from water. Glycolic acid grows as blocks from aqueous solutions[17], however crystals of an adequate size proved difficult to grow from water for this study. Glycolic acid was used directly from the bottle. It was concluded that long, thin needles were not suitable for the contacting experiments as the surface area in contact with the other crystal was too small. For those samples which formed needles small samples were taken directly from the bottle.

3.4.1.2 POWDER CONTACTING

On a microscope slide powdered samples of the two components were contacted and photographs taken over a number of days as the experiment progressed. Changes in colour, texture and position were all noted when observed. Images were recorded with a standard digital camera.

3.4.2 RESULTS OF CONTACT EXPERIMENTS

3.4.2.1 EPHEDRINE AND GLYCOLIC ACID

3.4.2.1.1 SINGLE CRYSTAL EPHEDRINE AND GLYCOLIC ACID

Small pieces of ephedrine and glycolic acid were initially contacted on a microscope slide and monitored using hotstage microscopy. The melting point of ephedrine is low at 37 °C; therefore the hotstage was not heated any higher than 28 °C. These initial results are shown below in Figure 33, where it is apparent that the uncovered sample at low temperatures takes up water readily. It was concluded that the sample dissolves in condensed water from the atmosphere rather than melting or forming a metastable liquid. From the theoretical binary phase diagram it would be expected that a metastable liquid would form around 24 °C and salt formation would follow. Glycolic acid is very hygroscopic which causes this issue.

To better assess whether this salt forms below room temperature, the experiment was repeated in a sealed system as described in Section 2.4.4.1 (Figure 34). Here it is apparent that liquid formation does not occur. This confirms that in the previous experiment water in the air was altering the results. From the sealed experiment the formation of a new product can be seen between the two components. This occurs at around 24 °C as predicted by the theoretical binary phase diagram. The formation of a liquid phase before nucleation was not observed, suggesting the mechanism occurring is not eutectic formation. Due to the apparent growth of needles without a liquid phase and the high vapour pressure of ephedrine, it appears that the diffusion mechanism is more feasible for this system. The formation of the racemic compound of ephedrine discussed by Duddu *et al*[18] suggests maybe even contact is not necessary. This theory will be explored further

after the contacting experiments of other ephedrine/acid salt systems have been discussed.

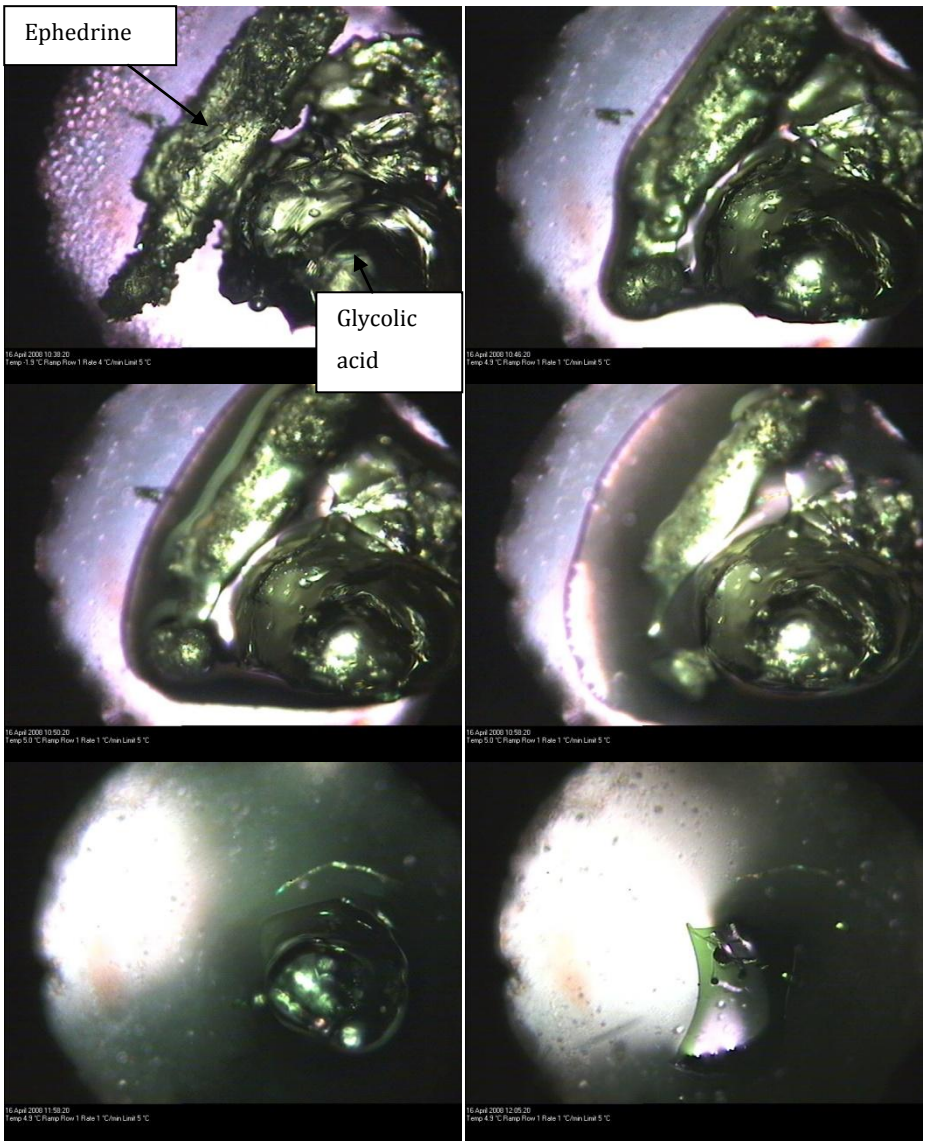

FIGURE 33- EPHEDRINE (RIGHT) AND GLYCOLIC ACID (LEFT) CONTACTED UNCOVERED ON A HOTSTAGE MICROSCOPE AT 5 °C OVER A PERIOD OF TWO HOURS

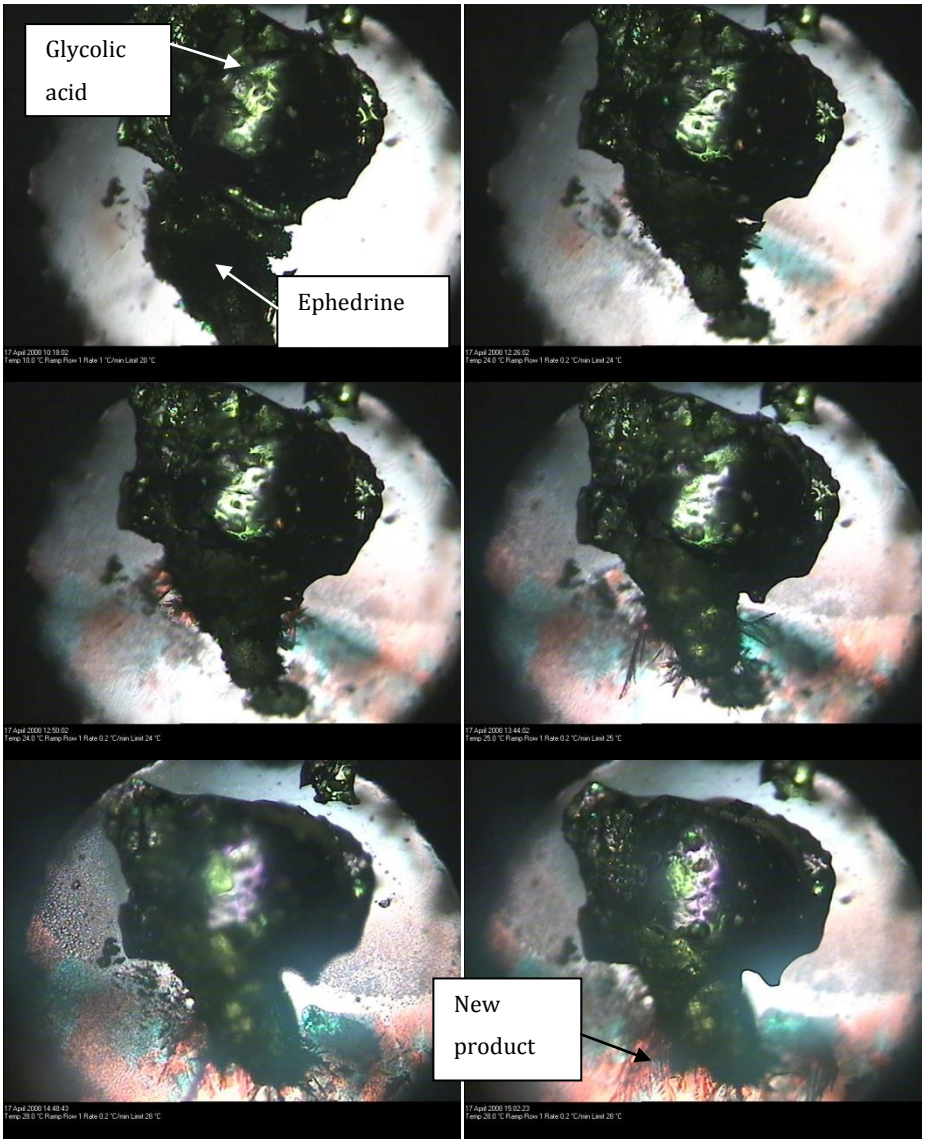

FIGURE 34- EPHEDRINE (BOTTOM) AND GLYCOLIC ACID (TOP) SEALED BETWEEN TWO COVERSLIPS AND HEATED FROM 20 TO 28 °C USING A HOTSTAGE MICROSCOPE OVER A PERIOD OF FIVE HOURS

The products formed in these small scale contact experiments were not successfully analysed due to the tiny amount of product formed. Larger scale experiments were undertaken to provide better sample volumes for analysis.

3.4.2.1.2 POWDER EPHEDRINE AND GLYCOLIC ACID

Ephedrine and glycolic acid in powdered form were contacted on a microscope slide and kept at room temperature in the laboratory, away from air flow. The images can be viewed in Figure 35 below. Here a reaction like that in the sealed microscope system can be seen, with small, needle-like crystals growing from the

contact region. Needle growth occurred on the glycolic acid side of the two components, while the ephedrine powder diminished in size. It appears that the mechanism occurring here may be the diffusion method discussed previously, however no vacuum was used. It is deduced that the vapour pressures involved must be relatively high. From these images it would appear that the ephedrine vapour travels further and forms the salt when the vapour reaches the solid acid.

The formation of this product is in agreement with the prediction made by the theoretical binary phase diagram (Figure 30) that the salt will form at room temperature without additional heat or grinding. The result observed here is not consistent with Chadwick's submerged eutectic mechanism as no liquid phase is observed.

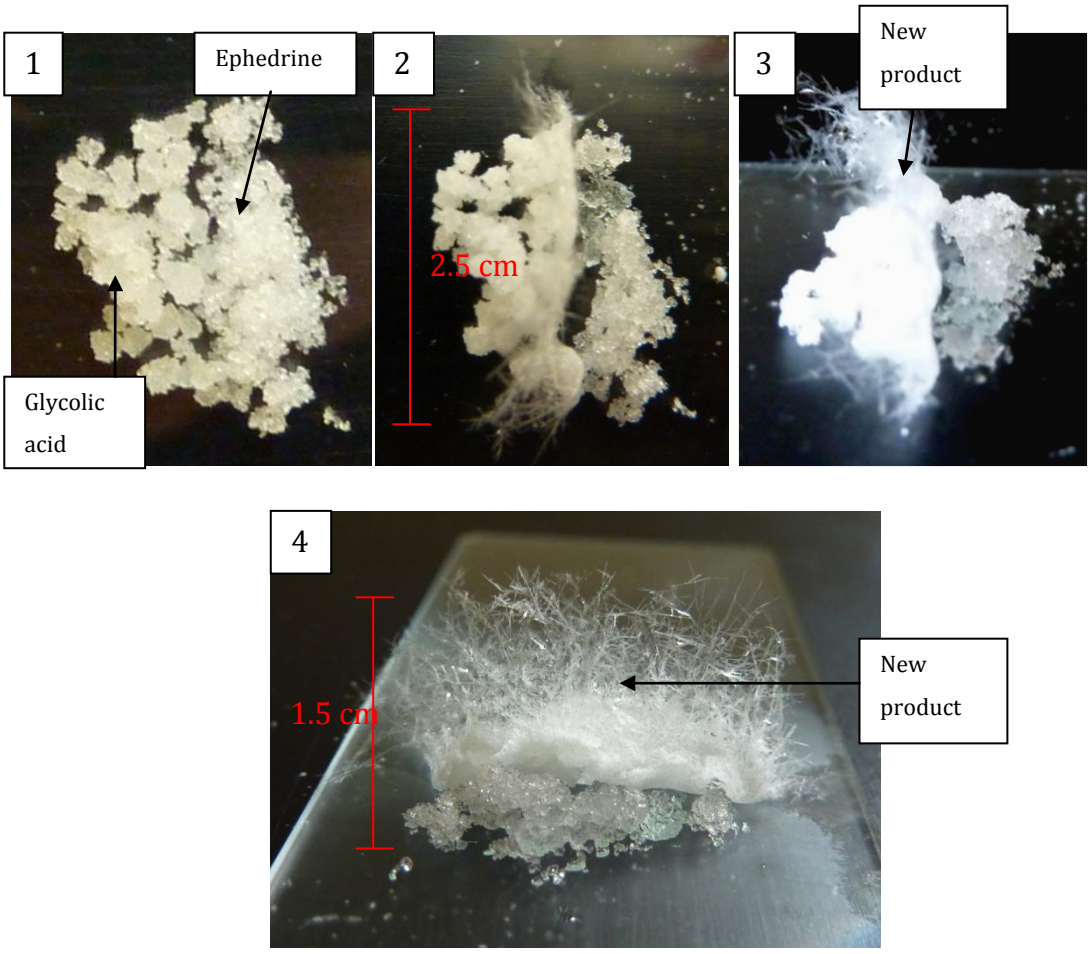

FIGURE 35- IMAGES OF EPHEDRINE IN CONTACT WITH GLYCOLIC ACID. IMAGE 1- INITIAL IMAGE OF EPHEDRINE (LEFT) AND GLYCOLIC ACID (RIGHT). IMAGE 2- SAMPLE LEFT FOR 1 DAY. IMAGE

3- SAMPLE LEFT FOR 5 DAYS. IMAGE 4- SAMPLE LEFT FOR 5 DAYS, EPHEDRINE AT FRONT OF IMAGE.

This new product was analysed by pXRD and FTIR and the results are displayed in Figure 36 and Figure 37 respectively. The pXRD pattern does not match the simulated pXRD pattern of ephedrine glycolate. The FTIR spectrum is identical to that of the salt previously formed by grinding and from solution. This suggests that by contacting, rather than grinding the components, a new polymorph of the salt has been formed. Unfortunately, due to the small, breakable nature of the crystals formed single crystal X-ray analysis could not be performed. The determination of a crystal structure to confirm this hypothesis was not possible.

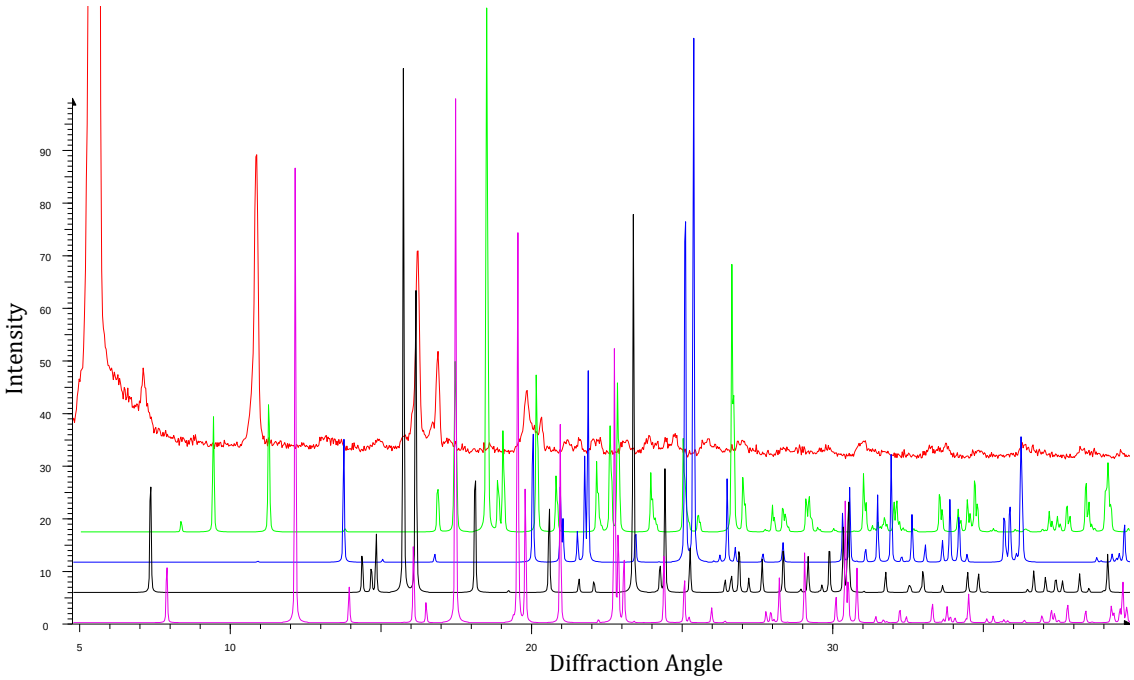

FIGURE 36- PXRD OF EPHEDRINE (PINK), EPHEDRINE HEMIHYDRATE (BLACK), GLYCOLIC ACID (BLUE), EPHEDRINE GLYCOLATE (GREEN) AND THE NEW PRODUCT FORMED BY CONTACT OF EPHEDRINE AND GLYCOLIC ACID

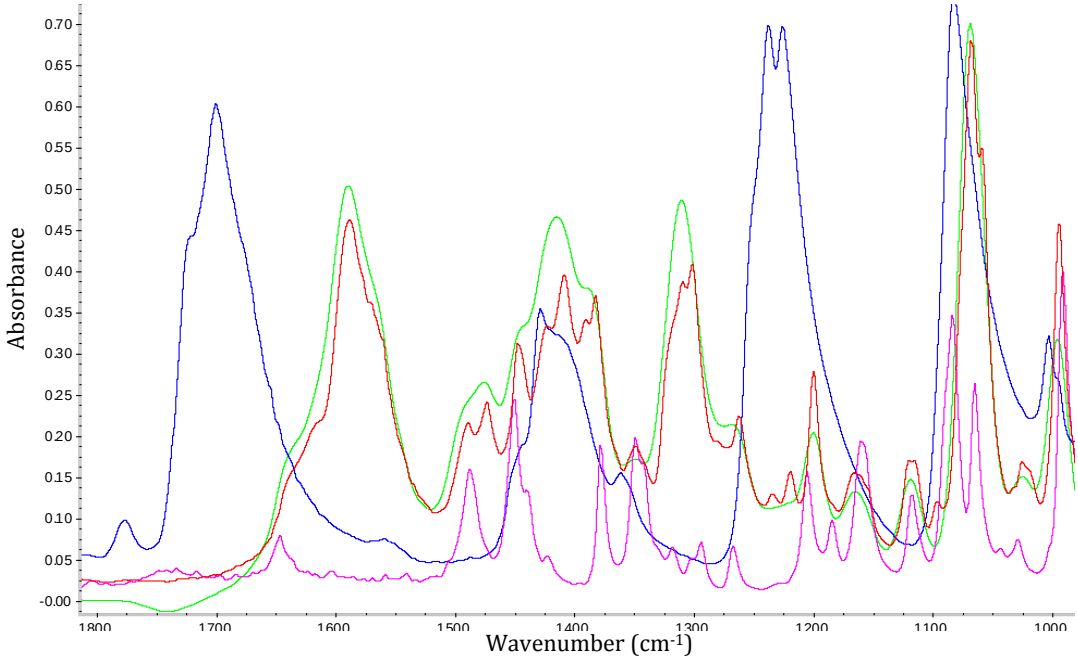

FIGURE 37- FTIR OF EPHEDRINE (PINK), GLYCOLIC ACID (BLUE), GROUND EPHEDRINE AND GLYCOLIC ACID (RED) AND THE NEW PRODUCT FORMED BY CONTACT OF EPHEDRINE AND GLYCOLIC ACID (GREEN).

3.4.2.2 EPHEDRINE AND BENZOIC ACID

3.4.2.2.1 SINGLE CRYSTAL EPHEDRINE AND BENZOIC ACID

The images below in Figure 38 show reaction occurred at the interface between the ephedrine and benzoic acid when they were held at 21 °C. This reaction occurred much more slowly than the reaction with glycolic acid. Due to the low melting temperature of ephedrine (37 °C) higher temperatures were not used. The reaction was allowed to proceed at a slow rate.

From the images in Figure 38 a metastable liquid phase, as would occur in eutectic formation, is not observable. The new product appears to grow along a line between the crystals, similarly to the ephedrine and glycolic acid, suggesting a diffusion mechanism may be controlling its formation. This may be due to the high vapour pressure of ephedrine.

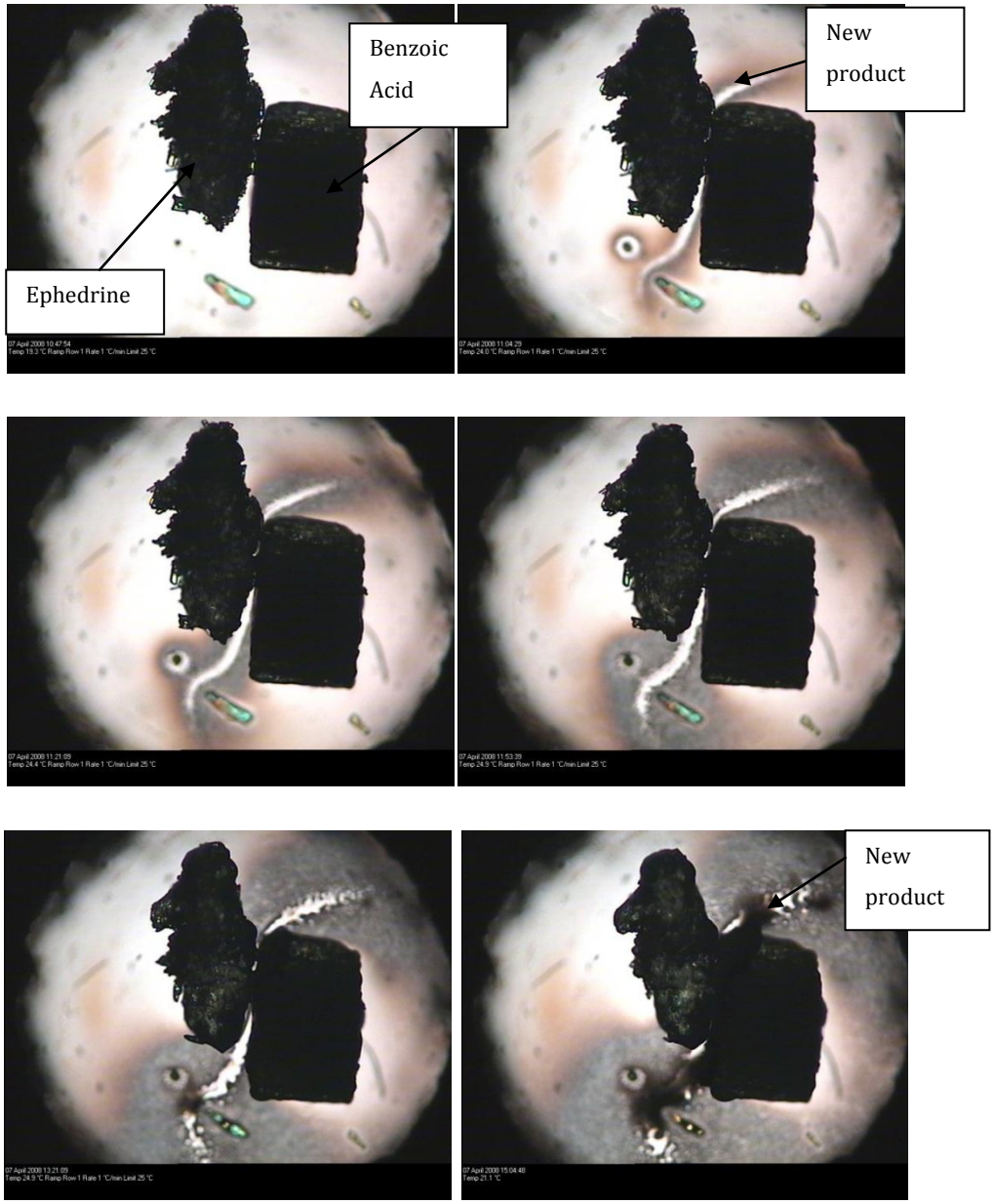

FIGURE 38- EPHEDRINE (LEFT) AND BENZOIC ACID (RIGHT) CONTACTED AT 25 °C FOR A PERIOD OF APPROXIMATELY FIVE HOURS

3.4.2.2.2 EPHEDRINE AND BENZOIC ACID POWDER CONTACT

The images shown in Figure 39 show the growth of a new product between the two pure components, as seen in the microscope images (Figure 38). The new product grows as tiny, fluffy, hair-like needles. The benzoic acid crystals (powder on the left) appear to be being covered by the new product as the reaction progresses. The amount of ephedrine (powder on the right) decreases. Again no

liquid phase appears to be present. The ephedrine vapour may be moving towards the acid with salt formation occurring upon its contact with the acid.

The formation of this product is in agreement with the prediction made by the theoretical binary phase diagram (Figure 31) that the salt would form below room temperature. As with the glycolic acid a liquid phase is not seen, the reaction appears to proceed via a vapour mechanism, rather than via a submerged eutectic.

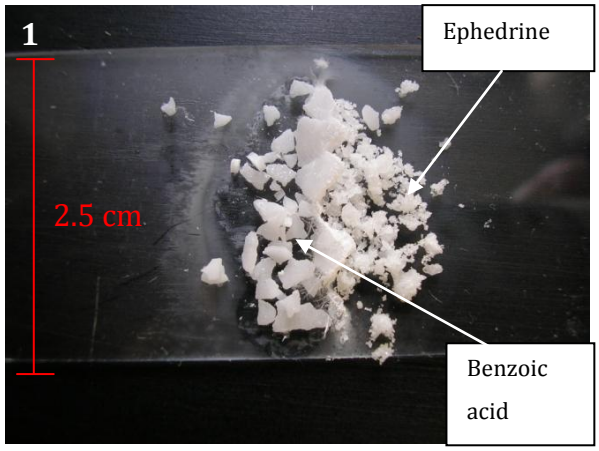

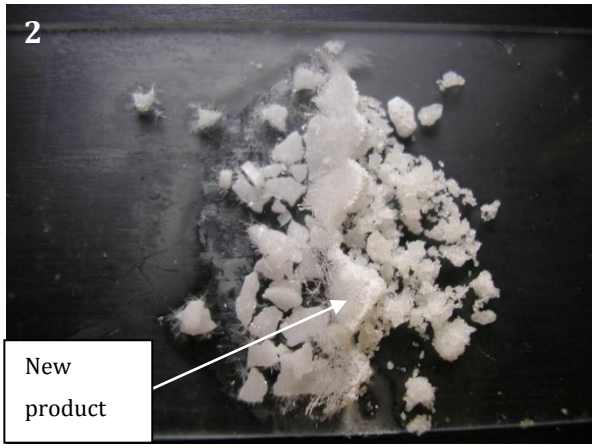

FIGURE 39- CAMERA IMAGES OF CONTACT BETWEEN EPHEDRINE (RIGHT) AND BENZOIC ACID (LEFT) AFTER 1 DAY (1), 3 DAYS (2) AND 1 WEEK (3)

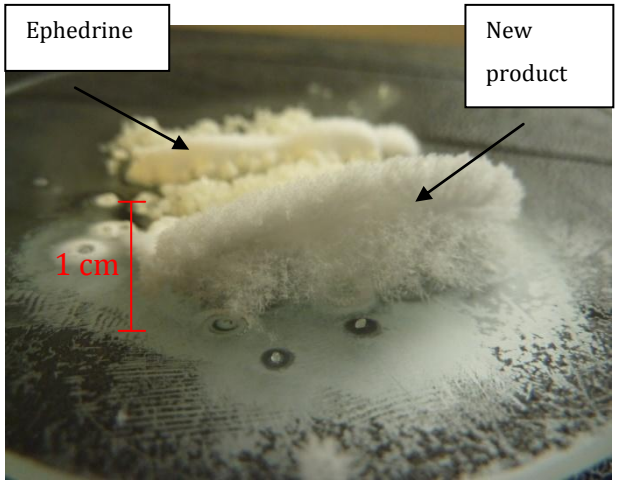

FIGURE 40- CAMERA IMAGE OF CONTACT BETWEEN EPHEDRINE AND BENZOIC ACID AFTER A MONTH. NOTE THE FINE 'FLUFFY' NEEDLES

Analysis of this product proved complex and due to this, data and discussion is included in the following chapter 'Ephedrine and Benzoic Acid' along with further work on this system.

3.4.2.3 EPHEDRINE AND PIMELIC ACID

3.4.2.3.1 SINGLE CRYSTAL CONTACTING OF EPHEDRINE AND PIMELIC ACID

A single crystal of pimelic acid was contacted with a small amount of ephedrine on a thin microscope slide. The slide was duly heated on a hotstage microscope to

35 °C (below the melting temperature of the pure ephedrine). Images were recorded every 10 seconds. A slightly higher temperature was chosen for the pimelic acid system than for the glycolic or benzoic systems due to information gained from the theoretical binary phase diagram (Figure 32). Sample images are shown here (Figure 41). The heat was increased slowly at 0.5 °C per minute, starting at 25 °C. No change was observed until just below 35 °C when the heating ramp was suspended to allow the reaction to proceed without an ephedrine melt. The ephedrine sample then appeared to gradually 'absorb' into the pimelic acid crystal. This left no ephedrine and the appearance of the pimelic acid crystal changed. At no point is a metastable liquid phase observable (as was expected from knowledge of the Chadwick *et al*[1] paper), however this does not mean it was not present. There is a possibility the new crystalline product formed very quickly or that it is hard to see on the images. The formation of a new product appeared to proceed by a very different mechanism to that of the ephedrine with benzoic or glycolic acids. There is no evidence that salt formation proceeds by a vapour process.

Analysis of the remaining sample proved difficult as a lot of pure pimelic acid remained (especially on the far left hand side, where ephedrine had not been directly contacted). Also the sample could not be ground as this may have induced a different reaction and/or introduced the extra pimelic acid into the system. To analyse the sample it was placed on the sample stage of a pXRD system and a pattern recorded (Figure 41). Some adjustments of the sample position were required to ensure the new, reacted parts of the sample were being analysed.

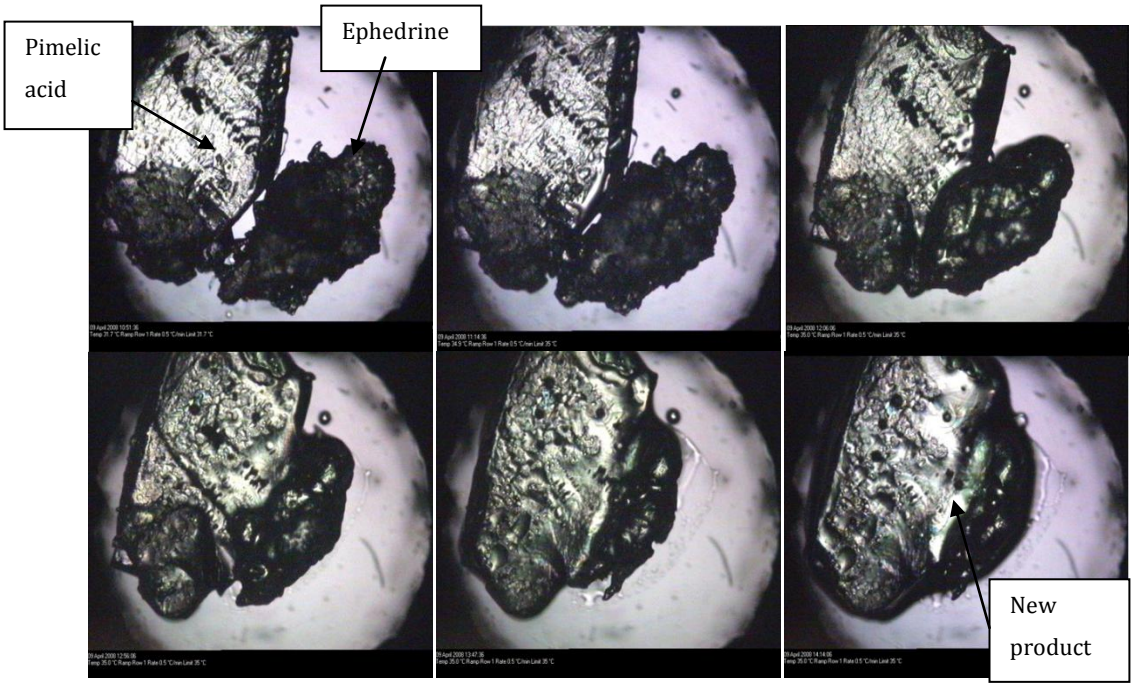

FIGURE 41- CONTACTING PIMELIC ACID (LEFT) AND EPHEDRINE (RIGHT) ON A HOTSTAGE MICROSCOPE AND HEATING FROM 25 TO 35 °C FOR A PERIOD OF APPROXIMATELY FOUR HOURS

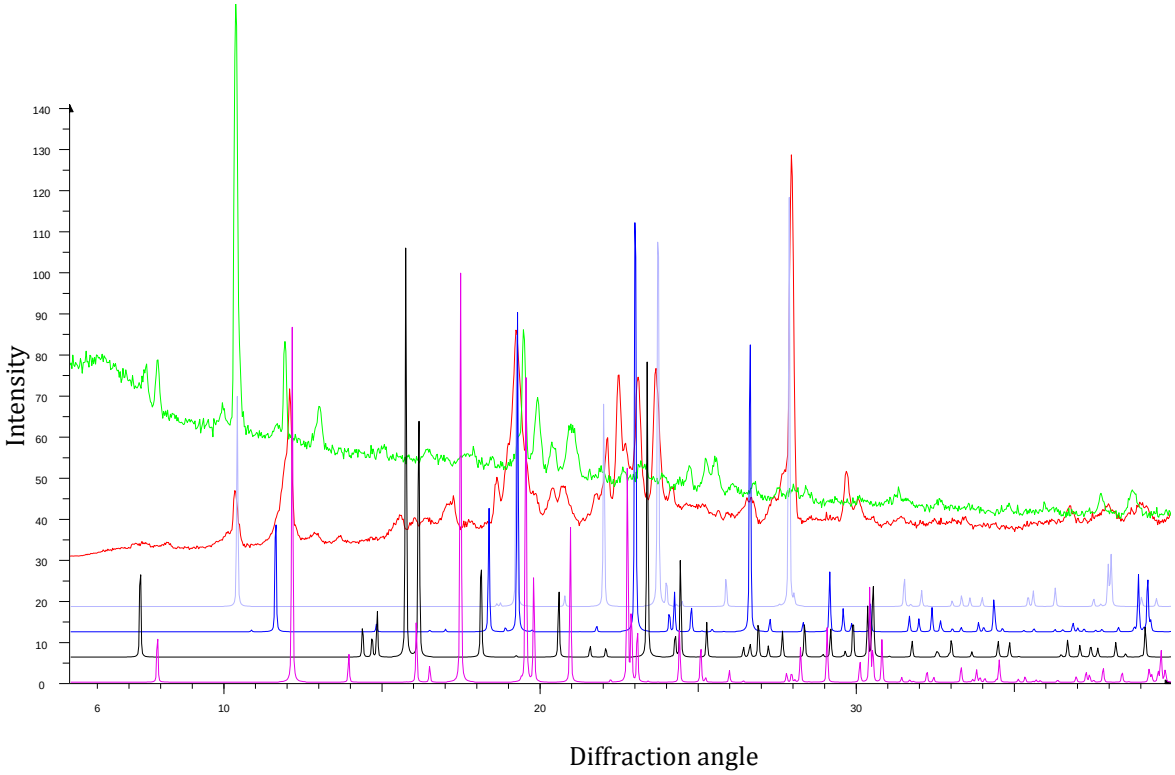

FIGURE 42- PXRD PATTERNS OF ANHYDROUS EPHEDRINE (PINK), EPHEDRINE HEMIYDRATE (BLACK), α PIMELIC ACID (BLUE), β PIMELIC ACID (LILAC), EPHEDRINE AND PIMELIC ACID GROUND (RED) AND THE CRYSTAL FORMED BY CONTACT OF EPHEDRINE AND PIMELIC ACID (GREEN)

3.4.2.3.2 POWDER EPHEDRINE AND PIMELIC ACID

Powdered samples of ephedrine and pimelic acid were contacted in the same way as ephedrine with benzoic or glycolic acids. The sample was left in contact for a month and no reaction was observed (Figure 43). For the ephedrine and pimelic acid system the addition of energy as heat or with grinding appears to induce reaction. This is in agreement with the theoretical binary phase diagram (Figure 32), which predicted a eutectic temperature just above room temperature. This suggests that, despite there being no obvious liquid phase, the Chadwick mechanism may be the cause of the formation of the salt.

FIGURE 43- CONTACT OF EPHEDRINE (LEFT) AND PIMELIC ACID (RIGHT) POWDERS AT ROOM TEMPERATURE

3.5 SUMMARY

From these experiments it has been determined that ephedrine not only forms salts by solution methods, but by grinding and contacting too. This occurs for a range of different acids and, as predicted by the 2009 review[5] of cocrystals, the mechanism for these results does not appear to be the same for all salt systems. The most interesting systems will be taken for continued study in following chapters, Ephedrine and Pimelic Acid (Chapter 4) and Ephedrine and Benzoic Acid (Chapter 5). The formation of ephedrine and pimelic acid salt was assessed to probably proceed via a submerged eutectic. The benzoic acid and glycolic acid systems showed similar effects (suspected salt formation by diffusion); therefore only the benzoic acid will be studied in more detail in order to investigate a salt

formed by vapour diffusion. Benzoic acid was selected from the two acids to eliminate the uptake of water as a factor affecting salt formation. The pimelic acid system will be taken to investigate an alternative salt formation mechanism. Both systems will also be investigated from solution perspectives.

3.6 REFERENCES

1. Chadwick, K., Davey, R. J. & Cross, W. How Does Grinding Produce Co-crystals? Insights from the Case of Benzophenone and Diphenylamine. Chemical Communications 9, 732-734 (2007).
2. Guo, K., Sadiq, G., Seaton, C., Davey, R. & Yin, Q. Co-Crystallisation in the Caffeine/ Maleic Acid System: Lessons from Phase Equilibria. Crystal Growth and Design 10, 268-273 (2010).
3. Trask, A. V. & Jones, W. Crystal Engineering of Organic Cocrystals by The Solid-State Grinding Approach. Topics in Current Chemistry 254, 41-70 (2005).
4. Trask, A. V., Motherwell, W. D. S. & Jones, W. Solvent Drop Grinding:Green Polymorph Control of Cocrystallisation. Chemical Communications, 890-891 (2004).
5. Friscic, T. & Jones, W. Recent Advances in Understanding the Mechanism for Cocrystal Formation via Grinding. Crystal Growth and Design 9, 1621-1637 (2009).
6. Nguyen, K. L., Friscic, T., Day, G. M., Gladden, L. F. & Jones, W. Terahertz Time-Domain Spectroscopy and the Quantitative Monitoring of Mechanochemical Cocrystal Formation. Nature Materials 6, 206-209 (2007).
7. Mallick, s. et al. Physiochemical Characterization of Interaction of Ibuprofen by Solid-State Milling with Aluminium Hydroxide. Drug Development and Industrial Pharmacy, 726-734 (2008).
8. Trask, A. V., Haynes, D. A., Motherwell, W. D. S. & Jones, W. Screening for Crystalline Salts via Mechanochemistry. Chemical Communications 51, 51-53 (2006).

9. Rastogi, R. P., Bassi, P. S. & Chadha, L. S. Kinetics of Reaction Between Naphthalene and Picric Acid in the Solid State. Journal of Physical Chemistry 66, 2707-2708 (1962).
10. Collier, E. A., Davey, R. J., Black, S. N. & Roberts, R. J. 17 Salts of Ephedrine: Crystal Structures and Packing Analysis. Acta Crystallographica, Section B: Structural Science B62, 498-505 (2006).
11. Collier, E. A. in Department of Chemical Engineering 179 (The Univeristy of Manchester Institute of Science and Technology, Manchester, 2004).
12. Brown, H. C., McDaniel, D. H. & Haflinger, O. Determination of Organic Structures by Physical Methods (eds. Braude, E. A. & Nachod, F. C.) (Academic Press, New York, 1955).
13. Dawson, R. M. C., Elliot, D. C., Elliot, W. H. & Jones, K. M. Data for Biochemical Research (Clarenden Press, Oxford, 1959).
14. Cox, J. D. & Pilcher, G. Thermochemistry of Organic and Organometallic Compounds (Academic Press, London 1970).
15. Myz, S. A. et al. Synthesis of Co-crystals of Meloxicam with Carboxylic Acids by Grinding. Mendeleev Communications 19, 272-274 (2009).
16. Adams, C. J., Colquhoun, H. M., Crawford, P. C., Lusi, M. & Orpen, A. G. Solid-State Interconversions of Coordination Networks and Hydrogen Bonded Salts. Angewandte Chemie. International edition in English 46, 1124-1128 (2007).
17. Pijper, W. The Molecular and Crystal Structure of Glycollic Acid. Acta Crystallographica, Section B: Structural Science B27, 344-348 (1971).
18. Duddu, S. P. & Grant, D. J. W. Formation of the Racemic Compound of Ephedrine Base from a Physical Mixture of Its Enantiomers in the Solid, Liquid, Solution, or Vapor State. Pharmaceutical Research 9, 1083-1091 (1992).

4 EPHEDRINE AND PIMELIC ACID

4.1 INTRODUCTION

Previous to this work the dicarboxylic acid pimelic acid had not been used to form any salts with ephedrine. The data collected and tabulated in Table 7 showed that it provided a good prospect for salt formation. Also, the study of salt formation by grinding (Section 3.2.2) showed that a new product formed when the two components were ground together at an equimolar ratio. This new product was shown to form by the contacting of the pure components when in the form of single crystals. Further study was needed to assess whether or not salt formation had occurred. This system will also be studied to assess salt formation from solution.

4.2 BACKGROUND DATA

The pK_a values of the acid and the base are greater than two units apart. As the general rule states[1] pK_a values greater than two units apart are favourable for salt formation, while a gap of less than two units means there is a greater likelihood of yielding the cocrystal. For this system both pK_a values for the acid are greater than two units from the base suggesting both 1:1 and 2:1 ratio salts could form from water. The aqueous solubilities of the two components are very similar at 5.39 wt% and 4.65 wt%. This suggests that congruent dissolution will occur for a 1:1 salt. Therefore this ensures the region of the phase diagram this salt forms within is easy to access. The molecular masses of the acid and ephedrine are reasonably similar at 165.23 $gmol^{-1}$ and 160.19 $gmol^{-1}$ respectively, making the measurement of equimolar amounts into solution easier. The same mass of each component can be used to achieve an equimolar ratio.

TABLE 7- EPHEDRINE AND PIMELIC ACID DATA

Physical Property	**Ephedrine**	**Pimelic Acid**
Melting Temperature (K)	310	378
Aqueous Solubility (wt %)	5.39	4.65
pKa in Water	9.74[2]	4.48, 5.42[3]
Enthalpy of Fusion (kJ/mol)	11.96	31.78
Polymorphs	No	3
Hydrates	Hemihydrate	No

The hydration of ephedrine is briefly discussed in Section 1.1.2.1, however some specific problems are dealt with within this chapter. The presence of the hemihydrate of ephedrine was a concern for the study of both binary and ternary phase diagrams. From pXRD the sample used from the bottle was roughly half anhydrous and half hemihydrate. In the binary system it was felt that the water would act as a third component. In the ternary system it was believed that it would alter the composition (with less ephedrine and more water present than anticipated). These issues were dealt with as and when the need arose and will be discussed as such in this chapter.

4.3 SALT SCREENING

Two techniques were used in the initial screen to determine whether salts of this system may occur. Firstly the two components were simply ground together in a pestle and mortar. The resulting powder was then analysed by pXRD, IR and DSC to assess whether salt formation had occurred. Secondly the binary phase diagram of the system was determined using DSC.

4.3.1 EPHEDRINE PIMELATE FORMATION BY GRINDING

As is discussed (Section 3.2.2), grinding the 1:1 ratio of ephedrine and pimelic acid in the absence of any solvent yielded a new product, suspected of being a salt. This hypothesis was based on several pieces of evidence. A new melting temperature of 132 °C (determined by DSC) was higher than either of the pure components

(Figure 44). An IR spectrum demonstrating a shifted and split carbonyl band (Figure 45) suggested salt formation. A new and unique pXRD pattern (Figure 46). Once ephedrine pimelate had been selected as a system for further study, dry grinding of the 2:1 base:acid ratio was also undertaken in an attempt to form a 2:1 salt. The 2:1 molar ratio of the ephedrine to the pimelic acid was ground in a pestle and mortar, as in the previous grinding work. As the components were ground the sample visibly changed, becoming a slightly darker colour and more cohesive consistency. This was potentially due to long range order being lost and the sample becoming increasingly amorphous, a common feature of grinding[4-8]. The sample was analysed to ascertain whether a change from the pure components had occurred, and if so, had yielded purely crystalline samples. While the 1:1 salt showed only crystalline characteristics, the 2:1 appeared to be partially amorphous.

The DSC traces of the two pure components and the 1:1 and 2:1 ratio ground samples are shown in Figure 44 below. The endotherm for the 2:1 ground sample is at a different temperature than those of the pure components and is also distinct from the 1:1 ratio ground sample. From this it can be deduced that there are two new products with melting temperatures of 123 °C and 132 °C. The endotherm of the 2:1 salt is also broader than the 1:1 implying greater amorphous character.

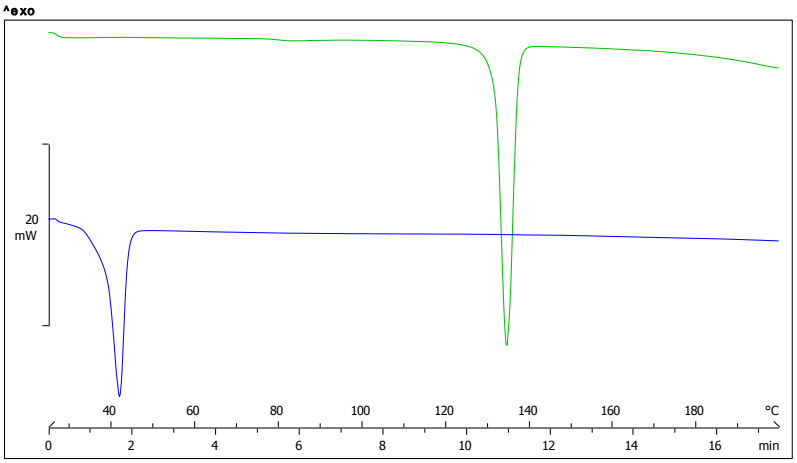

FIGURE 44- DSC OF PURE EPHEDRINE (BLUE), PURE PIMELIC ACID (BLACK), THE 2:1 GROUND SALT RATIO WITHOUT SOLVENT (RED) AND THE 1:1 GROUND RATIO WITHOUT SOLVENT (GREEN)

TABLE 8- TABLE OF DATA DETERMINED FROM DSC TRACES IN FIGURE 44

Compound	**Melting**	**Enthalpy of Fusion**
Ephedrine	310	11.97
Pimelic Acid	378	31.78
1:1 Ground Sample	405.5	44.66
2:1 Ground Sample	396.5	45.54

The new 2:1 ratio ground product was also analysed by FTIR to assess whether there was evidence a salt had been formed. As is discussed in Section 2.4.1.5 the shift of the carbonyl absorption stretch provides a good indication of the ionisation state of the ground products. The data seen in Figure 45 show a shift typical of ionisation. The carbonyl band of pimelic acid clearly shifts from a single absorption at 1681cm^{-1} in its unionised form (blue) to three bands with values of 1693 cm^{-1}, 1624 cm^{-1} and 1547 cm^{-1} in the 1:1 composition (red). In the 2:1 mixtures (green) a single broad peak at 1559 cm^{-1} with a shoulder at around 1620 cm^{-1} is apparent. For an ionised carboxylate two bands would be expected, as is seen in the 1:1 salt. The unionised carboxylic acid band is also still present. In the 2:1 salt the second carboxylate band is less clear. Either the broadened peak or shoulder may be the evidence of this. These changes are consistent with the expected salt formation in which the acid adopts mono-and doubly deprotonated forms[9].

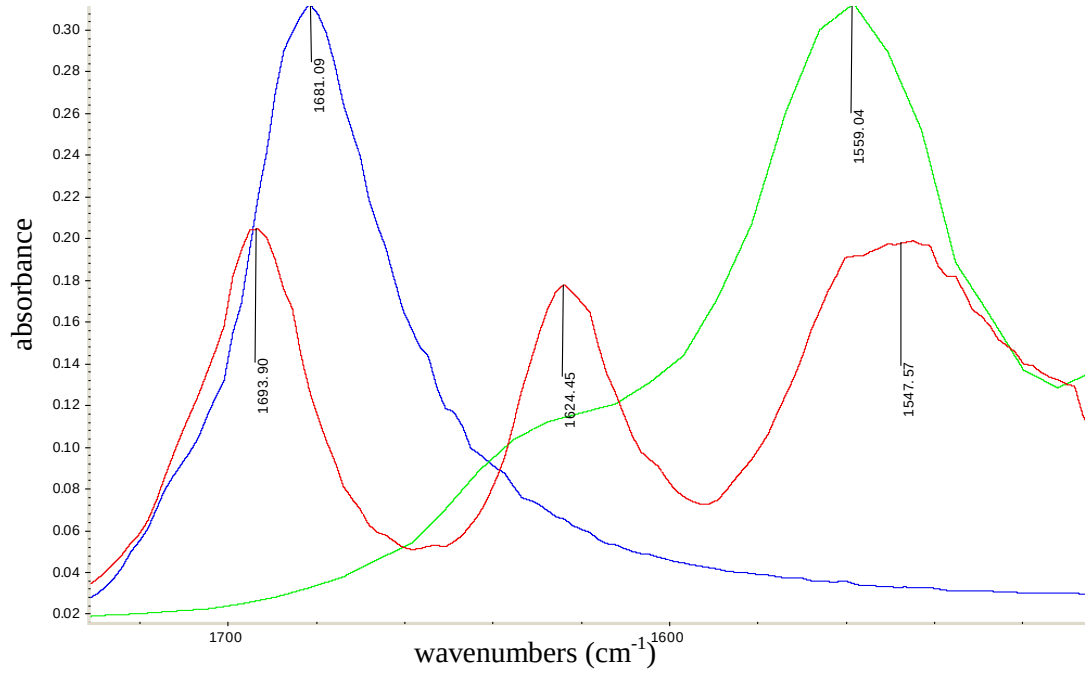

FIGURE 45- FTIR SPECTRA OF PURE PIMELIC ACID (BLUE), THE 1:1 GROUND SAMPLE (RED) AND THE 2:1 GROUND SAMPLE (GREEN)

The pXRD patterns of both the 1:1 and 2:1 ground samples are very different to those simulated for the pure components of acid and base (Figure 46). The 1:1 is mostly crystalline with only a very small amount of line broadening to suggest some amorphous characteristics are present. The 2:1 salt shows greater line broadening suggesting a greater amorphous presence. When the 2:1 sample was left at ambient conditions it became more visibly crystalline. This still could not be analysed by pXRD as regrinding would bring back the amorphous peak broadening. This suggests the 2:1 salt may form via an amorphous intermediate, via the mechanism proposed by Nguyen *et al*[10].

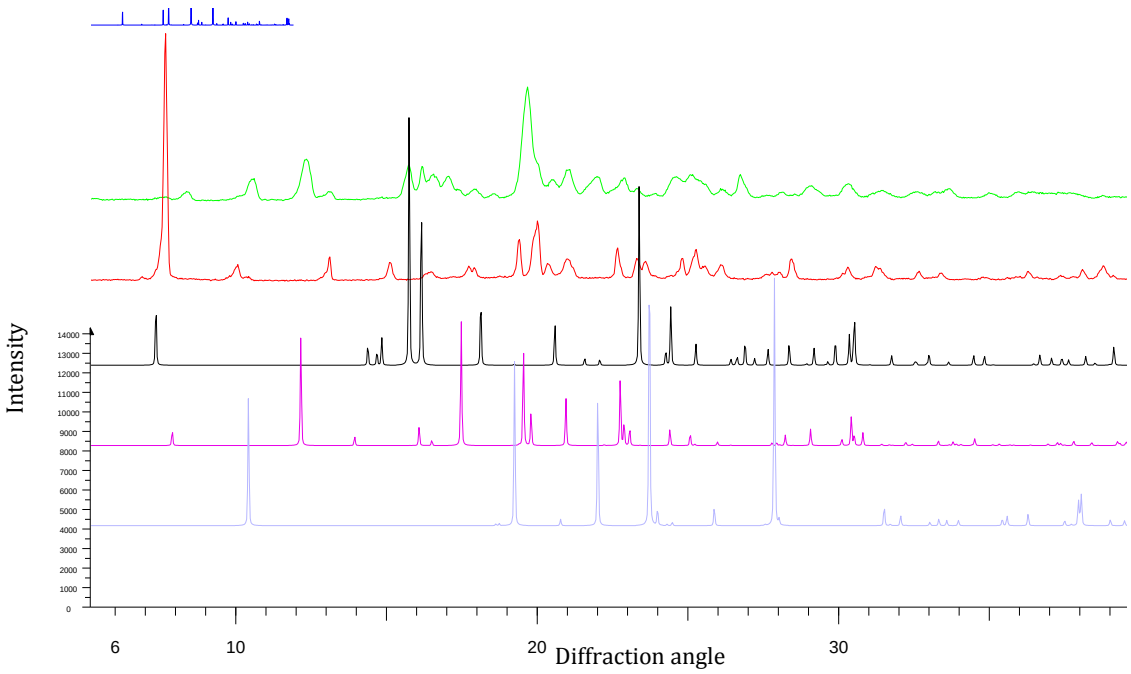

FIGURE 46- PXRD PATTERNS OF α PIMELIC ACID (BLUE), β PIMELIC ACID (LILAC), EPHEDRINE (PINK), EPHEDRINE HEMIHYDRATE (BLACK), 1:1 GROUND EPHEDRINE AND PIMELIC ACID (RED) AND 2:1 GROUND EPHEDRINE AND PIMELIC ACID (GREEN)

It was also noted in Section 3.4.2.3 that the 1:1 salt forms from the mere contact of the two constituent crystals at slightly elevated temperatures (35 °C). This implies that, as predicted by the ideal binary phase diagram (Figure 32), energy needs to be added to the system in the form of either heat or friction to induce reaction. This implies the 1:1 salt forms via the Chadwick method, despite there being no visible metastable liquid phase.

4.3.2 EPHEDRINE PIMELATE EXPERIMENTAL BINARY PHASE DIAGRAM DETERMINATION

To determine how the melting behaviour of one component changes in contact with the other different stoichiometric ratios were prepared and melting points established using DSC. As discussed in Section 2.2.4 with reference to a paper by Guarrera *et al*[11], the usual method for determining the binary phase diagram of a system using DSC entails an initial melting cycle, followed by a recrystallisation cycle using cooling and finally a second heating cycle. This is expected to give two well defined peaks. The eutectic line on the phase diagram is plotted from the first

peak onset. The liquidus curve is plotted from the second peak, caused by the melting of the pure component in contact with the other pure component[12, 13]. However, for this system no visible recrystallisation ever occurred in the cooling cycle. This same result was also observed for pure ephedrine, suggesting the presence of ephedrine in the samples may be the cause of this issue. Consequently samples were prepared as uniformly as possible by extended grinding and heated only once to determine the positions of the two endotherms. An example of such a DSC trace can be seen in Figure 47.

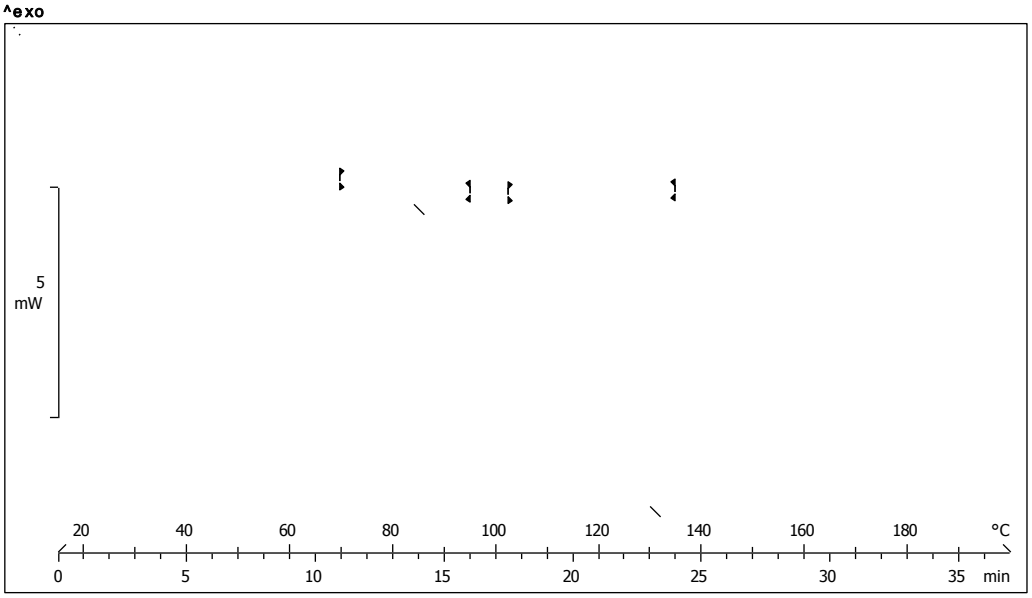

FIGURE 47- EXAMPLE DSC SHOWING A EUTECTIC PEAK (FIRST PEAK) AND A MELT PEAK (SECOND PEAK)

This method lead to some irreproducibility in the peak positions of the DSC due to broad peaks, such as the low temperature peak in Figure 47. The eutectic lines and liquidus curves on the binary phase diagram have some outlying points, as can be seen in Figure 48. Despite outlying points the general shape of the curves and position of the eutectic lines can be clearly observed and sketched lines fitting the points are used to guide the eye (Figure 49). The melting points determined agree closely with literature values for the pure single component solid phases and ground salt samples measured previously and shown in Figure 44 (Table 9)[1, 14].

As discussed in the experimental chapter and Section 4.2, the ephedrine used was roughly half anhydrous and half the hemihydrate form. In order to assess the effect of using this mixture ephedrine was placed in a desiccator for a week to ensure all water had been removed. Three of the DSC experiments for the binary phase diagram were then repeated using the anhydrous sample. No difference was seen in the results; therefore the presence of some hemihydrate in the ephedrine was not further considered with respect to the binary phase diagram.

TABLE 9- TABLE SHOWING MELTING TEMPERATURES OF GROUND SALT SAMPLES COMPARED TO THOSE DETERMINED IN THE BINARY PHASE DIGRAM.

Salt	**Melting Point from Ground Samples or Literature (°C)**	**Melting Point From Binary Phase Diagram (°C)**
Ephedrine	37.5[1]	37
Pimelic Acid	105[14]	107.2
1:1	132	130.7
2:1	123	124.4

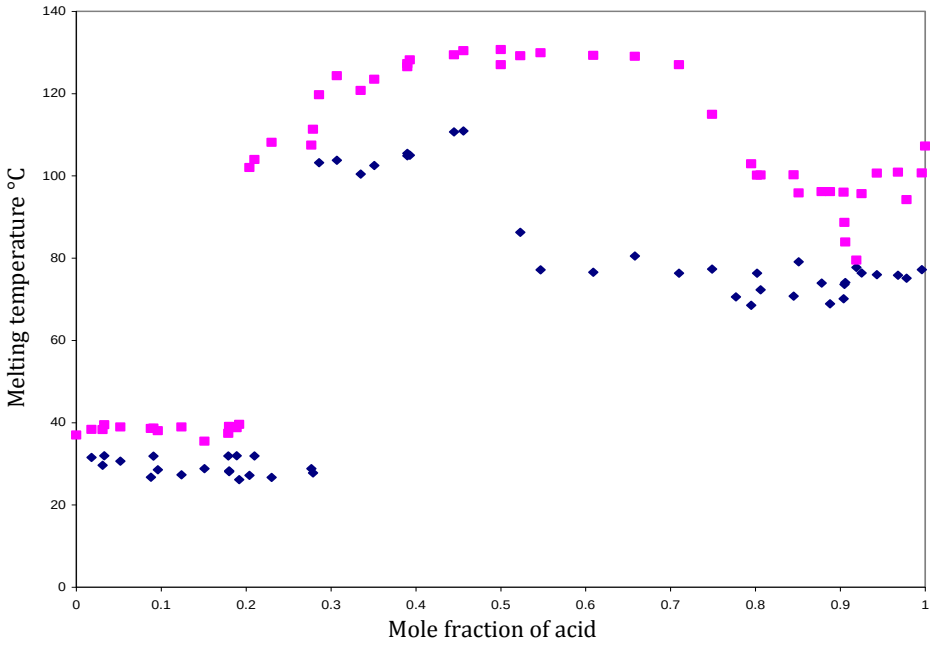

FIGURE 48- BINARY PHASE DIAGRAM OF EPHEDRINE AND PIMELIC ACID SHOWING EXPERIMENTALLY DETERMINED POINTS. PINK MARKERS DENOTE THE LIQUIDUS AND BLUE DATA POINTS SHOW THE EUTECTIC.

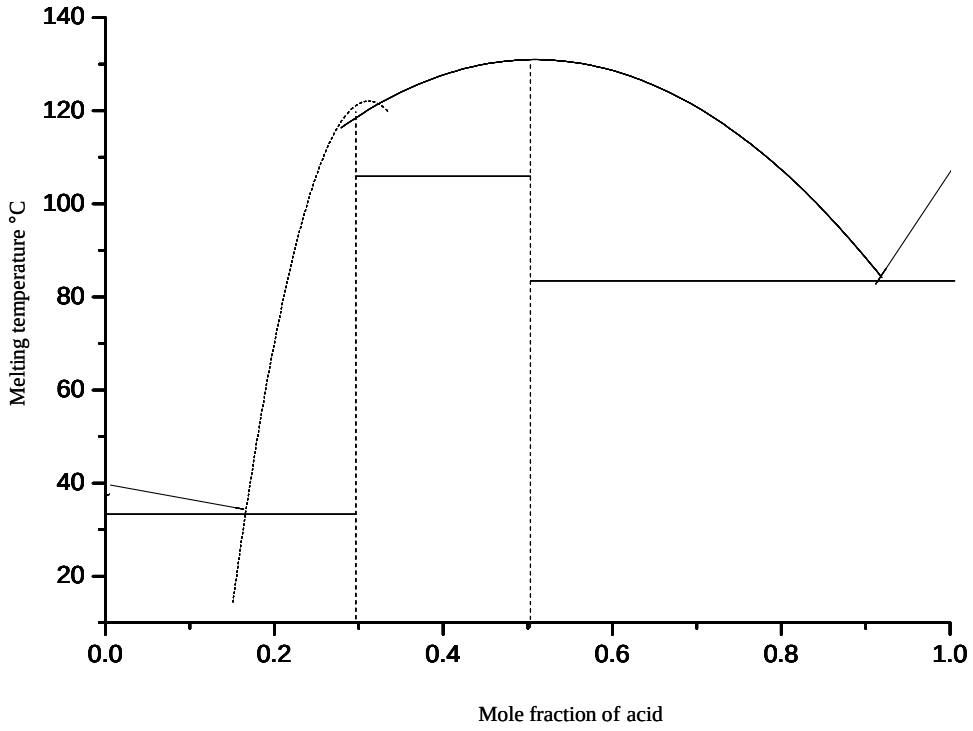

FIGURE 49- THE BINARY PHASE DIAGRAM OF EPHEDRINE AND PIMELIC ACID. THE SOLID HORIZONTAL LINES SHOW EUTECTIC LINES AND CURVES SHOW THE MELT TEMPERATURES OF THE COMPONENTS AND SALTS IN CONTACT WITH ONE ANOTHER. THE DASHED CURVED LINE IS THE SUSPECTED 2:1 SALT REGION. THE LINES ARE USED TO GUIDE THE EYE AND ARE NOT BEST FIT LINES.

From the binary phase diagram it is apparent that there is definitely a 1:1, and potentially a 2:1, salt in this system. The area thought to represent the 2:1 salt is small and positioned between 0.2 and 0.3 mole fraction of acid. The 1:1 salt region is large and dominates the phase diagram. The eutectic lines agree with this interpretation of the liquidus curve, providing greater evidence for the presence of the 2:1 region. The eutectic for the ephedrine/2:1 region is at ~30 °C, the eutectic for the 2:1/1:1 salts is ~105 °C and the eutectic for the 1:1 salt/pimelic acid region is at ~80 °C.

Having established that both a 1:1 and a 2:1 salt are present in the system by using simple grinding experiments, the determination of the binary phase diagram now appears to confirm this. Grinding offered a quicker alternative to a full determination and may provide valuable information when moving into solution based work. This may not be the case for all systems. The crystal structures are

needed for categorical identification and analysis of bonding and physical properties.

4.4 SALT FORMATION FROM SOLUTION

In order to confirm the existence of the 1:1 and 2:1 salts categorically, single crystals of both were grown from solution and analysed by single crystal XRD (sXRD).

4.4.1 SOLUTION SPECIATION

From the speciation diagram (Figure 50) it can be seen that the two pK_a values of the acid are both greater than 2 pK_a units from that of the base (in water). The general rule $\Delta pK_a > 2$ for salt formation is satisfied[1]. It is evident that at a pH of around 8, ephedrine is present exclusively as the anion and pimelate as the doubly deprotonated carboxylate. This pH region is where a 2:1 salt would be accessible. Upon lowering the pH to 5 the maximum proportion of singly deprotonated carboxylate is present, meeting the requirements of a 1:1 salt. The aqueous solubilities of the acid and base are similar. This suggests that the ternary phase diagram will potentially show two regions of salt formation occurring at 2:1 and equimolar ratios, the latter showing congruent dissolution.

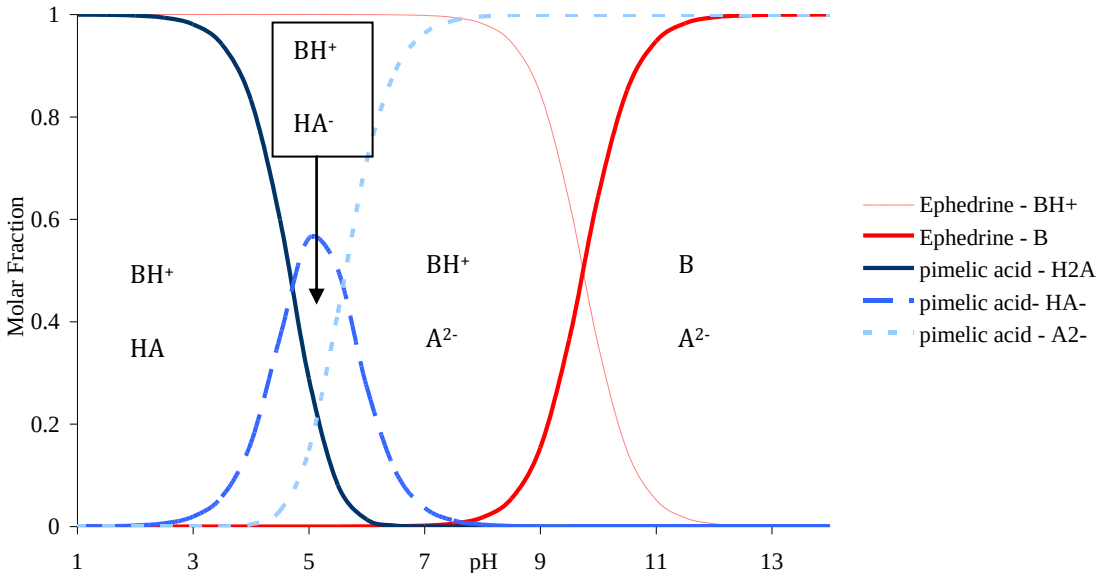

FIGURE 50- SPECIATION DIAGRAM OF EPHEDRINE AND PIMELIC ACID IN WATER SHOWING THE SPECIES PRESENT IN EACH REGION

4.4.2 CRYSTAL GROWTH

Single crystals and powders of the 1:1 salt were easily produced by slow evaporation of an aqueous solution. Typically, a solution was prepared by stirring a mixture of ephedrine, pimelic acid and water at 298 K for one day to give a solution 1 molar in both components. This solution was then left to evaporate slowly until crystals had formed after approximately 3 days. The pH of this solution was measured as 5.36. Using the speciation diagram it was concluded that pH adjustment was not necessary.

In applying a similar approach to the preparation of single crystals of the 2:1 salt (by adding 0.02 mol [3.304 g] ephedrine to 0.01 mol [1.602 g] pimelic acid at 298 K and adding 10 drops of water from a pipette) it was found that the resulting solutions were highly viscous. This viscosity increased upon evaporation, eventually solidifying to a clear mass rather than forming single crystals. PXRD and FTIR of this product showed it to be crystalline and identical to the material produced by grinding the 2:1 ratio of components. As an alternative method, cooling crystallisations were employed using identical compositions, but leaving the solutions to crystallise at 283 K. After a period of 3 weeks large needle like crystals had grown and were extracted for structural analysis by single crystal XRD.

4.4.3 BULK SAMPLE FORMATION

Attempts to prepare bulk samples of the 2:1 salt proved equally as difficult as single crystal formation. The results described above suggested that evaporative crystallisation would not be an effective means of preparing powder samples. A cooling method only worked at very low temperatures for an extended time and large product yields were never obtained. A drown-out method using acetone was tested. Addition of 50 mL of acetone to 100 mL of the 2:1 salt solution caused solids to precipitate. This suggested that acetone acts as an anti-solvent for this system and is shown in Figure 51. A sample of the 2:1 salt solution was placed on a microscope slide and a couple of drops of acetone added. The images in Figure 51 were taken using an optical microscope (instrumentation described in Section

2.4.4) over a matter of seconds. Crystallisation using acetone as an anti-solvent is a very fast process. The solid samples formed were found not to be phase pure, but a mixture of the 2:1 salt with solid ephedrine by pXRD and DSC.

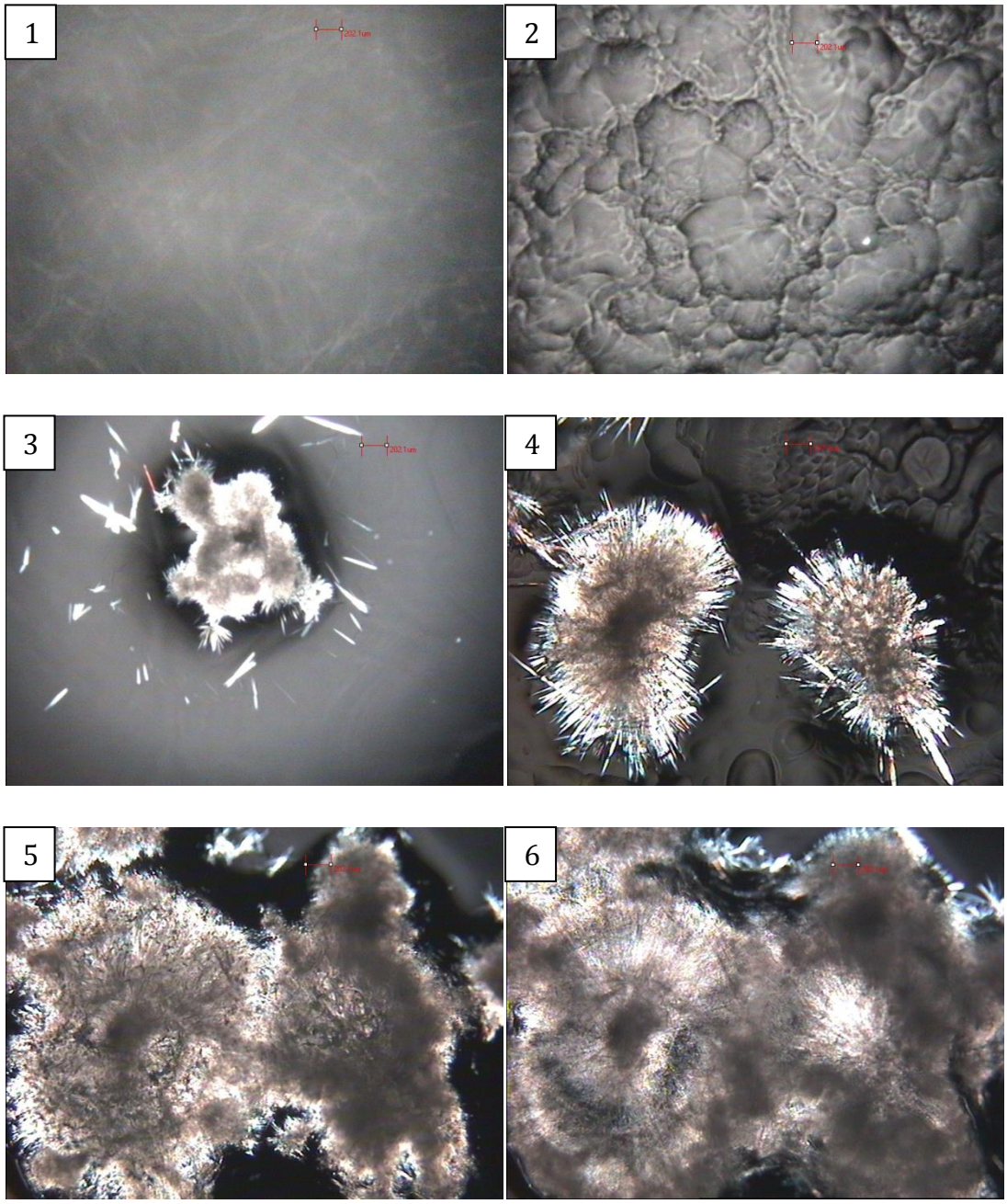

FIGURE 51- IMAGES 1-6 SHOWING THE ADDITION OF ACETONE TO A SOLUTION OF 2:1 EPHEDRINE PIMELATE. IMAGE 1- 2:1 EPHEDRINE PIMELATE SOLUTION BEFORE ACETONE ADDITION. IMAGE 2- AFTER INITIAL ACETONE ADDITION. IMAGE 3- INITIAL CRYSTAL GROWTH. IMAGE 4- CRYSTAL GROWTH. IMAGE 5- FURTHER CRYSTAL GROWTH. IMAGE 6- TOTAL CRYSTALLISATION.

In a continuation of this work, an experiment was conducted to see if larger crystals could be grown when the contact area with acetone was limited. This was conducted using an experiment based on the set-up used for the well-known Kofler experiment[15], first discussed by Lehmann in 1888[16]. The 2:1 salt solution was trapped between a microscope slide and coverslip. Acetone was then introduced and was 'sucked' under the coverslip, providing an interface with the solution. Crystals were shown to grow at the interface of the 2:1 ephedrine pimelate solution and acetone (Figure 52). From this interface experiment crystallisation only appears to occur at the points of contact and does not induce nucleation throughout the salt solution. From Figure 53 it is apparent that continued addition of acetone to the system causes some of the sample to dissolve. It has not been possible to determine a reliable process for the formation of larger samples of the pure 2:1 salt in this way.

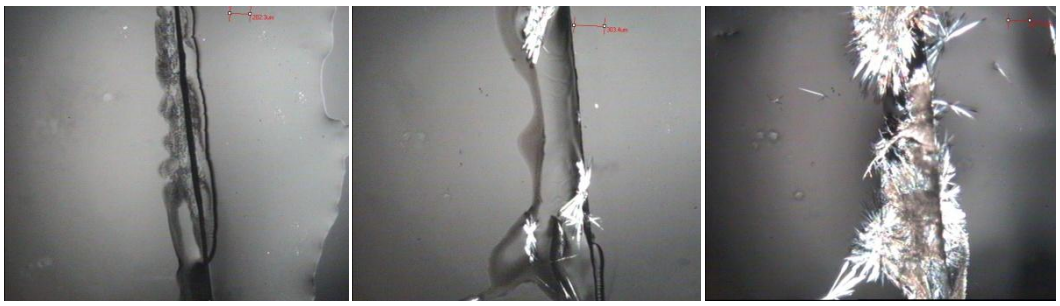

FIGURE 52- THE GROWTH OF THE 2:1 AT THE INTERFACE BETWEEN THE 2:1 EPHEDRINE PIMELATE SOLUTION AND ACETONE.

FIGURE 53- THE EFFECT OF CONTINUED ADDITION OF ACETONE ON THE CRYSTALLINE PRECIPITATE OF 2:1 SALT FROM ACETONE USE AS AN ANTI-SOLVENT.

4.4.4 SALT CRYSTAL IMAGES

Images of the 1:1 salts were collected using an optical microscope and an example is shown in Figure 54. Images of the crystals of the 2:1 salt are not available due to the small number of crystals grown. The collection of single crystal XRD data was deemed to be of greater importance.

FIGURE 54- IMAGES OF 1:1 EPHEDRINE PIMELATE CRYSTALS GROWN FROM WATER

4.4.5 CRYSTALLOGRAPHIC DATA

Table 9 shows the details of the single crystal X-ray diffraction experiments used to determine the crystal structures of both the 1:1 and 2:1 salts. The R factors (or residual electron density) are a measure of the accuracy of the data collected. For the 1:1 salt a 'good' value of 0.037 and for the 2:1 salt an acceptable value of 0.067 was attained.

TABLE 10- CRYSTALLOGRAPHIC DATA TABLE FOR 1:1 AND 2:1 EPHEDRINE PIMELATE

System	**1:1 Ephedrine Pimelate**	**2:1 Di-ephedrine Pimelate**
Empirical Formula	C10H16NO.C7H11O4	2(C10H16NO).C7H10O4
M_r (g/mol)	325.40	490.63
Temperature (K)	100	100
Radiation Type, Wavelength	MoK$_\alpha$, 0.71073	MoK$_\alpha$, 0.71073
Crystal System, Space Group	Monoclinic, P2$_1$	Monoclinic, P2$_1$

a,b,c (Å)	5.5353 (5), 13.4324 (13), 11.9231 (11)	13.9597 (10), 5.8075 (4), 16.7716 (15)
α, β, γ (°)	90, 101.574 (9), 90	90, 91.690 (3), 90
Volume (Å^3)	868.48 (14)	1359.10 (18)
Z, Density (mg.m^{-3})	2, 1.244	2, 1.199
Absorption Coefficient (mm^{-1})	0.09	0.08
Crystal Size (mm)	1.00 x 0.4 x 0.25	0.3 x 0.1 x 0.05
$\theta_{min}/\theta_{max}$	3.8° /26.4°	3.1° /26.0°
Reflection Collected/Unique (R_{int})	0.034	0.096
Data/ restraints/ parameters	2887/1/316	2658/1/324
Goodness of fit on F^2	0.93	1.05
Residual Electron Density	0.037	0.067
Final R indices [I>2σ(I)] R1/wR2	0.037/0.079	0.067/0.176

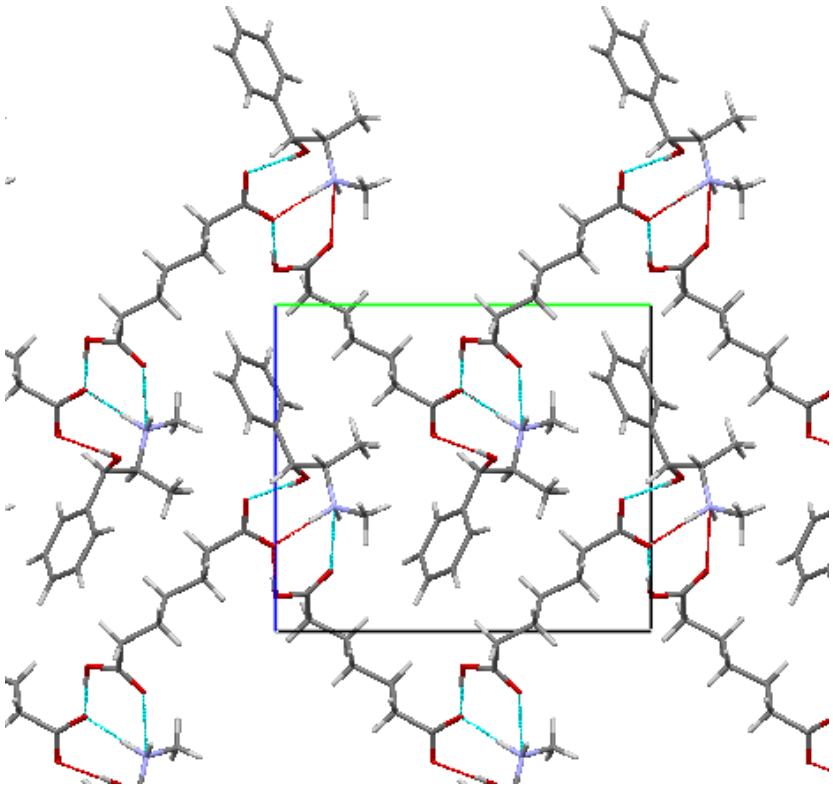

FIGURE 55- 1:1 SALT STRUCTURE VIEWED DOWN A

In the 1:1 salt (Figure 55) the pimelic acid molecules utilise hydrogen bonding interactions (O…O distance 2.61 Å) between protonated and deprotonated carboxylic acid groups on adjacent molecules to create an infinite chain running along the b axis. To this acid chain are bound ephedrine molecules. One is held via two hydrogen bonds in which the protonated amine nitrogen interacts with the carbonyl (O…N distance 2. 84 Å) of one acid and the carboxylate of a second (O…N distance 2.695 Å). The second ephedrine is held through a hydroxyl – carboxylate hydrogen bond (O…O distance 2.66 Å). These ephedrine molecules then interact again to the adjacent chain through identical hydrogen bonds such that they form π stacks with a C…H distance of 3.29 Å. There are no inter ephedrine hydrogen bonds in this structure. None of the structures previously determined by Collier *et al*[17] had this bonding motif.

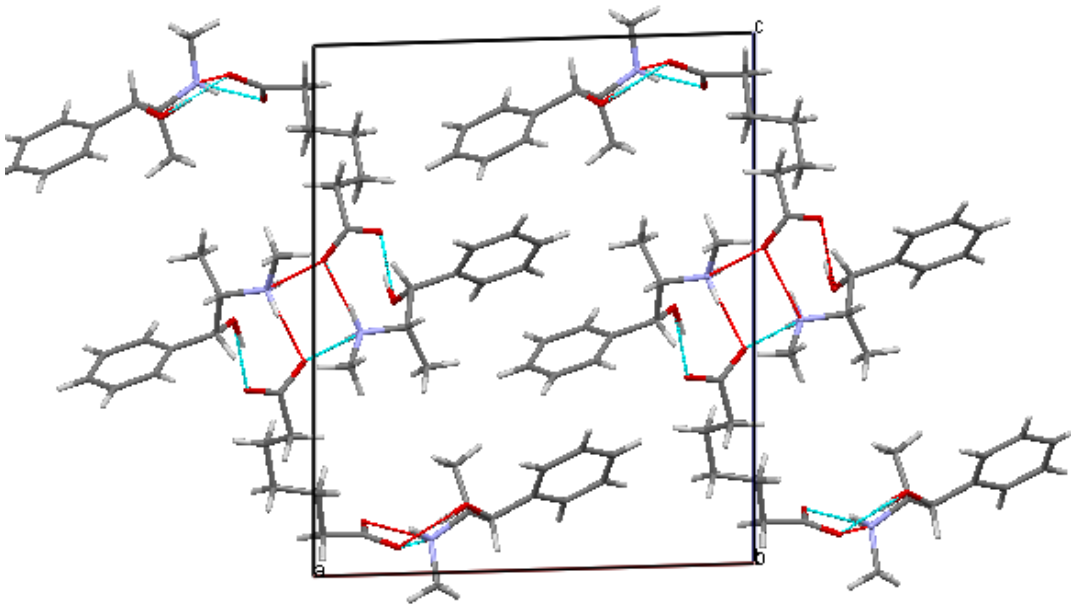

FIGURE 56- 2:1 SALT STRUCTURE VIEWED DOWN B

The 2:1 salt is quite different in that both ends of the deprotonated acid chain bind separate ephedrine molecules and there are no acid-acid interactions. In one carboxylate group, one oxygen forms a bifurcated hydrogen bond to amines on two separate ephedrine molecules (O…N 2.75 and 2.80 Å) while the second interacts with the hydroxyl of a third ephedrine molecule. The other carboxylate binds only two ephedrine molecules through O…N and O…O interactions (2.63 Å) to one

molecule and O...N (2.77 Å) to the second. Four ephedrine molecules and two pimelic acid molecules bond in this manner to form tetramer units as shown in Figure 66, which are then interlinked via π - π bonding (3.45 Å). These units are the same as those seen in other ephedrine salts and are further considered in Section 4.6.1 below.

Knowledge of the crystal structures allowed confirmation that the new products formed by grinding were the salts grown from solution. The melting temperatures were determined to be identical using DSC. From DSC experiments the temperature and enthalpy of fusion determined from the ground 1:1 salt sample matches that of the salt formed from solution. PXRD patterns of the new products match the simulated powder patterns of the single crystals (Figure 57). Due to the difficulties in forming the 2:1 salt from solution and limited sample mass, it was not possible to perform any thermal analysis on the sample.

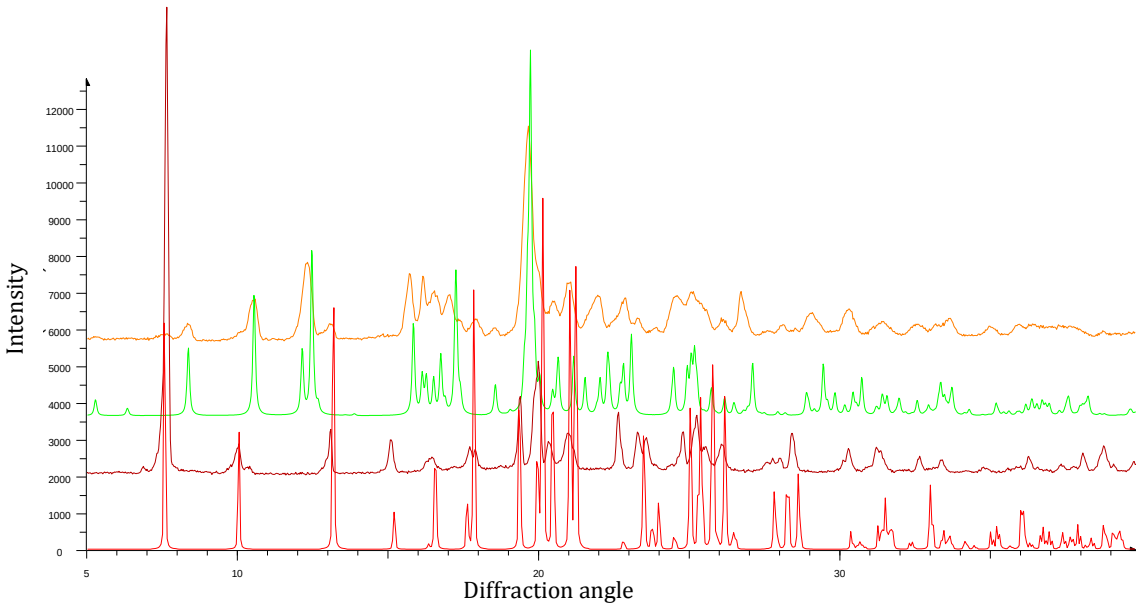

FIGURE 57- PXRD PATTERNS OF THE GROUND SALT SAMPLES AND SALT PATTERNS SIMULATED FROM THE KNOWN CRYSTAL STRUCTURES. SIMULATED 1:1 SALT (RED), GROUND 1:1 SALT (BROWN), SIMULATED 2:1 (GREEN) AND GROUND 2:1 SALT (ORANGE).

4.5 TERNARY PHASE DIAGRAM

The ternary phase diagram of this system was determined to assess the size and shape of the pure phase regions. This provides information on the compositions

that could be used to form the salts or pure components with a high degree of accuracy.

4.5.1 METHOD

To measure the ternary phase diagram different known ratios of pure acid and base were dissolved in known volumes of solvent and the solubility determined. By analysing the solid phase/phases remaining in solution once equilibration had been achieved and using the lever rule (Section 2.2.3), the liquidus curve could be plotted on the ternary phase diagram.

4.5.1.1 THE LEVER RULE

An example data table for ternary phase diagram calculations is given below in Table 11.

TABLE 11- DATA TABLE USED TO CALCULATE LIQUID PHASE COMPOSITION FOR A SINGLE PHASE SOLID REGION. ALL VALUES ARE IN MOLE FRACTION

	Ephedrine	**Pimelic Acid**	**Water**
Starting Composition	0.225	0.025	0.75
Solid Phase	1	0	0
Liquid Phase	x	y	0.863

Using the lever rule x and y in Table 11 can be calculated using,

$$\frac{x_C^i}{x_B^i} = \frac{x_C^l}{x_B^l}$$ EQUATION 4:1

Therefore for the data in the above table,

$$0.75/0.025 = 0.863/y$$

$$y = 0.029$$

$$x = 1- (0.863+0.029)$$

$$x = 0.108$$

TABLE 12- DATA TABLE USED TO CALCULATE LIQUID PHASE COMPOSITION FOR A TWO COMPONENT SOLID PHASE REGION. ALL VALUES ARE IN MOLE FRACTION

	Ephedrine	**Pimelic Acid**	**Water**
Starting Composition	0.14	0.193	0.667
Solid Phase	0.5	0.5	0
Liquid Phase	X	y	0.760

Using the lever rule x and y in Table 12 can be calculated using,

$$x_{AB}^{l} = x_{AB}^{i} - (x_{AB}^{s} \times (x_{C}^{l} - x_{C}^{i})) \qquad \text{EQUATION 4:2}$$

Therefore using the data in the above table,

$$x = 0.14 - (0.5 * (0.760 - 0.667))$$

$$x = 0.0935$$

$$y = 1 - (0.760 + 0.0935)$$

$$y = 0.146$$

4.5.2 EXPERIMENTAL TERNARY PHASE DIAGRAM

Figure 58 shows the ephedrine-pimelic acid-water phase diagram measured at 296 K in which there are 7 regions and 2 eutectic points. Region 1 is the undersaturated liquid region in which all compositions are single phase liquids. In all other regions (2-7) solid phases exist in equilibrium with solutions. Regions 2, 4, 5 and 7 are pure solid phases of either starting materials (ephedrine or pimelic acid) or salts (either 1:1 or 2:1) in contact with their saturated solutions. Regions 3 and 6 are areas where mixtures of solid phases exist (ephedrine and 1:1 salt, and 1:1 and pimelic acid respectively). These solid phases are in equilibrium with solutions of different invariant compositions (exact compositions only estimated in the 2:1 region of this ternary phase diagram due to issues with the solubility determination discussed below).

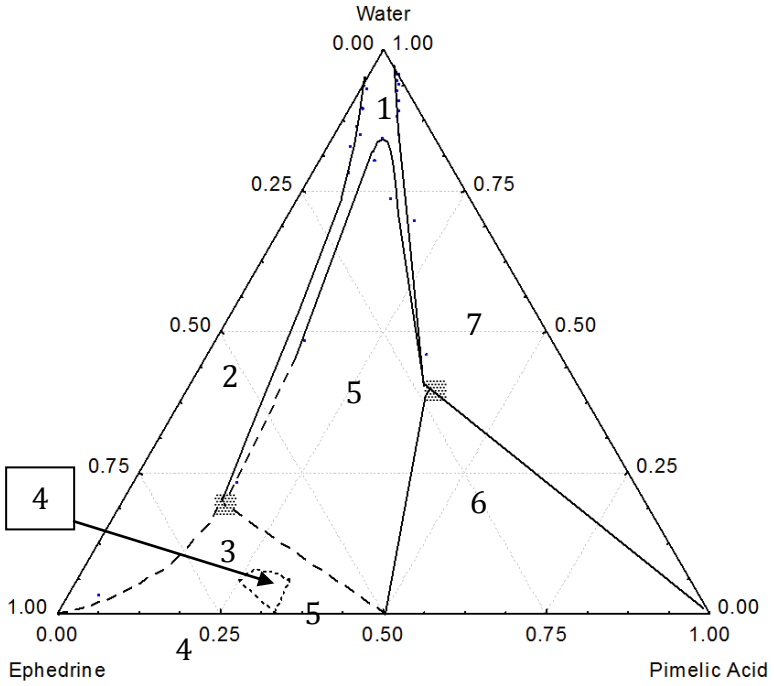

FIGURE 58- THE EXPERIMENTAL TERNARY PHASE DIAGRAM OF EPHEDRINE-PIMELIC ACID-WATER AT 23°C IN MASS %. (1) LIQUIDUS, (2) EPHEDRINE + LIQUID, (3) EPHEDRINE + 1:1 SALT+ LIQUID, (4) METASTABLE 2:1 SALT (5) 1:1 SALT + LIQUID, (6) 1:1 SALT AND PIMELIC ACID + LIQUID, (7) PIMELIC ACID + LIQUID. ▒ INDICATES UNCERTAINTY OF THE EUTECTIC POSITIONS.

The pH values of the salt solutions, Table 13, are naturally within the pH regions required for salt formation at the given stoichiometries. This eliminates the need to alter the pH. Tabulated alongside are the solubilities at 23 °C.

TABLE 13- SOLUBILITY AND pH DATA AT 23 °C FOR PURE PHASES

Compound	**Solubility (wt %)**	**pH of solution**
Ephedrine	5.39	11.20
Pimelic acid	4.65	2.25
1:1 salt	16.00	5.36
2:1 salt	~80	~9

Ephedrine hemihydrate accounts for half of the ephedrine sample added. This was a concern as the presence of water would change the ternary composition and the

mole fractions would be different to those used to plot Figure 12. In order to assess the extent of the effect, the sample that would be most greatly affected was assessed. This was the sample in the ephedrine pure phase region with the highest solubility. It was assumed that the ephedrine sample used was approximately 50 % anhydrous and 50 % hemihydrate. The assumption is for every gram of ephedrine, the composition is half of a gram of anhydrous and half a gram of hemihydrated ephedrine. By altering the original masses used for composition calculations, the amounts of ephedrine and water in the starting ternary composition could be adjusted. From this the liquid phase compositions could be recalculated and the result checked against that plotted on the ternary phase diagram. The difference between the two values was very small and the error was calculated as less than 1 %. In conclusion the presence of ephedrine hemihydrate was deemed negligible in the ternary system. The final product was known to be pure anhydrous ephedrine (determined by pXRD analysis), as the sample was placed in a desiccator.

4.5.3 GVS ANALYSIS OF SALTS

To shed further light on any hydration effects, GVS experiments were performed on powdered samples of both salt forms. For the 1:1 salt a mass increase of 1.8 % was observed at humidity levels up to 80 % with all water being lost on the reduction of humidity levels back to zero (Figure 59). According to Table 4 in the Section 2.4.5 this makes the sample hygroscopic.

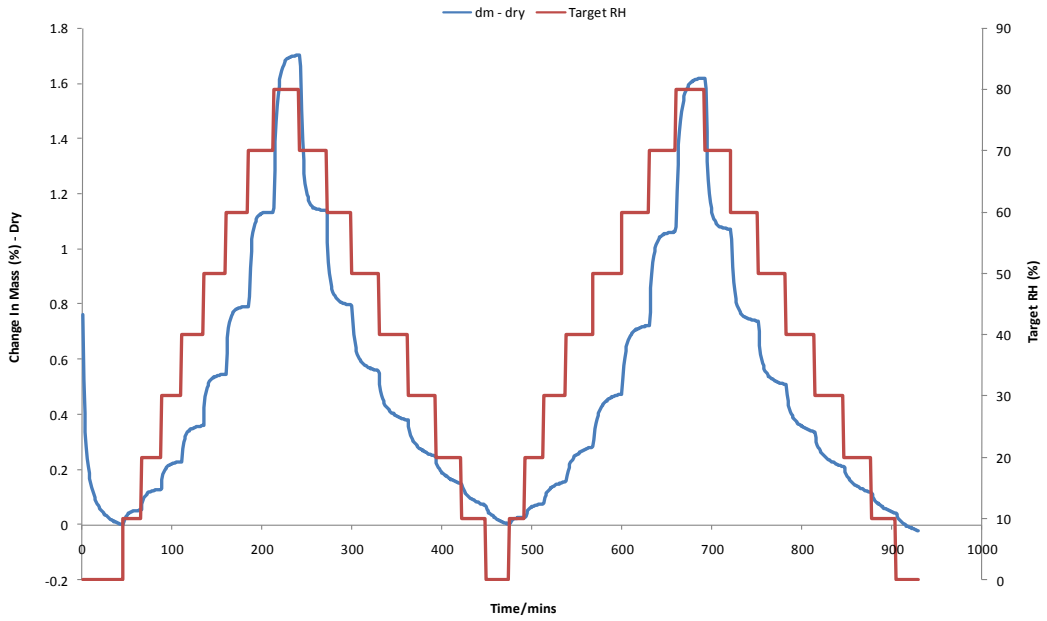

FIGURE 59- GVS OF 1:1 EPHEDRINE PIMELATE AT 24.6 °C

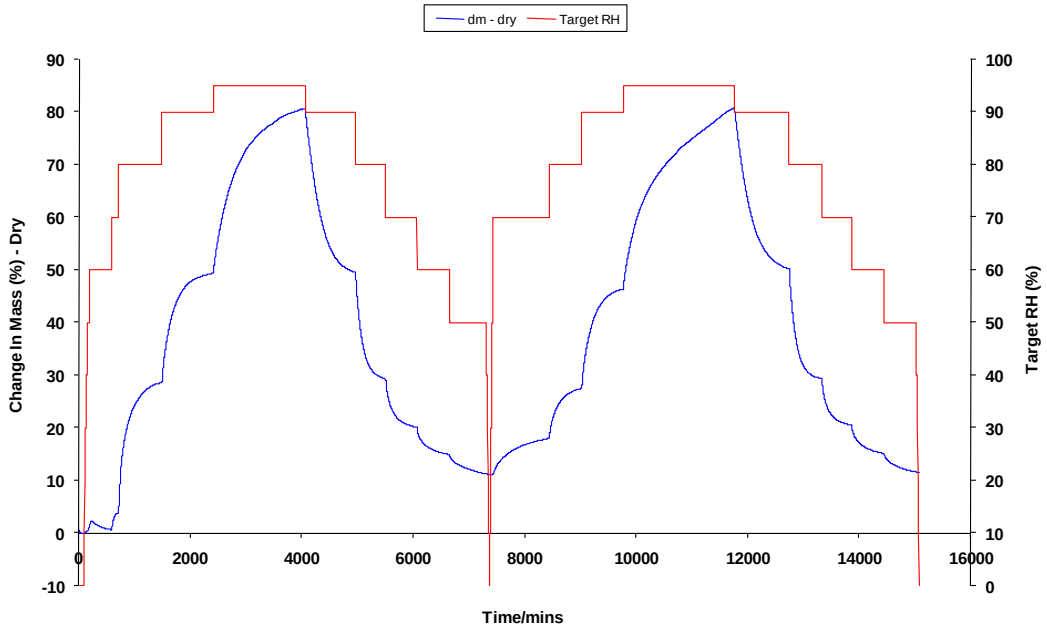

FIGURE 60- GVS OF 2:1 EPHEDRINE PIMELATE AT 24.6 °C.

The 2:1 salt undergoes a change of mass around 70 % at a humidity of 95 % with 10 % water remaining when the humidity levels were reduced to 0 % (Figure 60). This makes the sample deliquescent (Table 4). Since the sample was a liquid during the cycle and solid at the end of the GVS run this suggests the possible

formation of a crystalline trihydrate. To replicate this experiment on a larger scale a powdered sample of the 2:1 salt (formed by grinding) was placed in a desiccator with a saturated solution of potassium sulphate (used to provide a humidity of 96.3 %). The resulting liquid sample was then placed in the laboratory and evaporation allowed to naturally occur. The resulting solids were analysed by pXRD, DSC and IR.

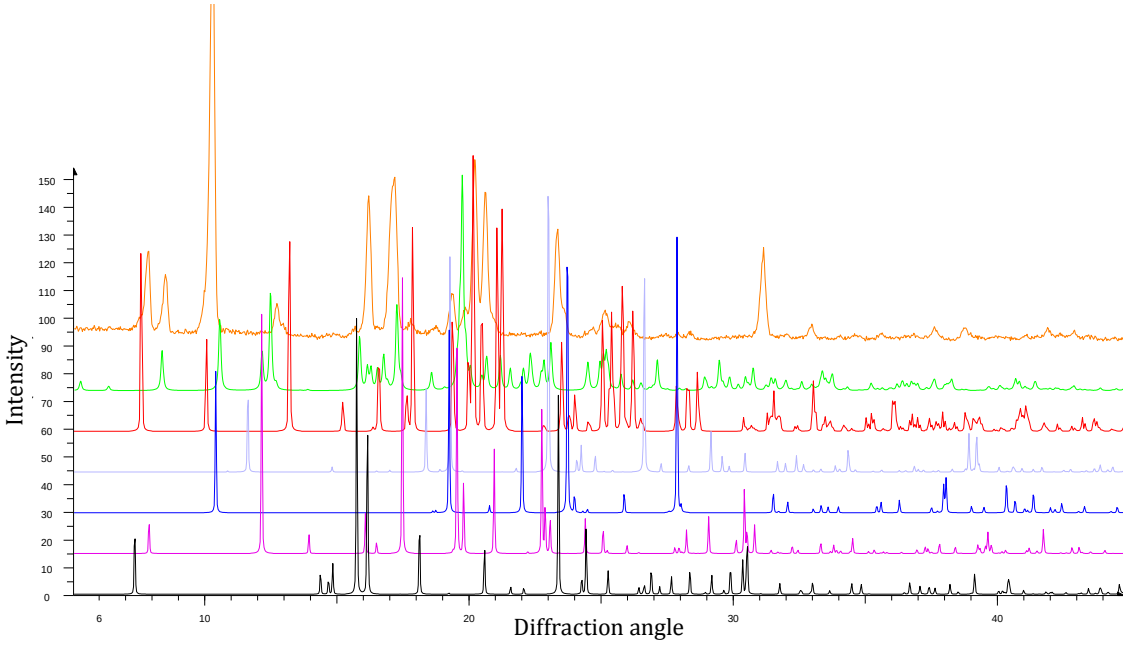

FIGURE 61- SIMULATED PXRD PATTERNS OF EPHEDRINE HEMIHYDRATE (BLACK), ANHYDROUS EPHEDRINE (PINK), β PIMELIC ACID (BLUE), α PIMELIC ACID (LILAC), 1:1 SALT (RED) AND 2:1 SALT (GREEN) COMPARED TO THE NEW SUSPECTED HYDRATE (ORANGE).

The pXRD pattern is different to that of the pure 2:1, with extra peaks at 13 and 21 2θ, however it was found that the different peaks all corresponded to those observed for the 1:1 salt. This suggests that rather than forming a hydrate, as suspected from the GVS, the sample is partially converting to the mono protonated salt (Figure 61).

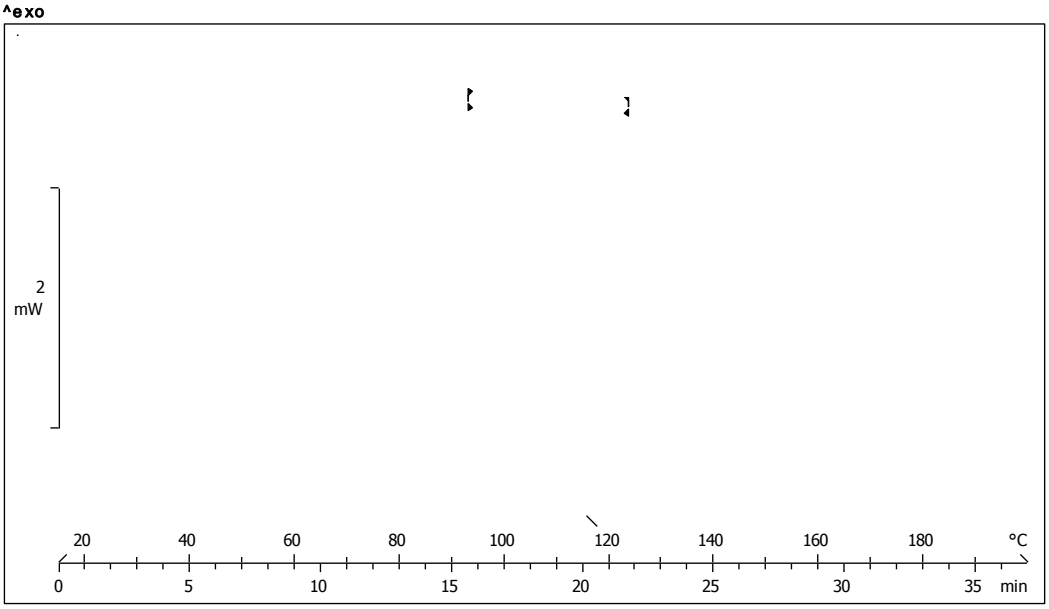

FIGURE 62-DSC OF 2:1 SALT AFTER 5 DAYS IN AN ENVIRONMENT WITH 96.3 % HUMIDITY, ALLOWED TO RECRYSTALLISE IN THE LABORATORY FOR 5 DAYS AFTERWARDS.

The DSC of the 2:1 salt after 5 days in a 96.3 % humidity environment recrystallised in the laboratory (Figure 62) shows a shoulder to a large, relatively sharp peak starting around 100 °C. This peak suggests water is being removed before the main body of the endotherm peaks just below 120 °C, the melt of the 2:1 salt. The melting temperature of the 2:1 salt may have been depressed by the water acting as an impurity. Therefore, from DSC evidence, a conversion is not apparent. However, the lower melt of the 2:1 salt may be obscuring the melt of any 1:1 salt present.

The IR spectrum recorded (Figure 63) appears to be the same as the pure 2:1 salt. There is no evidence of the 1:1 also being present. It appears that any water in this amine salt would be able to interact with the complex hydrogen bonding process already present, even if the water molecules are well separated from each other. This possibly would explain the extra relative band strengths of the ~2700 and 2500 cm^{-1} bands[18]. However, this result is not conclusive and it is felt that the pXRD results offer more detailed information.

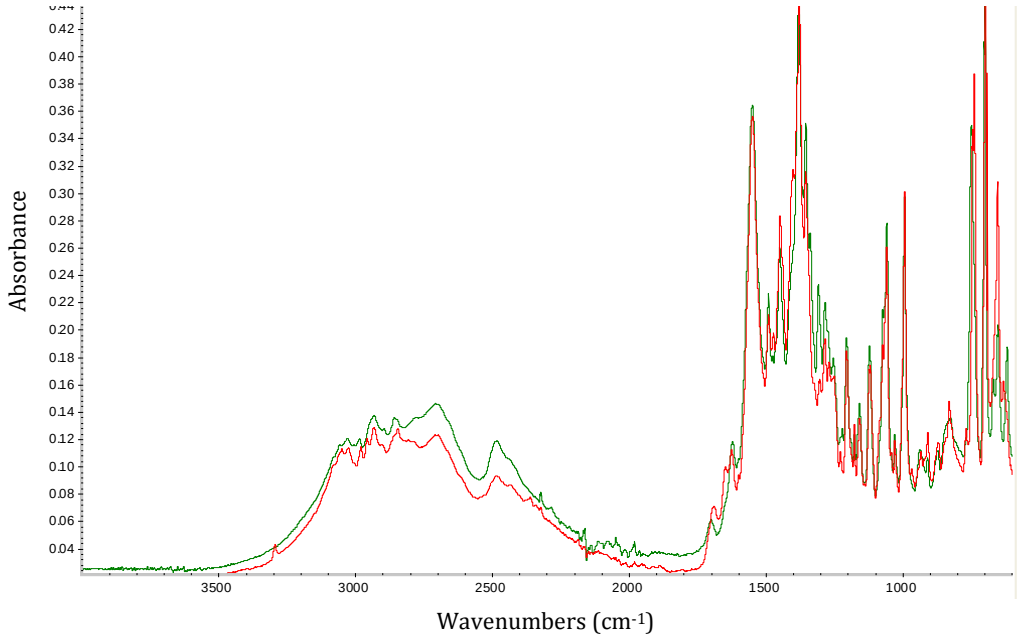

FIGURE 63- IR SPECTRA OF PURE 2:1 SALT (RED) AND 2:1 SALT AFTER 5 DAYS IN AN ENVIRONMENT WITH 96.3 % HUMIDITY (GREEN), ALLOWED TO RECRYSTALLISE IN THE LABORATORY FOR 5 DAYS.

In order to further assess the stability of the 2:1 salt, the recrystallised humidity sample was reanalysed three months later. Due to instrument failure, DSC analysis was not possible, but from the pXRD an even greater similarity with the simulated 1:1 salt pattern is now apparent (Figure 64), with all peaks accounted for.

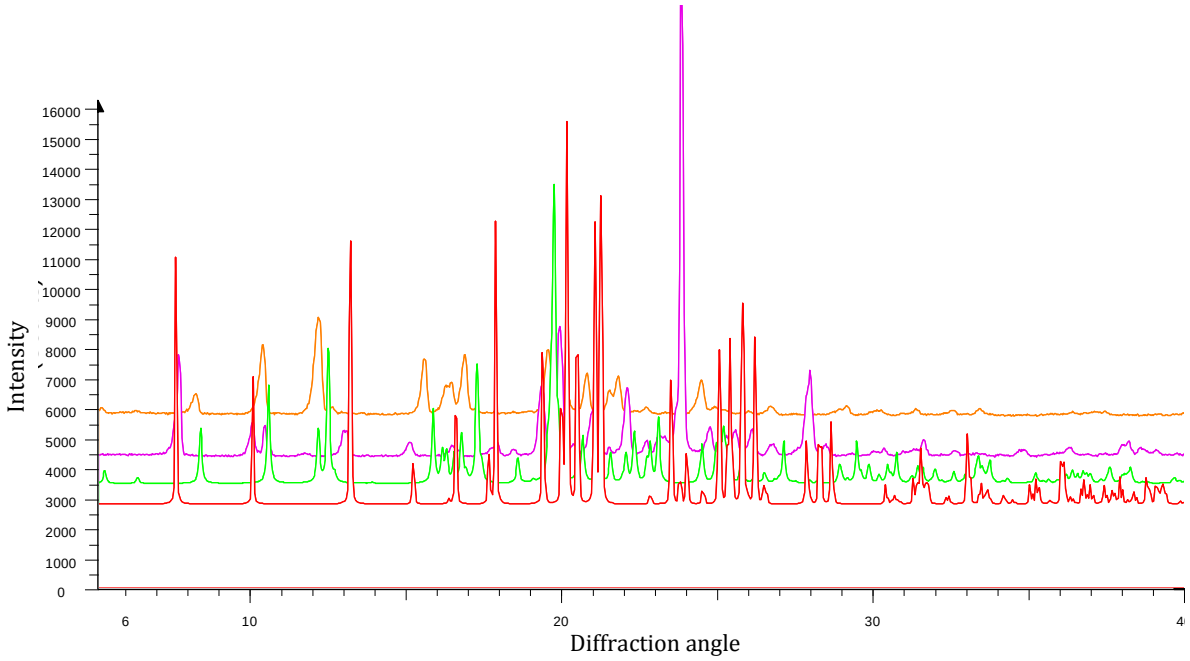

FIGURE 64- SIMULATED PXRD PATTERNS OF 1:1 SALT (RED) AND 2:1 SALT (GREEN) COMPARED TO THE PREVIOUSLY SUSPECTED HYDRATE (ORANGE) AND THE SAME SAMPLE LEFT FOR THREE MONTHS (PINK).

From the IR spectrum the carbonyl has become entirely mono, rather than di-, protonated (Figure 65) with three distinct peaks observable due to the carbonyl stretching bands at 1694, 1624 and 1547 cm^{-1}. Therefore from IR the 1:1 salt appears to have wholly formed.

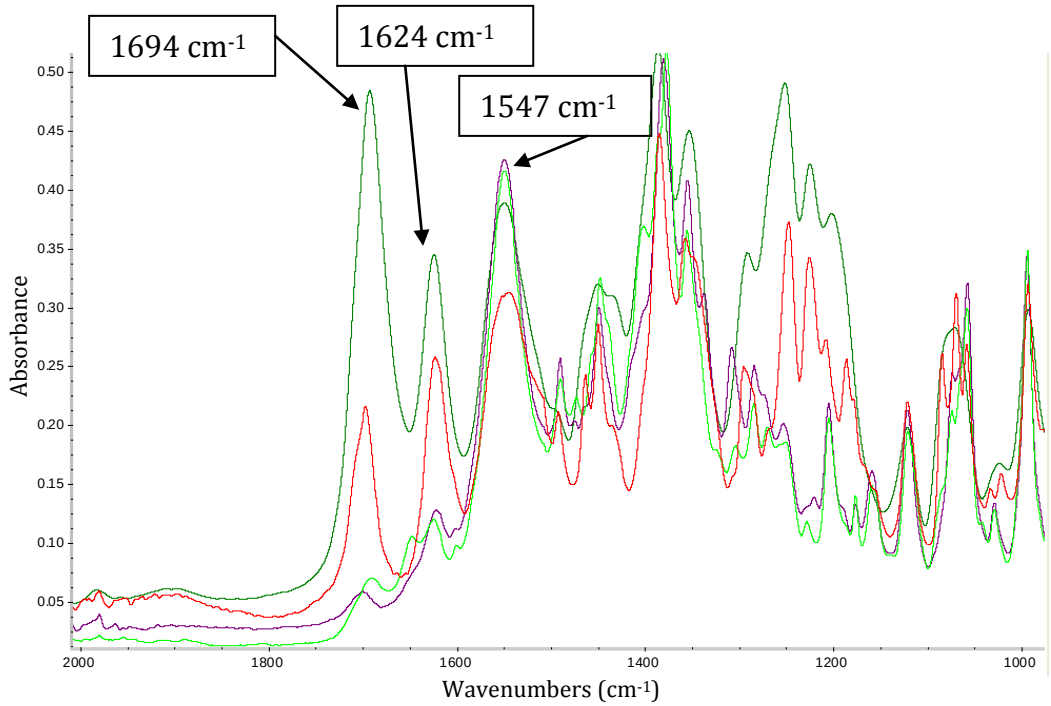

FIGURE 65- IR SPECTRA OF PURE 1:1 SALT (RED), PURE 2:1 (BRIGHT GREEN) AND 2:1 SALT AFTER 5 DAYS IN AN ENVIRONMENT WITH 96.3 % HUMIDITY ALLOWED TO RECRYSTALLISE IN THE LABORATORY FOR 5 DAYS ANALYSED IMMEDIATELY (DARK GREEN) AND AFTER 3 MONTHS (PURPLE)

It can be concluded that after three months the potentially hydrated sample entirely converted from the 2:1 to the 1:1 salt. When the 2:1 salt is kept at ambient humidity it is stable, however if any 1:1 salt is present in the 2:1 sample, as it appears happens after deliquescence and recrystallisation, it eventually all converts.

From studying the ternary phase diagram above in Figure 58 this result can be rationalised. The 1:1 salt is significantly less soluble than the 2:1 salt, hence will crystallise out of solution first. After the difficulties encountered in the formation of the 2:1 salt its inability to recrystallise after deliquescing is unsurprising. When left at ambient conditions in the laboratory the 2:1 salt has shown good stability,

not converting to the less soluble 1:1 salt. It appears that at humidity levels greater than ambient conversion to the 1:1 salt occurs.

4.6 DISCUSSION

4.6.1 COMMON EPHEDRINE SALT BONDING MOTIF

The tetramer motif is the same as that seen in the adipate (Figure 67), glycolate (Figure 68) and malonate (Figure 69) salts (1:1 ratio) reported by Collier *et al*[17]. The (-)-(1R,2S)-Ephedrine ent-2-methoxycarbonyl-cyclohex-4-ene-1-carboxylate[19] (Figure 70) found on the CSD also shows the same motif. Interestingly all of the salts subjected to GVS (adipate, glycolate and malonate) proved to be deliquescent, as is the 2:1 salt. The deliquescence of the 2:1 salt is discussed in more detail in Section 1.5.3 above.

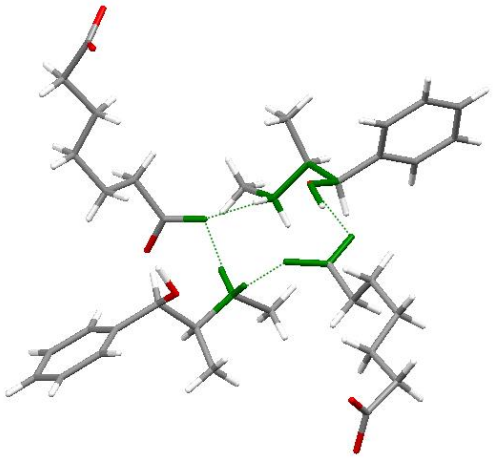

FIGURE 66- 2:1 SALT STRUCTURE SHOWING HYDROGEN BONDING MOTIF (HIGHLIGHTED IN GREEN) COMMON TO A NUMBER OF EPHEDRINE SALTS.

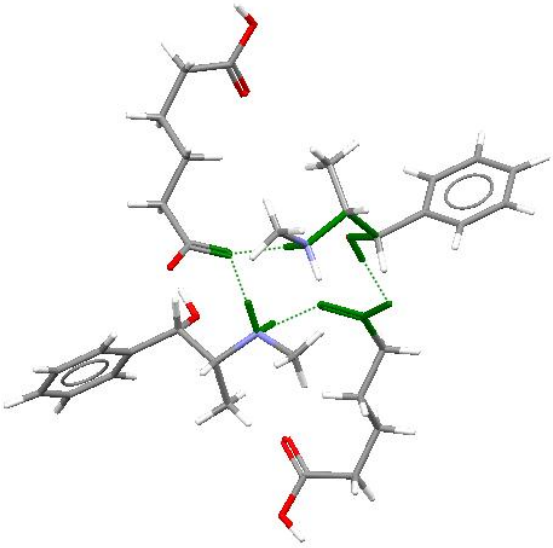

FIGURE 67- (-)-(1R,2S)-EPHEDRINE ADIPATE WITH THE COMMON HYDROGEN BONDING MOTIF HIGHLIGHTED IN GREEN

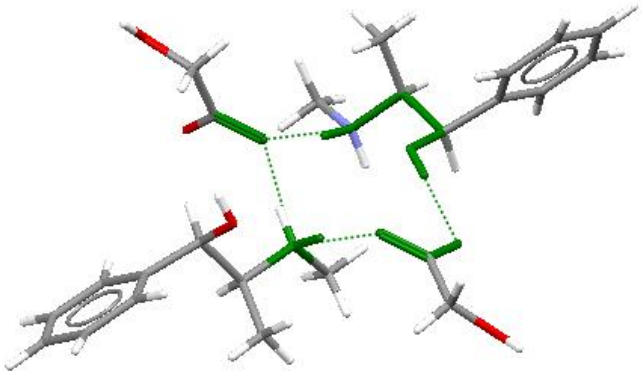

FIGURE 68- (-)-(1R,2S)-EPHEDRINE GLYCOLATE WITH THE COMMON HYDROGEN BONDING MOTIF HIGHLIGHTED IN GREEN

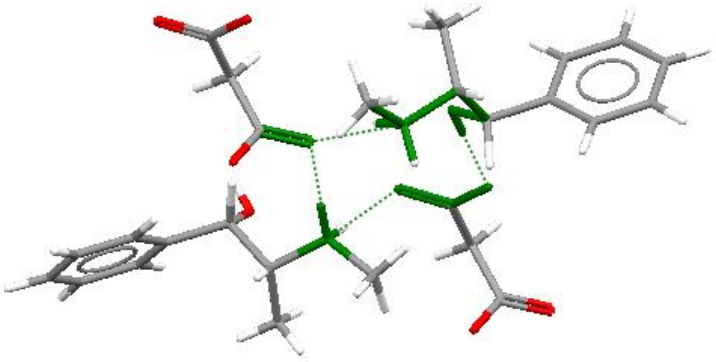

FIGURE 69- (-)-(1R,2S)-EPHEDRINE HEMIKIS(MALONIC ACID) WITH THE COMMON HYDROGEN BONDING MOTIF HIGHLIGHTED IN GREEN

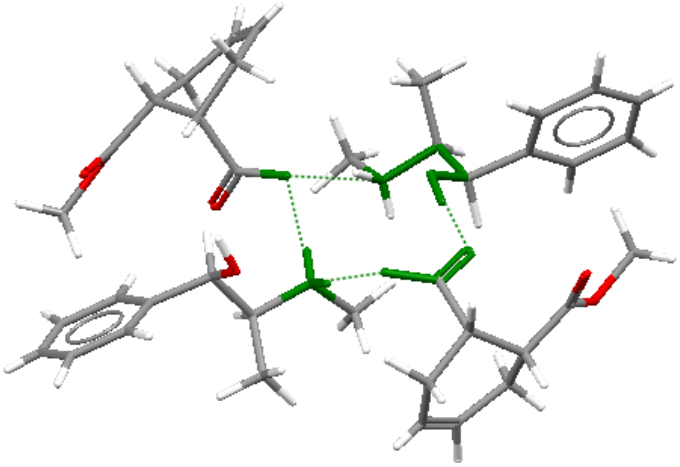

FIGURE 70- (-)-(1R,2S)-EPHEDRINE ENT-2-METHOXYCARBONYL-CYCLOHEX-4-ENE-1-CARBOXYLATE WITH THE COMMON HYDROGEN BONDING MOTIF HIGHLIGHTED IN GREEN.

4.6.2 PIMELIC ACID CONFORMATION

The conformations of the pimelic acid molecules in the two salts are both different to the conformations in two of the polymorphs of the pure acid (all shown in Figure 71). There are only three other examples of pimelate salts in the CSD and none show the same conformations of pimelic acid as are found in these two ephedrine salts (Figure 72). The 1:1 salt shows rotation at the sixth carbon in the chain and the 2:1 salt shows a twist at the fifth carbon. Of the other known salts all but one contain pimelic acid in straight chain conformations like those of the pure

acid polymorphs. Only bis (DL-arginium) pimelate hemihydrate (blue in Figure 72) shows another conformation with the twist at carbon four. As the 2:1 salt has a very high solubility it was suspected that the chains may be in an especially high energy/unfavourable conformation, however by visual inspection, this does not seem to be the case, as shown in Figure 71 and Figure 72.

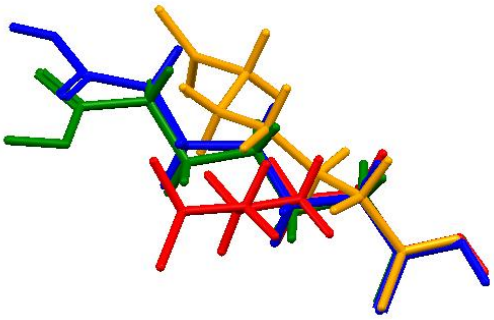

FIGURE 71- THE DIFFERENT CONFORMATIONS OF PIMELIC ACID IN α PIMELIC ACID (GREEN), β PIMELIC ACID (BLUE), 1:1 SALT (RED) AND 2:1 SALT (YELLOW)

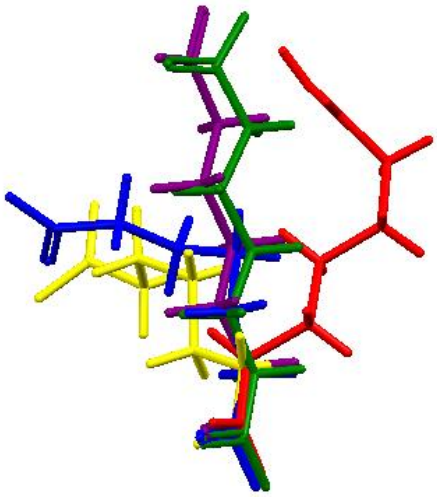

FIGURE 72- THE DIFFERENT CONFORMATIONS OF PIMELIC ACID IN DL-LYSINIUM HEMIPIMELATE ETHANOL SOLVATE HYDRATE (GREEN), BIS(DL-ARGININIUM) PIMELATE DIHYDRATE (BLUE), POTASSIUM HYDROGEN PIMELATE (PURPLE), 1:1 SALT (RED) AND 2:1 SALT (YELLOW)

4.6.3 EPHEDRINE CONFORMATION

Ephedrine can exist in two conformations, folded or extended[17]. The extended conformation is the most common and lower energy state[20, 21], and is displayed in the pure ephedrine, ephedrine hemihydrate and both salt structures discussed in

this thesis. Salts of ephedrine previously formed, including the majority published by Collier *et al*[17], appear to favour the extended conformation. Therefore, the high solubility of the 2:1 salt cannot be assigned to the conformation of the ephedrine molecules.

4.6.4 TERNARY PHASE DIAGRAMS OF EPHEDRINE SALTS

It is worth noting that Figure 58 shows a markedly different shape from those ternary phase diagrams hypothesised in the 2007 paper by Black *et al*[1]. In this publication the ternary phase diagram showing the congruent dissolution of adipic acid and ephedrine shows a much more 'orthodox' shape. As both adipic and pimelic acids are dicarboxylic acids it would be a reasonable assumption that the phase diagrams may look similar. Therefore, this highlights the need to fully determine a phase diagram rather than just predicting its shape from the solubilities of the salt/cocrystal and the two pure components.

4.7 SUMMARY

From this chapter it can be seen that to fully understand a salt system a range of different analyses should be employed and appropriate phase diagrams determined. In this system, determination of the binary phase diagram gave useful support to the grinding experiments performed, providing strong evidence for the existence of both salts. The formation of the 2:1 salt by grinding was hypothesised to proceed via an amorphous intermediate, as crystallinity of the salt increased as the sample aged. This is unlike the 1:1 salt which was hypothesised to proceed via a submerged eutectic. Without the evidence gained from non-solution experiments the presence of the 2:1 salt may not have been discovered.

Discovery of the 2:1 salt from ternary systems was considerably complicated by the high aqueous solubility and led to an inability to determine a consistent preparative route. For the 1:1 salt a consistent preparative route was easily developed in the aqueous system. In determining the ternary phase diagram it became clear why the 2:1 salt was hard to form. From an industrial perspective the ternary phase diagram suggests the formation of the 2:1 salt is probably not worth

attempting. It also gives a good indication of the ratios of acid, base and solution that should be avoided due to issues with very high solubility.

Investigation into the potential for a hydrate provided evidence of the instability of the 2:1 salt at high humidity levels. It was determined by GVS that the 2:1 salt was deliquescent at high levels of humidity. When the sample recrystallised it was contaminated with some of the less soluble 1:1 salt, eventually leading to total conversion. From a pharmaceutical perspective this would be an important consideration, especially for marketing and safety in countries with humid climates.

The complimentary effects of pimelic acid and ephedrine on their solubilities in water are clearly highly non-ideal. Both components significantly increase the solubility of the other. Similar effects were reported by Lorenz *et al*[22] in aqueous racemic mandelic acid and Chadwick *et al*[23] in the benzophenone/diphenylamine/methanol system. In the present case, the solubility of the pimelic acid increases to over 50 wt% in the presence of ephedrine, due to the ionisation of the components. On the ephedrine rich side of the phase diagram regions 2, 3, 4 and 5 could not be fully determined, as indicated by the dashed lines. This was due to the extremely high aqueous solubility of both ephedrine and the 2:1 salt which lead to inherent problems of stirring and filtering solutions of high viscosity. These issues also hampered both equilibration and effective gravimetric analysis. The solubility of ephedrine rose to over 90 wt%, suggesting significant ionisation and potentially also complexation of the two components. This could not be determined with accuracy. Although this area of the phase diagram is poorly determined, further evidence for the metastability of the 2:1 salt comes from GVS analysis. The ideal ternary phase diagram determined and discussed in Section 6.1.3 reinforces this theory.

4.8 REFERENCES

1. Black, S. N., Collier, E. A., Davey, R. J. & Roberts, R. J. Structure, Solubility, Screening, and Synthesis of Molecular Salts. Journal of Pharmaceutical Sciences 96, 1053-1068 (2007).

2. Florey, K. Analytical Profiles of a Drug Substance (Academic Press, Inc., 1986).
3. Brown, H. C., McDaniel, D. H. & Haflinger, O. Determination of Organic Structures by Physical Methods (eds. Braude, E. A. & Nachod, F. C.) (Academic Press, New York, 1955).
4. Bahl, D. & Bogner, R. H. Amorphization of Indomethacin by Co-Grinding with Neusilin US2: Amorphization Kinetics, Physical Stability and Mechanism. Pharmaceutical Research 23, 2317-2325 (2006).
5. Bruneel, E., Verbist, K., Fiermans, L. & Hoste, S. Amorphization During Mechanical Grinding of Bi-Pb-Sr-Ca-Cu-O Ceramic Superconductors. Applied Superconductivity 4, 357-364 (1996).
6. Ikeya, T. & Senna, M. Amorphizationand Phase Transformation of Niobium Pentoxide by Fine Grinding. Journal of Material Science 22, 2497-2502 (1987).
7. Vucelic, D., Simic, D., Kovacevic, O., Dojcinovic, M. & Mitrovic, M. The Effects of Grinding on the Physiochemical Characteristics of White Sepiolite from Golesh. Journal of Serbian Chemical Society 67, 197-211 (2002).
8. Willart, J. F. & Deshamps, M. Solid State Amorphization of Pharmaceuticals. Molecular Pharmaceutics 5, 905-920 (2008).
9. Bellamy, L. J. in The Infrared Spectra of Complex Molecules (Chapman and Hall, London and New York, 1980).
10. Nguyen, K. L., Friscic, T., Day, G. M., Gladden, L. F. & Jones, W. Terahertz time-domain spectroscopy and the quantitative monitoring of mechanochemical cocrystal formation. Nature Materials 6, 206-209 (2007).
11. Guarrera, D., Taylor, L. D. & Warner, J. C. Molecular Self Assembly in the Solid State- The Combined Use of Solid-State NMR and Differential Scanning Calorimetry for the Determination of Phase Constitution. Chemistry of Materials 6, 1293-1296 (1994).
12. Davey, R. (ed. Hilton, A.) Fax concerning work on Melt Equilibria-DSC Scans (Blackley, Manchester, 1994).
13. Dyer, U. C., Henderson, D. A. & Mitchell, M. B. Application of Automation and Thermal Analysis to Resolving Agent Selection. Organic Process Research and Development 3, 161-165 (1999).

14. Burger, A., Henck, J.-O. & Dunser, M. N. On the Polymorphism of Dicarboxylic Acids:1 Pimelic Acid. Mikrochimica Acta 122, 247-257 (1996).
15. Kofler, L. & Kofler, A. Die Polymorphie des Nicotinsaureamids. Berichte der deutschen chemischen Gesellschaft (A and B Series) 76, 246-248 (1943).
16. Lehmann. MolecularPhysik 2, 398-415 (1877).
17. Collier, E. A., Davey, R. J., Black, S. N. & Roberts, R. J. 17 Salts of Ephedrine: Crystal Structures and Packing Analysis. Acta Cryst. B62, 498-505 (2006).
18. Dent, G. (ed. Cooke, C.) Email correspondance with University spectroscopy specialist (Manchester, 2010).
19. Gais, H.-J. & Lukas, K. L. Enantioselective and Enantioconvergent Syntheses of Building-Blocks for the Total Synthesis of Cyclopentanoid Natural-Products. Angewandte Chemie. International edition in English 23, 142-143 (1984).
20. Leusen, F. J. J. et al. Towards a Rational Design of Resolving Agents. Part III. Structural Study of Two Pairs of Diastereomeric salts of Ephedrine and a Cyclic Phosphoric Acid. Recl. Trav. Chim. Pays-Bas 110, 13-18 (1991).
21. Leusen, F. J. J., Noordik, J. H. & Karfunkel, H. R. Racemate Resolution via Crystallization of Diastereomeric Salts: Thermodynamic Considerations and Molecular Mechanics Calculations. Tetrahedron 49, 5377-5396 (1993).
22. Lorenz, H. & Seidel-Morgenstern. Binary and Ternary Phase Diagrams of Two Enantiomers in Solvent Systems. Thermochimica Acta 382, 129-142 (2002).
23. Chadwick, K., Davey, R. J. & Cross, W. How Does Grinding Produce Co-crystals? Insights from the Case of Benzophenone and Diphenylamine. Chem Comm 9, 732-734 (2007).

5 EPHEDRINE AND BENZOIC ACID

5.1 INTRODUCTION

In the grinding study discussed earlier in this work (Chapter 3- Solid State Methods in the Formation of Ephedrine Salts) a new product formed when ephedrine and benzoic acid were ground together. This product was partially crystalline and it was suspected that a route to producing the crystalline version of the amorphous salt previously formed[1] had been discovered. In Section 3.4.2.2 it was also observed that a new product formed on contacting the two components in both single crystal and powder states. The same effect was also observed with another ephedrine salt former, glycolic acid. The ephedrine and benzoic acid system is analysed here and the results applied to both systems. Although previous work has reported ephedrine benzoate grown from solution to be amorphous[2] this is re-examined here and reasoned modifications of the method applied.

5.2 BACKGROUND DATA

The physical properties of ephedrine and benzoic acid are presented in Table 14. Inspection of the table shows the pK_a values of the acid and the base to be greater than 2 units apart. This suggests salt formation is favoured in the system. The solubilities of the two components in this system are drastically different, with ephedrine over 20 times more soluble. This means the ternary phase diagram will be skewed and perhaps this will offer insight into why a crystalline salt has not previously been formed from aqueous solutions.

TABLE 14- EPHEDRINE AND BENZOIC ACID DATA

Physical Property	**Ephedrine**	**Benzoic Acid**
Melting Temperature (K)	310	393
Aqueous Solubility (wt %)	5.39[3]	0.27

pKa in Water	9.74[4]	4.19[5]
Enthalpy of Fusion (kJ mol^{-1})	11.96	16.70
Polymorphs	No	No
Hydrates	Hemihydrate	No

5.3 SALT SCREENING

Two techniques were used in the initial screen to determine whether salts of this system may occur. Firstly the two components were simply dry ground together using a pestle and mortar (see Section 3.2.2). The resulting powder was then analysed by pXRD, IR and DSC to assess whether salt formation had occurred. Secondly, following the work on the ephedrine pimelate salt, the binary phase diagram was explored using thermal analysis.

5.3.1 GRINDING

As was reported in Chapter 3, ephedrine and benzoic acid formed a new product when ground together at an equimolar ratio in the absence of solvent. This was characterised by pXRD, FTIR and DSC. The pXRD pattern is different to those of the pure components with some new unique peaks at 6° and 11° 2θ (Figure 73). The pattern also shows considerable amorphous character (from broadened pXRD peaks in Figure 73). The IR spectrum shows total ionisation of the carbonyl as the corresponding peak shifts from 1676 cm^{-1} to two peaks at 1590 cm^{-1} and 1545 cm^{-1} (Figure 74). This shift and split is characteristic of the change from the carbonyl of a carboxylic acid to the carbonyl of a carboxylate salt[6]. DSC (Figure 75) shows two small endotherms at 65 °C and 91 °C corresponding to melts/transformations in the system. The large, broad peak at around 240 °C is most likely indicative of a decomposition event. The melting temperatures of ephedrine (37 °C) and benzoic acid (128 °C) are unlikely to account for these endotherms. This implies a new product had been formed. The presence of two peaks raises the question of whether the new product is polymorphic. As with other ephedrine salts the sample does not recrystallise in the DSC pan upon cooling.

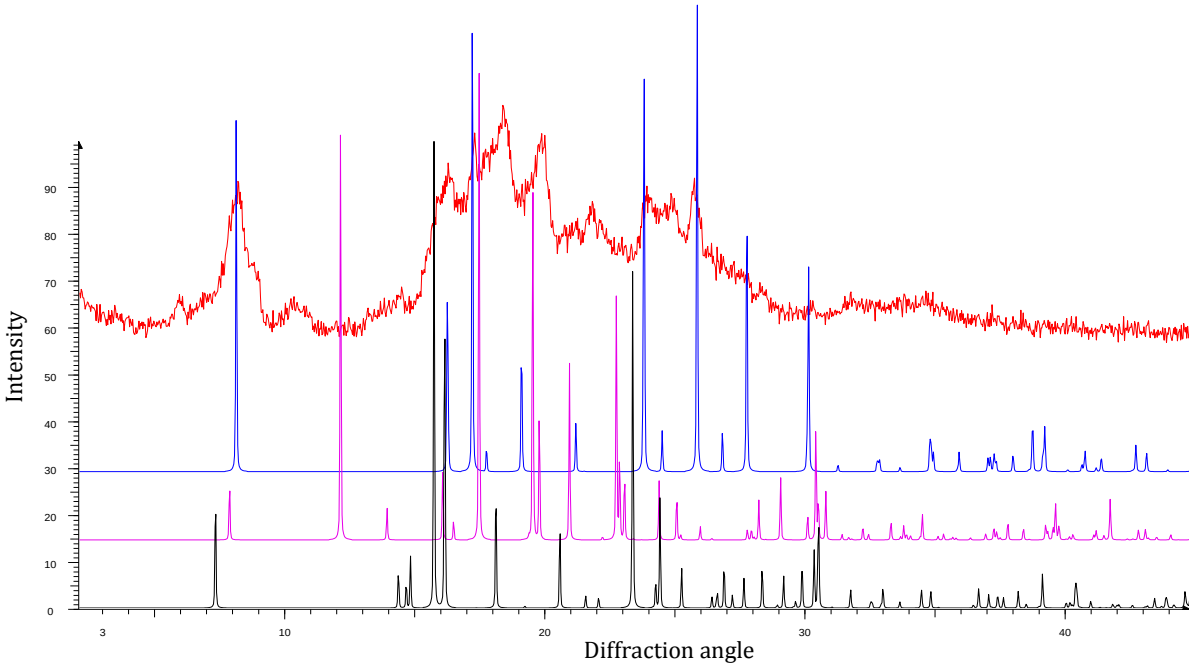

FIGURE 73- SIMULATED PXRD OF EPHEDRINE HEMIHYDRATE (BLACK), EPHEDRINE (PINK) AND BENZOIC ACID (BLUE) SHOWN WITH THE GROUND SAMPLE OF EPHEDRINE AND BENZOIC ACID (RED)

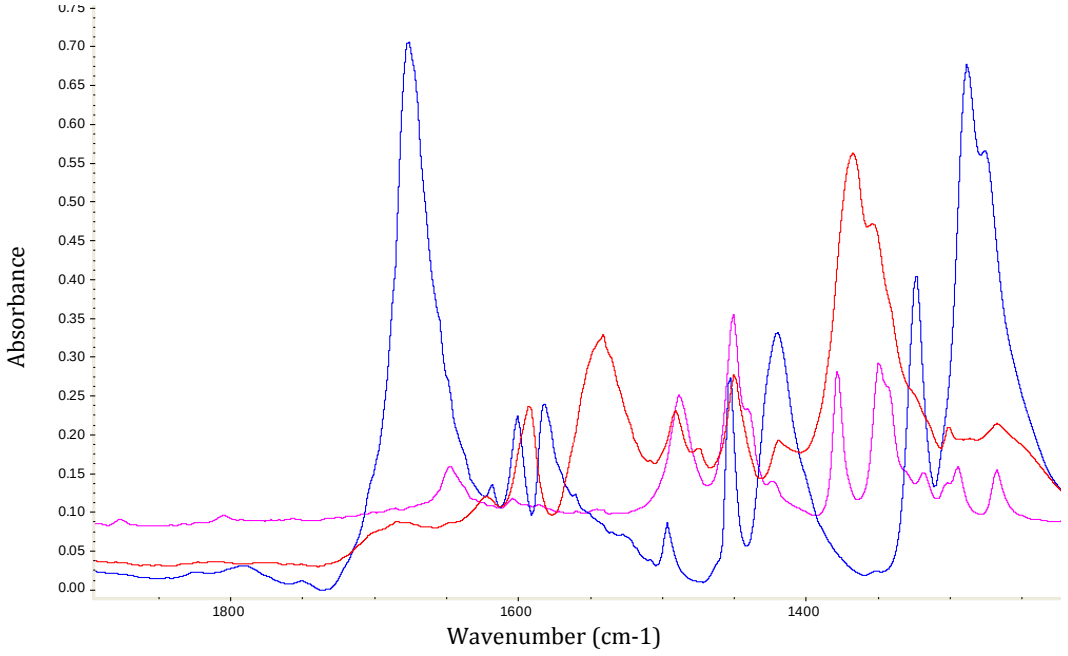

FIGURE 74- IR SPECTRA OF BENZOIC ACID (BLUE), EPHEDRINE (PINK) AND THE GROUND SAMPLE OF EPHEDRINE AND BENZOIC ACID (RED)

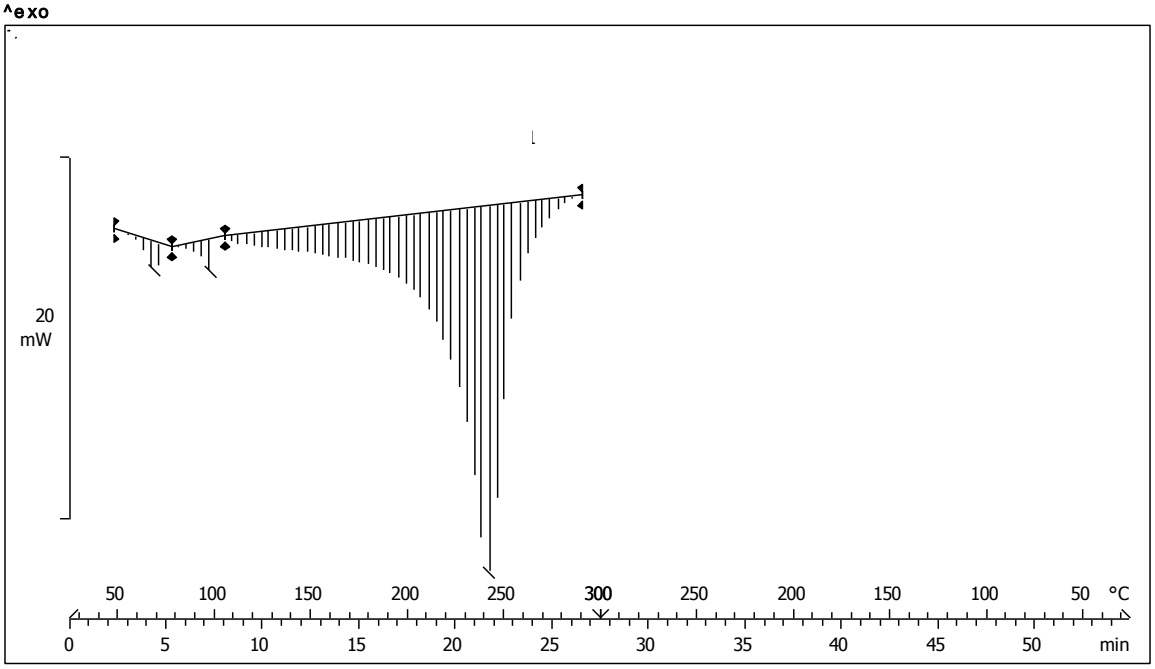

FIGURE 75- DSC OF GROUND EPHEDRINE AND BENZOIC ACID IN A 1:1 RATIO

5.3.2 EXPERIMENTAL BINARY PHASE DIAGRAM DETERMINATION

Determination of the binary phase diagram of this system using DSC was unsuccessful. DSC patterns were recorded for a range of compositions between pure ephedrine and pure benzoic acid. Assessment of the traces showed there to be major issues. On the ephedrine-rich side of the diagram the only endotherm visible in the DSC traces was that corresponding to the melt of ephedrine (36 °C), as shown in Figure 76. No salt peak was identified until a 1:1 ratio of acid to base had been used. PXRD of these samples showed that some salt formation occurs at the lower ratios of acid (Figure 77). For the benzoic acid rich side of the phase diagram, an endotherm relating to the melt of the salt was present (Figure 78). The peaks in the traces were also broad, an effect caused by the amorphous nature of the samples (Figure 78).

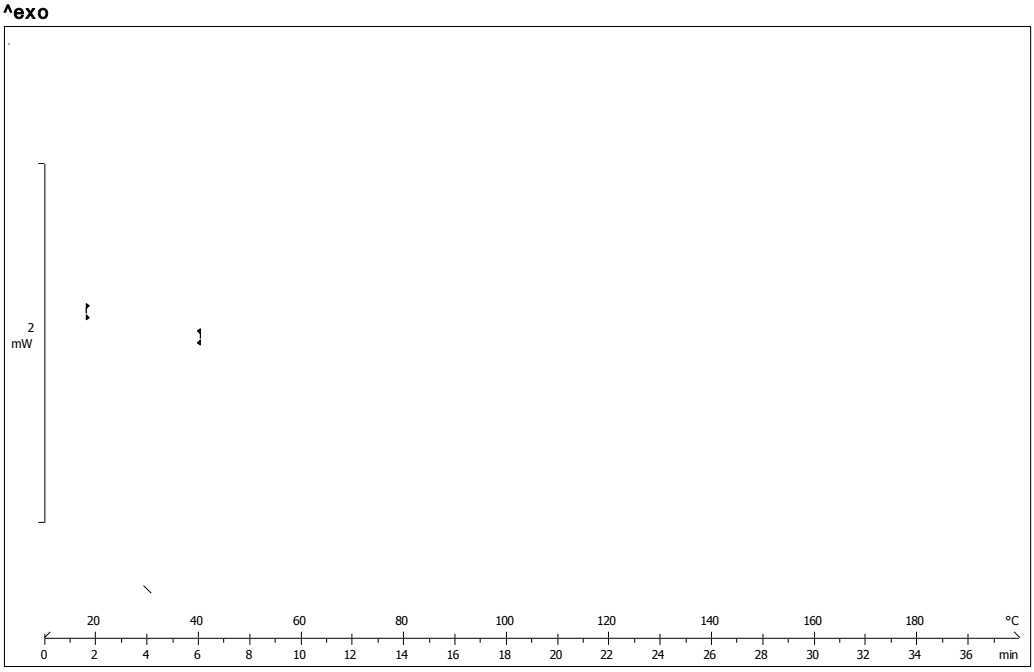

FIGURE 76- DSC OF EPHEDRINE (0.6 BY MOLE FRACTION) AND BENZOIC ACID (0.4 BY MOLE FRACTION)

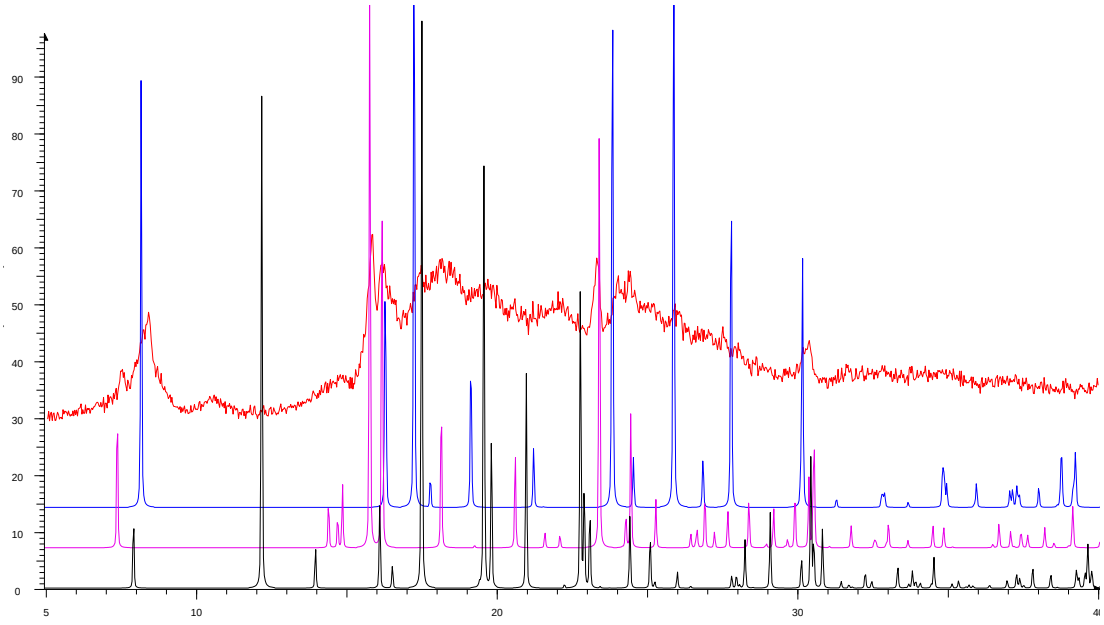

FIGURE 77- PXRD OF EPHEDRINE (PINK), EPHEDRINE HEMIHYDRATE (BLACK), BENZOIC ACID AND GROUND BENZOIC ACID AND EPHEDRINE (0.4 AND 0.6 BY MOLE FRACTION RESPECTIVELY)

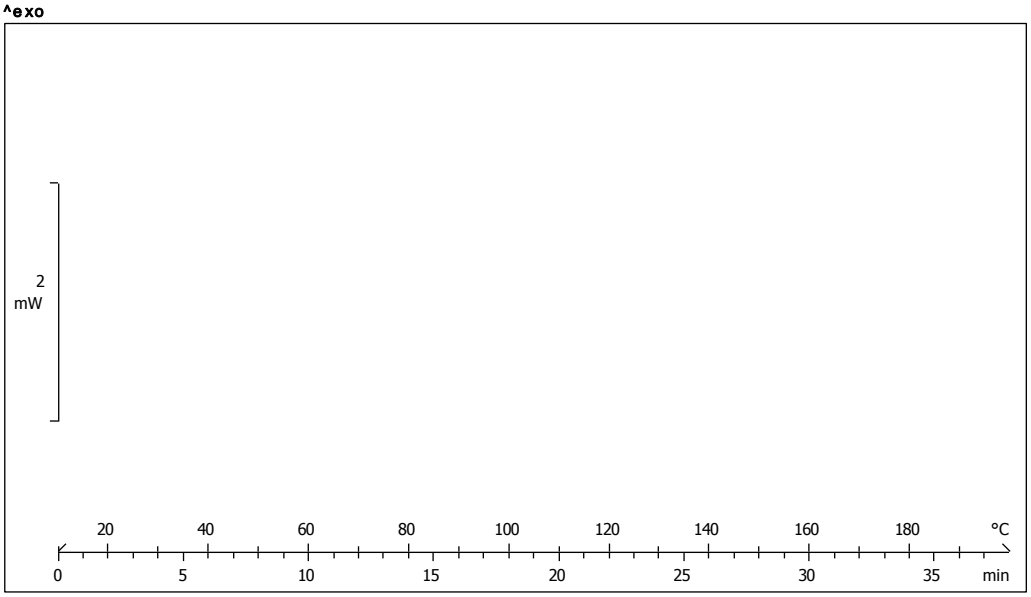

FIGURE 78- DSC TRACE OF GROUND EPHEDRINE AND BENZOIC ACID (0.3 EPHEDRINE AND 0.7 BENZOIC ACID BY MOLE FRACTION RESPECTIVELY)

In Chapter 4 (Ephedrine and Pimelic Acid) it became clear that the determination of a binary phase diagram was not imperative to understanding the phases accessible by solid state techniques. It only provided reinforcement for results already known from grinding. The grinding work completed was deemed to have provided sufficient information. The phase diagram for this system was not pursued as the grinding experiments appeared to have been successful in the formation of the salt.

5.3.3 CONTACT

As can be seen in Chapter 3 a new product also appears to grow from the contact of these two pure components. This can be seen again in Figure 79 and Figure 80, showing the growth of the new contact product with time at room temperature. This new product formed slowly over days and weeks rather than hours. Significant growth could still be observed after a month. Due to time restrictions a long term optical microscopy study from initial contact to total formation was not completed.

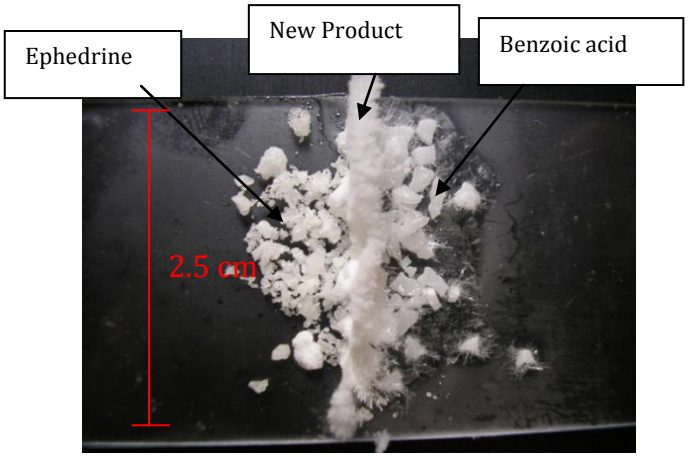

FIGURE 79- CAMERA IMAGE OF CONTACT BETWEEN EPHEDRINE (LEFT), BENZOIC ACID (RIGHT) AND THE NEW PRODUCT FORMED (CENTRE).

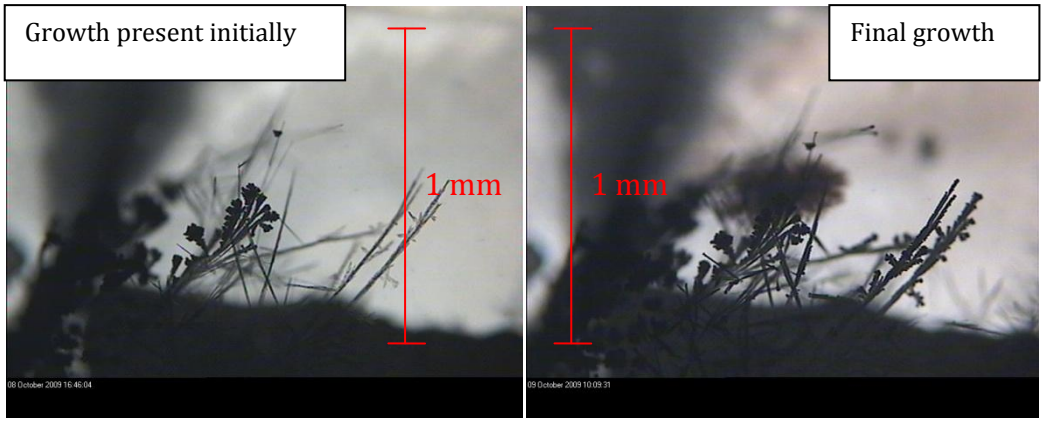

FIGURE 80- MICROSCOPE IMAGES OF NEW PRODUCT GROWTH FROM CONTACT OF EPHEDRINE AND BENZOIC ACID AT ROOM TEMPERATURE. IMAGES RECORDED OVER ONE DAY.

5.3.3.1 ANALYSIS OF THE NEW PRODUCT

Analysis of this new product proved difficult, as pure components were also still present in the sample. It can clearly be seen that the benzoic acid and ephedrine powders remain in Figure 79. The new fluffy, 'hair like' needles (seen more closely in Figure 80) had to be carefully separated. They also easily compressed leaving very little sample to work with. An IR spectrum, pXRD pattern and DSC trace were recorded in an attempt to characterise the sample.

The pXRD pattern of the sample formed by contact is very similar to that of the sample formed by grinding and both can be studied in Figure 81. The contact sample (green pattern in Figure 81) contains more crystalline and less amorphous material than the ground sample (red pattern in Figure 81). From the pattern of the contact sample, unique peaks can be more clearly observed, most notably at 6° and 11° 2θ. Due to the less amorphous nature of the contact sample other new unique peaks (at 7° and 22° 2θ) can now also be observed.

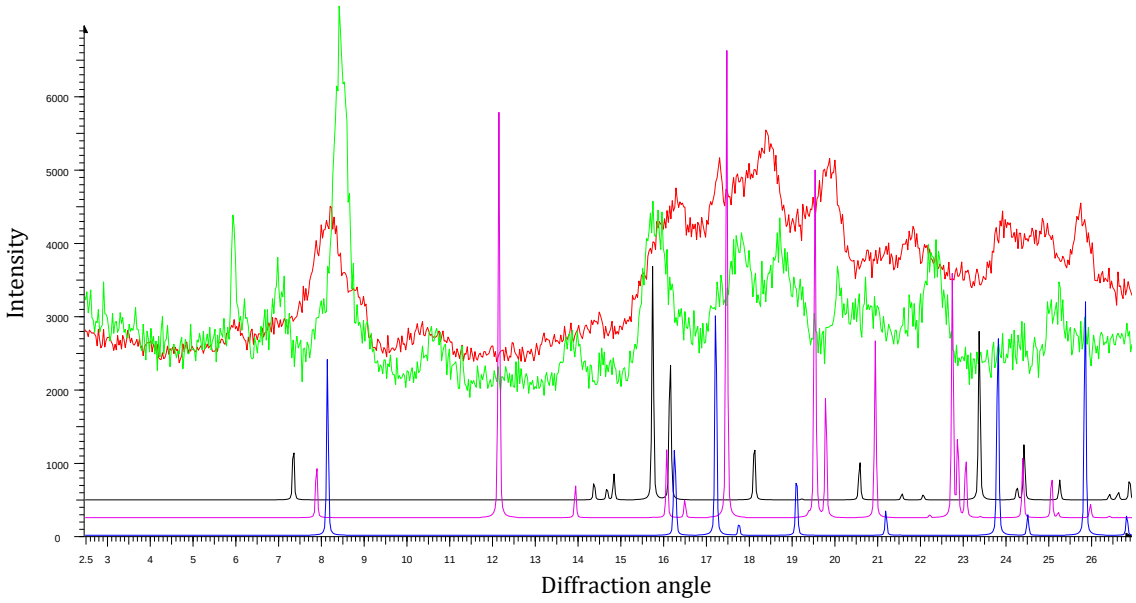

FIGURE 81- PXRD PATTERNS OF ANHYDROUS EPHEDRINE (PINK), EPHEDRINE HEMIHYDRATE (BLACK), BENZOIC ACID (BLUE), SAMPLE FORMED BY GRINDING EPHEDRINE AND BENZOIC ACID (RED) AND SAMPLE FORMED BY CONTACTING EPHEDRINE AND BENZOIC ACID (GREEN)

The IR spectrum of the contacted sample is identical to the IR of the ground sample. This confirms that the addition of grinding does not cause any change to the product formed, merely accelerates product formation and amorphisation. Both spectra, along with the pure components, are plotted in Figure 82. In this spectrum the same shift of the carbonyl seen in the ground sample can be observed and it can be concluded that a salt has probably formed.

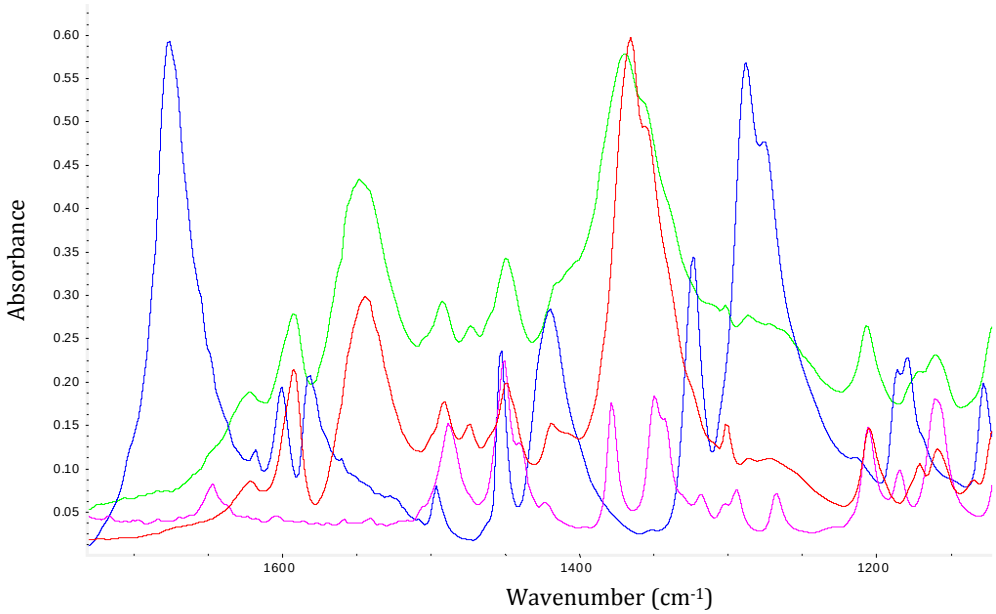

FIGURE 82- IR SPECTRA BETWEEN 1000 AND 1800 CM^{-1} OF EPHEDRINE (PINK), BENZOIC ACID (BLUE), GROUND EPHEDRINE AND BENZOIC ACID (RED) AND CONTACTED EPHEDRINE AND BENZOIC ACID (GREEN)

The DSC of this sample is shown in Figure 83 and displays a number of endotherms. The first at around 30 °C is due to the pure ephedrine. The needles are hard to separate so some ephedrine must still have remained. The second peak at 70 °C is new and may be related to the peak at 65 °C in the ground sample (Figure 75). The next peak at 95 °C may correspond to the second peak in the ground DSC shown to occur at 91 °C. There is also a final peak at 100 °C. The discrepancies between these temperatures are likely to be due to the presence of impurities (such as pure compound) lowering the melting point. The endotherms are all broad, due to some amorphisation, making the determination of peak position less accurate. This suggests the new product formed in the contact experiment is the same as that formed by grinding and is probably the salt. More investigation is required into whether other polymorphic phases are forming in the heating process.

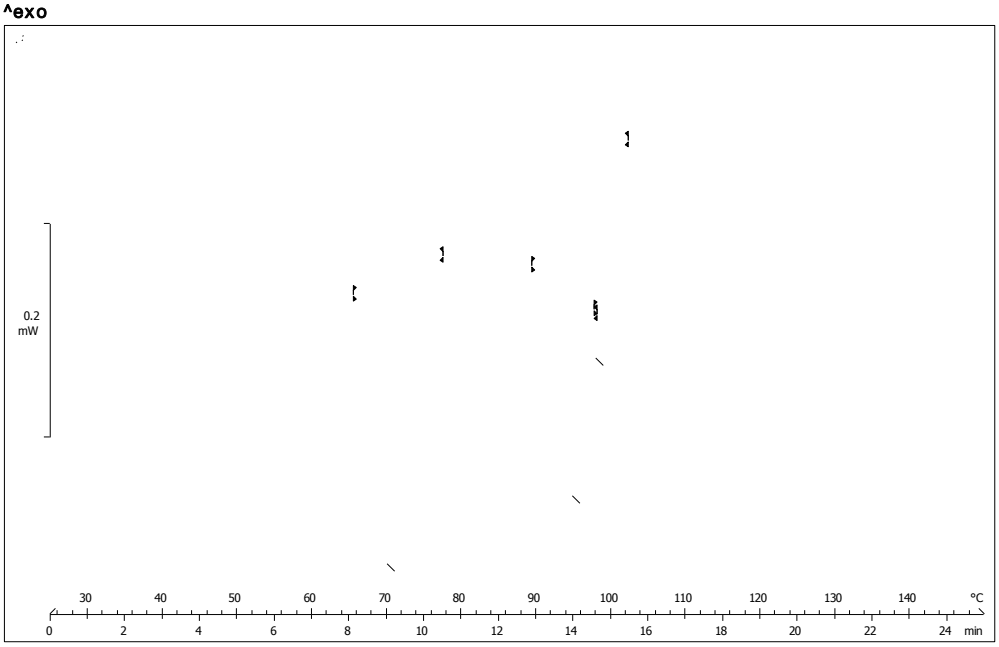

FIGURE 83- DSC OF THE SAMPLE FROM THE EPHEDRINE AND BENZOIC ACID CONTACT EXPERIMENT

As the DSC trace does not give a single, sharp melt peak, hotstage microscopy was utilised to provide more conclusive answers about the thermal behaviour of the sample formed by contacting. The sample was sandwiched between two coverslips and heated. The heating rate was initially 10 ° per minute until 50 °C, then a rate of 1 °C per minute followed by holding at 60 °C for 10 minutes. The ramp was then continued at the same rate, holding every 10 °C for 10 minutes. Images of the effects of the heating process on the contact sample are shown in Figure 84. As in the DSC an initial change occurs at around 65 °C when the original tiny fluffy needles melt. This is accompanied by the growth of new needles, as can be seen in Image 2, Figure 84. These needles continue to grow until a temperature just below 80 °C, where this needle phase begins to melt (Image 6, Figure 84). The heating is then continued and the new needles continue to melt (Images 7 and 8, Figure 84). This melt corresponds to the second peak in the DSC at around 90 °C. As the tiny needles melt they reveal larger needles present in the cluster (Image 9, Figure 84). It was not possible to determine at which stage of the process these larger needles grew. At just over 100 °C the remaining sample melted, corresponding to the final peak in the DSC at 100 °C.

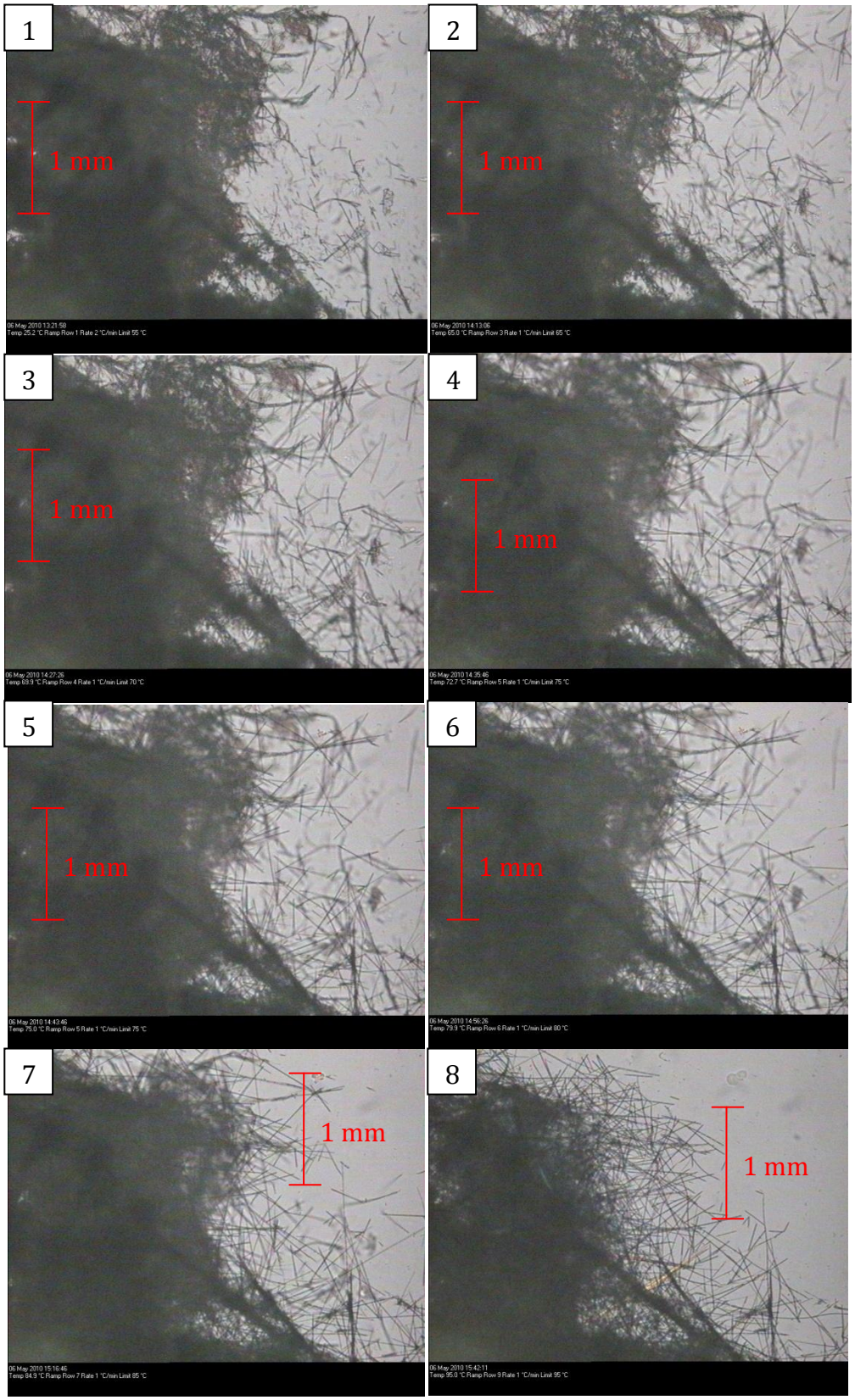
1
1 mm
2
1 mm
3
1 mm
4
1 mm
5
1 mm
6
1 mm
7
1 mm
8
1 mm

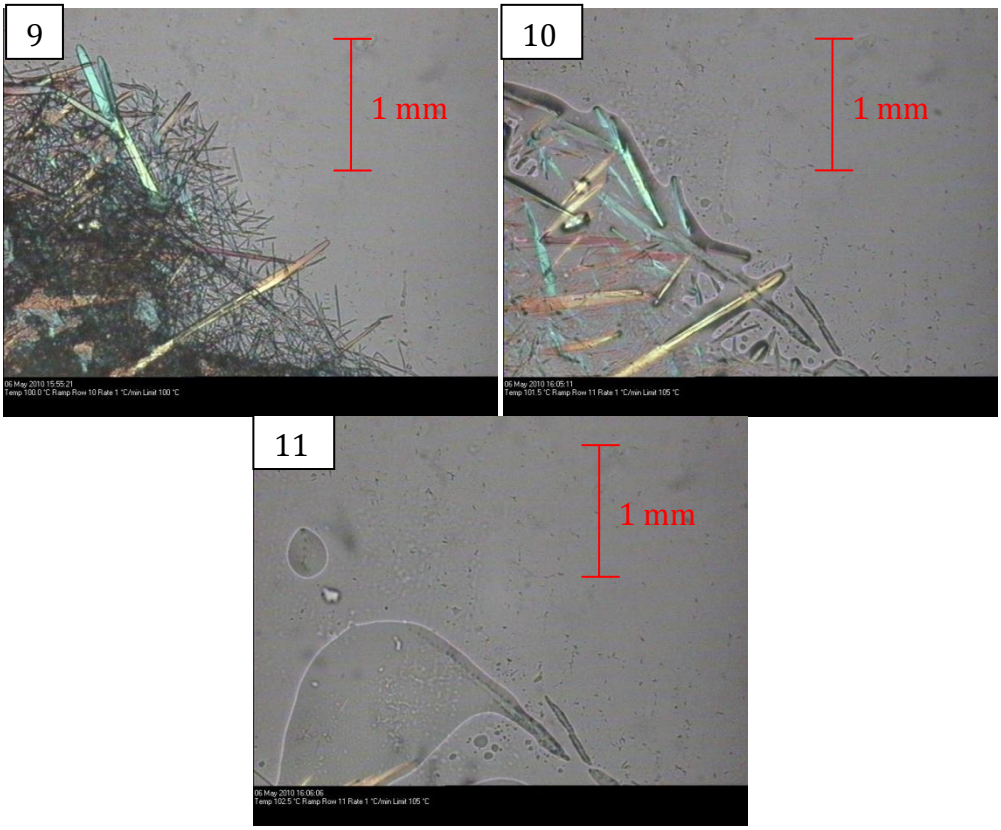

FIGURE 84- HOTSTAGE MICROSCOPY OF THE MELTING OF THE EPHEDRINE AND BENZOIC ACID CONTACT SAMPLE

The tiny needles formed during the microscopy experiment are too small and unstable to perform single crystal analysis on. The structure of the crystals cannot be determined by this method.

IR spectroscopy was carried out in conjunction with a hotstage to assess whether the new phases formed in the heating process have different spectra. If the new phases are different polymorphs, the IR spectra may not be different. The results are displayed below in Figure 85 and are inconclusive. The intensity of certain areas of the spectra change as the temperature is increased, especially between 1800 cm^{-1} and 4000 cm^{-1}. The intensities stop getting any greater in this region after 85 °C, well before the melt (as determined by hotstage microscopy). The positions of the peaks do not show many significant alterations. The broad peak at 3100 cm^{-1} shifts to 3000cm^{-1} at between 75 °C and 80 °C. This peak is probably due to the C-H stretch in the ring, as although the secondary amine N-H stretch appears in the same region, it is notoriously weak and variable[7]. The carbonyl is ionised

throughout and the intensity of this band appeared to vary randomly. The carbonyl was not further interrogated during these heating experiments.

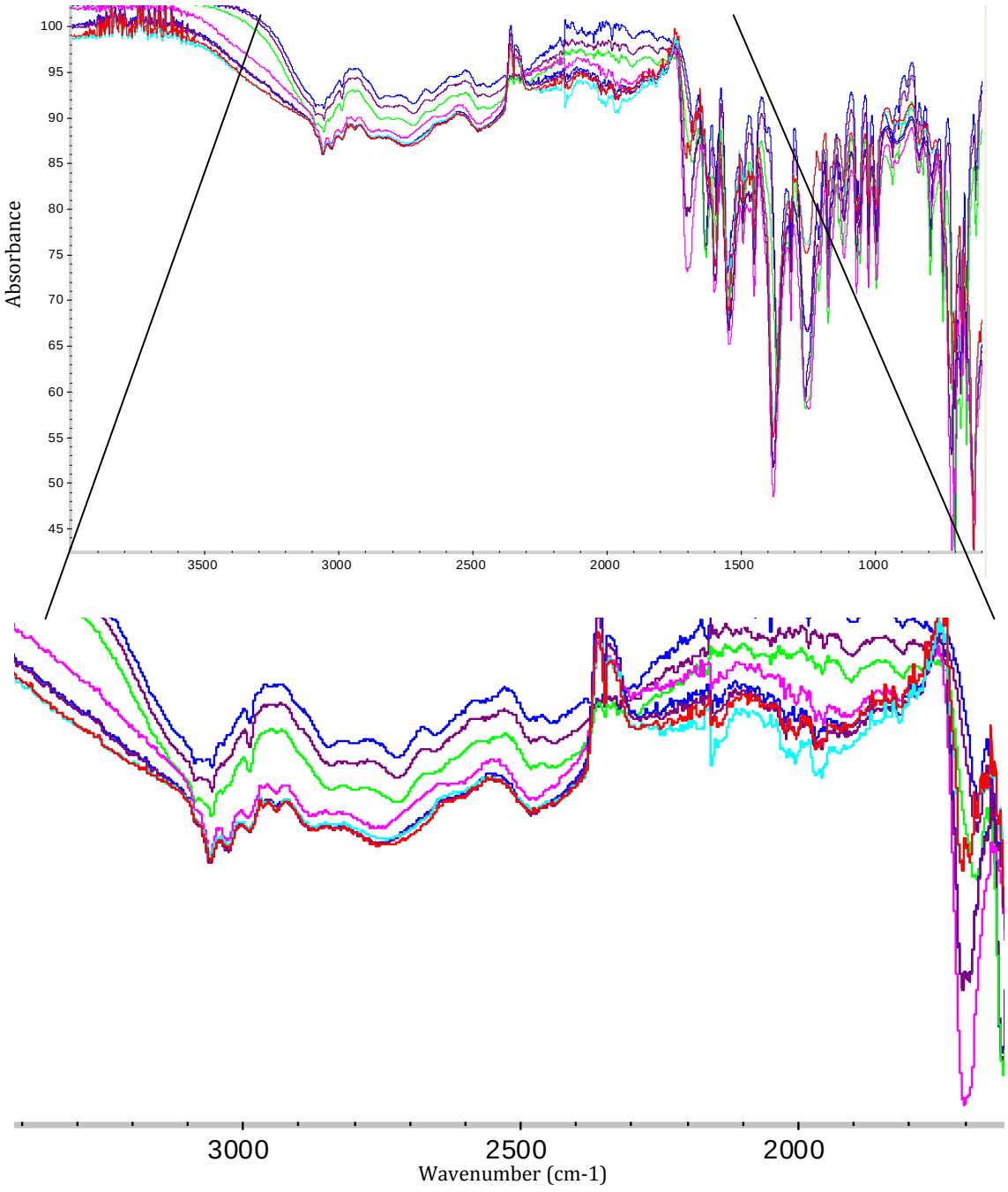

FIGURE 85-TOP- FULL IR SPECTRA SHOWING THE HEATING OF THE SUSPECTED EPHEDRINE BENZOATE SALT. 50 °C (DARK BLUE), 60 °C (PURPLE), 75 °C (BRIGHT GREEN), 80 °C (PINK), 85 °C (DARK BLUE), 90 °C (PURPLE), 95 °C (RED) AND 110 °C (LIGHT BLUE). BOTTOM- ZOOMED IN REGION OF SPECTRA SHOWING THE INTENSITY DIFFERENCES BETWEEN DIFFERENT TEMPERATURE READINGS.

Hotstage pXRD was also performed to assess the change in form. This technique should show any changes in form/phase as the crystal structure would be

different. Unfortunately as this sample is so light and compresses to a very small size, the technique did not provide a good analytical route. The sample holder was filled with the fully compressed sample. The pXRD pattern gave fewer peaks, as would be expected upon melting, without the addition of any new peaks. It is possible that heating did not give a new product, although this seems unlikely from the microscopy evidence. It is also possible that the sealed heating environment of the pXRD chamber is different to sealing between two coverslips, meaning the sample merely melts and does not transform. It is also possible that due to the nature of the sample as it melts or transforms it becomes too small or badly positioned for the system to analyse.

5.3.3.2 THE EFFECT OF CLOSE PROXIMITY OF COMPONENTS

To assess whether the two components need to be in contact for reaction to occur, the contact experiment (Section 5.3.3) was repeated with the components separated by a gap of 1 cm (Figure 86). As can be seen in Figure 87, Figure 88 and Figure 89 below, formation of the new product again occurred. In Figure 87 it can be seen that the product grows as a 'wall' between the two components. This 'wall' appears to be closer to the benzoic acid than the ephedrine. On the benzoic acid side small needle-like crystals can be observed and are visible more clearly in Figure 88. On the ephedrine side the surface of the 'wall' is much smoother, as is seen in Figure 89. This suggests that growth is a vapour phase process and is occurring closer to the benzoic acid. As the melting point of ephedrine is significantly lower than the melting point of benzoic acid it would be expected that ephedrine would have a higher vapour pressure. This links with the conclusions of previous ephedrine research published by Duddu and Grant[8]. In this publication the racemic compound of ephedrine was grown from the two enantiomers kept diametrically separated. The authors concluded that the vapour pressure of ephedrine is sufficiently high to enable reaction in the vapour state to form the racemic compound. They also found crystals of the racemic compound grew on the pure enantiomers. As discussed in Section 1.6 Rastogi[9] proposed diffusion of the vapour phase as a cocrystal formation mechanism method in 1963.

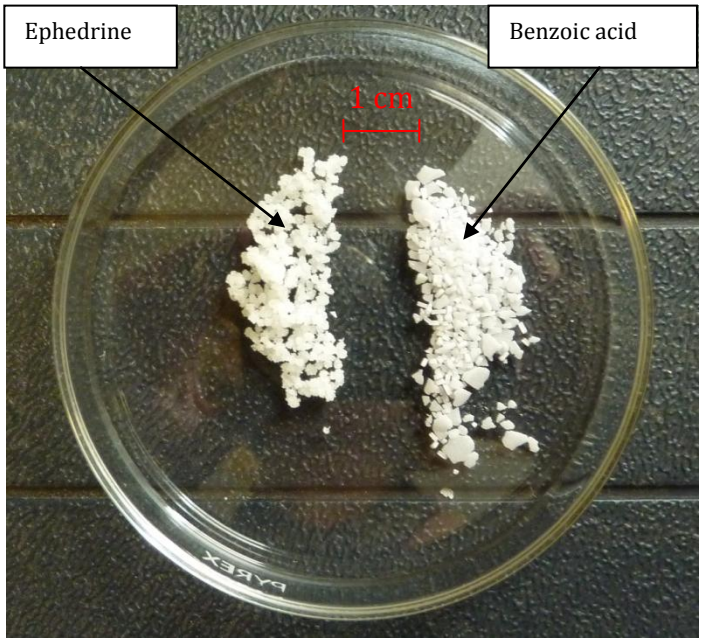

FIGURE 86- INITIAL IMAGE OF EPHEDRINE (LEFT) AND BENZOIC ACID (RIGHT) 1 CM APART. THE REACTION OCCURS WITH NO FURTHER MOVEMENT OF EITHER COMPONENT

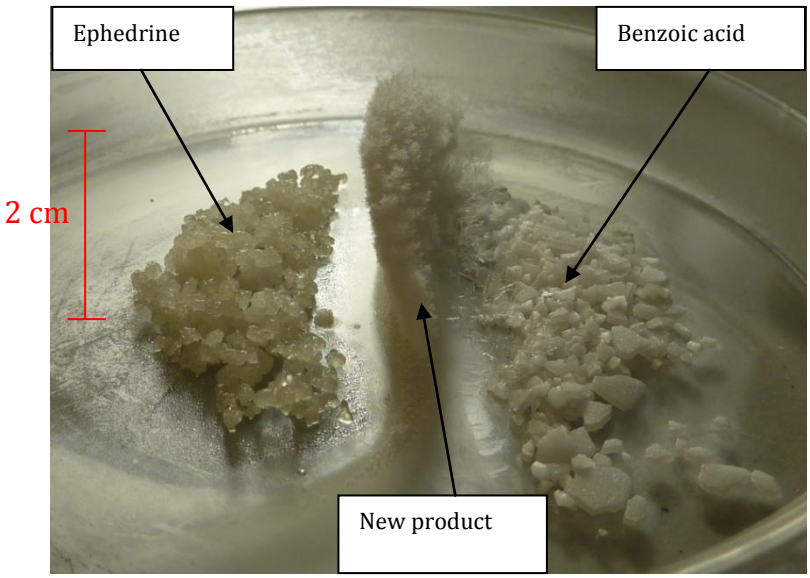

FIGURE 87- IMAGE OF PRODUCT FORMATION WITH 1 CM BETWEEN THE COMPONENTS. EPHEDRINE IS ON THE LEFT AND BENZOIC ACID IS ON THE RIGHT. THE NEW PRODUCT GROWS IN A 'WALL' BETWEEN

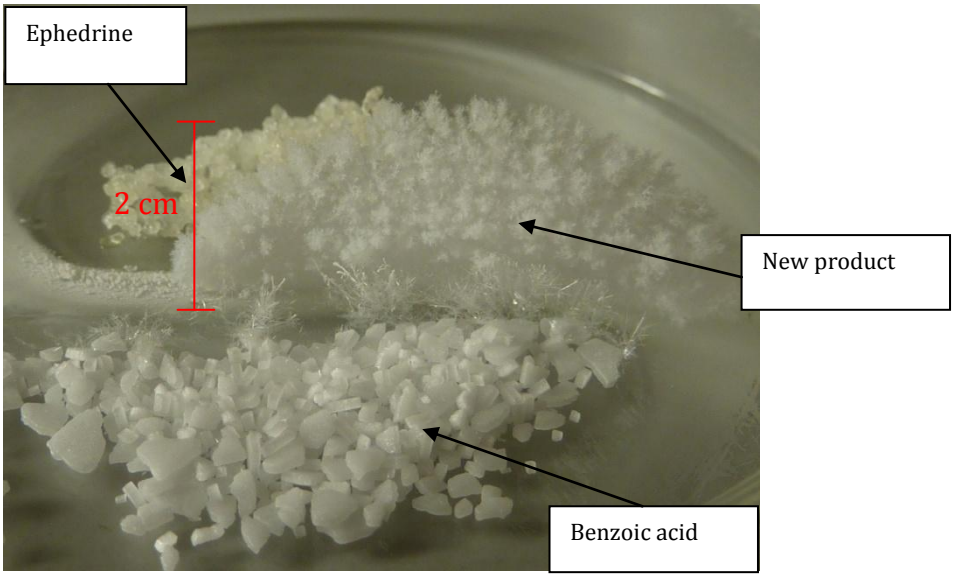

FIGURE 88- IMAGE OF PRODUCT FORMATION WITH 1 CM BETWEEN THE COMPONENTS. PURE BENZOIC IS AT THE FRONT WITH THE 'WALL' OF PRODUCT BEHIND. JUST SEEN IS THE EPHEDRINE BEHIND.

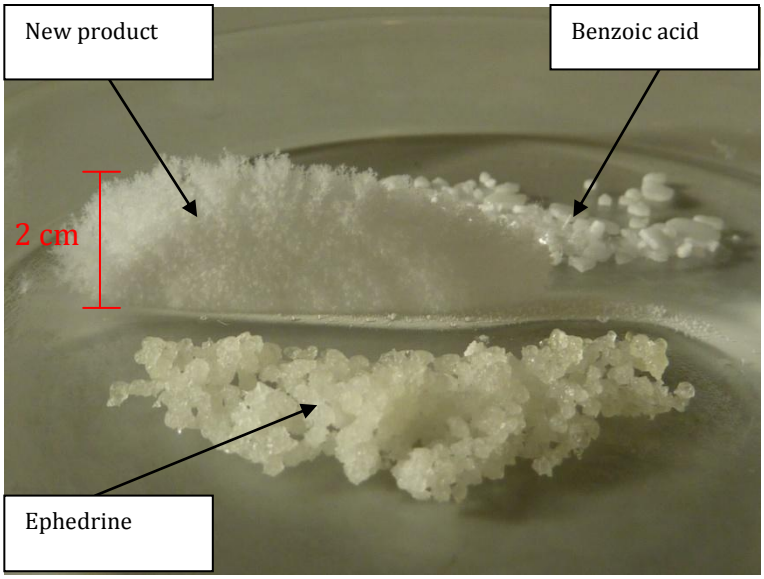

FIGURE 89- IMAGE OF PRODUCT FORMATION WITH 1 CM BETWEEN THE COMPONENTS. PURE EPHEDRINE IS AT THE FRONT WITH THE 'WALL' OF PRODUCT BEHIND. JUST SEEN IS THE BENZOIC ACID BEHIND.

To further assess this effect the components were positioned 4 cm apart in an otherwise identical experiment. The result is displayed in Figure 90. Here, unexpectedly, it can be seen that the new product grew closer to the ephedrine. In

the contact samples it appeared that the sample grew closer to the benzoic acid. This suggests the vapour pressure of the benzoic acid is having a greater effect than anticipated from early results.

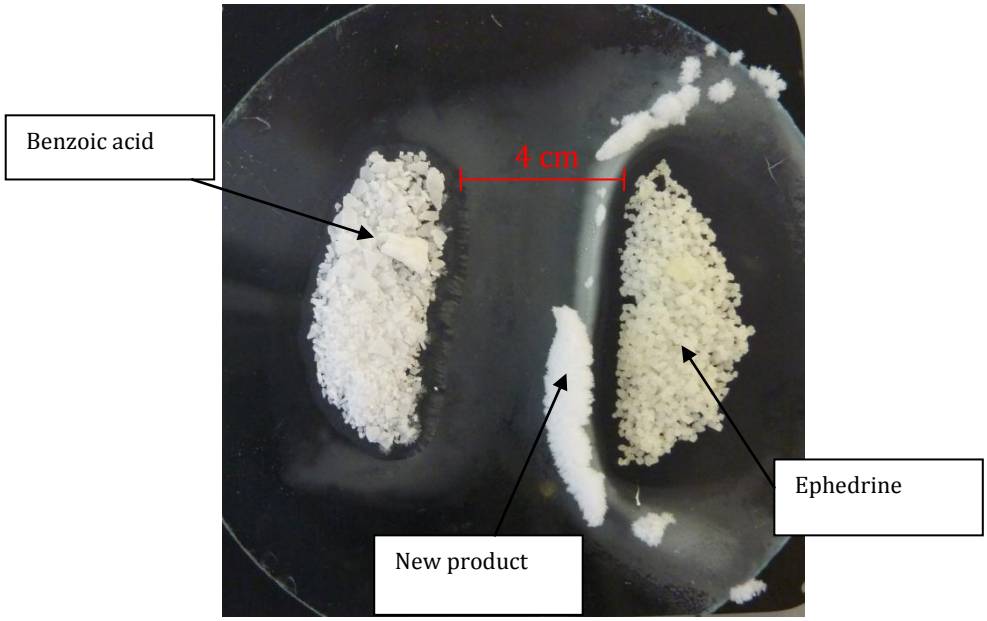

FIGURE 90- IMAGE OF PRODUCT FORMATION WITH 4 CM BETWEEN THE COMPONENTS. PURE EPHEDRINE IS ON THE RIGHT. BENZOIC ACID IS ON THE LEFT. THE LINE OF NEW PRODUCT CAN BE SEEN IN THE MIDDLE.

To assess whether this product is the same as that grown in the contact experiments FTIR and pXRD were performed on the samples. They proved the samples formed in close proximity are ionised and, despite the highly amorphous pXRD patterns, appear the same as the product formed by contacting. These spectra and patterns are given in the Appendix. As a final assessment into the distances these salts would form over, the samples were placed 14 cm apart on a large petri dish. No salt formation was noted after one month. Further work should be carried out into understanding the conditions required and the mechanism (see Section 7.2).

5.4 SALT FORMATION FROM SOLUTION

In order to confirm the existence of a 1:1 salt of this system (potentially in a number of polymorphic forms) attempts were made to grow a single crystal from solution. Previous work by Collier *et al*[2] only formed an amorphous salt by cooling an equimolar ratio in water or methanol. Due to the large difference in solubility

between the acid and base a 1:1 molar ratio does not necessarily mean the correct region of the ternary phase diagram would be targeted. In order to determine the composition needed to target the correct region an ideal ternary phase diagram was used (Figure 91).

The actual solubilities of the acid and base in water were plotted on the appropriate sides of the diagram. Assuming the system behaves ideally (see Section 1.5.2) these line run parallel to the opposite side (as can be seen more clearly on the zoomed in phase diagram in Figure 91). At the point just below where they cross it can be assumed that the solid phase present is the salt, if it is accessible from an aqueous system. This is the point that was targeted to access the salt region.

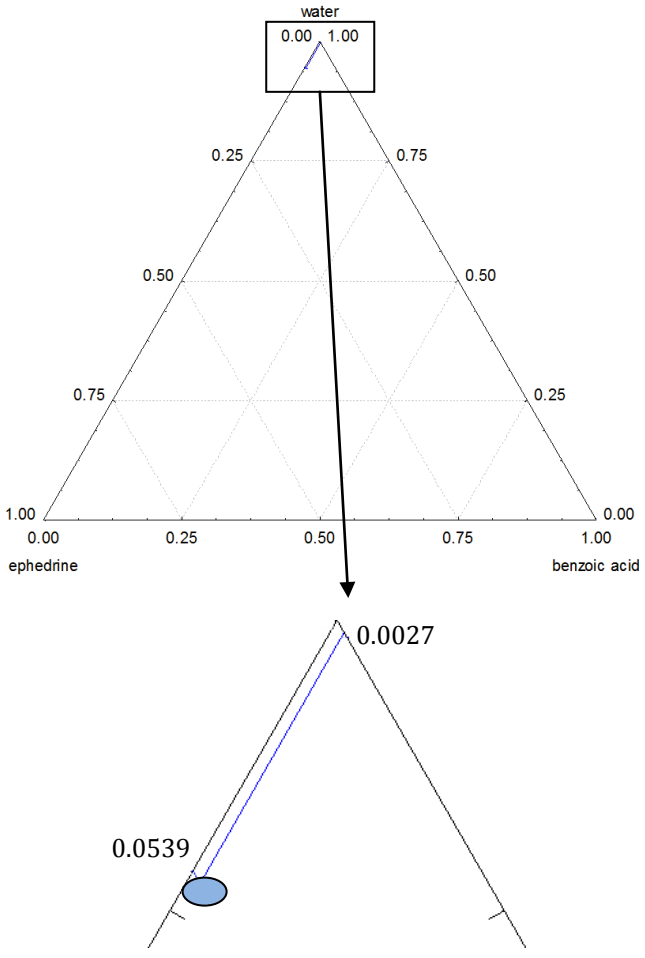

FIGURE 91- IDEAL TERNARY PHASE DIAGRAM OF EPHEDRINE AND BENZOIC ACID IN WATER BASED UPON EXPERIMENTAL SOLUBILITIES OF THE PURE COMPONENTS

In the speciation diagram in Figure 92 it can be seen that the difference in pK_a between the acid and the base is greater than two units, which by the general rule suggests salt formation is possible[3]. The pH range a salt solution should form within is between 4.5 and 9.5.

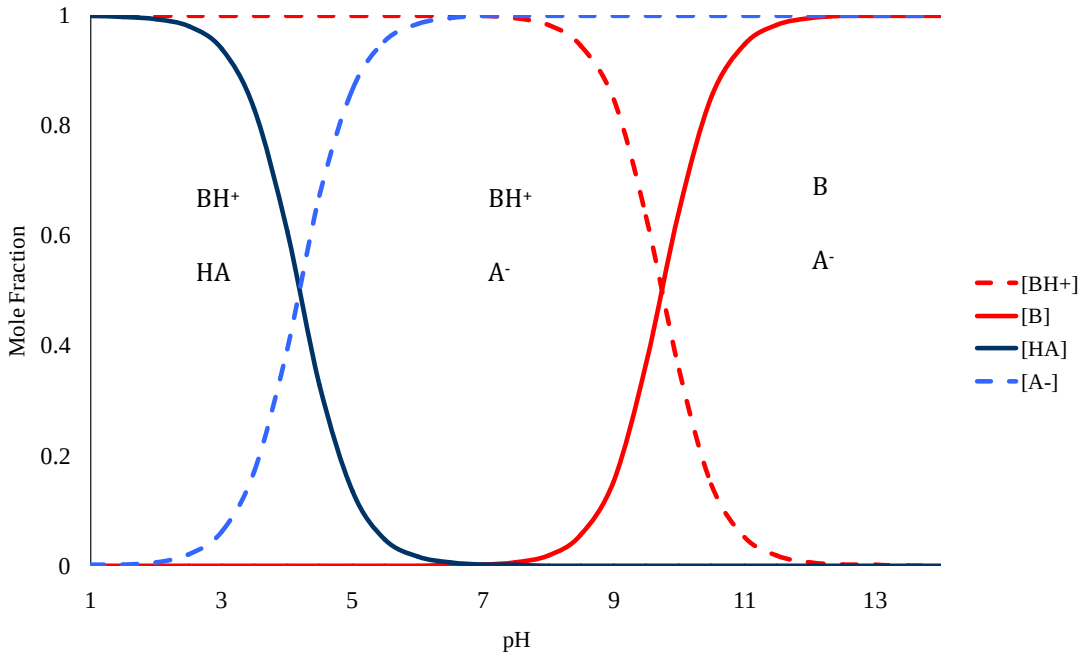

FIGURE 92- SPECIATION DIAGRAM OF EPHEDRINE AND BENZOIC ACID

5.4.1 SALT FORMATION FROM AQUEOUS SOLUTIONS WITHOUT PH ALTERATION

In order to assess whether the salt is accessible from the system, $5.1x10^{-3}$ moles (0.844 g) of ephedrine and $3.27x10^{-4}$ moles (0.040 g) of benzoic acid were slurried in 10 g of water. The initial volume of water (determined from the ternary phase diagram- Figure 91) had to be reduced as all solid dissolved. This was due to the non-ideality of salt systems (explored further in Chapter 7). The solution was allowed to stir for 3 days at 298 K to ensure equilibrium had been reached before the solution was filtered. The solid was then analysed by pXRD (Figure 93) and the liquid sample left at room temperature for slow evaporation to occur. The analysis of the solid showed it to be a mixture of the pure components (mostly ephedrine hemihydrate), suggesting salt formation does not occur in this system.

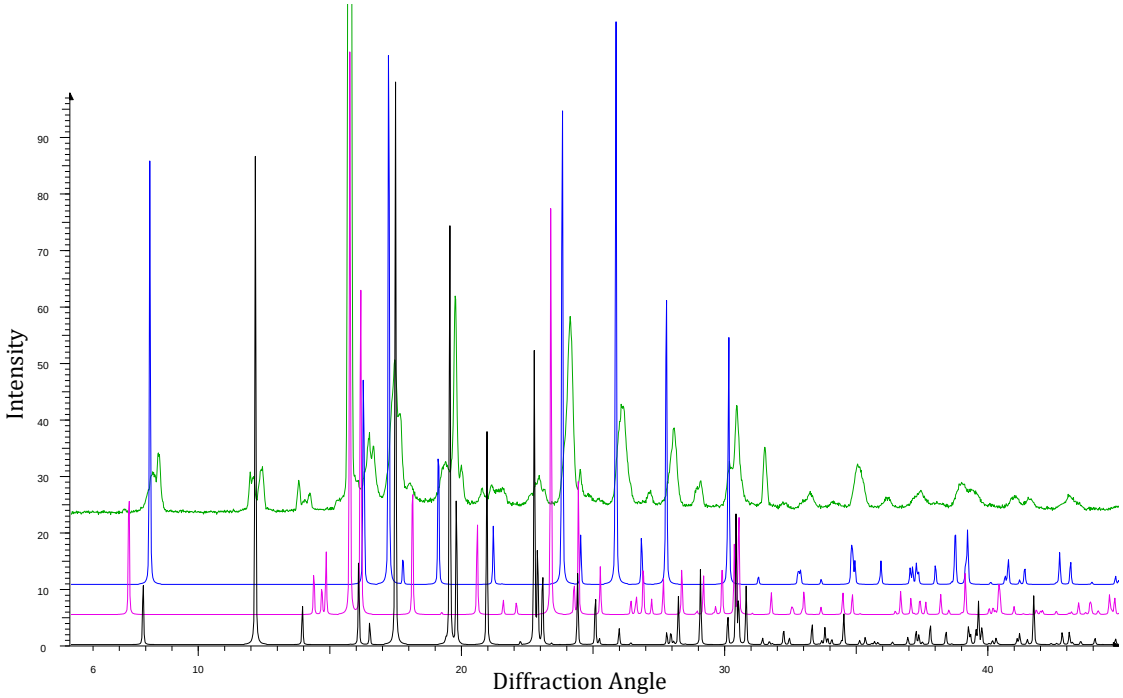

FIGURE 93- PXRD PATTERNS OF EPHEDRINE (PINK), EPHEDRINE HEMIHYDRATE (BLACK), BENZOIC ACID (BLUE) AND THE FILTERED SAMPLE (GREEN).

After a week, without any pH manipulation, small needle like crystals had formed in the solution (Figure 94). There was some concern that the needles may consist of many conjoined needles as they failed to extinguish as the plane of polarised light was rotated (Figure 95). These crystals also dissolved in the mounting oil used in sXRD. The crystals had to be mounted without the use of oil.

FIGURE 94- CRYSTAL FORMED FROM EPHEDRINE AND BENZOIC ACID IN WATER

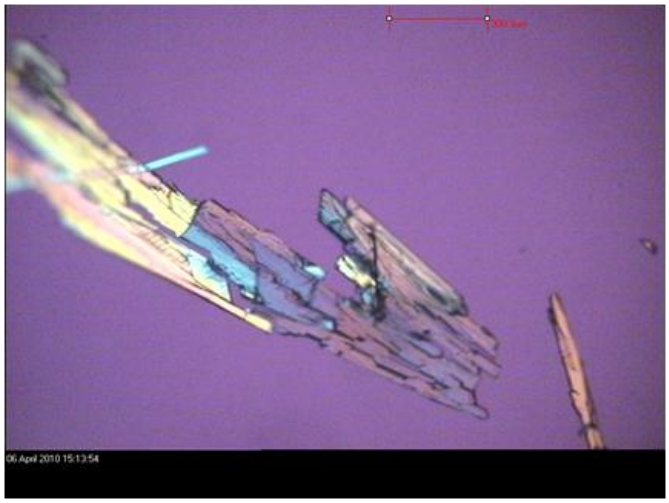

FIGURE 95- CRYSTAL FORMED FROM EPHEDRINE AND BENZOIC ACID IN WATER VIEWED UNDER CROSS POLARS

The crystals did diffract well enough to allow the crystal structure to be solved.

The components had not ionised to form the salt, but instead reacted, undergoing a condensation reaction forming 2-phenyl-3,4-dimethyl-5 phenyl-1,3-oxazolidine. The pH of the solution was measured as 10.88. The solution lies in the region of the speciation diagram where the base would be expected to exist mostly in the non-ionised form. This provides the explanation for why the salt does not form.

5.4.1.1 CRYSTAL STRUCTURE DATA

Crystal structure information is tabulated (Table 15) and the bonding is shown in Figure 96, Figure 97 and Figure 98.

TABLE 15- CRYSTALLOGRAPHIC DATA TABLE FOR 2-PHENYL-3,4-DIMETHYL-5 PHENYL-1,3-OXAZOLIDINE

System	2-phenyl-3,4-dimethyl-5 phenyl-1,3-oxazolidine
Empirical Formula	C17ONH19
M_r (g/mol)	253.34
Temperature (K)	100
Radiation Type, Wavelength	MoK_α, 0.71073
Crystal System, Space Group	Monoclinic, $P2_1$
a,b,c (Å)	9.1340(18) , 7.6087(12) 10.5102(19)

α, β, γ (°)	90, 103.585(18), 90
Volume (Å^3)	710.0(2)
Z, Density (mg.m^{-3})	2, 1.185
Absorption Coefficient (mm^{-1})	0.073
Crystal Size (mm)	?*
$\theta_{min}/\theta_{max}$	3.32°/28.32°
Reflection Collected/Unique (R_{int})	0.065
Data/ restraints/ parameters	2413/1/174
Goodness of fit on F^2	0.813
Residual Electron Density	0.065
Final R indices [I>2σ(I)] R1/wR2	0.065/0.156

*for crystal size, due to crystals sticking together, it was not possible to measure individual crystal lengths.

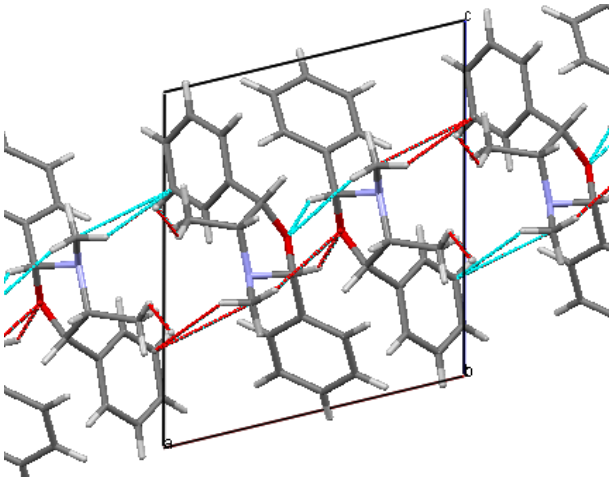

FIGURE 96- CRYSTAL STRUCTURE OF 2-PHENYL-3,4-DIMETHYL-5 PHENYL-1,3-OXAZOLIDINE VIEWED DOWN A

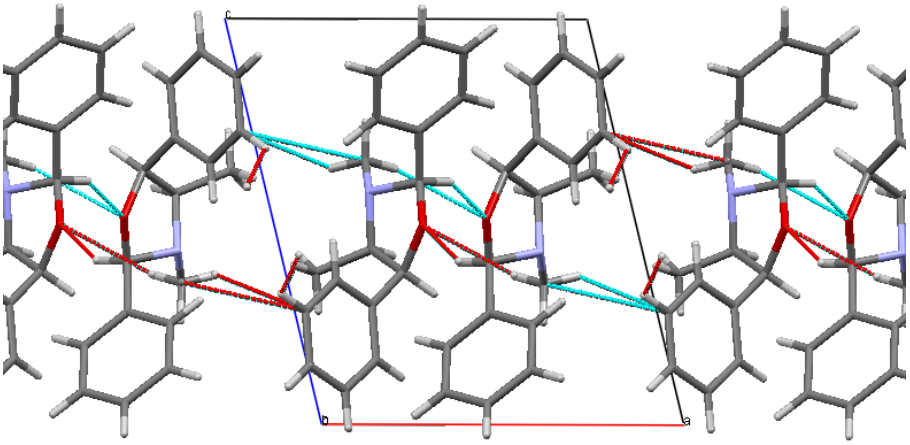

FIGURE 97- CRYSTAL STRUCTURE OF 2-PHENYL-3,4-DIMETHYL-5 PHENYL-1,3-OXAZOLIDINE VIEWED DOWN B

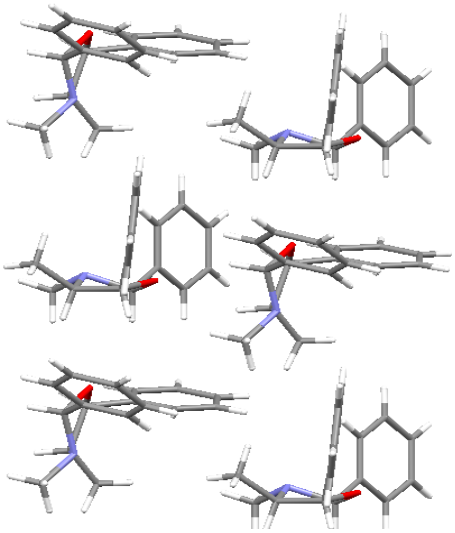

FIGURE 98- CRYSTAL STRUCTURE OF 2-PHENYL-3,4-DIMETHYL-5 PHENYL-1,3-OXAZOLIDINE

5.4.1.2 ANALYSIS OF 2-PHENYL-3,4-DIMETHYL-5 PHENYL-1,3-OXAZOLIDINE

The new product formed contains three chiral centres at the three carbons of the central cyclic structure, labelled in Figure 99. A chiral structure lacks an internal plane of symmetry and can be easily identified when a carbon has four different groups attached to it. It is not superimposable on its mirror image[10]. As there are three chiral centres the van't Hoff formula can be applied to calculate the number

of possible stereoisomers. This formula states that for n chiral centres the number of optical isomers is 2^n, hence for 2-phenyl-3,4-dimethyl-5 phenyl-1,3-oxazoline there are eight possible isomeric structures[11]. All three of the centres, labelled 1, 2 and 3 in Figure 99 are in the R configuration. Theory and methods detailing the determination of configurations is discussed in detail in well regarded publications[12] and is not relevant to this work.

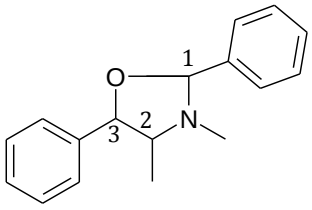

FIGURE 99- 2-PHENYL-3,4-DIMETHYL-5 PHENYL-1,3-OXAZOLIDINE WITH THE CHIRAL CENTRES HIGHLIGHTED AND NUMBERED.

From the crystal structure projections shown in Figure 96, Figure 97 and Figure 98 it can be seen that there is no hydrogen bonding in this structure, only van der Waals bonding. The absence of hydrogen bonds makes the structure weaker, and is a potential cause of the low melting point (for a large organic molecule) and its solubility in oil. The melting point is confirmed by DSC (Figure 100) where a melting point of 71 °C is observed.

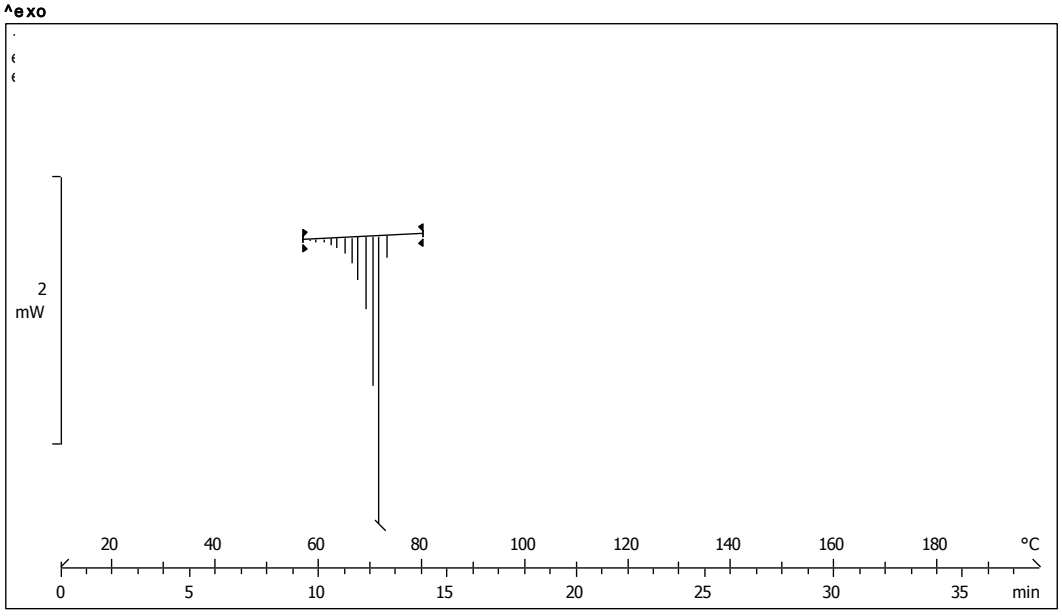

FIGURE 100- DSC OF 2-PHENYL-3,4-DIMETHYL-5 PHENYL-1,3-OXAZOLIDINE

The new structure is easily identified using IR spectroscopy (Figure 101) due to the absence of a carbonyl, as would be present in the acid or salt. This absence can be more clearly seen in Figure 102.

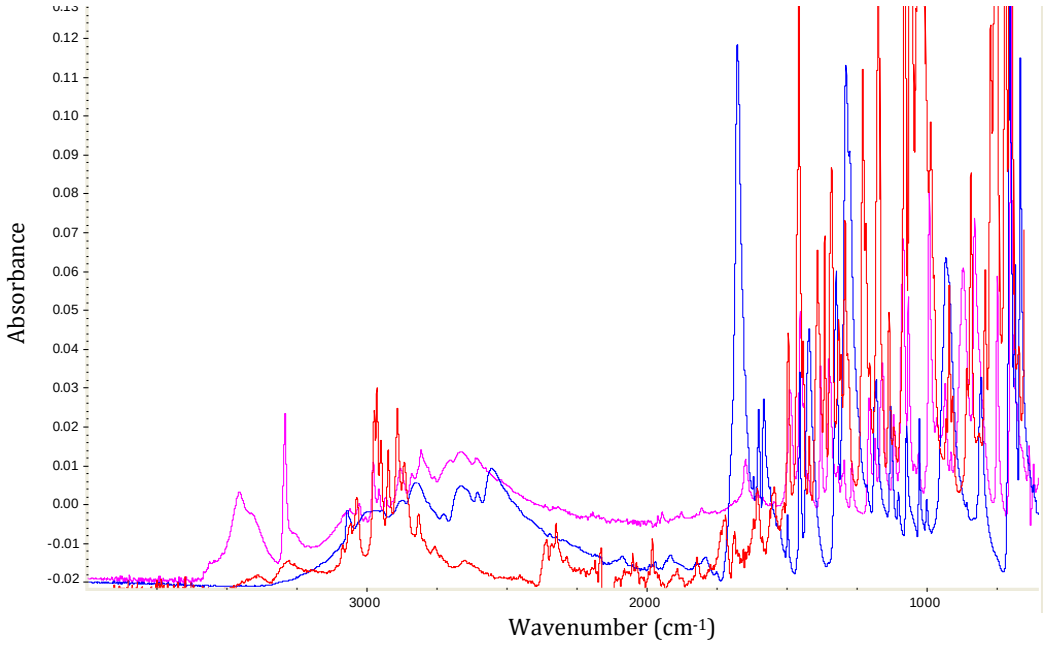

FIGURE 101- COMPLETE IR SPECTRA OF 2-PHENYL-3,4-DIMETHYL-5 PHENYL-1,3-OXAZOLIDINE (RED) AND THE PURE COMPONENTS, EPHEDRINE (PINK) AND BENZOIC ACID (BLUE)

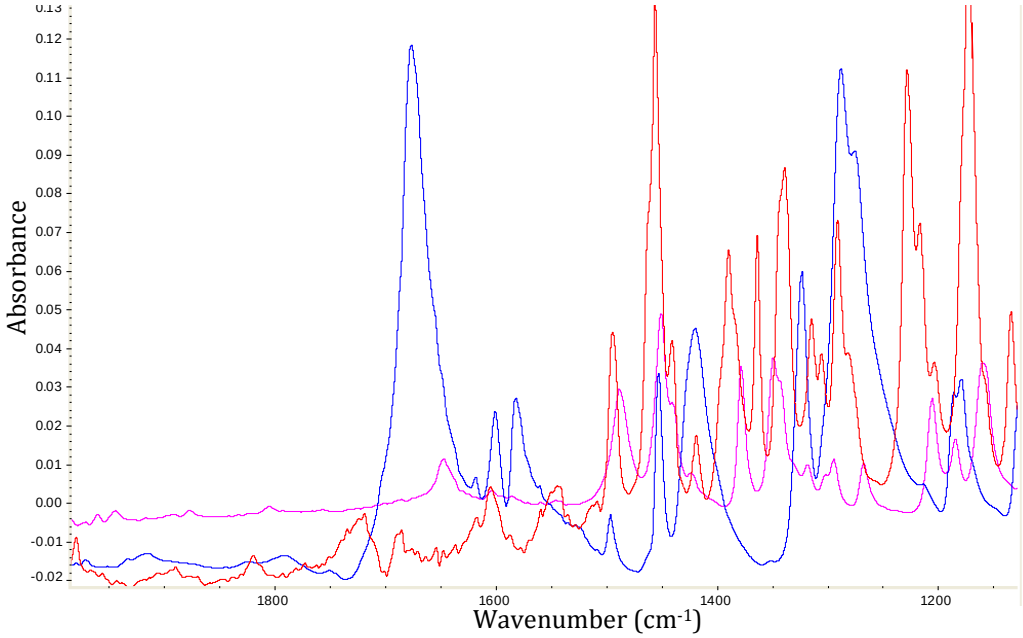

FIGURE 102- IR CARBONYL REGION OF 2-PHENYL-3,4-DIMETHYL-5 PHENYL-1,3-OXAZOLIDINE (RED) AND THE PURE COMPONENTS, EPHEDRINE (PINK) AND BENZOIC ACID (BBLUE)

The simulated powder pattern for 2-phenyl-3,4-dimethyl-5 phenyl-1,3-oxazolidine is totally unlike those recorded from samples of grinding or contact experiments (Figure 103). This has also been shown by the DSC trace and IR spectra in Figure 100 and Figure 102 respectively. This new compound formed from aqueous solution reaction is not the product formed using solid state techniques. The hypothesis that the product formed in grinding and contact experiments is the salt remains strong.

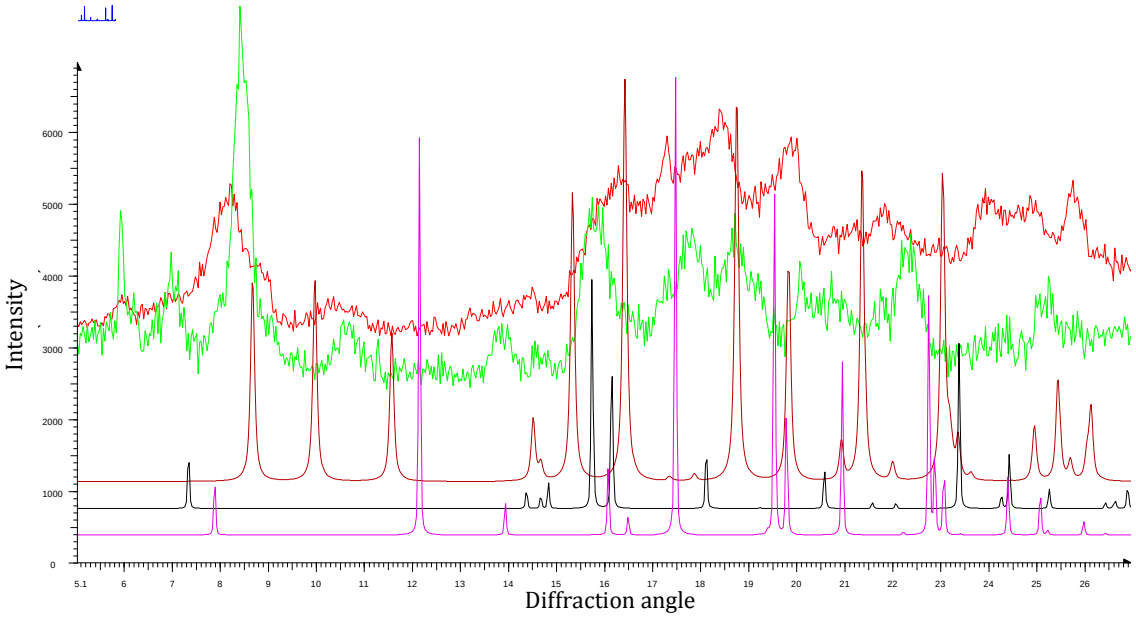

FIGURE 103- PXRD PATTERNS OF ANHYDROUS EPHEDRINE (PINK), EPHEDRINE HEMIHYDRATE (BLACK), BENZOIC ACID (BLUE), SAMPLE FORMED BY GRINDING EPHEDRINE AND BENZOIC ACID (RED), SAMPLE FORMED BY CONTACTING EPHEDRINE AND BENZOIC ACID (GREEN) AND 2-PHENYL-3,4-DIMETHYL-5 PHENYL-1,3-OXAZOLIDINE (BROWN)

5.4.1.3 ANALYSIS OF THE REACTION MECHANISM

The proposed mechanism was determined with the aid of James Clayton, an organic chemist, and is a common reaction mechanism studied in organic chemistry. This reaction normally requires more extreme conditions and is carried out using an aldehyde, rather than an acid (further discussion of other similar reactions is given in Section 5.5.2).

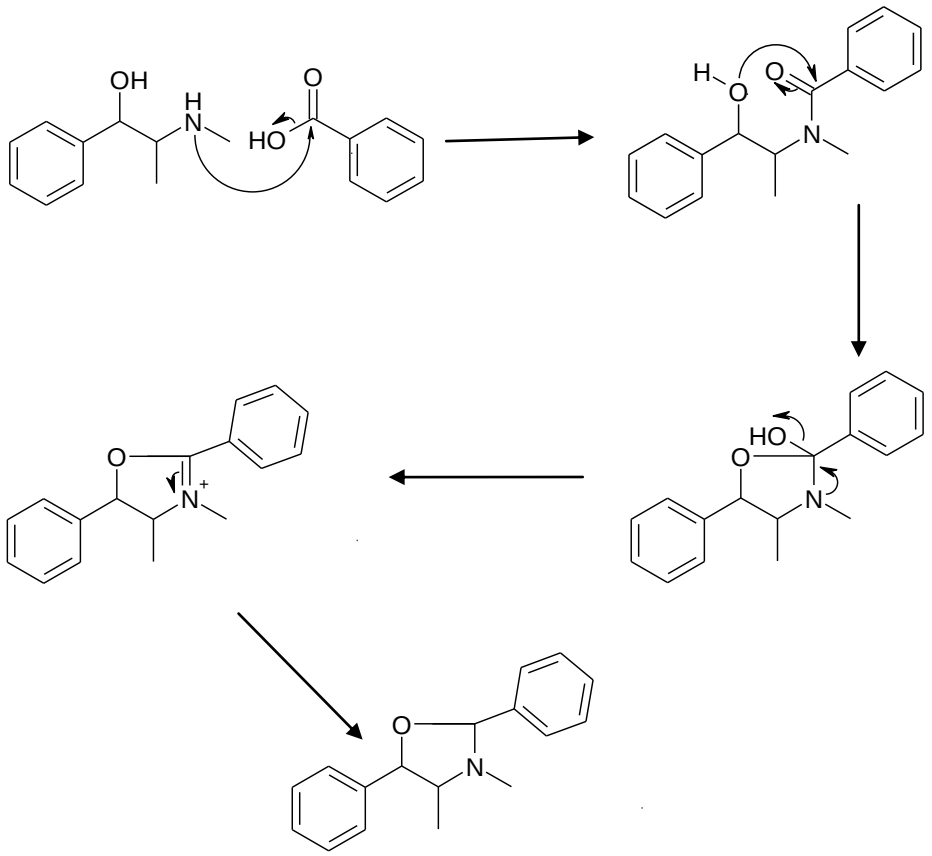

REACTION 3- THE REACTION OF EPHEDRINE AND BENZOIC ACID IN WATER TO FORM 2-PHENYL-3,4-DIMETHYL-5-PHENYL-1,3-OXAZOLIDINE

The electron pair of the ephedrine nitrogen attacks the electropositive end of the benzoic acid carbonyl. The benzoic acid hydroxyl group is then lost. The oxygen lone pair of the ephedrine then attacks the electropositive end of the benzoic acid carbonyl again, reducing it. A cyclic structure remains and with some rearrangement leaves the product.

Solution FTIR was undertaken in an attempt to understand how this new compound forms from such mild conditions (in comparison with the reactions in the papers[13-17] discussed below). The answer to the question 'does ionisation occur in solution as a precursor to reaction or does the reaction occur between the neutral species (as proposed in REACTION 3 above)' was sought. If no ionisation occurs this is reinforcement for the proposed reaction mechanism.

The solution IR spectrum of the pure solvent (water) was recorded, and used for solvent subtraction in the cases of the other solutions (using the solution IR software described in Section 2.4.1.3). The aqueous solution was prepared in the same way as described previously (Section 5.4.1) and agitated. The solution was then filtered and analysed. IR spectra of the slurry and the clear, filtered solution until crystallisation was noted are shown below (Figure 104). A spectrum of pure solid 2-phenyl-3,4-dimethyl-5 phenyl-1,3-oxazolidine (pink) is included in Figure 104 and was recorded by immersing the probe in the powdered sample.

By studying the spectra it can be observed that the carbonyl band is absent in the pure powdered 2-phenyl-3,4-dimethyl-5 phenyl-1,3-oxazolidine. In the solution samples the carbonyl remains at an equal intensity to the unionised acid. This suggests the 2-phenyl-3,4-dimethyl-5 phenyl-1,3-oxazolidine does not exist in solution. The acid does not ionise in the solution, as would be expected from the pH and the speciation diagram. The spectra recorded are noisy and do not show very strong intensities as they are recorded in water. Water has a very strong IR spectrum and although the water background is removed it leaves little intensity from the sample.

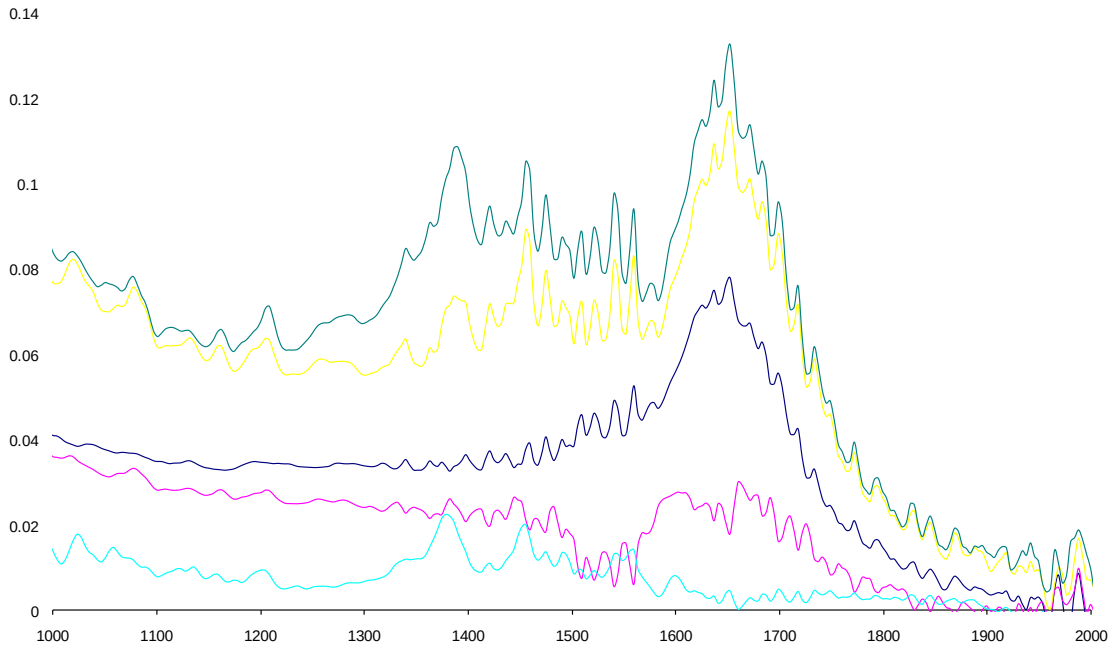

FIGURE 104- IR SPECTRA OF BENZOIC ACID DISSOLVED IN WATER (BLUE), EPHEDRINE AND BENZOIC ACID SLURRY (PINK), SOLID 2-PHENYL-3,4-DIMETHYL-5 PHENYL-1,3-OXAZOLIDINE

(LIGHT BLUE), EPHEDRINE AND BENZOIC ACID SOLUTION (YELLOW) AND EPHEDRINE AND BENZOIC ACID SOLUTION WITH CRYSTAL FORMATION (AQUA)

The results in Figure 104 confirm that the pure components remain present in the solution throughout the experiment. It can also be confirmed that the acid is not ionised in this solution from the position of the carbonyl peak.

5.4.2 SALT FORMATION FROM AQUEOUS SOLUTIONS WITH PH ALTERATION

In order to access the correct region of the predicted ternary phase diagram (Figure 91) a large excess of ephedrine must be used. This causes a high solution pH of 10.88, outside the pH range it would be expected that salt formation would occur within (Figure 92). To lower the pH of the solution hydrochloric acid (37 %) was added dropwise and the pH monitored using a probe. Once a pH of 7 had been attained (approximately 5 drops) the sample was filtered and left to evaporate slowly at ambient conditions until crystallisation was observed.

The crystals grown by this method were determined to be pure ephedrine hydrochloride (Figure 105). Attempts to grow single crystals of ephedrine benzoate were not pursued further. Discussion of the potential methods if further attempts are made is included in Section 5.6 below.

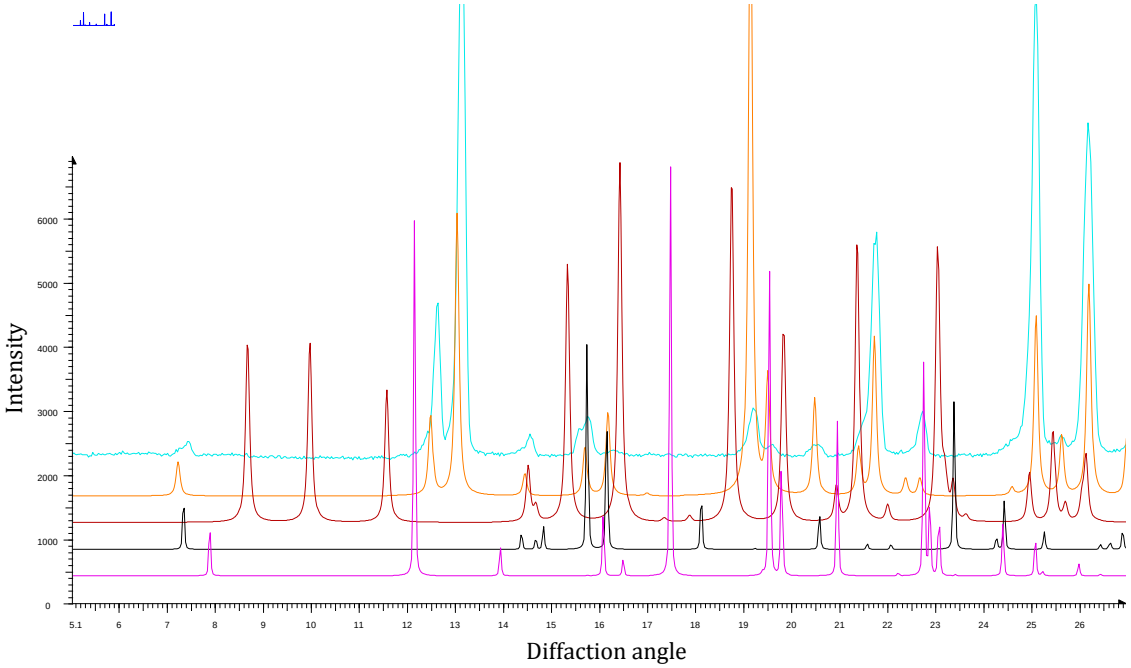

FIGURE 105- PXRD PATTERNS OF ANHYDROUS EPHEDRINE (PINK), EPHEDRINE HEMIHYDRATE (BLACK), BENZOIC ACID (BLUE), 2-PHENYL-3,4-DIMETHYL-5 PHENYL-1,3-OXAZOLIDINE

(BROWN), SAMPLE FORMED BY pH ALTERING (BLUE) AND SIMULATED EPHEDRINE HYDROCHLORIDE (ORANGE)

5.5 DISCUSSION

5.5.1 VAPOUR PRESSURE OF THE COMPONENTS

The vapour pressure of ephedrine is high; however exact values have not been published. The vapour pressure, sublimation and vaporisation enthalpies of benzoic acid have been determined a number of times in a range of papers[18-24]. In 'Perry's Chemical Engineers' Handbook'[25] and 'Thermochemistry of Organic and Organometallic Compounds'[26] large amounts of physical chemistry data are tabulated, including the vapour pressures of benzoic and pimelic acids at a range of temperatures. These are tabulated in Table 16 and converted to SI units. Neither publication contains the vapour pressure of glycolic acid. According to a 2004 paper by Wright *et al*[27], measurement of the vapour pressure of glycolic acid was not possible. This was due to simultaneous decomposition and evaporation. Inspection of the tabulated data in Table 16 shows the vapour pressure of benzoic acid is lower than that of pimelic acid. Pimelic acid does not show the same salt formation growth effect when in contact, or in close proximity, with ephedrine. Ephedrine and pimelic acid require the addition of energy (in the form of heat or friction) to induce salt formation. From this data it can be seen that just because an acid has a higher vapour pressure it does not necessarily form a salt in the same way. The papers published in 1962[28] and 1963[9] by Rastogi *et al* discuss formation of a new product due to the high vapour pressure of at least one of the components.

TABLE 16- VAPOUR PRESSURES OF BENZOIC ACID AND PIMELIC ACID AT A RANGE OF TEMPERATURES IN MMHG AND CONVERTED INTO ATMOSPHERES[25]

Temperature (°C)	Benzoic Acid Vapour Pressure (mmHg)	Benzoic Acid Vapour Pressure (atm)	Pimelic Acid Vapour Pressure (mmHg)	Pimelic Acid Vapour Pressure (atm)
1	96	0.126	163.4	0.215
5	119.5	0.157	196.2	0.258
10	132.1	0.174	212.0	0.279
20	146.7	0.193	229.3	0.302
40	162.6	0.214	247.0	0.325

5.5.2 COMPARISON WITH STRUCTURES SIMILAR TO 2-PHENYL-3,4-DIMETHYL-5 PHENYL-1,3 OXAZOLIDINE

The new molecular structure determined in this chapter is similar to a number of other compounds on the CSD. The first of these structures was formed by Neelakantan and Molin-Case in 1971[15]. This molecule was formed as part of a study of asymmetric synthesis and the structure was determined using sXRD. They found the reaction of ephedrine hydrate and *p*-bromobenzaldehyde led to the product shown in Figure 106. The melting point is low at 87-88 °C, as with 2-phenyl-3,4-dimethyl-5 phenyl-1,3 oxazolidine, and again this is due to the absence of hydrogen bonding between molecules in the crystal structure. The crystal structure was also redetermined in 1983 by Just *et al*[14].

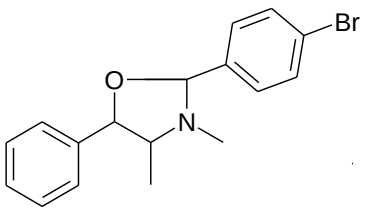

FIGURE 106- 2-*p*-BROMOPHENYL-3,4-DIMETHYL-5-PHENYLOXAZOLIDINE

Thirty years later another paper was published by Bukeeva *et al* featuring a similar structure[17] (shown in Figure 107). To form this molecule d-pseudoephedrine and anisaldehyde were reacted giving the authors an unexpected result. Instead of the molecule in Figure 107, they were attempting to form an α-aminonitrile. The authors claim this unexpected result came about due to the presence of sodium cyanide in the reaction mixture causing the ephedrine to act as a base.

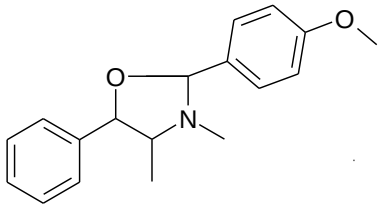

FIGURE 107- 2-(*p*-METHOXYPHENYL)-3,4-DIMETHYL-5-PHENYL-1,3-OXADIAZOLIDINE

In 2004 Duffy *et al*[13] published a structure very similar to that formed by Burkeeva *et al*, with a propyl group in place of the methyl (Figure 108). The product is formed by the condensation of *l*-ephedrine with 4-propoxyaldehyde in the study of systems lacking strong hydrogen-bond donors and acceptors. This compound has a melting point of 65-67 °C and again no hydrogen bonding in the structure.

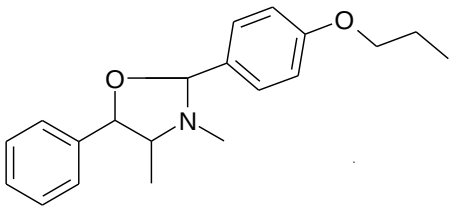

FIGURE 108- (2S,4S,5R)-(-)-2-(4-PROPOXYPHENYL)-3,4-DIMETHYL-5-PHENYL-1,3-OXAZOLIDINE

In 2007 Nurkenov *et al* published the structure displayed in Figure 109[16]. Again, as with the other previously published reactions, an aldehyde was reacted with ephedrine. In this case the reaction was carried out in benzene under reflux. The melting point of this compound is significantly higher at 179-180 °C than the others discussed. There is still no intermolecular hydrogen bonding. This suggests the van der Waals bonding is significantly stronger than in the other similar molecules. Unlike the other structures, this crystal structure does include intramolecular hydrogen bonding.

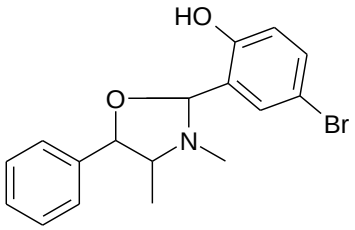

FIGURE 109- 2-*p*-BROMOPHENYL-3,4-DIMETHYL-5-PHENYLOXAZOLIDINE

The reaction that occurs between ephedrine and benzoic acid here is the only one of these reactions featuring an acid, rather than an aldehyde, in reaction with ephedrine. This reaction was probably facilitated by the high pH, due to the excess of ephedrine, counteracting the acidity of the benzoic acid present.

5.5.3 THE PRESENCE OF EPHEDRINE HEMIHYDRATE

The partial hydration of the ephedrine samples used has not been discussed in this chapter as no binary or ternary phase diagrams were determined and no other form of quantitative measurement used. The presence of a small amount of water may have facilitated or accelerated salt formation by grinding. This was not felt to be pertinent to the overall points for discussion and further investigation. The growth of 2-phenyl-3,4-dimethyl-5 phenyl-1,3-oxazolidine occurred while using a large excess of ephedrine. There appears no reason why switching to the anhydrous ephedrine and increasing the volume of ephedrine used would alter the product formation. This would increase the pH further. A higher water proportion in the samples may partially account for the higher solubility observed at the predicted salt ratio.

5.6 SUMMARY

Previous work on ephedrine and benzoic acid had only formed what was concluded to be an amorphous salt from solution[1]. No pXRD patterns or DSC traces were published, but IR spectroscopy supported this. By the grinding of the two components a new product, which appears to be the salt, has been formed. This is confirmed by pXRD patterns and IR spectra. The same new material was also

concluded to have formed from merely contacting the two components at ambient temperature. From the DSC traces and hotstage microscopy it has also been concluded that this salt is polymorphic, with two other forms available at higher temperatures. A diffusion mechanism appears to control salt formation in this system.

The formation of this salt by contact (or close proximity) has been attributed to the high vapour pressures of ephedrine and benzoic acid. It has also been concluded that a high vapour pressure of the acid does not automatically ensure salt formation by this method.

Unsuccessful attempts to form ephedrine benzoate from aqueous solutions have been attributed to the massive difference in aqueous solubility between the two constituents. Attempting crystallisation by evaporation would leave the solution in the wrong region of the ternary phase diagram for the salt to crystallise. This eventually leads to all of the solution evaporating, leaving only the amorphous solid. Adjustment of these ratios to account for the skewed solubilities leads to the reaction of the components due to the large shift in solution pH from that at a 1:1 ratio. This pH shift moves the solution pH into the wrong region of the speciation diagram for salt formation to occur. The adjustment of pH using HCl did not successfully compensate for this effect as ephedrine hydrochloride was formed instead due to its high stability. If this work is continued with the main aim of forming the ephedrine benzoate salt, different solvents should be assessed. The components should show similar solubilities in the solvents selected. The addition of other acids should also be considered. Ideally the acid added will not form a salt with ephedrine. If a salt is known to form between ephedrine and the added acid, it should be ensured it is less stable than an ephedrine benzoate salt.

The new product formed, 2-phenyl-3,4-dimethyl-5 phenyl-1,3-oxazolidine, was unexpected, but highlights the need for pH control when forming salts. The reaction itself was unexpected due to the relatively mild experimental conditions when compared to similar reactions. Most similar products were formed by reaction of ephedrine with an aldehyde rather than an acid. Further work into this

reaction should be considered to assess whether this may be a reaction route that has not been assessed previously in the study of this type of condensation reaction.

In order to form a salt from a given solvent both the ternary phase diagram and speciation diagram should be considered. In this system the two diagrams were incompatible. The solubilities were so skewed that adjustment of this pushed the solution pH too far into the wrong region of the speciation diagram.

5.7 REFERENCES

1. Collier, E. A. in Department of Chemical Engineering 179 (The Univeristy of Manchester Institute of Science and Technology, Manchester, 2004).
2. Collier, E. A., Davey, R. J., Black, S. N. & Roberts, R. J. 17 Salts of Ephedrine: Crystal Structures and Packing Analysis. Acta Crystallographica, Section B: Structural Science B62, 498-505 (2006).
3. Black, S. N., Collier, E. A., Davey, R. J. & Roberts, R. J. Structure, Solubility, Screening, and Synthesis of Molecular Salts. Journal of Pharmaceutical Sciences 96, 1053-1068 (2007).
4. Florey, K. Analytical Profiles of a Drug Substance (Academic Press, Inc., London, 1986).
5. Dawson, R. M. C., Elliot, D. C., Elliot, W. H. & Jones, K. M. Data for Biochemical Research (Clarenden Press, Oxford, 1959).
6. Bellamy, L. J. in The Infrared Spectra of Complex Molecules (Chapman and Hall, London and New York, 1980).
7. Dent, G. (The School of Chemical Engineering, The University of Manchester, 2007).
8. Duddu, S. P. & Grant, D. J. W. Formation of the Racemic Compound of Ephedrine Base from a Physical Mixture of Its Enantiomers in the Solid, Liquid, Solution, or Vapor State. Pharmaceutical Research 9, 1083-1091 (1992).
9. Rastogi, R. P., Bassi, P. S. & Chadha, L. S. Mechanism of the Reaction Between Hydrocarbons and Picric Acid in the Solid State. Journal of Physical Chemistry 67, 2569-2573 (1963).

10. Stevenson, D. & Williams, G. A. in Chiral Separations (eds. Stevenson, D. & Wilson, I. D.) (Plenum Press, New York and London, 1988).
11. Morris, D. G. Stereochemistry (The Royal Society of Chemistry, Cambridge, 2001).
12. North, M. in Principles and Applications of Stereochemistry (Stanley Thornes, Cheltenham, 1998).
13. Duffy, M., Gallagher, J. F. & Lough, A. J. C-H...O and C-H...π(arene) interactions in (2S,4S,5R)-(-)-2-(4-propoxyphenyl)-3,4-dimethyl-5-phenyl-1,3-oxazolidine. Acta Crystallographica, Section E: Structural Reports Online E60, 234-236 (2004).
14. Just, G., Potvin, P. & Uggowitzer, P. Configuration at the 2-Position of Oxazolidines Derived from l-Ephedrine and p-Bromobenzaldehyde. An X-ray Structure Redetermination. Journal of Organic Chemistry 48, 2923-2924 (1983).
15. Neelakantan, L. & Molin-Case, J. A. Crystal and Molecular Structure of 2-p-Bromophenyl-3,4-dimethyl-5-phenyloxazolidine. Journal of Organic Chemistry 36, 2261-2262 (1971).
16. Nurkenov, O. A., Gazaliev, A. M., Turdybekov, D. M., Dzhandigulov, A. R. & Adekenov, S. M. Synthesis and Crystal Structure of (2S,4S,5R)-2-(5-Bromo-2-hydroxyphenyl)-3,4-dimethyl-5-phenyl-1,3-oxazolidines. Russian Journal of General Chemistry 77, 1614-1617 (2007).
17. Bukeeva, A. B. et al. Reaction of d-Pseudoephedrine Hydrochloride with Anisaldehyde in the Presence of Sodium Cyanide. Russian Journal of General Chemistry 73, 831-833 (2003).
18. Ashcroft, S. J. The measurement of enthalpies of sublimation by thermogravimetry. Thermochimica Acta 2, 512 (1971).
19. Davies, M. & Jones, J. I. The sublimation pressures and heats of sublimation of some carboxylic acids. Transactions of the Faraday Society 61, 1608 (1954).
20. Davies, M. & Kybett, B. Sublimation and vaporization heats of long-chain alcohols. Transactions of the Faraday Society 61, 1608 - 1617 (1965).
21. Klosky, S., Woo, L. P. L. & Flanigan, R. J. Vapor Pressure of Benzoic Acid. Journal of the American Chemical Society 49 (1927).

22. Morawetz, E. Enthalpies of vaporization for a number of aromatic compounds Journal of Chemical Thermodynamics 4, 455 (1972).
23. Malaspina, L., Gigli, R. & Bardi, G. Microcalorimetric determination of the enthalpy of sublimation of benzoic acid and anthracene. Journal of Chemical Physics 59, 387 (1973).
24. McEachern, D. M. & Sandoval, O. A molecular flow evaporation apparatus for measuring vapour pressures and heats of sublimation of organic compounds. Journal of Physics E 6, 155 (1973).
25. Liley, P. E., Thomson, G. H., Friend, D. G., Daubert, T. E. & Buck, E. Perry's Chemical Engineers' Handbook (eds. Perry, R. H. & Green, D. W.) (McGraw Hill, New York, 1997).
26. Cox, J. D. & Pilcher, G. Thermochemistry of Organic and Organometallic Compounds (Academic Press, London 1970).
27. Wright, S. F., Dollimore, D., Dunn, J. G. & Alexander, K. Determination of the Vapour Pressure Curves of Adipic Acid and Triethanolamine using Thermogravimetric Analysis. Thermochimica Acta 421, 25-30 (2004).
28. Rastogi, R. P., Bassi, P. S. & Chadha, L. S. Kinetics of Reaction Between Naphthalene and Picric Acid in the Solid State. Journal of Physical Chemistry 66, 2707-2708 (1962).

6 THE BEHAVIOUR OF SALTS IN LIQUIDS

6.1 INTRODUCTION

In solid structures such as crystals, salts are known to exist as two (or more) ionised molecules in their ionised states. For salts in solutions ionisation of the components is also known to occur. The effect of this ionisation on the ideality of the systems (both binary and ternary) is less well understood. In liquids formed by the melt of salt components, the ionisation states of the components have not been previously investigated. This chapter will also endeavour to increase understanding of how ionisation affects ideality in both melt and solution systems (using binary and ternary phase diagrams). The contribution of pH to the solubility change is assessed from fundamental equations.

6.2 BEHAVIOUR OF SALT COMPONENTS IN THE MOLTEN STATE

6.2.1 INFRARED MICROSCOPY OF EPHEDRINE PIMELATE

The ionisation of molten salt components in the ephedrine/pimelic acid system as the ratio of components changes was of considerable interest. The ionisation was assessed using IR microscopy. The theory of FTIR and the equipment used for IR microscopy is discussed in Section 2.4.1.4. The samples were ground in a pestle and mortar and then melted on a microscope slide using a sealed hotplate. The molten sample was then placed under the microscope, imaged and spots for analysis selected (Figure 110). The selection of a number of spots allowed some understanding of the homogeneity of the system. IR spectra of the selected spots were then collected.

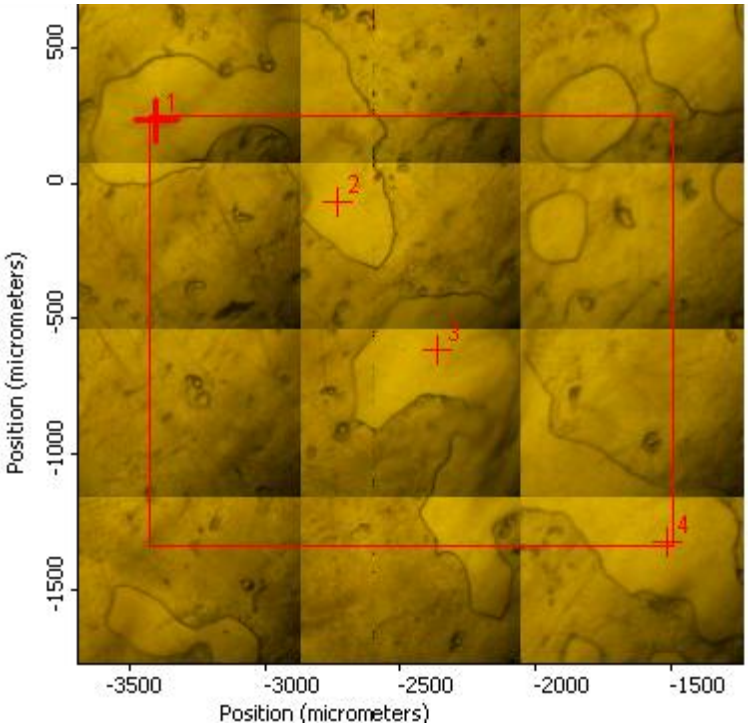

FIGURE 110- IMAGE OF THE MOLTEN EPHEDRINE AND PIMELIC ACID SALT SAMPLE FROM IR MICROSCOPY. NUMBERED POINTS (1-4) ARE THOSE SELECTED FOR SPECTROSCOPY.

From the IR spectra collected it can clearly be seen that as the ratio of ephedrine to pimelic acid increases, so does the ionisation of the carboxylic acid groups of the pimelic acid molecules. This is shown by the increase in peak size at 1559 cm^{-1} and a decrease in peak size at 1681 cm^{-1}. In Figure 111 the peak is large at 1559 cm^{-1} and no peak is present at 1681 cm^{-1}. This indicates total ionisation, as would be expected from 0.1 moles of acid and 0.9 moles of ephedrine. In Figure 119 the peak is large at 1681 cm^{-1} and no peak is present at 1559 cm^{-1}, as expected from a ratio of 0.9 moles of acid and 0.1 moles of ephedrine.

The spectra in Figure 111 to Figure 119 focus on the region 1200 cm^{-1} to 1900 cm^{-1} so the shift of the carbonyl can be interrogated.

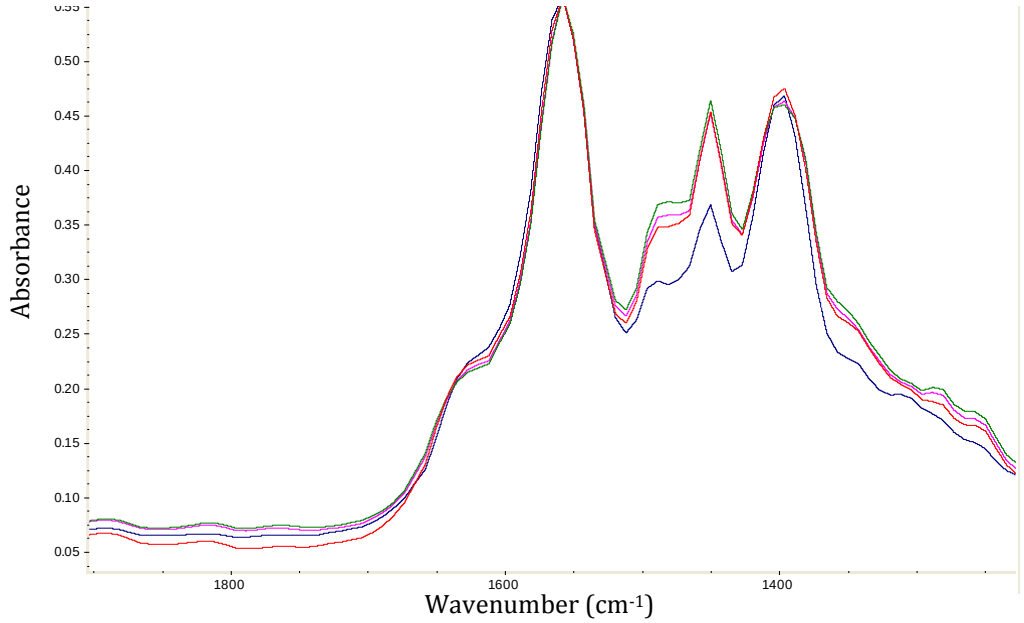

FIGURE 111- IR SPECTRA OF SIX SPOTS SELECTED FROM A MOLTEN SAMPLE COMPOSED OF 0.1 MOLES OF PIMELIC ACID AND 0.9 MOLES OF EPHEDRINE.

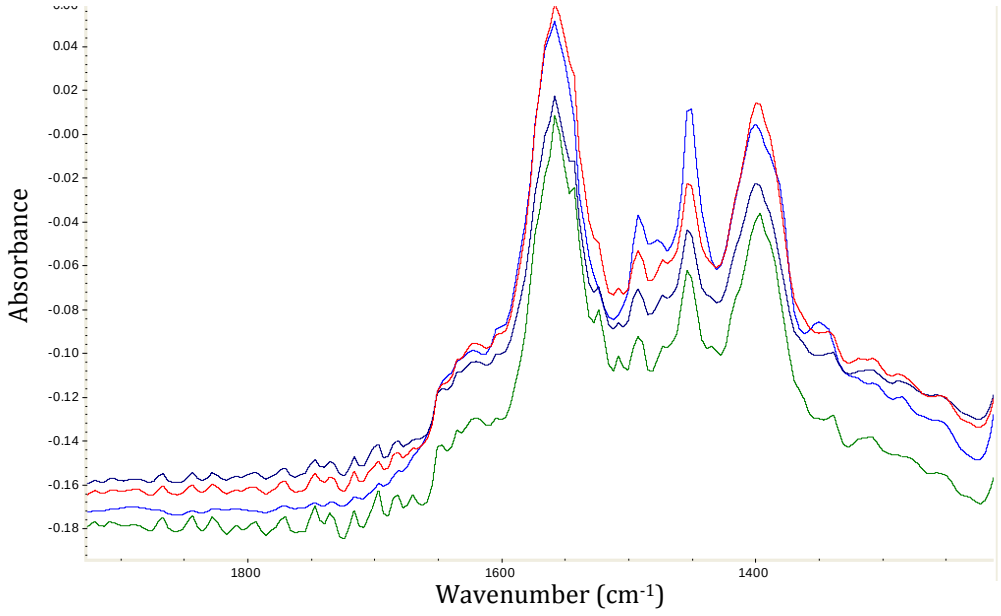

FIGURE 112- IR SPECTRA OF SIX SPOTS SELECTED FROM A MOLTEN SAMPLE COMPOSED OF 0.2 MOLES OF PIMELIC ACID AND 0.8 MOLES OF EPHEDRINE.

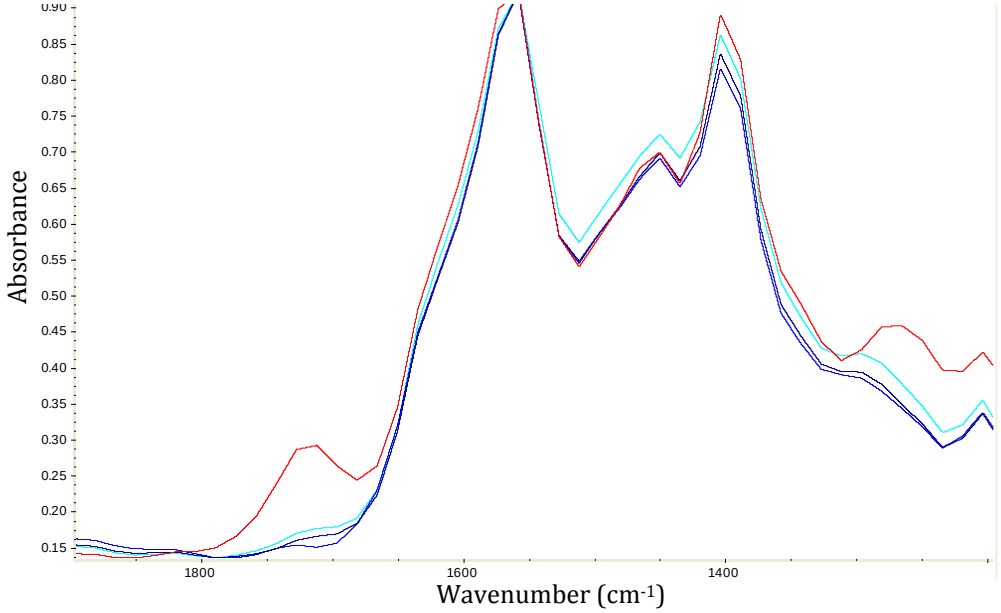

FIGURE 113- IR SPECTRA OF SIX SPOTS SELECTED FROM A MOLTEN SAMPLE COMPOSED OF 0.3 MOLES OF PIMELIC ACID AND 0.7 MOLES OF EPHEDRINE.

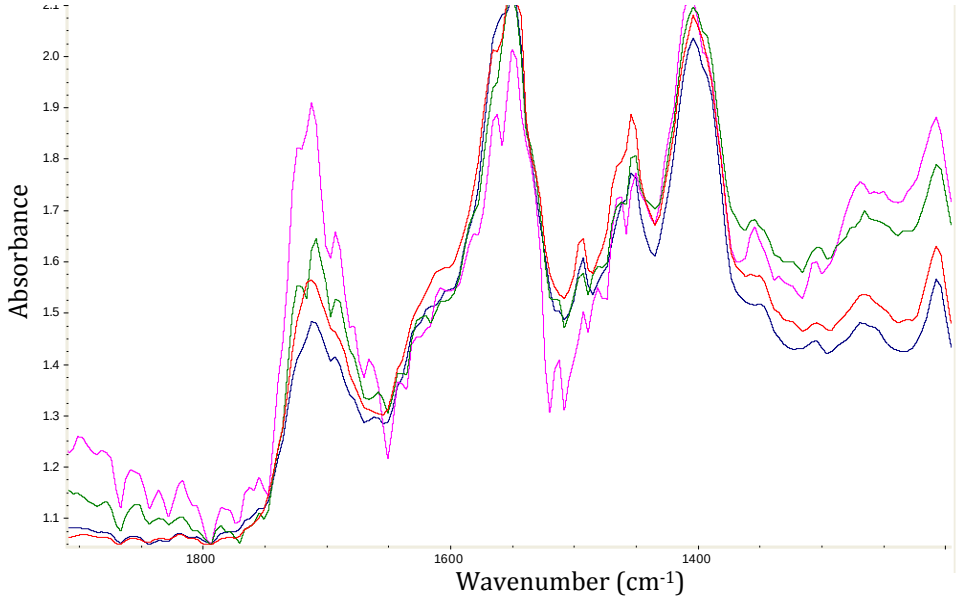

FIGURE 114- IR SPECTRA OF SIX SPOTS SELECTED FROM A MOLTEN SAMPLE COMPOSED OF 0.39 MOLES OF PIMELIC ACID AND 0.61 MOLES OF EPHEDRINE.

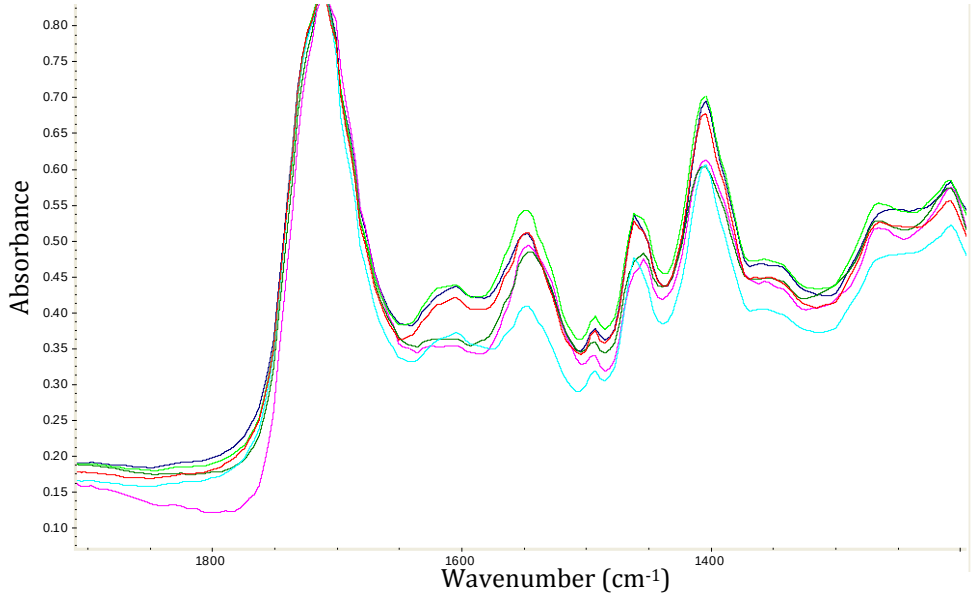

FIGURE 115- IR SPECTRA OF SIX SPOTS SELECTED FROM A MOLTEN SAMPLE COMPOSED OF 0.54 MOLES OF PIMELIC ACID AND 0.46 MOLES OF EPHEDRINE.

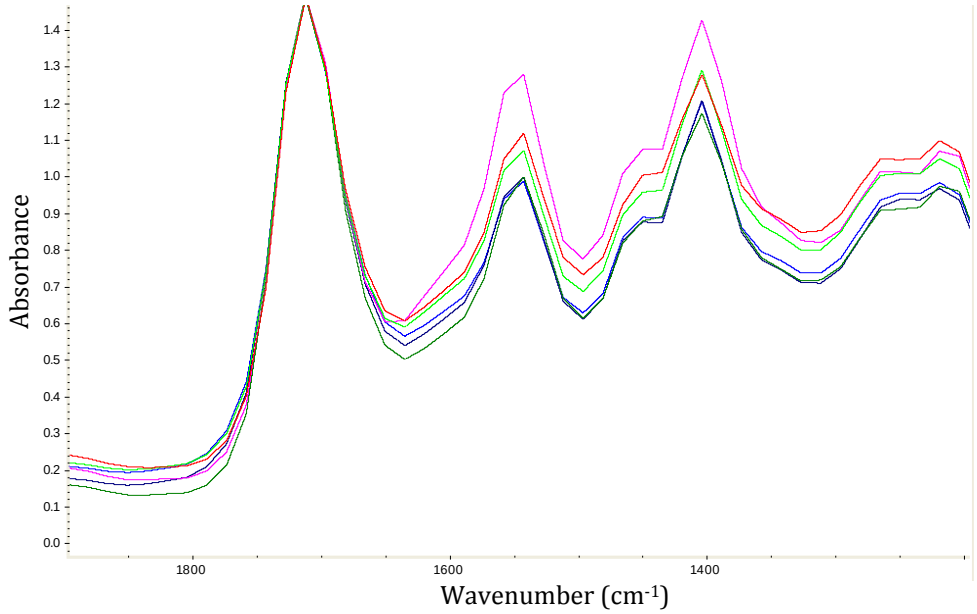

FIGURE 116- IR SPECTRA OF SIX SPOTS SELECTED FROM A MOLTEN SAMPLE COMPOSED OF 0.65 MOLES OF PIMELIC ACID AND 0.35 MOLES OF EPHEDRINE.

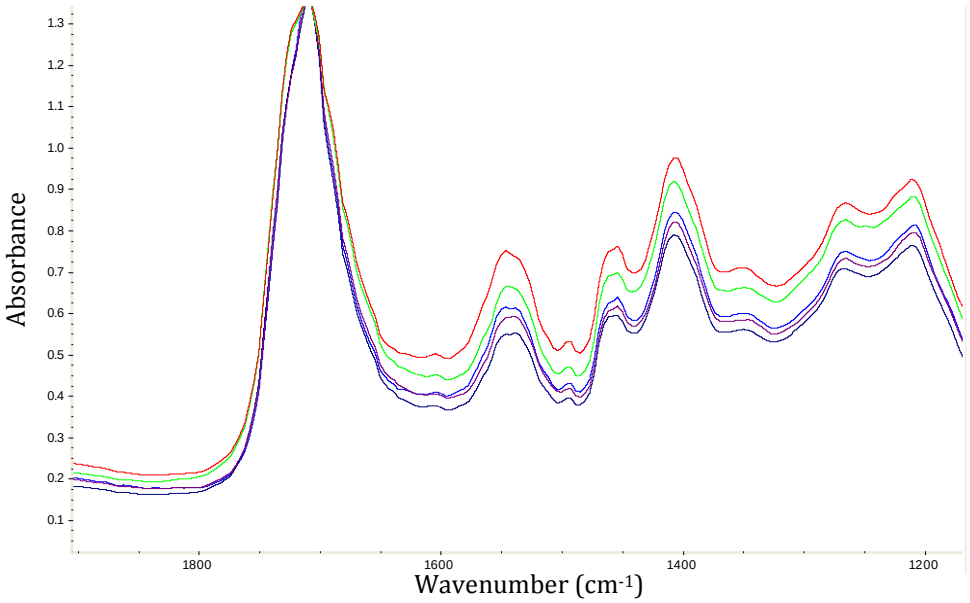

FIGURE 117- IR SPECTRA OF SIX SPOTS SELECTED FROM A MOLTEN SAMPLE COMPOSED OF 0.7 MOLES OF PIMELIC ACID AND 0.3 MOLES OF EPHEDRINE.

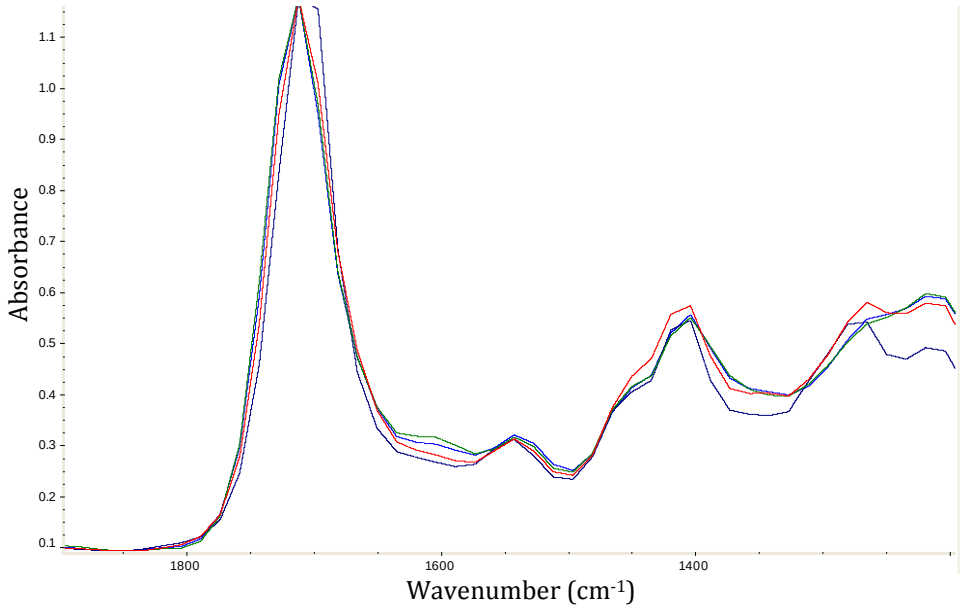

FIGURE 118- IR SPECTRA OF SIX SPOTS SELECTED FROM A MOLTEN SAMPLE COMPOSED OF 0.8 MOLES OF PIMELIC ACID AND 0.2 MOLES OF EPHEDRINE.

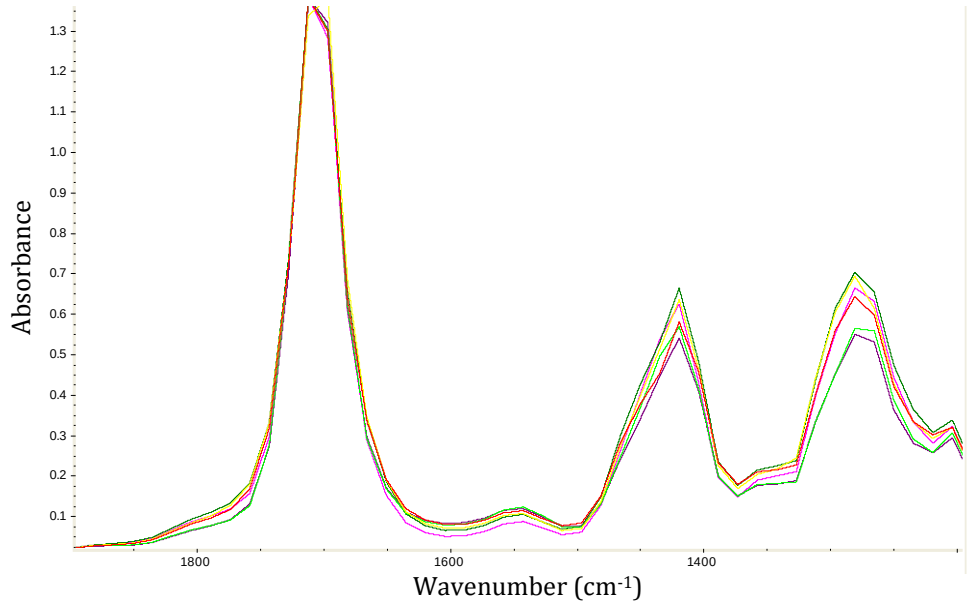

FIGURE 119- IR SPECTRA OF SIX SPOTS SELECTED FROM A MOLTEN SAMPLE COMPOSED OF 0.9 MOLES OF PIMELIC ACID AND 0.1 MOLES OF EPHEDRINE.

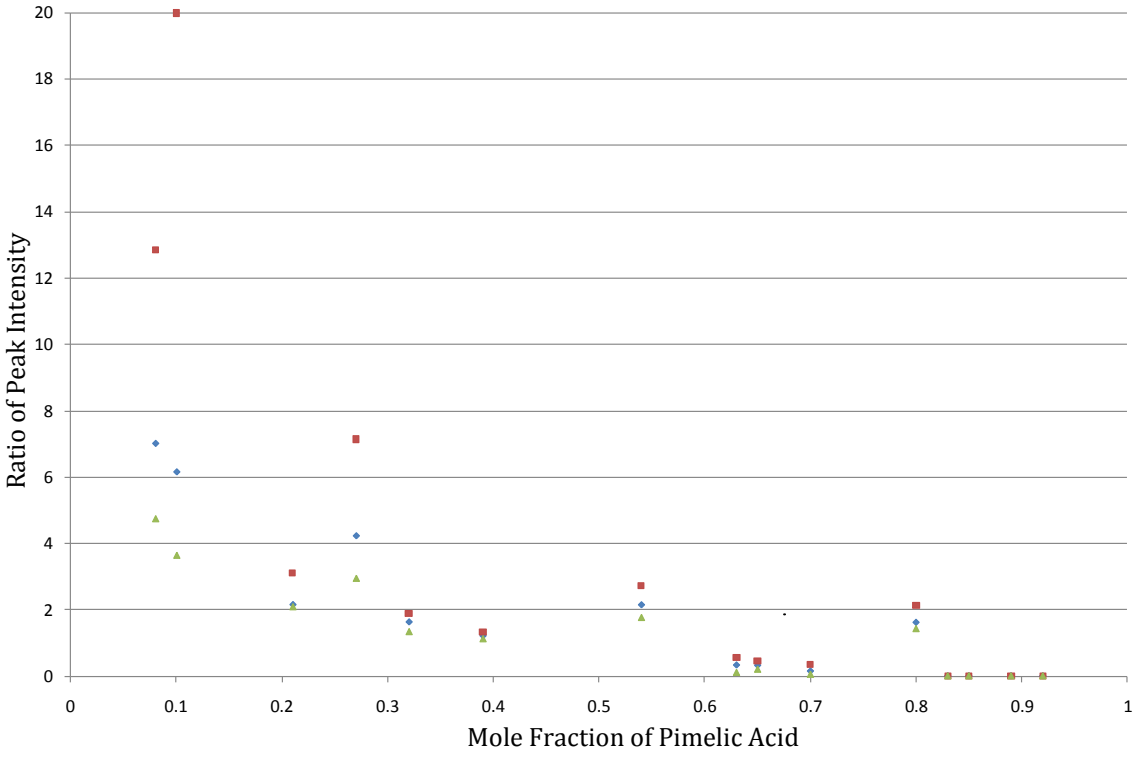

FIGURE 120- RATIO OF FTIR PEAK INTENSITY BETWEEN THE PEAK AT 1681 cm^{-1} AND THE PEAK AT 1559 cm^{-1} PLOTTED AGAINST MOLE FRACTION OF PIMELIC ACID (BLUE POINTS). THE RED AND GREEN POINTS RESPECTIVELY SHOW THE MAXIMUM AND MINIMUM DEVIATION BETWEEN PEAKS IN SPECTRA.

In Figure 120 the ratio between the ionised and unionised peaks is shown for each IR spectrum (including some not displayed above). For the calculation the intensity of the peak at 1559 cm^{-1} (ionised carbonyl) was divided by the intensity of the peak at 1681 cm^{-1} (unionised carbonyl). Red and green markers show the deviation between the highest intensity difference (red) and the lowest intensity difference (green) at that concentration. From these errors it can be seen that the samples were not entirely homogeneous.

From Figure 120 it can be seen that no ionisation occurs until just before a mole fraction of 0.2 ephedrine is present (mole fraction of 0.8 acid). This is consistent with the results from the far right hand side of the experimental binary phase diagram (Figure 121). Here it can be seen that the pure pimelic acid region goes to under 0.9 moles of acid. There is some uncertainty in the exact position of the region due to issues with binary phase diagram determination discussed in Section 4.3.2. It can be concluded that for the pimelic acid region of the binary phase diagram no ionisation is occurring in the acid.

Between acid mole fractions of 0.7 and 0.35 (Figure 120) the ratio of peak intensities is around 2, suggesting the ionised peak is around twice as intense as the unionised. This does not mean there are twice as many ionised carbonyl groups as there are unionised groups, merely that the intensity of this stretch is greater. What can be taken from this is the relatively consistent ionisation level in this region, corresponding to the 1:1 salt region in the binary phase diagram (Figure 121).

Between acid mole fractions of 0.2 and 0.35 is the 2:1 salt region, according to Figure 121. Total ionisation would be expected in this region but was not recorded in the molten sample IR spectra. The ionisation states of the solid and molten salt samples appear to be different.

Over an ephedrine mole fraction of 0.8 (0.2 mole fraction of acid), total ionisation can be seen to have occurred from the IR spectra in Figure 118 and Figure 119. Here the intensity ratio is not relevant as the result is merely the intensity of only one significant peak. It can be assumed that the 2:1 salt would be favoured to form. In the phase diagram this is seen to (briefly) be the case until entry into the pure

ephedrine region. Here it can be assumed that the 2:1 salt fails to form due to the ionisation state of ephedrine, not the acid. From the intensity differences between individual spectra (between red and green spots) a large amount of variability in this region can be seen. This is because a small difference in the size of the low intensity unionised peak has a major effect on the ratio when the intensity of the large peak was divided by it.

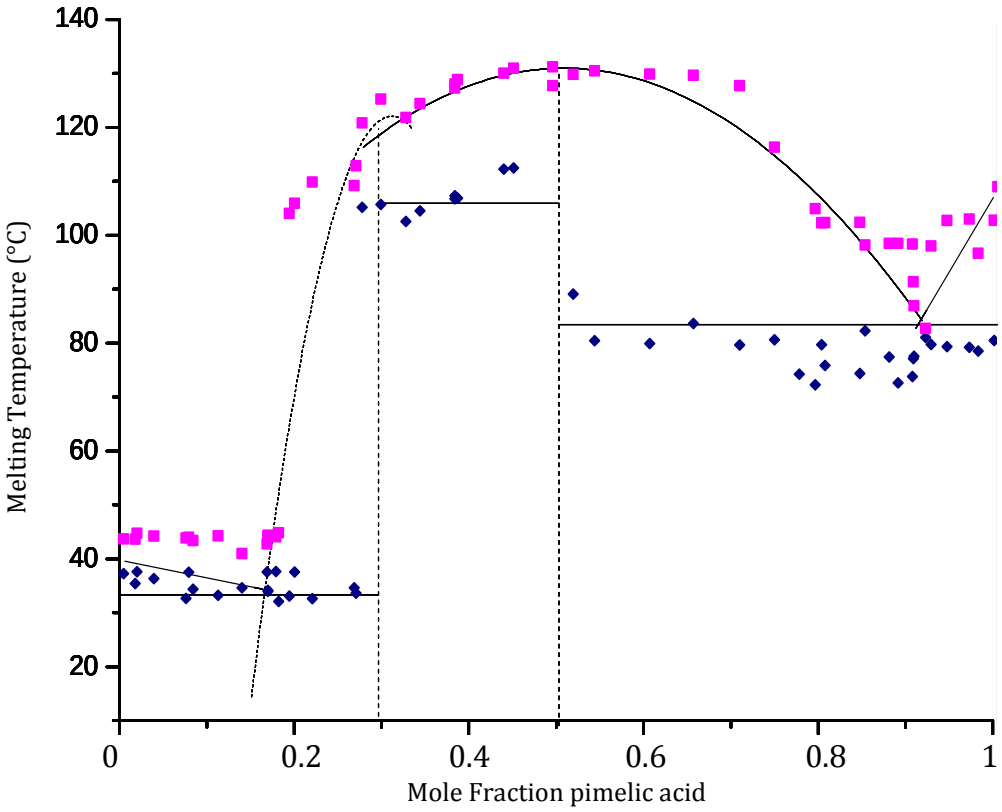

FIGURE 121- BINARY PHASE DIAGRAM OF EPHEDRINE AND PIMELIC ACID SHOWING EXPERIMENTALLY DETERMINED POINTS, PINK = MELT CURVES, BLUE = EUTECTIC LINES AND A SCHEMATIC TO GUIDE THE EYE IN WHICH THE SOLID HORIZONTAL LINES SHOW THE EUTECTIC AND THE CURVES SHOW THE MELT TEMPERATURES OF THE COMPONENTS AND SALTS IN CONTACT WITH ONE ANOTHER. THE DASHED CURVED LINE IS THE SUSPECTED 2:1 SALT REGION.

6.2.2 IDEALITY IN THE BINARY PHASE SYSTEM

The experimental binary phase diagram for ephedrine and pimelic acid (Figure 121) was determined by DSC using the method described in Section 2.2.4 and

plotted as a function of the mole fraction of acid. The phase diagram is given in Figure 122 and shows both ideal lines and also experimental results.

The ideal binary phase diagram was calculated using the Schröder-Van Laar[1] (for the pure components), Prigogine-Defay[2] (for 1:1 salt) and Rastogi[2] equations (for the 2:1 salt). The derived equations are given below for Schröder-Van Laar (Equation 6.1), Prigogine-Defay (Equation 6.2) and Rastogi (Equation 6.3) while the derivations can be found in Section 1.5.3.2. The enthalpy of fusion per mole of ions was calculated by dividing the molar enthalpy of fusion for the salt by the number of ions per molecule (1 for ephedrine or pimelic acid, 2 for the 1:1 salt and 3 for the 2:1 salt).

$$\ln x = \frac{\Delta_f H}{R}\left(\frac{1}{T} - \frac{1}{T_c}\right) \qquad \text{EQUATION 6:1}$$

$$\ln 4x(1-x) = \frac{\Delta_f H}{R}\left(\frac{1}{T} - \frac{1}{T_c}\right) \qquad \text{EQUATION 6:2}$$

$$\ln \frac{27}{4}(1-x)x^2 = \frac{\Delta_f H}{R}\left(\frac{1}{T} - \frac{1}{T_c}\right) \qquad \text{EQUATION 6:3}$$

The ideal lines on the phase diagram in Figure 122 show how the components behave if the interactions between the components are identical to the interactions between two identical molecules. The 1:1 salt can be seen to behave relatively ideally in its molten state, especially at the right hand side of the diagram with high proportions of pimelic acid. This suggests similar interactions occur between salt and acid as between the salt molecules. At the left hand side with a high proportion of ephedrine, the ideal region is broader than in the experimental diagram. This means a lower melting temperature of the salt is measured in reality than would be predicted ideally. The ephedrine stability region is larger than predicted. In the 1:1 salt region the ionisation state does not change upon melting (from IR melt data) and hence follows ideality.

Ideally the 2:1 salt is metastable, while in reality it is a small but definitely accessible stable region. The position and melting temperature of the ideal 2:1 liquidus is quite similar to that measured experimentally. The metastability is

caused by the broadness of the ideal 1:1 liquidus, which in reality is less broad (as discussed above). In the pure ephedrine region the melting point does not decrease with the addition of the acid as expected, instead remaining constant. This means it is showing a positive deviation from ideality. The ephedrine to 2:1 salt interactions are weaker than those between two molecules of the pure base. The pimelic acid experiences a negative deviation from ideality on the addition of ephedrine. The melting point of the pimelic acid decreases much more than would be expected ideally. This suggests it is strongly affected by the presence of another component. From the IR melt data from the 2:1 region, the total ionisation expected is not apparent. This means the ionisation states of the solid and molten samples are different. This may be the partial cause of the deviation from ideality.

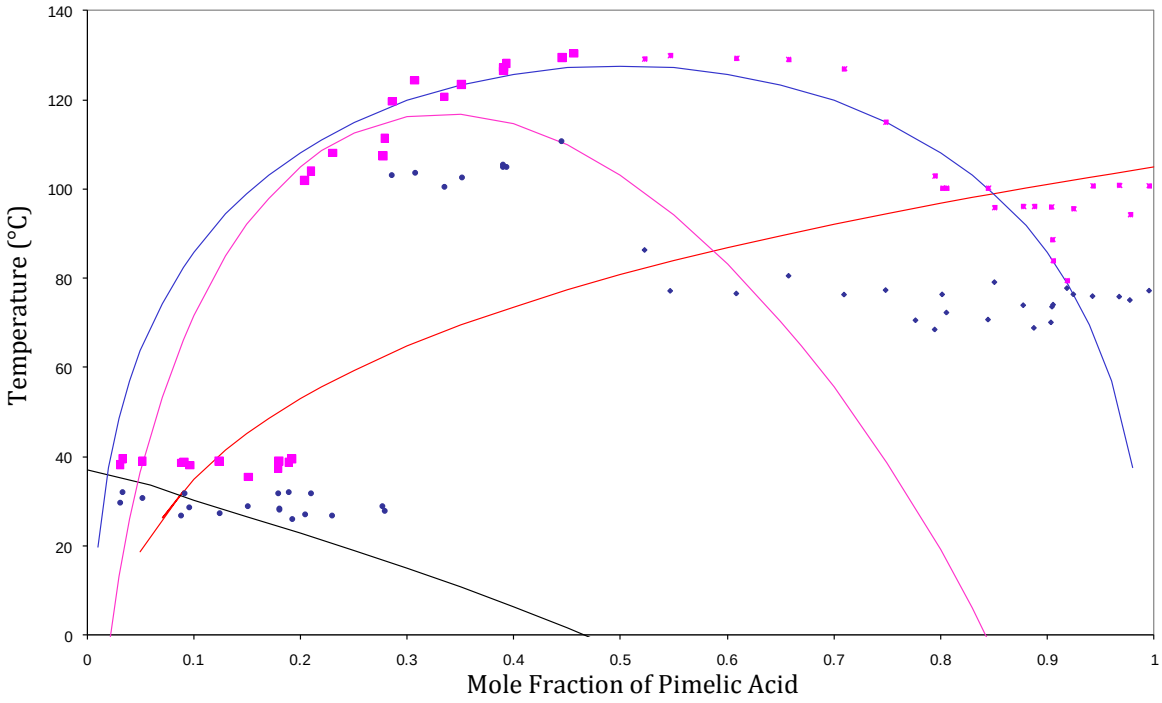

FIGURE 122- EPHEDRINE AND PIMELIC ACID. THE IDEAL BINARY PHASE DIAGRAM OVERLAID WITH THE EXPERIMENTAL BINARY PHASE DIAGRAM. PINK SPOTS- EXPERIMENTAL LIQUIDUS, BLUE SPOTS- EXPERIMENTAL EUTECTIC LINES, BLUE CURVE- IDEAL 1:1 LIQUIDUS, PINK CURVE- IDEAL 2:1 LIQUIDUS, RED LINE- IDEAL PIMELIC ACID LIQUIDUS, BLACK LINE- IDEAL EPHEDRINE LIQUIDUS.

From the ideal binary phase diagram it would appear possible that both the 1:1 and 2:1 ephedrine pimelate salts are accessible without the use of solvents. Although the ideal binary phase diagram does not provide a perfect representation

of the experimental results for this system, it accurately predicts the solid phases that are accessible without the use of solvents.

6.3 SOLUBILITY OF SALT COMPONENTS

The ideal solubilities of the pure starting components in the ephedrine and pimelic acid salt system were calculated using the Schröder-Van Laar (Equation 6.1), Prigogine-Defay (Equation 6.2) and Rastogi (Equation 6.3) equations used previously for the ideal binary system (Section 6.2.2).

TABLE 17- EXPERIMENTAL AND IDEAL SOLUBILITY DATA FOR SALTS AND SALT COMPONENTS IN THE EPHEDRINE AND PIMELIC ACID SYSTEM

	Actual Solubility (mole fraction)	**Ideal Solubility (mole fraction)**	**Ratio of Ideal to Measured Solubility**
Ephedrine	0.0539	0.8000	14.84
Pimelic Acid	0.0465	0.0679	1.46
1:1 Salt	0.16	0.3250	2.03
2:1 Salt	~0.80	0.6149	0.77

6.3.1 IDEALITY IN THE TERNARY PHASE SYSTEM

The ideal ternary phase diagram (Figure 123) displays how the components of the ephedrine pimelate system (including water) would behave if the interactions between them were identical to those between two identical molecules. If this is compared to the actual ternary phase diagram (Figure 124) the system can be seen to be highly non-ideal. The ideal calculations predict the metastability of the 2:1 salt.

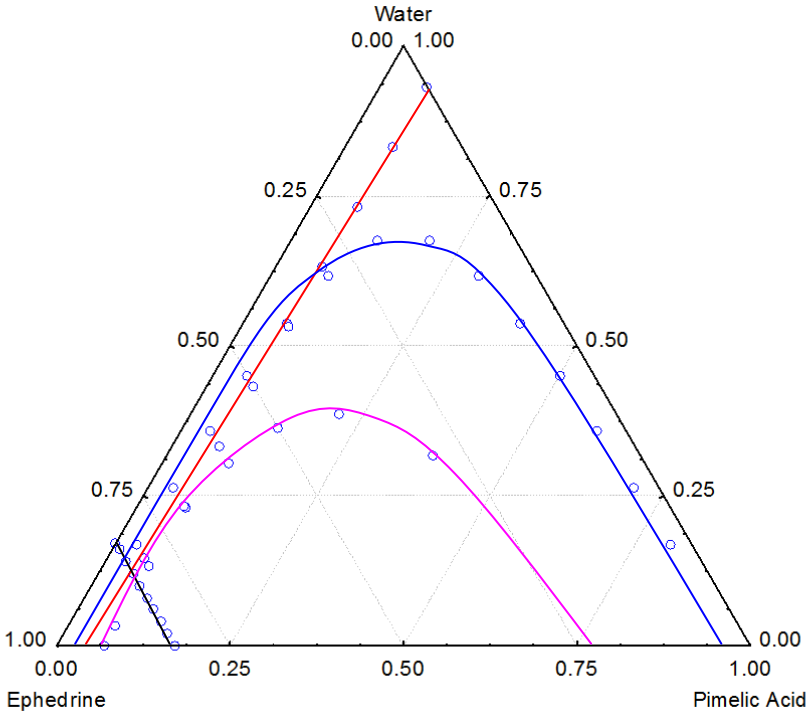

FIGURE 123- IDEAL TERNARY PHASE DIAGRAM OF EPHEDRINE AND PIMELIC ACID IN WATER AT 23°C IN MOLE FRACTION. LINES REPRESENT THE LIQUIDUS FOR PIMELIC ACID (RED), EPHEDRINE (BLACK), 1:1 SALT (BLUE) AND 2:1 SALT (PINK)

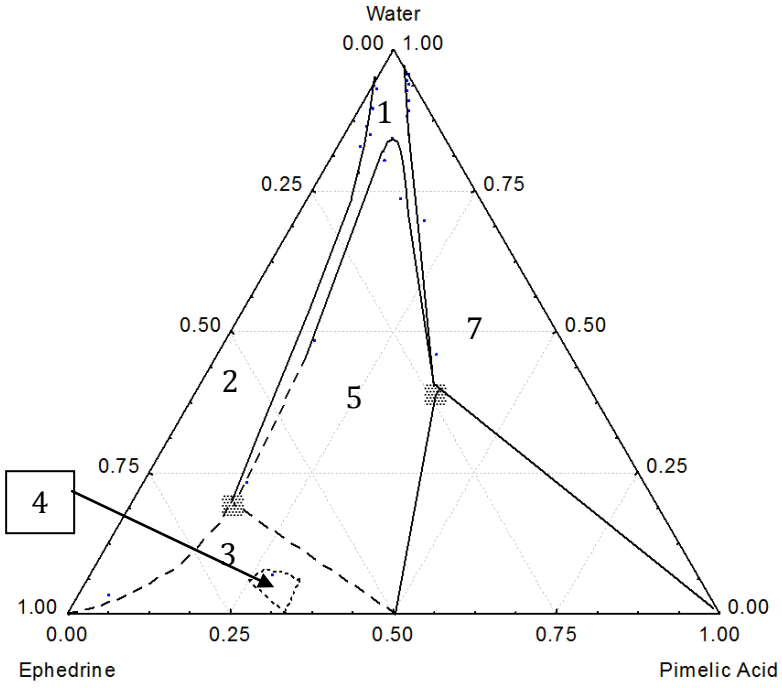

FIGURE 124- THE TERNARY PHASE DIAGRAM OF EPHEDRINE-PIMELIC ACID-WATER AT 23°C IN MOLE FRACTION (1) LIQUIDUS, (2) EPHEDRINE + LIQUID, (3) EPHEDRINE + 1:1 SALT + LIQUID,

(4) 2:1 SALT (5) 1:1 SALT + LIQUID, (6) 1:1 SALT + PIMELIC ACID + LIQUID, (7) PIMELIC ACID + LIQUID. ▒ INDICATES UNCERTAINTY OF THE EUTECTIC POSITIONS. THE DASHED LINES INDICATE UNCERTAINTY OF THE LIQUIDUS LINES DUE TO VERY HIGH SOLUBILITIES.

It is already well known that the ideal solubility of ephedrine is very different to the aqueous solubility determined experimentally[3] and this is displayed again in Figure 123. This is because of the difficulty in hydrating the phenyl ring due to its unfavourable interactions with water. Ideally the solubility is unaffected by the increase in counter-ion concentration and runs parallel to the opposite side of the triangle. Similarly when the actual solubility is plotted for an invariant system (where solubility is unaffected by the presence of another component) there is no increase in solubility on addition of acid. In reality the ephedrine solubility increases much more sharply with a negative deviation from ideality. This can be viewed more clearly in Figure 125 below. The points gained in this region with higher proportions of acid present are also not as accurate as at lower concentrations. This is due to the very high solubility and inherent issues with agitation and equilibration. The solubility of the ephedrine increases to a mole fraction of over 0.8 in the water and pimelic acid solution. This suggests strong solution phase interactions between ephedrine and pimelic acid in this region of the diagram. The R factor of the trendline in Figure 125 is 0.945.

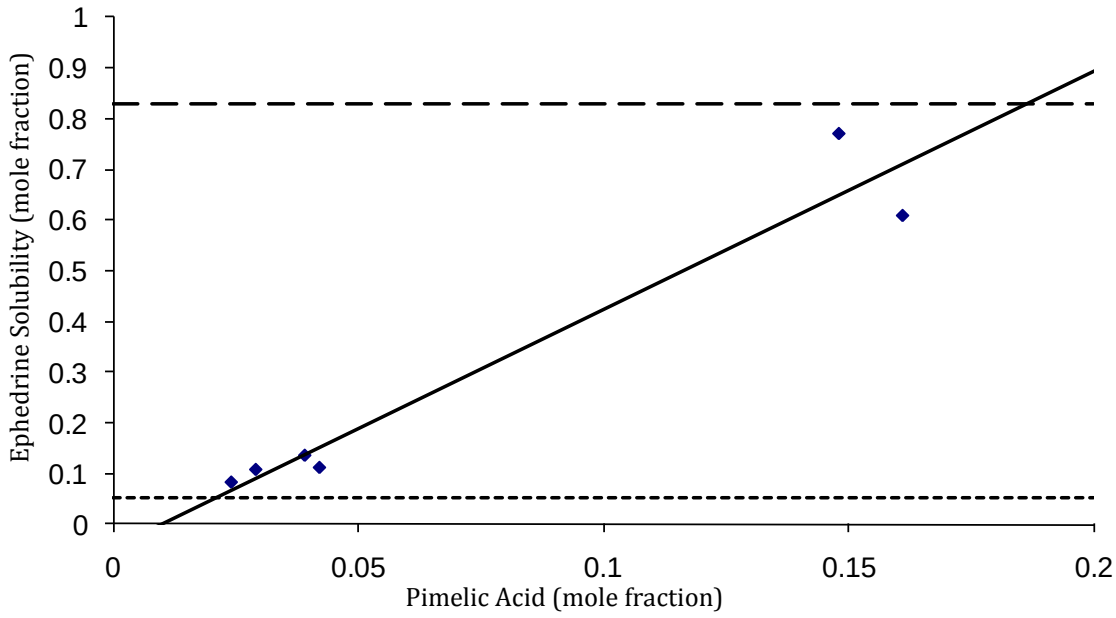

FIGURE 125- GRAPH SHOWING HOW THE EXPERIMENTALLY MEASURED SOLUBILITY OF EPHEDRINE VARIES WITH THE ADDITION OF PIMELIC ACID (SOLID LINE), THE EXPERIMENTAL SOLUBILITY IN AN INVARIANT SYSTEM (SMALL DASHED LINE) AND THE IDEAL SOLUBILITY (CALCULATED USING SCHRÖDER- VAN LAAR) IN AN IDEAL SYSTEM (LARGE DASHED LINE). ALL SOLUBILITES ARE GIVEN IN MOLE FRACTION.

The ideal solubility of pimelic acid is very similar to the experimental value in water. Pure pimelic acid has similar interactions with water as with itself and hence behaves ideally. The pimelic acid does not behave ideally as the ephedrine is added. Studying Figure 123 and Figure 124 the solubility of the pimelic acid can be seen to increase rapidly as ephedrine is added, rather than remaining parallel to the opposite side of the triangle. This is shown in more detail in Figure 126 where the extent of the non-ideality is obvious. The interactions between the pimelic acid and ephedrine in water are much stronger than those between pure pimelic acid molecules. It appears that as the proportion of singly charged anion increases, the deviation from ideality becomes increasingly positive. The pimelic acid is not as soluble as the ephedrine and only reached a maximum mole fraction of approximately 0.25. Agitation and equilibration did not pose a problem. More data points were collected than for the ephedrine side of the diagram. The R factor of the trendline in Figure 126 is 0.9184.

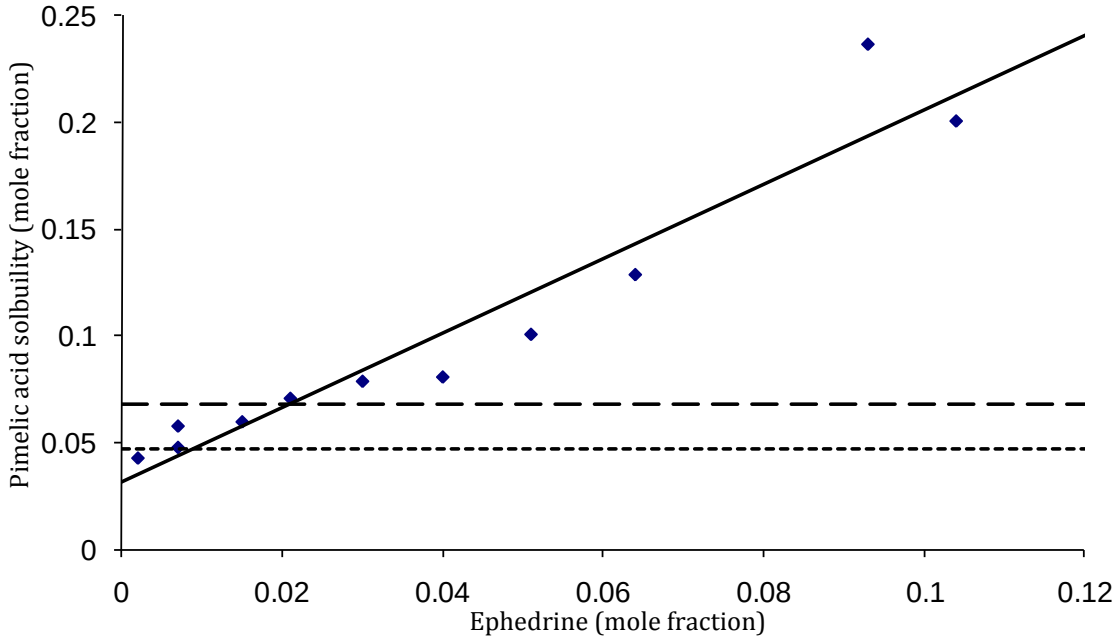

FIGURE 126- GRAPH SHOWING HOW THE EXPERIMENTALLY MEASURED SOLUBILITY OF PIMELIC ACID VARIES WITH THE ADDITION OF EPHEDRINE (SOLID LINE), THE EXPERIMENTAL SOLUBILITY IN AN INVARIANT SYSTEM (SMALL DASHED LINE) AND THE IDEAL SOLUBILITY (CALCULATED USING SCHRÖDER- VAN LAAR) IN AN IDEAL SYSTEM (LARGE DASHED LINE). ALL SOLUBILITES ARE GIVEN IN MOLE FRACTION.

From Figure 125 and Figure 126 it can be observed that neither salt component behaves anything like it would in ideal or invariant systems.

According to the ideal scenario the 2:1 salt is metastable to the 1:1 salt and will always convert to the 1:1 stoichiometry in water. In reality the 2:1 salt proved very hard to form from water (see Section 4.4). Single crystals were only successfully grown on one occasion and the formation of crystalline powder was never achieved. The 2:1 salt was found to convert to a mixture of 2:1 and 1:1 salts after deliquescence occurred. As the sample recrystallised the more stable 1:1 salt also crystallised out due to its lower solubility and hence greater stability (evidence in Section 4.5.3). Upon leaving this sample at ambient conditions it was found to convert to the 1:1 salt. It appears the ideal system offered a correct prediction and the 2:1 salt is metastable to the 1:1. This conclusion proved elusive from only the ternary phase diagram due to the very high aqueous solubility in this region and hence a lack of accurate points measured.

6.4 THE EFFECT OF pH ON SOLUBILITY

As is demonstrated and discussed in the 2005 paper by Jones *et al*[4], the solubilities of salts and their components are considerably more complicated than those of neutral species. They are defined by the species of acid and base in the solution under a given set of conditions. The speciation is dependent upon the pH and the solvent used (and hence the pK_a of the compound in that solvent). The solubility of the base is defined as the sum of all the component species in solution. Equivalently, the solubility of the acid is the sum of all the acidic component species. The solubility of the salt can be determined by combining these equations.

6.4.1 VARIATION IN BASE SOLUBILITY WITH CHANGING pH

For the component base the mass balance equations combined with the base equilibria give the relationship,

$$\text{Solubility} = [B] + [BH^+]; \; K_b = [H^+][B]/[BH^+] \qquad \text{EQUATION 6:4}$$

The ionisation of the basic component can be described thus,

$$[B] + [BH^+] = K_{sp}*(1 + ([H^+]/10^{-pKb})) \qquad \text{EQUATION 6:5}$$

The K_{sp} is determined using this equation, according to the method discussed by Black *et al*[3]. If pH $\gg$ pK_b then [B] = K_{sp} and the K_{sp} of ephedrine used is 0.345 mol^2/L^2.

When the solubility is calculated as a function of pH using this equation it is seen that the ephedrine solubility increases exponentially as the pH decreases (as shown in Figure 127). This is in agreement with the ternary phase diagram shown in Figure 124. Ephedrine is becomes increasingly soluble as the proportion of acid is increased and the pH decreases.

Also plotted on the graph shown in Figure 127 are three experimentally determined solubility points for which the pH was measured. These can be seen to show the same trend with solubility increasing as pH decreases. The increase in solubility is much sharper in reality than predicted by the pH alone. For ephedrine it can be concluded that the change in pH is not the only cause of the increased

solubility as the proportion of acid is increased. It appears some other form of association/dissociation is occurring that is not explicitly captured by these equations.

The initial curve in the exponential plot (Figure 127) is due to the position above the pK_a of the base. Once below the pK_a a true exponential curve can be seen.

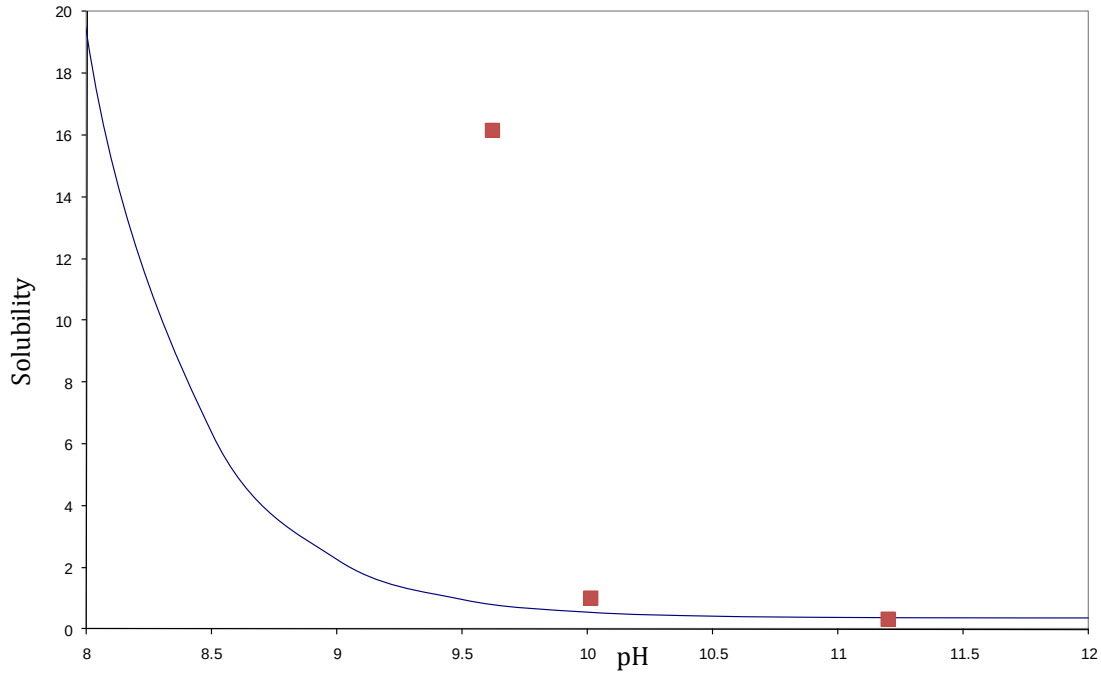

FIGURE 127- THE CALCULATED SOLUBILITY OF EPHEDRINE PLOTTED AGAINST THE pH OF THE SOLUTION (BLUE LINE). RED MARKERS INDICATE THE POSITION OF EXPERIMENTALLY DETERMINED DATA.

6.4.2 VARIATION IN ACID SOLUBILITY WITH CHANGING pH

For the component acid the mass balance equations combined with the acid equilibria give the relationship,

$$\text{Solubility} = [A^{2-}]+[HA^{-}]+[H_2A];$$

$$K_{a1} = [H^{+}][HA^{-}]/[H_2A];$$

$$K_{a2} = [H^{+}][A^{2-}]/[HA^{-}] \qquad \text{EQUATION 6:6}$$

The ionisation of the acidic component can be described thus,

$$[H_2A]+[HA^{-}]+[A^{2-}]=$$

$$K_{sp}*(1+(10^{-pKa2}/[H^+])+((10^{-pKa1}*10^{-pKa2})/[H^+]^2)) \quad \text{EQUATION 6:7}$$

The K_{sp} is determined using this equation. If pH $\ll$ pK_a, then K_{sp} = $[H_2A]$ or more specifically in this case 0.29 mol^3/L^3.

When the solubility is calculated as a function of pH using this equation it can be seen that the acid solubility increases drastically as the pH increases (as shown in Figure 128). This is in agreement with the ternary phase diagram shown in Figure 124, where the pimelic acid becomes increasingly soluble as the proportion of base is increased causing pH to increase.

Also plotted on the graph shown in Figure 128 are five experimentally determined solubility points for which the pH was measured. These can be seen to show the same trend with solubility increasing as pH increases. The increase in solubility is much sharper in reality than predicted by the pH alone. As for the ephedrine, it can be concluded that the change in pH is not the only cause of the increased solubility. Some other form of association/dissociation is occurring that is not explicitly captured by these equations.

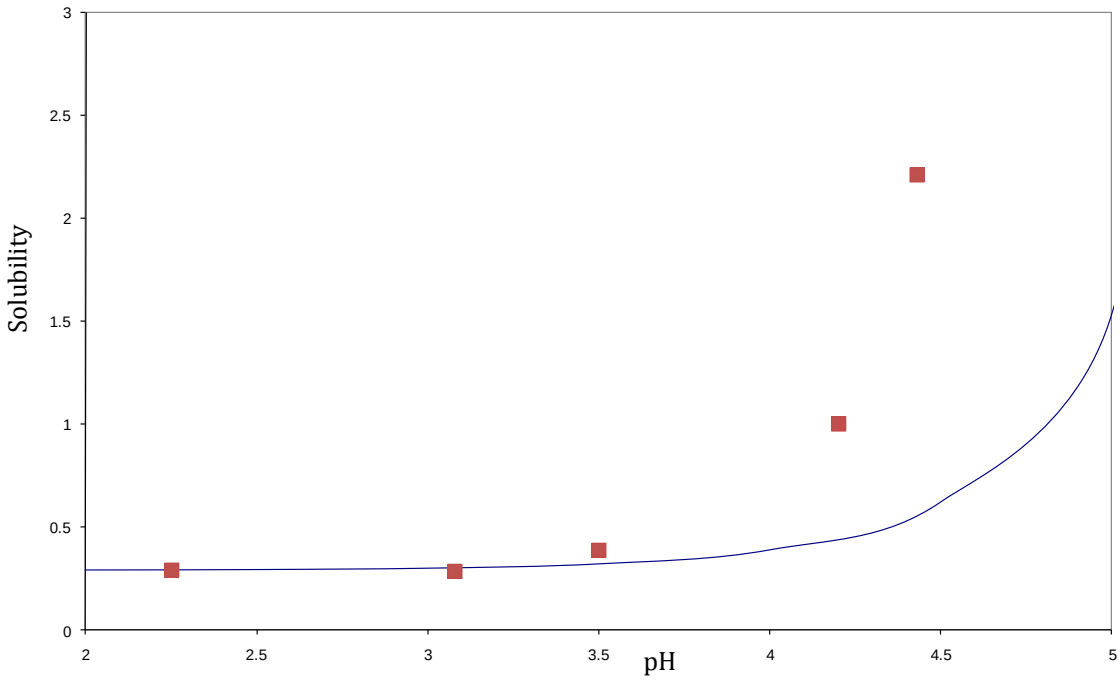

FIGURE 128- THE CALCULATED SOLUBILITY OF PIMELIC ACID PLOTTED AGAINST THE pH OF THE SOLUTION (BLUE LINE). RED MARKERS INDICATE THE POSITION OF EXPERIMENTALLY DETERMINED DATA.

The initial curve in the exponential plot (Figure 128) is due to the position below the pK_a of the base. Once above the pK_a a true exponential curve can be seen.

6.4.3 VARIATION IN SALT SOLUBILITY WITH CHANGING pH

For the ephedrine and pimelic acid system a mono-base and di-acid were being used. The equations required were different to those published by Jones *et al*[4], where a di-base and mono-acid were used.

It is possible to describe the ionisation of the whole system thus,

$$[A^{2-}]+[HA^{-}]+[H_2A]=[BH^{+}]+[B] \qquad \text{EQUATION 6:8}$$

Equations 6.6 and 6.7 combined with Equation 6.8 can then be used to quantify the species in solution in terms of the dissociation constants thus,

$$\text{Solubility}=(1/4*K_{sp}*((1+([H^{+}]/K_b))^2)*(1+(K_{a1}/[H^{+}])+((K_{a1}*K_{a2})/[H^{+}]/[H^{+}]))^{1/3} \qquad \text{EQUATION 6:9}$$

As the plot is only for a 1:1 salt, despite the di-acid present, the equations can be simplified to that for a monoprotic acid (providing the pH remains above the pK_a value of 4.48). For the mono-acid, as for a di-acid above,

$$[A^{-}] + [HA] = [BH^{+}] + [B] \qquad \text{EQUATION 6:10}$$

$$\text{Solubility} = (K_{sp}*(1 + (K_a/[H^{+}]))*(1 + ([H^{+}]/K_b)))^{1/2} \qquad \text{EQUATION 6:11}$$

The K_{sp} for use in these equations was determined using the Solver function in Microsoft Excel. A measured pH value was added to the list of arbitrary pH values giving a calculated pH as a function of K_{sp}. The difference between the calculated solubility at this pH value and the measured solubility was then minimised by varying the K_{sp}. When the difference between the two solubilities was zero the K_{sp} value had been determined. The K_{sp} was determined as 0.0017 (mol^2/L^2). This method was also employed in the 2008 paper[5] concerning the solubility of saccharinate salts and cocrystals. The full paper can be found in the Appendix.

The solubility can be plotted as a function of pH using these calculations and giving the blue line in the plot shown in Figure 129. This shows maximum solubilities are achieved at very high and very low pH values and a minimum solubility is attained at between 4.5 and 6.5. While measuring the ternary phase diagram it was determined that the pH range of the salt region was between approximately 4.5 and 8. The minimum solubility would be expected in this region. Also plotted in Figure 129 are the experimental solubilities with known pH values. From these it can be seen that in reality the increase in solubility at both ends of the pH scale is slightly greater than the pH calculations predict. The fit between the predicted and measured solubilities is relatively accurate (compared to the pure components) and ionisation is the major governing factor in the solubility increase.

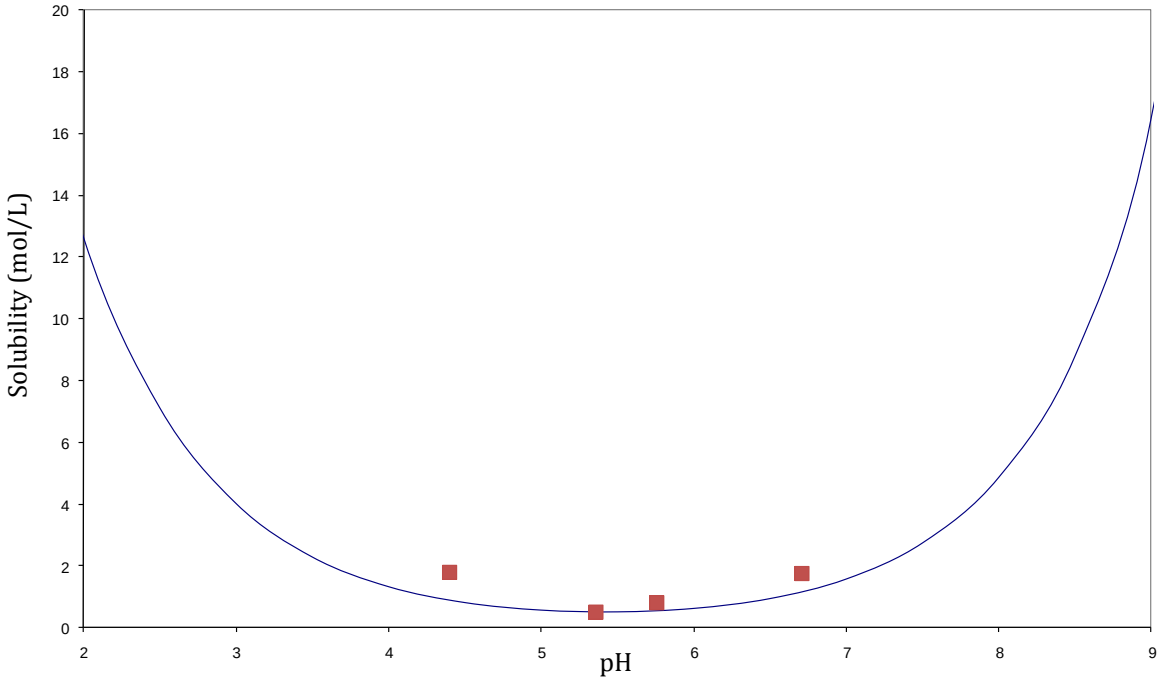

FIGURE 129- THE CALCULATED SOLUBILITY OF THE 1:1 SALT PLOTTED AGAINST THE pH OF THE SOLUTION (BLUE LINE). RED MARKERS INDICATE THE POSITION OF EXPERIMENTALLY DETERMINED DATA.

6.5 DETERMINATION OF THE pH WITH KNOWN SOLUBILITIES

Using the fundamental equations given below it was felt that it would be possible to calculate the pH of solutions along the liquidus line of the ternary phase diagram. The full derivations of the equations used for these calculations are given in the Section 8.3 with the key equations given below. The square brackets used in

concentration annotation (e.g. $[H^+]$) are omitted in order to simplify the equations, however it should be noted that H^+, OH^-, HA^-, H_2A, B and BH^+ are all concentrations, not constants.

Fundamental Equations

$$Kw = H^+OH^- \qquad \text{EQUATION 6:12}$$

$$Ka_1 = H^+HA^- / H_2A \qquad \text{EQUATION 6:13}$$

$$Ka_2 = H^+A^{2-} / HA^- \qquad \text{EQUATION 6:14}$$

$$Kb = BH^+OH^- / B \qquad \text{EQUATION 6:15}$$

$$c_1 = H_2A + HA^- + A^{2-} \qquad \text{EQUATION 6:16}$$

$$c_2 = B + BH^+ \qquad \text{EQUATION 6:17}$$

$$H^+ + BH^+ = HA^- + A^{2-} + OH^- \qquad \text{EQUATION 6:18}$$

Known Values

$pKa_1 = 4.48$
$pKa_2 = 5.42$
$pKb = 9.74$
$pKw = 14$

An equation for A^{-2} was derived in terms of known values and concentrations, starting with Equation 6.16 giving,

$$\frac{Ka_1Ka_2c_1}{Ka_1Ka_2 + \left(H^+\right)^2 + H^+Ka_1} = A^{2-} \qquad \text{EQUATION 6:19}$$

An equation for HA^- was then derived in terms of known values and concentrations, starting with Equation 6.16 giving ,

$$HA^- = \frac{H^+ Ka_1 (Ka_2)^2 c_1}{Ka_1 Ka_2 + (H^+)^2 + H^+ Ka_1} \qquad \text{EQUATION 6:20}$$

An equation for BH^+ was derived in terms of known values and concentrations, starting with Equation 6.17 giving,

$$BH^+ = \frac{c_2 KbH^+}{H^+ Kb + Kw} \qquad \text{EQUATION 6.21}$$

By combining equations for A^{2-}, HA^- and BH^+ given above into Equation 6.18, multiplying out all of the terms and setting the equation to zero,

$$(H^+)^5 Kb + (H^+)^4 (KbKa_1 + Kw + c_2 Kb) +$$
$$(H^+)^3 (KbKa_1 Ka_2 + KwKa_1 + c_2 KbKa_1 - Ka_1 c_1 Kb - KwKb) +$$
$$(H^+)^2 (KwKa_1 Ka_2 + c_2 KbKa_1 Ka_2 - Ka_1 c_1 Kw - 2KbKa_1 Ka_2 c_1 - KwKa_1 Kb - (Kw)^2) -$$
$$(H^+)(2KwKa_1 Ka_2 c_1 + KwKa_1 Ka_2 Kb + (Kw)^2 Ka_1) - (Kw)^2 Ka_1 Ka_2 = 0$$

The value of H^+ can be determined using the iteration tool in Microsoft Excel. The value of H^+ determined can then be converted into the solution pH. Prediction can now be made of the pH of the ternary solution across the measured liquidus of the ternary phase diagram by inputting concentrations (in mole per litre). Predicted pH values are tabulated below (Table 18) for four points on the liquidus of the ternary phase diagram. By comparing the predicted and experimental pH values it can be seen that, from the theoretical calculations, a narrower range of pH values would be expected than those achieved experimentally. The theoretical pH range for these concentrations is only 0.61, while the experimental is 2.31. This strongly correlates with the results from Section 6.4 where the solubility was seen to increase more sharply with pH change than was theoretically predicted. Again it can be concluded that these equations do not fully explain the relationship

between pH and solubility in this system and suggests other association/dissociation factors may also be involved.

The ternary phase diagram cannot be plotted using these equations with known pH values, as the concentrations of acid and base feature as independent variables and values for both cannot be determined.

TABLE 18- COMPARISON BETWEEN EXPERIMENTAL AND THEORETICAL pH VALUES AT KNOWN CONCENTRATIONS ALONG THE LIQUIDUS LINE OF THE MEASURED TERNARY PHASE DIAGRAM.

Concentration of acid (M/L)	Concentration of base (M/L)	Experimental pH	Theoretical pH
3.81	1.76	4.4	4.04
0.595	0.577	5.36	4.30
1.43	2.36	5.76	4.48
1.78	4.73	6.71	4.65

6.6 SUMMARY

From IR microscopy it is known that the ionisation of the acid increases across the binary phase diagram with the addition of ephedrine and an increase in pH.

The ephedrine and pimelic acid system can be seen to show relatively ideal behaviour in the binary system, especially for the 1:1 salt at high levels of pimelic acid. It can be concluded that the 1:1 salt interacts similarly with the acid as it does with itself. The ephedrine rich side of the diagram shows a greater deviation from ideality as the salt interacts less strongly with the ephedrine than it does with itself.

In the ternary system major deviations from ideality can be seen as the solubility increases much more rapidly upon the addition of the other component than would be expected in an ideal system (for both components). This suggests stronger interactions with the other component and water than with itself. The salt is also more soluble as greater proportions of either component are added than would be expected from ideality.

By using acid-base equilibria and mass balances it has been shown that the solubility of the components and the salt can be calculated and plotted as a function of the solution pH. By doing this it is apparent that the increase in solubility cannot be wholly accounted for in either the components or the salt.

Equations were derived relating solution pH and concentration of pure components without the need to calculate K_{sp}. Using an iteration tool pH values can now be determined when the concentrations of acid and base from measured points on the liquidus are inputted along with known constants. The theoretical pH values show the correct trend across the phase diagram (rising with increasing basic content). They did not predict the extent of change that has been shown to occur experimentally and can only provide an approximation.

6.7 REFERENCES

1. Jacques, J., Collet, A. & Wilen, S. H. Enantiomers, Racemates and Resolutions (Wiley-Interscience, New York, 1981).
2. Rastogi, R. P. Thermodynamics of Phase Equilibria and Phase Diagrams. Journal of Chemical Education 41, 443-448 (1964).
3. Black, S. N., Collier, E. A., Davey, R. J. & Roberts, R. J. Structure, Solubility, Screening, and Synthesis of Molecular Salts. Journal of Pharmaceutical Sciences 96, 1053-1068 (2007).
4. Jones, H. P., Davey, R. J. & Cox, B. G. Crystallization of a Salt of a Weak Organic Acid and Base: Solubility Relations, Supersaturation Control and Polymorphic Behaviour. Journal of Physical Chemistry 109, 5273-5278 (2005).
5. Cooke, C. & Davey, R. J. On the Solubility of Saccharinate Salts and Cocrystals. Crystal Growth and Design 8, 3483-3485 (2008).

7 CONCLUSIONS AND FURTHER WORK

7.1 CONCLUSIONS

A range of salts were either partially or fully formed by non-solution techniques. These salts have been shown to form by a number of mechanisms, some of which have been heavily discussed in the literature and some that have not. From study of these systems it is apparent that the grinding of acid and base can provide a quick, cheap and environmentally friendly salt screening technique.

By grinding both the 1:1 and 2:1 ratios of ephedrine and pimelic acid the respective salts were formed. It has been shown that salt formation also occurs when the components are only contacted and the temperature is increased. Under ambient conditions the salt did not form by contacting the pure components. It has been concluded that the energy provided by grinding or heating is required to initiate reaction. To extend this solvent-free work the binary phase diagram was determined, demonstrating the size of each solid phase region. From this it was possible to determine the ratios of acid and base required to ensure salt formation at a given temperature.

In order to allow the crystal structure of the ephedrine pimelate salts to be determined traditional solution techniques were used to grow single crystals. These proved unequivocally that the samples formed by grinding were the 1:1 and 2:1 salts. As salt formation from the aqueous solution proved easy for the 1:1 and difficult for the 2:1 salt, the ternary phase diagram was determined. From this it was apparent that the 2:1 salt is very soluble and metastable to the 1:1 salt. From an industrial perspective determination of the diagram highlights the compositions (in the salt region with high ephedrine content) that should be avoided. This ensures issues with stirring and equilibrating viscous liquids are not encountered.

The system of ephedrine and benzoic acid was also studied in terms of solvent free salt formation. The product formed by grinding was determined to be an amorphous salt, as was formed from solution in a previous thesis. This was stated

but evidence not presented. This same salt was also formed by contacting the two components at ambient conditions. Salt formation was concluded to occur via by a vapour diffusion mechanism due to the high vapour pressures of the two components. The salt also appears to be polymorphic with two other forms available at higher temperatures. In attempts to form a crystalline salt a ratio of acid to base was chosen based on the components aqueous solubilities. This led to reaction, rather than ionisation, of components in water forming a condensation product. This was deemed to be due to the high solution pH, meaning the wrong region of the speciation diagram was targeted. From this system it has been concluded that while the region of the ternary phase diagram where the two pure component solubilities cross should be targeted, this should not mean the speciation diagram is overlooked. It has also been demonstrated that the ternary phase diagram and speciation diagrams may not be compatible for some systems, explaining why salt formation may not occur.

From IR microscopy it has been ascertained that the ionisation of the acid goes through different periods. It is unionised at very low ephedrine concentrations, partially ionised at concentrations where the 1:1 salt will form and totally ionised at both 2:1 salt and pure pimelic acid regions of the binary phase diagram. It is now known that salt components are present as their ions in the molten state as well as solid state if the correct ratios are studied.

The ideality of the solvent free ephedrine pimelate system has been assessed and the system shown to be relatively ideal in some regions and non-ideal in others. Greater deviations from ideality are apparent on the ephedrine rich side of the phase diagram. This suggests ephedrine interacts with the salts and acid more strongly than it does with itself.

The aqueous ternary system shows substantial deviations from ideality. Massive increases in solubility on both sides of the diagram are observable when greater amounts of the opposing components are added. This means stronger interactions are occurring between both ephedrine and pimelic acid with either water or the other component.

By studying acid-base equilibria it has been shown that estimations can be made of the solubility of each pure phase if the pH is known. By comparison of these estimated solubilities and measured data it has been determined that pH does not wholly control the increase in solubility seen between the pure phase regions in the ternary phase diagram.

Equations have been derived to relate solution pH and the concentrations of the pure components. From these equations the solution pH can be calculated when the concentration of acid and base at the liquidus line are known. The results from these calculations agree with the acid-base equilibria result. The increase in solubility on the addition of another component is controlled by more factors than just pH.

7.2 SUGGESTED FURTHER WORK

7.2.1 SOLVENT FREE SALT FORMATION MECHANISMS

More work is required on the mechanisms by which solvent free salt formation takes place. Within this work three previously proposed cocrystal formation methods have been studied and conclusions drawn as to which is occurring for three different salts. Despite the conclusions drawn more work should be undertaken to further understand these phenomena. For example in the ephedrine pimelate system no metastable liquid is seen, yet it is assumed that a submerged eutectic formation method is occurring.

7.2.1.1 SALT FORMATION BY VAPOUR

From the work on ephedrine with both glycolic and benzoic acids it was noted that salt formation occurred by the diffusion of vapours. While there is some literature on this subject more investigation is needed. The vapour pressures of both components are obviously important and there is currently no measurement for ephedrine. Investigation should be carried out into the vapour pressures of both acid and base required to initiate this reaction. The reaction environment should also be further investigated in terms of proximity of reactant, temperature and the presence of air.

7.2.2 EPHEDRINE BENZOATE SALT

The formation of ephedrine benzoate salt from solution was unsuccessful in this work. In order to attempt the formation of this salt different solvents should be used. Preferably the acid and base will have similar solubilities in the chosen solvent. This will mean the ternary phase diagram will be congruent, with the salt forming when equimolar amounts of the two components are used. The pK_as of the acid and base will need to be known in the chosen solvent so the speciation diagram can be plotted. If equimolar amounts of the two components are used a mid-range pH will be more likely This would increase the chance of finding both components in their appropriate ionised states. If a salt could be grown it would be interesting to compare the properties with the potentially amorphous behaviour shown by the salt formed by contact.

7.2.3 2-PHENYL-3,4-DIMETHYL-5 PHENYL-1,3-OXAZOLIDINE

The formation of 2-phenyl-3,4-dimethyl-5 phenyl-1,3-oxazolidine was unexpected in this work. It is felt that from literature searches this reaction may be of interest to organic chemists where this type of cyclisation reaction is commonly used. Mostly more extreme reaction conditions are usually used and reactions conducted between ephedrine and an aldehyde.

8 APPENDIX

8.1 PROOF OF SALT FORMATION BY GRINDING

Table 6 in Chapter 3 gives a summary of salt formation by grinding from three techniques. The pXRD patterns, FTIR spectra and DSC traces are provided here as evidence.

8.1.1 EPHEDRINE AND ADIPIC ACID

8.1.1.1 PXRD

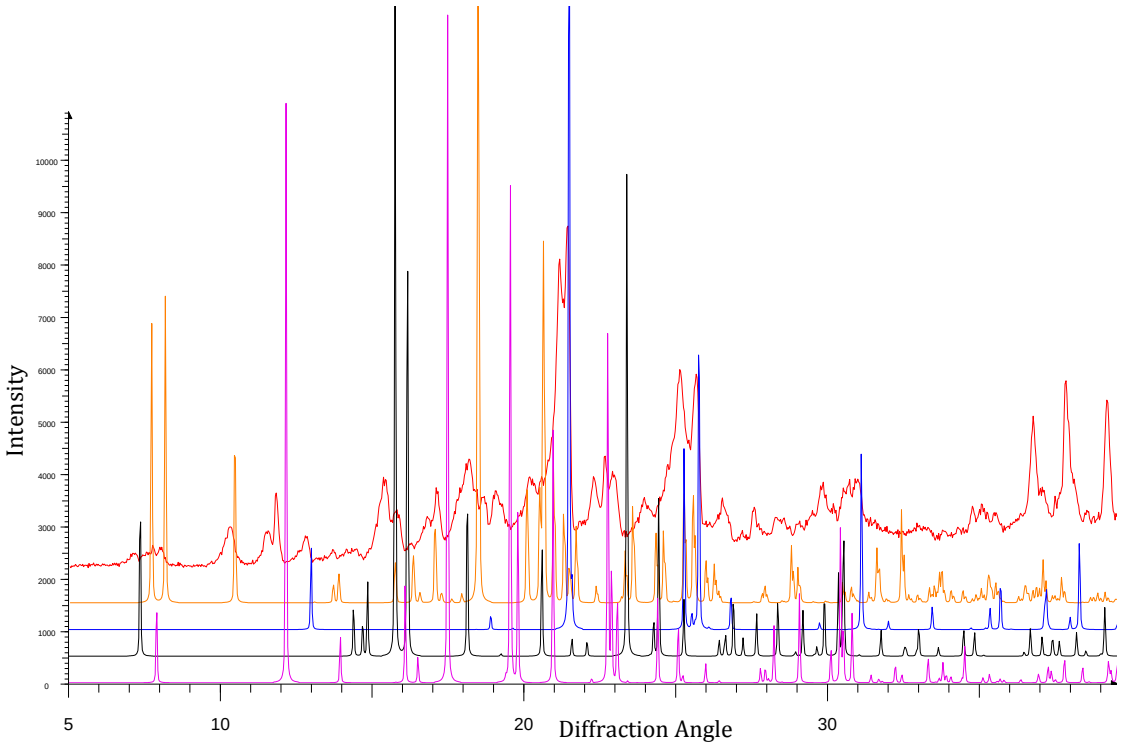

FIGURE 130- PXRD PATTERNS OF ANHYDROUS EPHEDRINE (PINK), EPHEDRINE HEMIHYDRATE (BLACK), ADIPIC ACID (BLUE), SIMULATED EPHEDRINE ADIPATE (ORANGE) AND THE GROUND EPHEDRINE AND ADIPIC ACID SAMPLE (RED).

8.1.1.2 FTIR

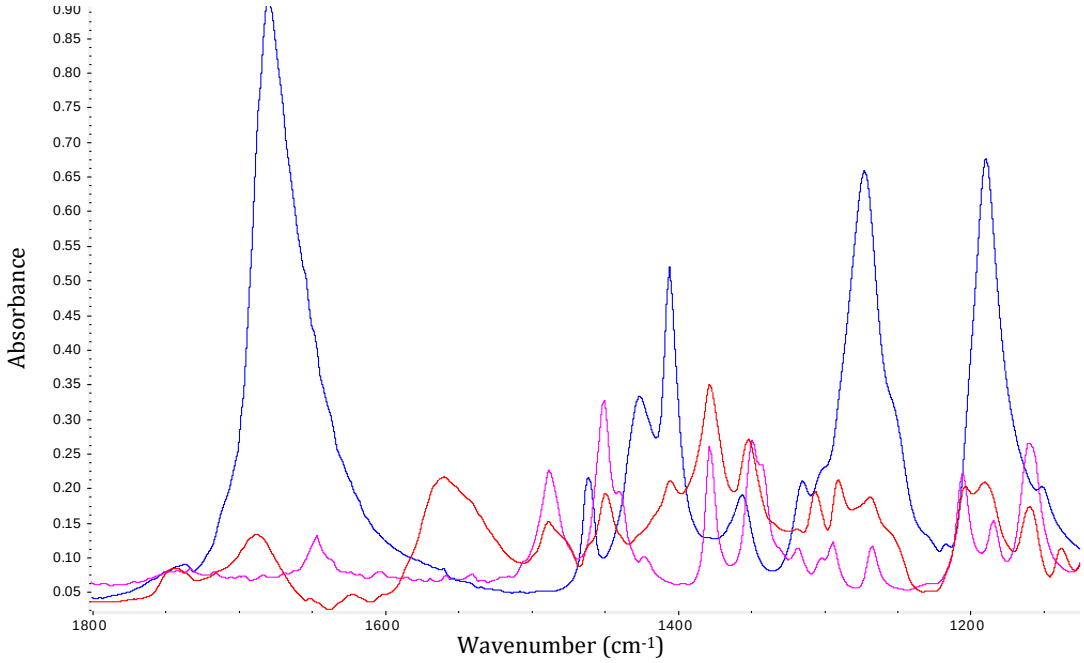

FIGURE 131- FTIR SPECTRA SHOWN BETWEEN 1000 AND 1800 CM^{-1} OF ADIPIC ACID (BLUE), EPHEDRINE (PINK) AND THE GROUND EPHEDRINE AND ADIPIC ACID SAMPLE (RED).

8.1.1.3 DSC

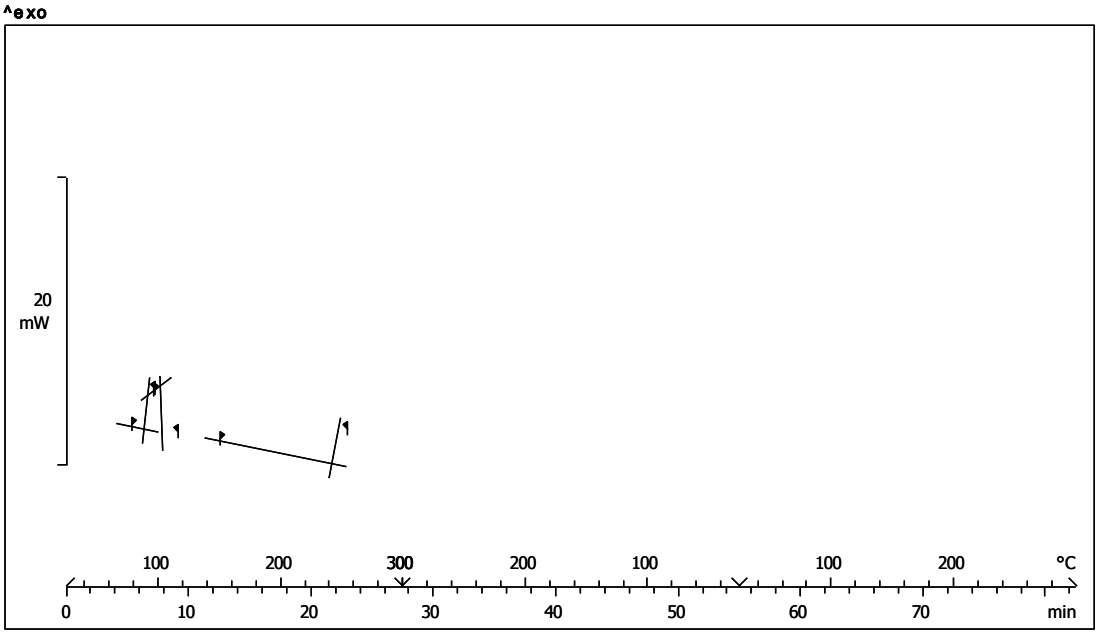

FIGURE 132-DSC TRACE OF GROUND EPHEDRINE AND ADIPIC ACID

8.1.2 EPHEDRINE AND FUMARIC ACID

8.1.2.1 PXRD

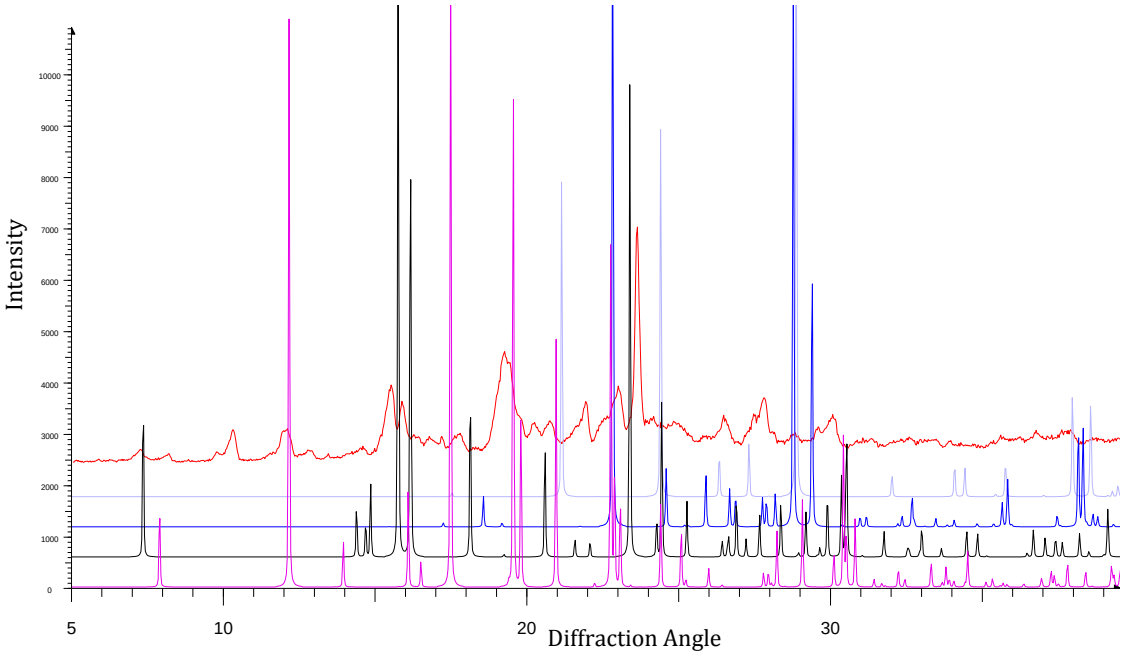

FIGURE 133- PXRD PATTERNS OF ANHYDROUS EPHEDRINE (PINK), EPHEDRINE HEMIHYDRATE (BLACK), α FUMARIC ACID (BLUE), β FUMARIC ACID (LILAC) AND THE GROUND EPHEDRINE AND FUMARIC ACID SAMPLE (RED).

8.1.2.2 FTIR

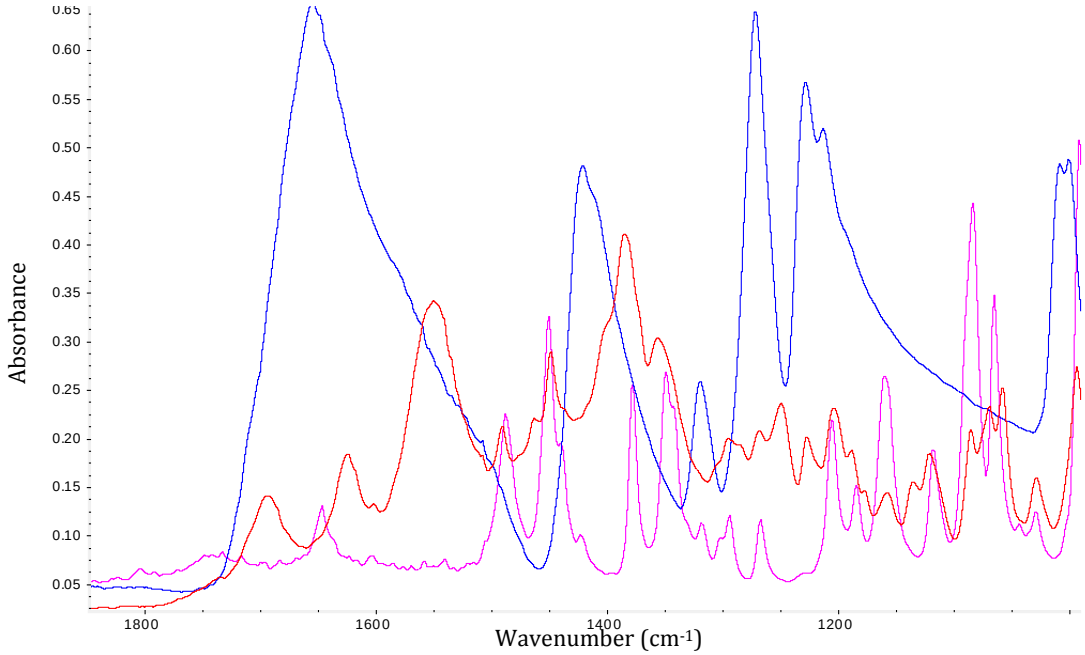

FIGURE 134- FTIR SPECTRA SHOWN BETWEEN 1000 AND 1800 CM^{-1} OF FUMARIC ACID (BLUE), EPHEDRINE (PINK) AND THE GROUND EPHEDRINE AND FUMARIC ACID SAMPLE (RED).

8.1.2.3 DSC

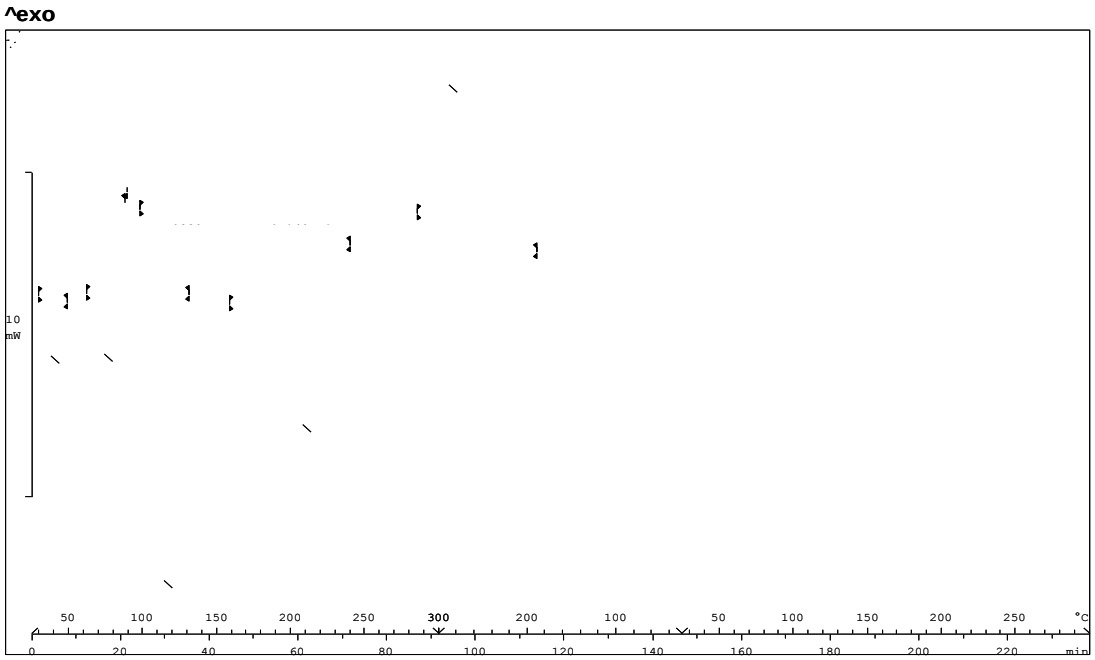

FIGURE 135- DSC TRACE OF GROUND EPHEDRINE AND FUMARIC ACID

8.1.3 EPHEDRINE AND GLUTARIC ACID

8.1.3.1 PXRD

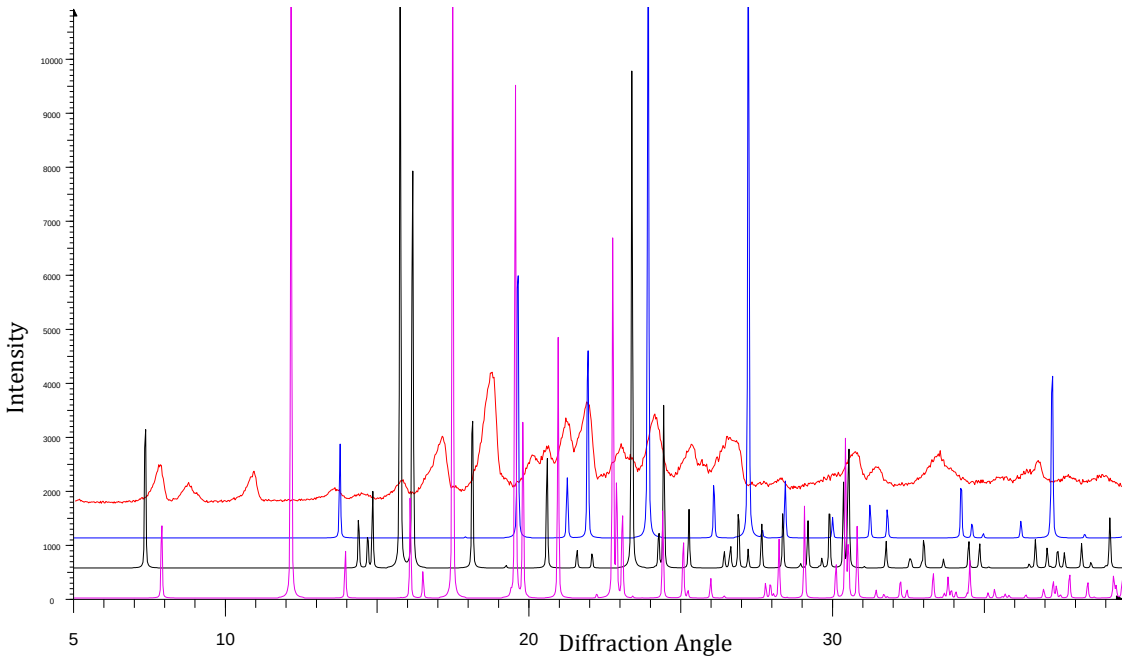

FIGURE 136- PXRD PATTERNS OF ANHYDROUS EPHEDRINE (PINK), EPHEDRINE HEMIHYDRATE (BLACK), GLUTARIC ACID (BLUE) AND THE GROUND EPHEDRINE AND GLUTARIC ACID SAMPLE (RED).

8.1.3.2 FTIR

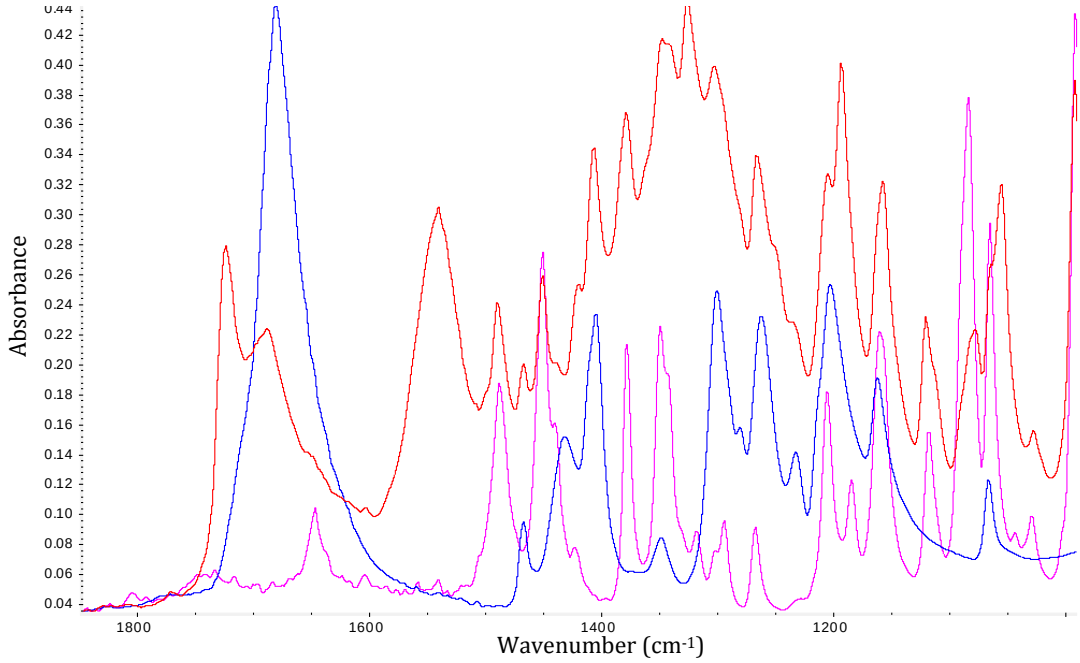

FIGURE 137- FTIR SPECTRA SHOWN BETWEEN 1000 AND 1800 CM^{-1} OF GLUTARIC ACID (BLUE), EPHEDRINE (PINK) AND THE GROUND EPHEDRINE AND GLUTARIC ACID SAMPLE (RED).

8.1.3.3 DSC

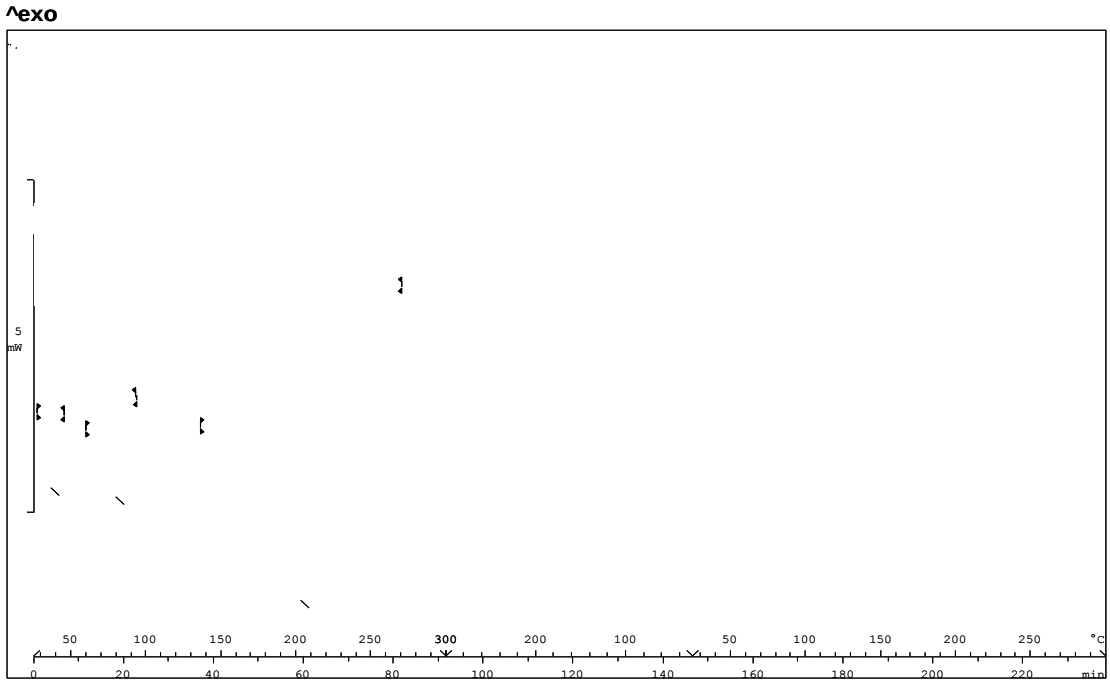

FIGURE 138- DSC TRACE OF GROUND EPHEDRINE AND GLUTARIC ACID.

8.1.4 EPHEDRINE AND MALEIC ACID

8.1.4.1 PXRD

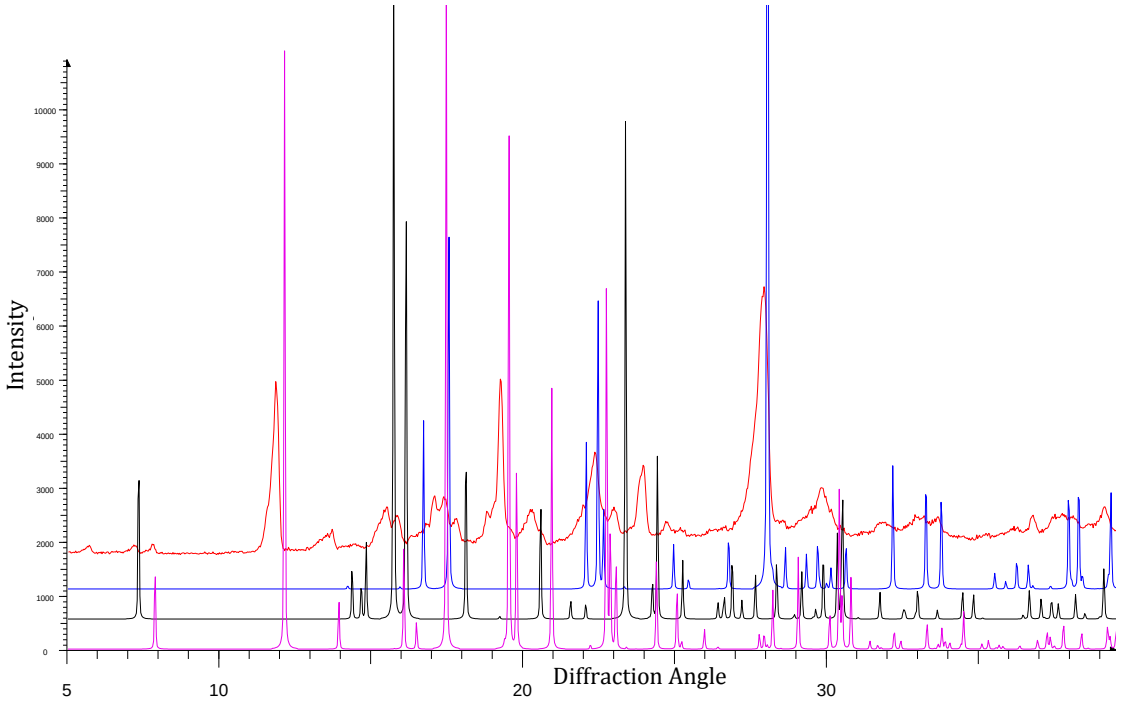

FIGURE 139- PXRD PATTERNS OF ANHYDROUS EPHEDRINE (PINK), EPHEDRINE HEMIHYDRATE (BLACK), MALEIC ACID (BLUE) AND THE GROUND EPHEDRINE AND MALEIC ACID SAMPLE (RED).

8.1.4.2 FTIR

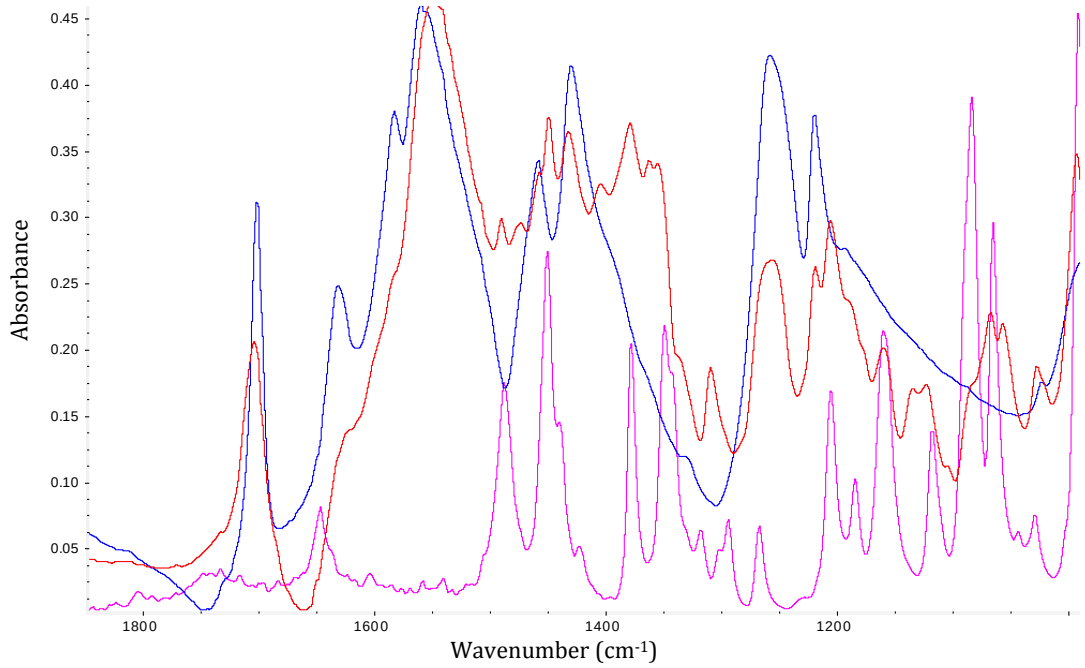

FIGURE 140- FTIR SPECTRA SHOWN BETWEEN 1000 AND 1800 CM^{-1} OF MALEIC ACID (BLUE), EPHEDRINE (PINK) AND THE GROUND EPHEDRINE AND MALEIC ACID SAMPLE (RED).

8.1.4.3 DSC

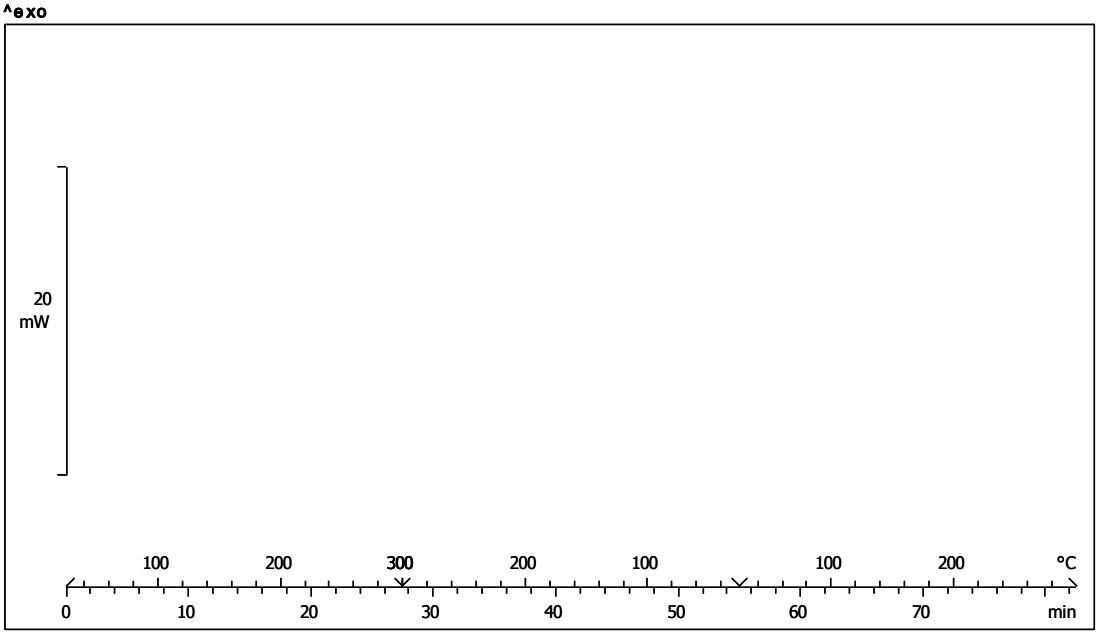

FIGURE 141- DSC TRACE OF GROUND EPHEDRINE AND MALEIC ACID.

8.1.5 EPHEDRINE AND MALIC ACID

8.1.5.1 PXRD

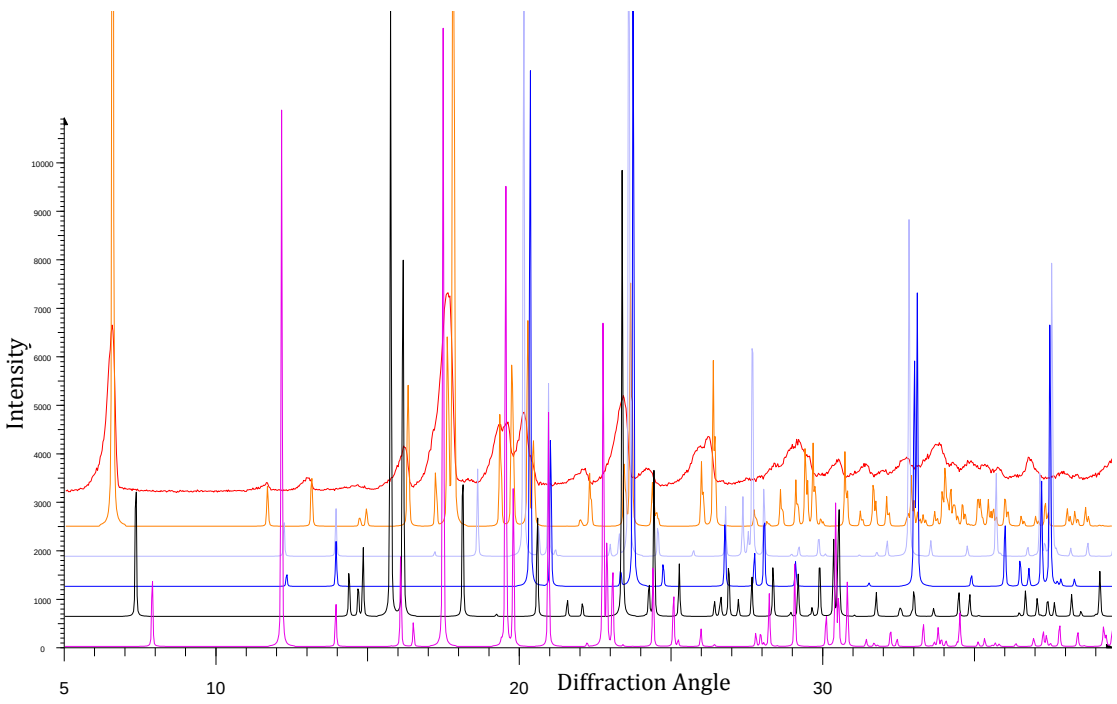

FIGURE 142- PXRD PATTERNS OF ANHYDROUS EPHEDRINE (PINK), EPHEDRINE HEMIHYDRATE (BLACK), α DL MALIC ACID (BLUE), β DL MALIC ACID (LILAC), SIMULATED EPHEDRINE MALATE (ORANGE) AND THE GROUND EPHEDRINE AND DL MALIC ACID SAMPLE (RED).

8.1.5.2 FTIR

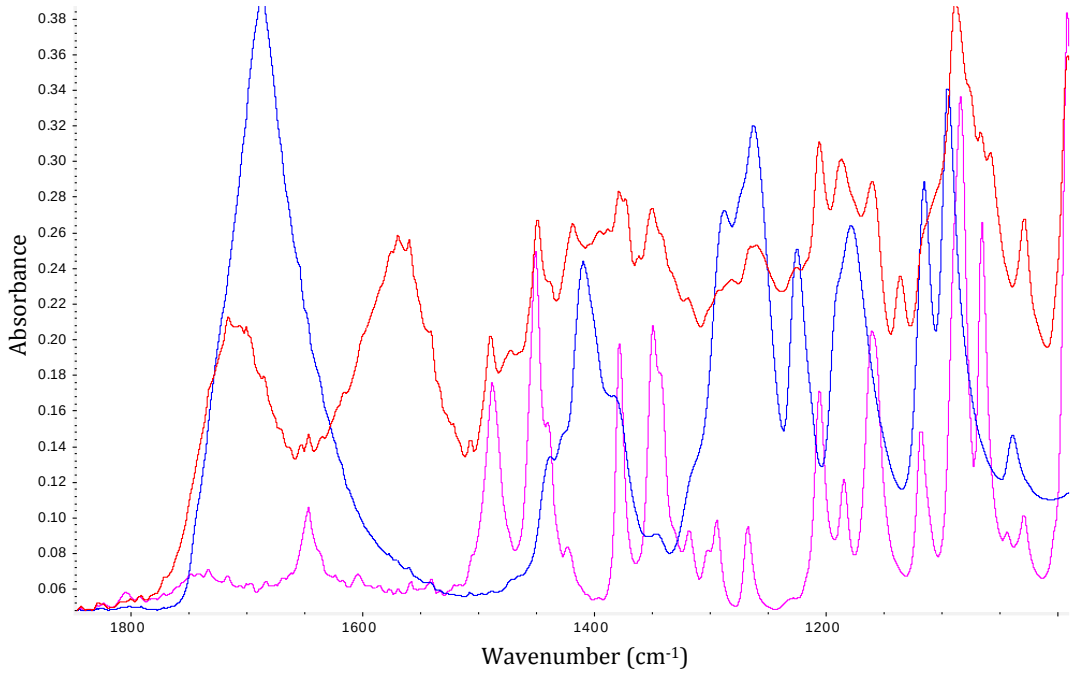

FIGURE 143- FTIR SPECTRA SHOWN BETWEEN 1000 AND 1800 CM^{-1} OF DL-MALIC ACID (BLUE), EPHEDRINE (PINK) AND THE GROUND EPHEDRINE AND DL-MALIC ACID SAMPLE (RED).

8.1.5.3 DSC

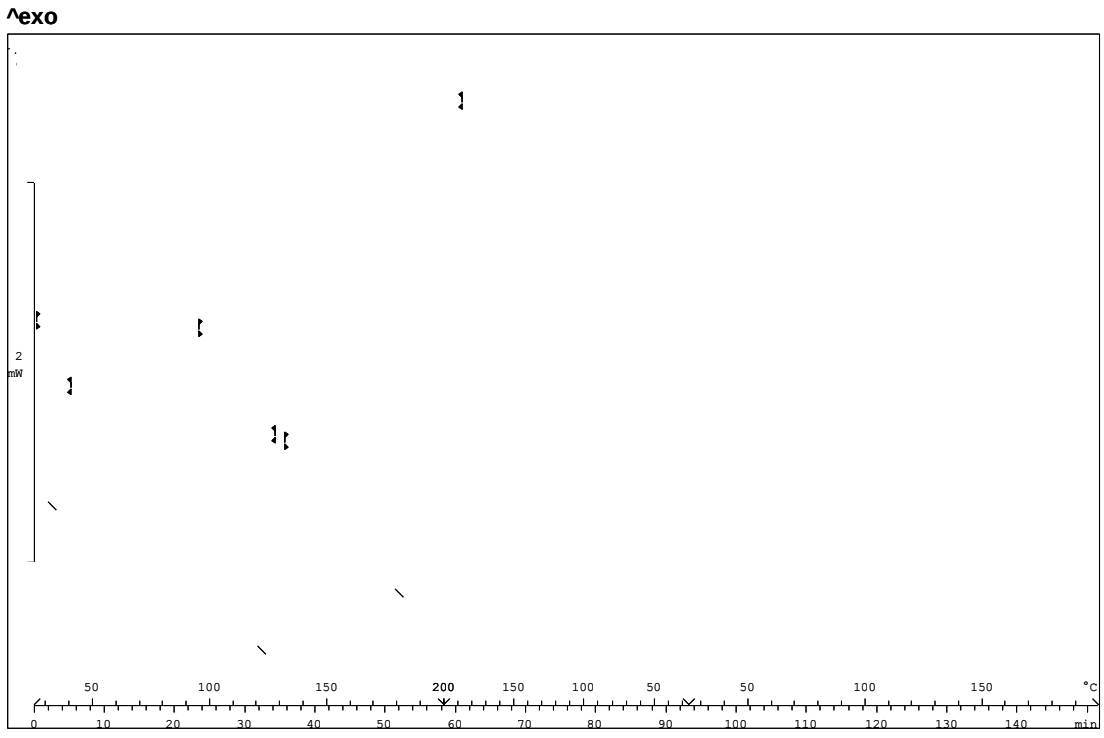

FIGURE 144- DSC TRACE OF GROUND EPHEDRINE AND DL MALIC ACID.

8.1.6 EPHEDRINE AND MALONIC ACID

8.1.6.1 PXRD

The product formed was very amorphous and therefore was unsuitable for pXRD analysis.

8.1.6.2 FTIR

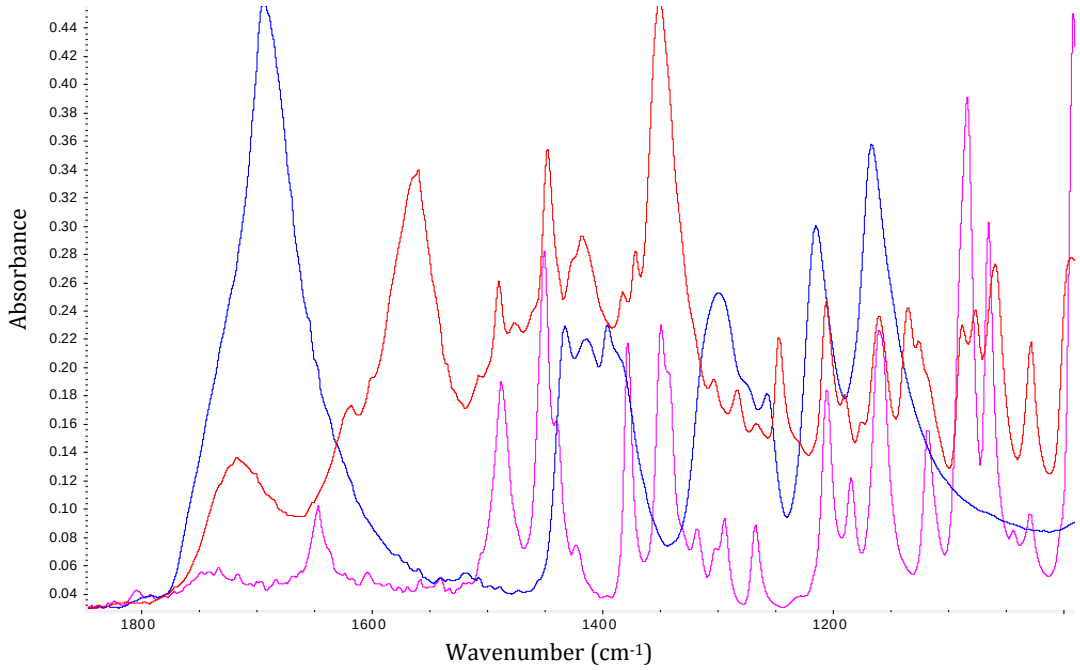

FIGURE 145- FTIR SPECTRA SHOWN BETWEEN 1000 AND 1800 CM^{-1} OF MALONIC ACID (BLUE), EPHEDRINE (PINK) AND THE GROUND EPHEDRINE AND MALONIC ACID SAMPLE (RED).

8.1.6.3 DSC

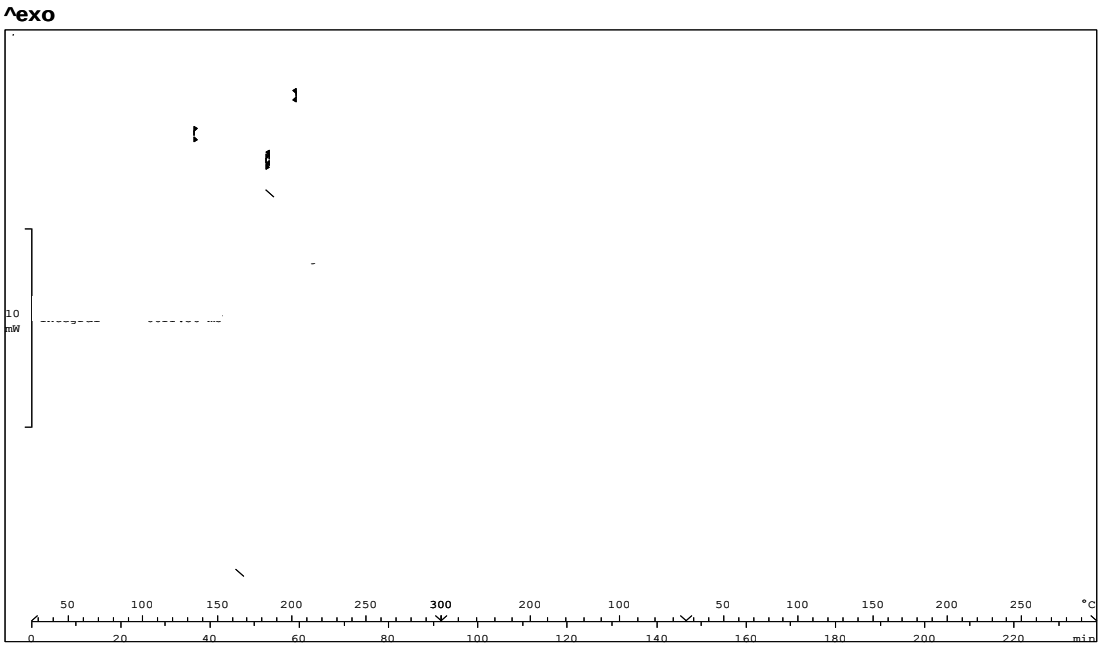

FIGURE 146- DSC TRACE OF GROUND EPHEDRINE AND MALONIC ACID.

8.1.7 EPHEDRINE AND OXALIC ACID

8.1.7.1 PXRD

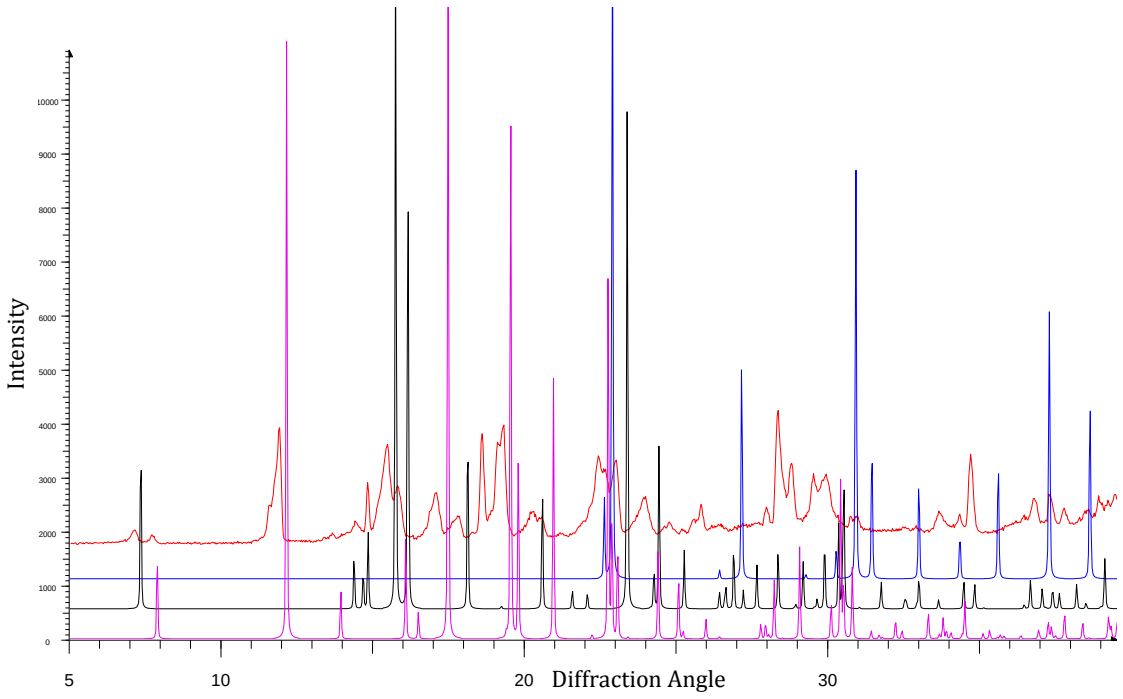

FIGURE 147- PXRD PATTERNS OF ANHYDROUS EPHEDRINE (PINK), EPHEDRINE HEMIHYDRATE (BLACK), OXALIC ACID (BLUE) AND THE GROUND EPHEDRINE AND OXALIC ACID SAMPLE (RED).

8.1.7.2 FTIR

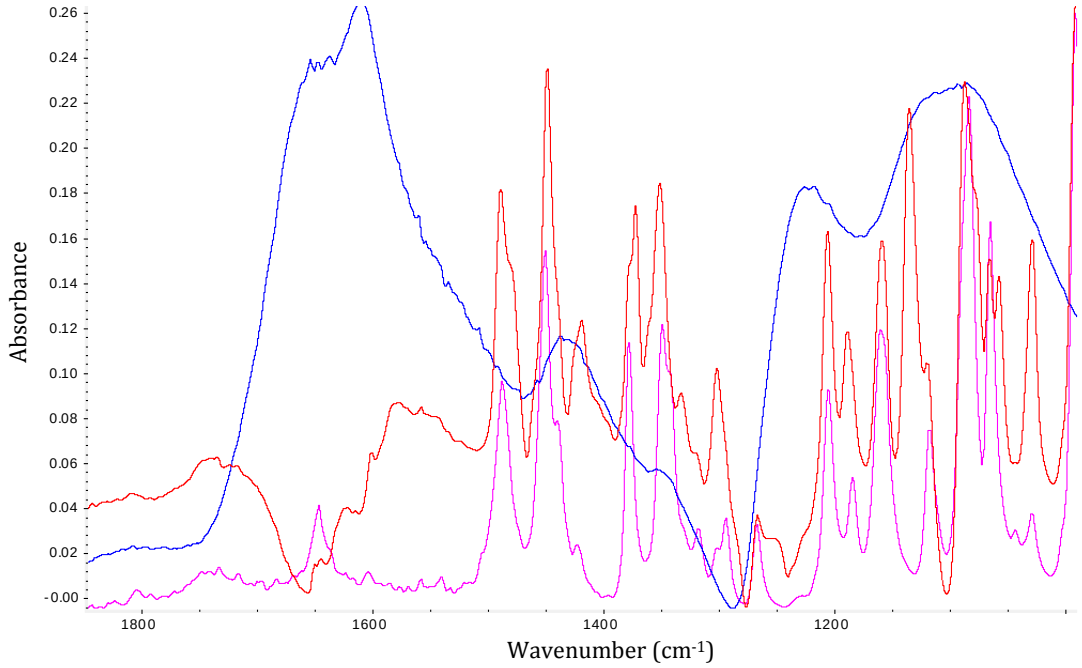

FIGURE 148- FTIR SPECTRA SHOWN BETWEEN 1000 AND 1800 CM^{-1} OF OXALIC ACID (BLUE), EPHEDRINE (PINK) AND THE GROUND EPHEDRINE AND OXALIC ACID SAMPLE (RED).

8.1.7.3 DSC

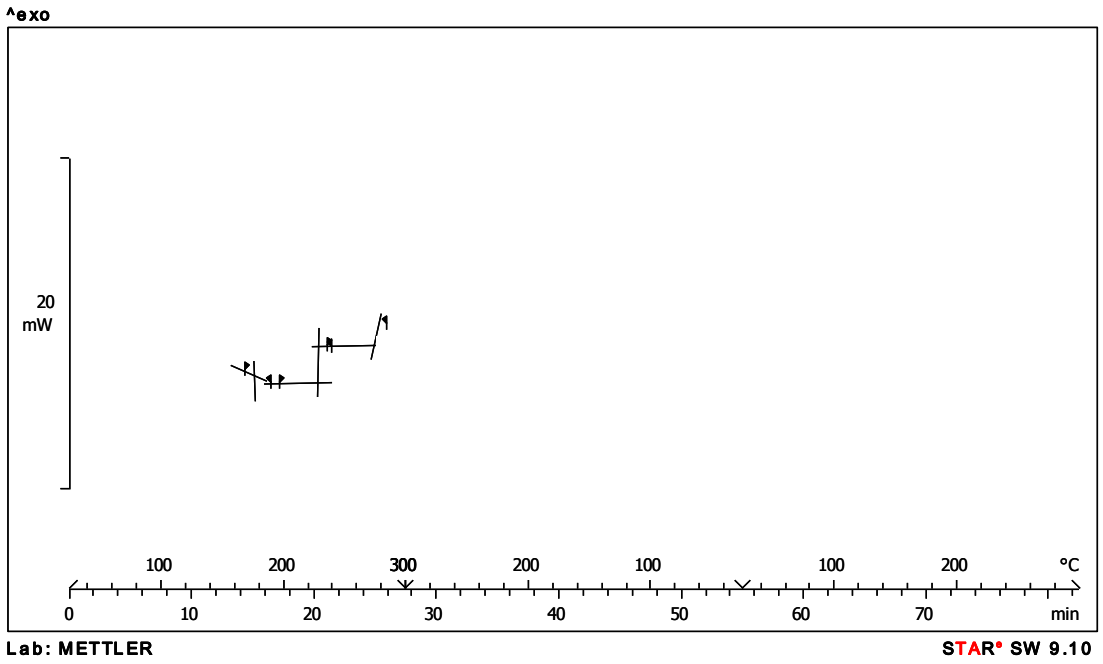

FIGURE 149- DSC TRACE OF GROUND EPHEDRINE AND OXALIC ACID.

8.1.8 EPHEDRINE AND SUBERIC ACID

8.1.8.1 PXRD

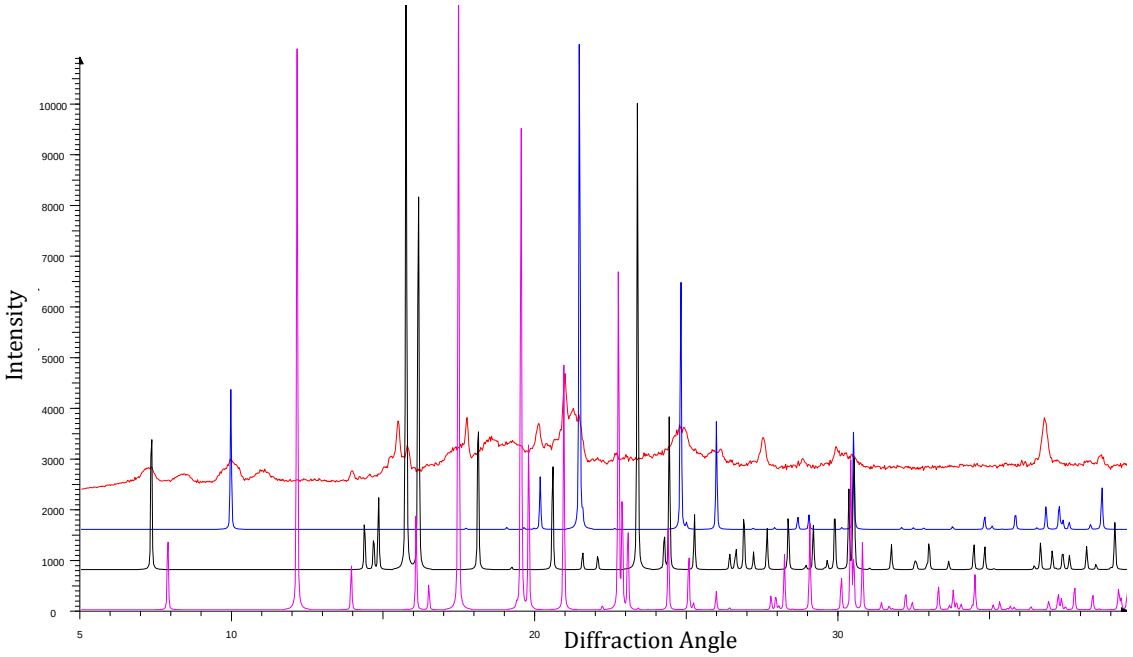

FIGURE 150- PXRD PATTERNS OF ANHYDROUS EPHEDRINE (PINK), EPHEDRINE HEMIHYDRATE (BLACK), SUBERIC ACID (BLUE) AND THE GROUND EPHEDRINE AND SUBERIC ACID SAMPLE (RED).

8.1.8.2 FTIR

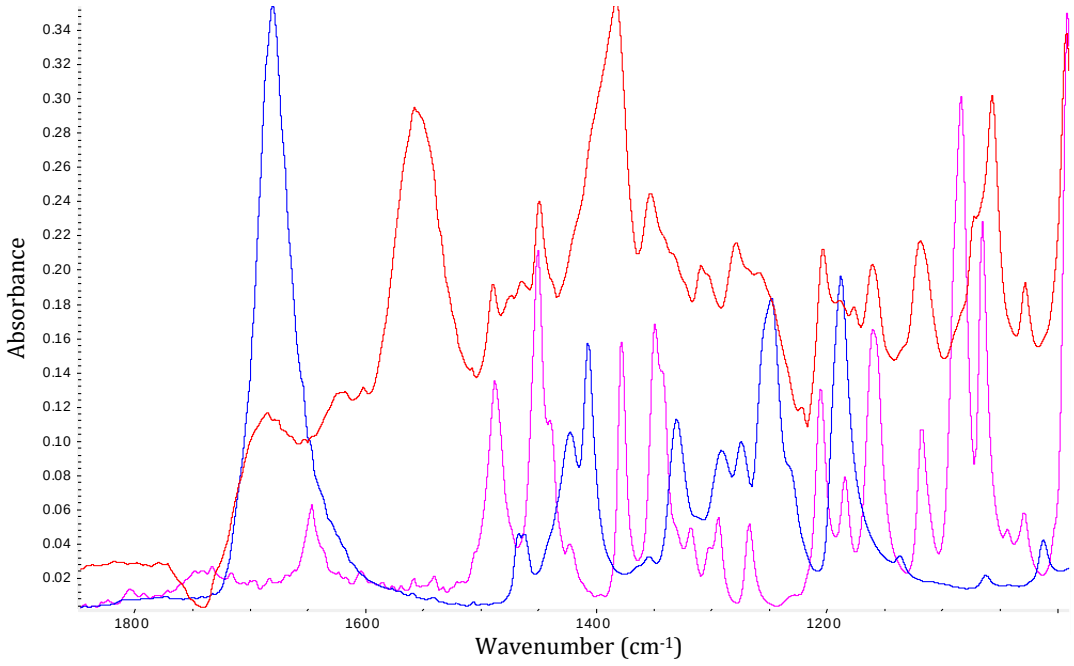

FIGURE 151- FTIR SPECTRA SHOWN BETWEEN 1000 AND 1800 CM^{-1} OF SUBERIC ACID (BLUE), EPHEDRINE (PINK) AND THE GROUND EPHEDRINE AND SUBERIC ACID SAMPLE (RED).

8.1.8.3 DSC

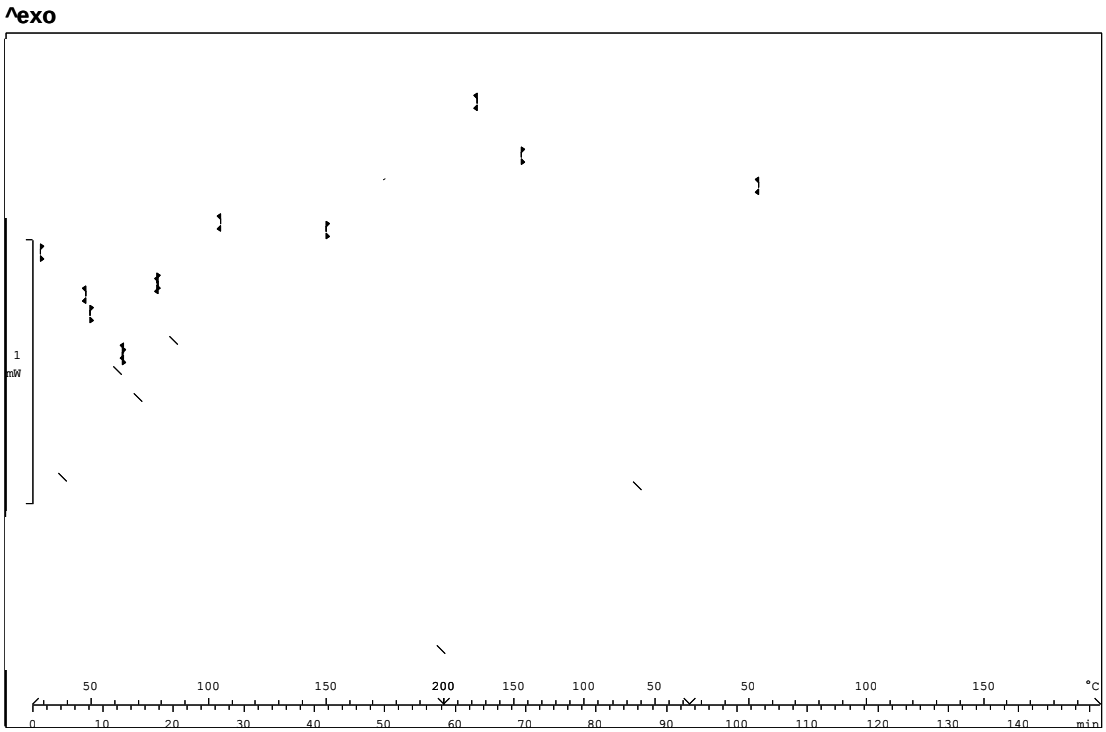

FIGURE 152- DSC TRACE OF GROUND EPHEDRINE AND SUBERIC ACID

8.1.9 EPHEDRINE AND SUCCINIC ACID

8.1.9.1 PXRD

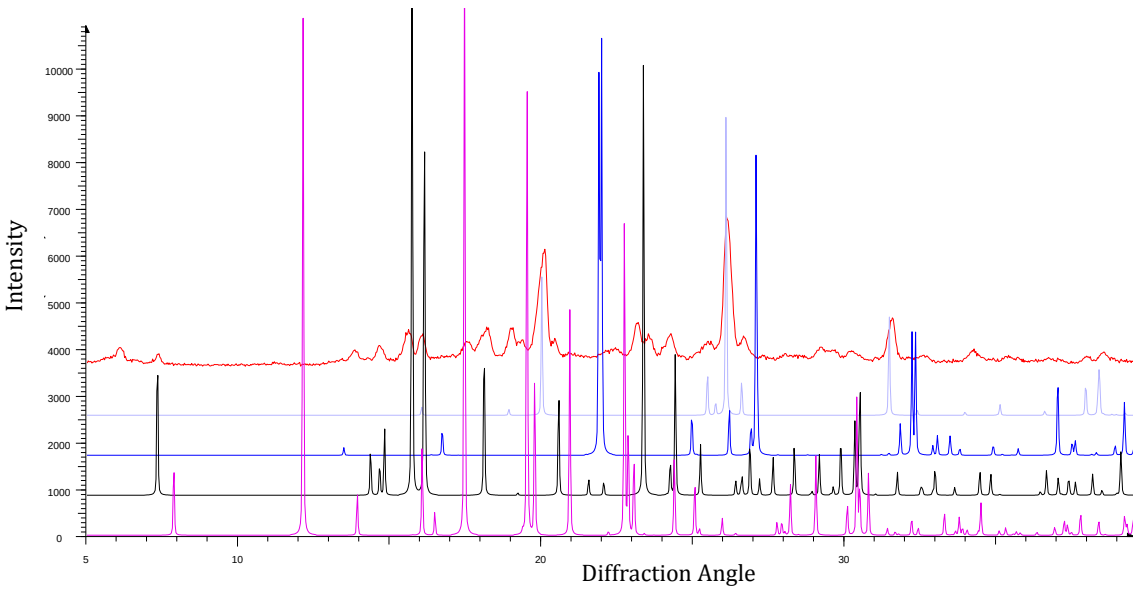

FIGURE 153- PXRD PATTERNS OF ANHYDROUS EPHEDRINE (PINK), EPHEDRINE HEMIHYDRATE (BLACK), α SUCCINIC ACID (BLUE), β SUCCINIC ACID (LILAC) AND THE GROUND EPHEDRINE AND SUCCINIC ACID SAMPLE (RED).

8.1.9.2 FTIR

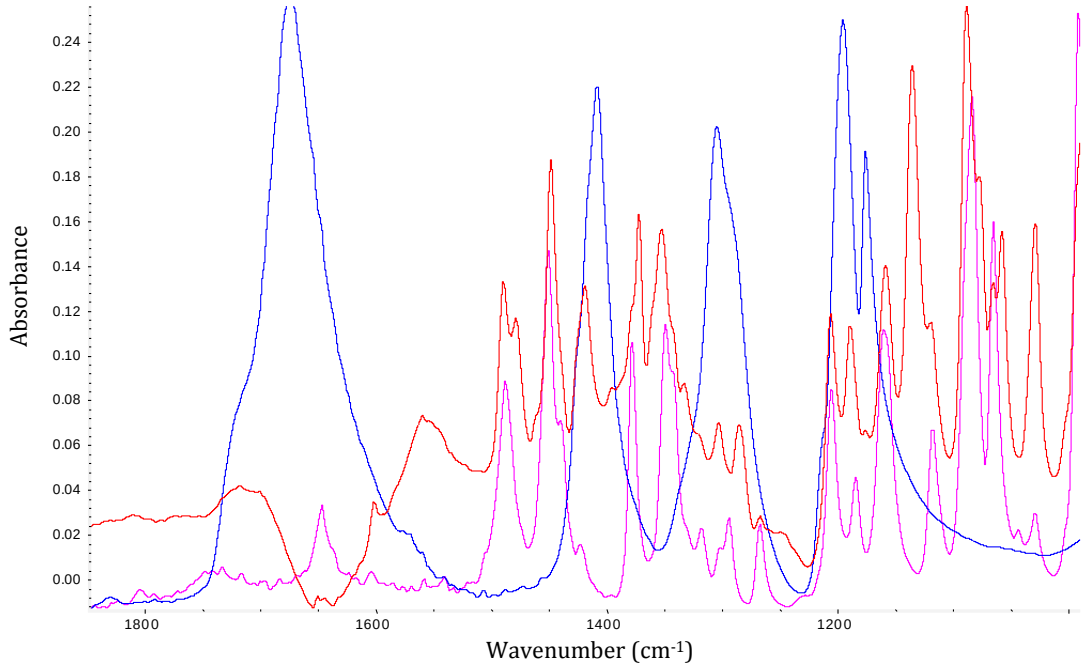

FIGURE 154- FTIR SPECTRA SHOWN BETWEEN 1000 AND 1800 CM^{-1} OF SUCCINIC ACID (BLUE), EPHEDRINE (PINK) AND THE GROUND EPHEDRINE AND SUCCINIC ACID SAMPLE (RED).

8.1.9.3 DSC

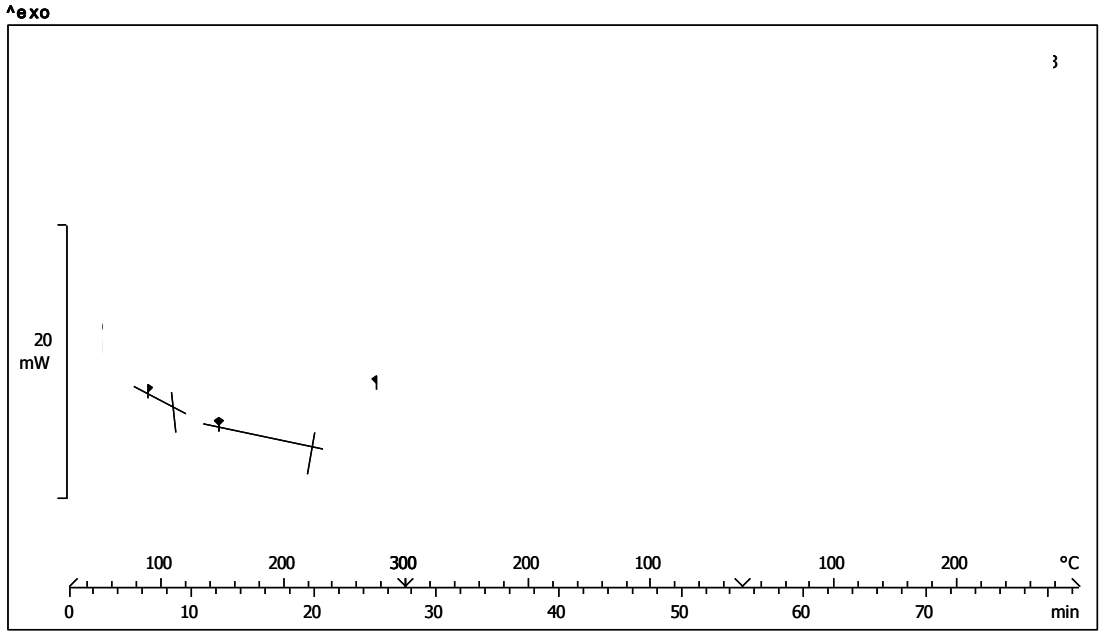

FIGURE 155- DSC TRACE OF GROUND EPHEDRINE AND SUCCINIC ACID.

8.1.10 EPHEDRINE AND TARTARIC ACID

8.1.10.1 PXRD

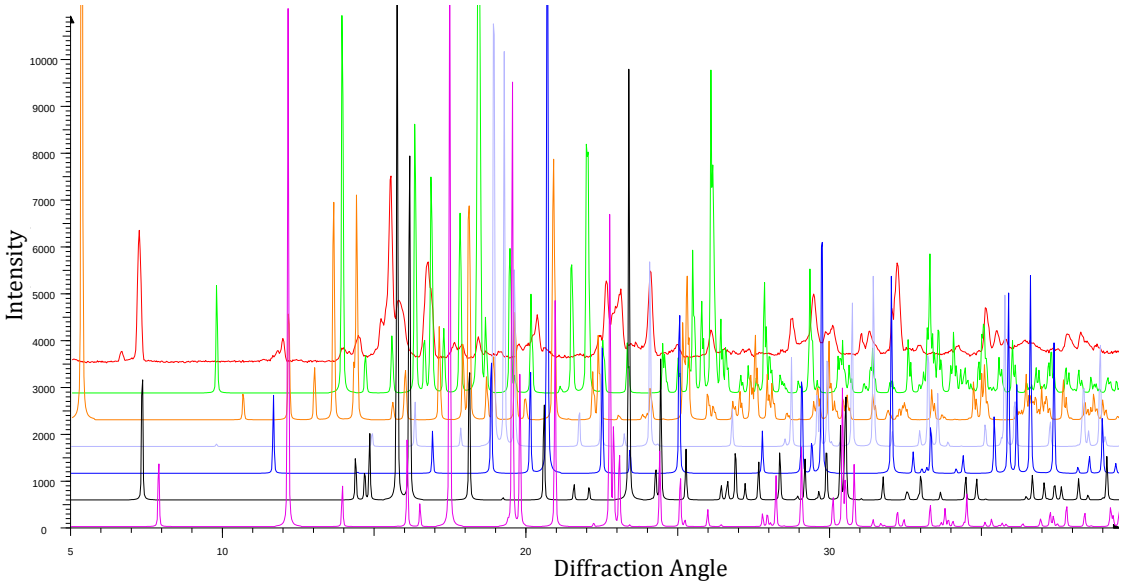

FIGURE 156- PXRD PATTERNS OF ANHYDROUS EPHEDRINE (PINK), EPHEDRINE HEMIHYDRATE (BLACK), α TARTARIC ACID (BLUE), β TARTARIC ACID (LILAC), SIMULATED EPHEDRINE TARTRATE (ORANGE), SIMULATED EPHEDRINE TARTRATE MONOHYDRATE (GREEN) AND THE GROUND EPHEDRINE AND TARTARIC ACID SAMPLE (RED).

8.1.10.2 FTIR

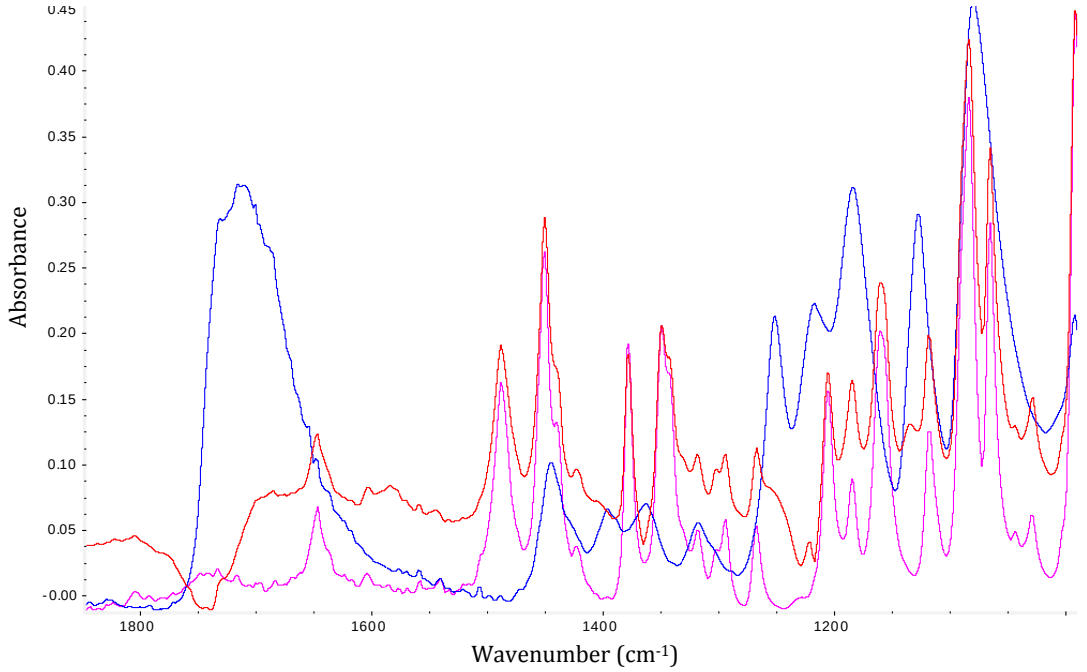

FIGURE 157- FTIR SPECTRA SHOWN BETWEEN 1000 AND 1800 CM^{-1} OF TARTARIC ACID (BLUE), EPHEDRINE (PINK) AND THE GROUND EPHEDRINE AND TARTARIC ACID SAMPLE (RED).

8.1.10.3 DSC

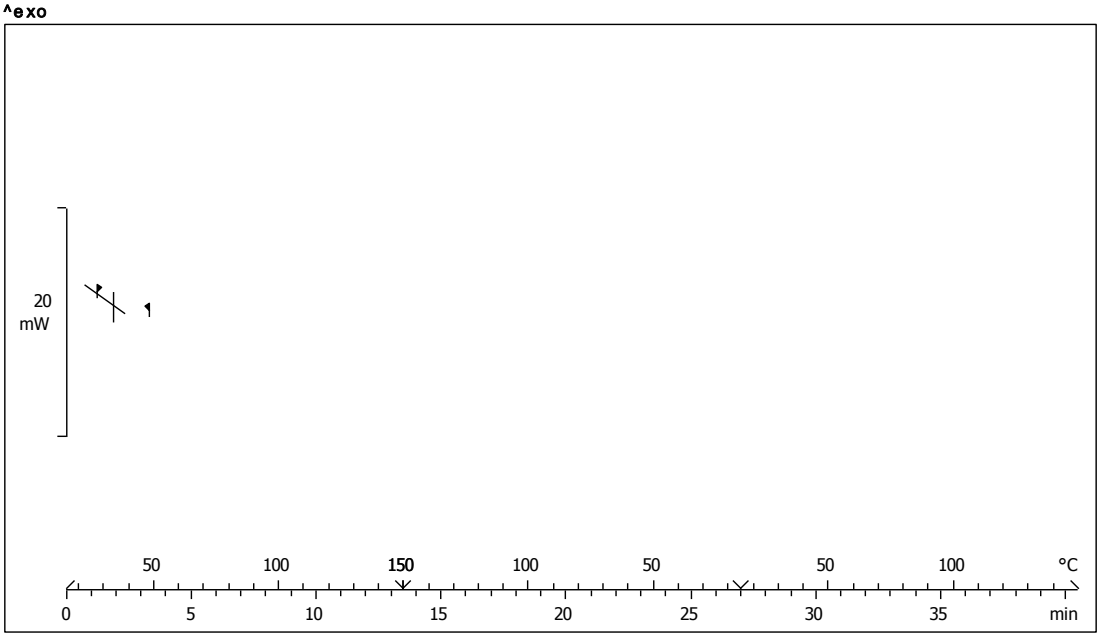

FIGURE 158- DSC TRACE OF GROUND EPHEDRINE AND TARTARIC ACID

8.2 ANALYSIS OF PRODUCT FORMATION BY CLOSE PROXIMITY OF EPHEDRINE AND BENZOIC ACID

8.2.1 PXRD

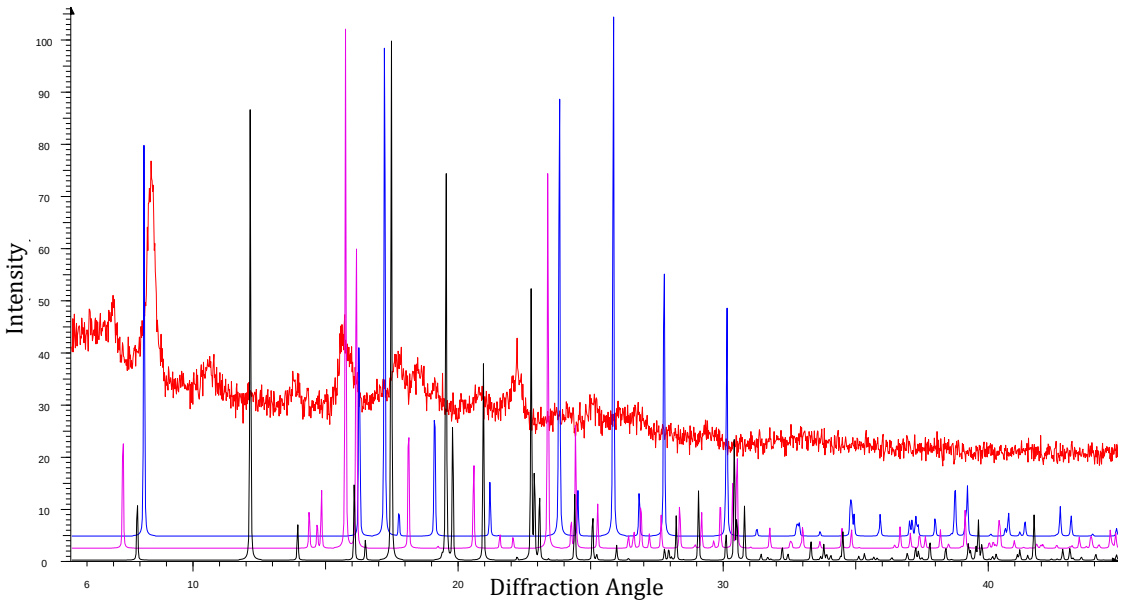

FIGURE 159- PXRD OF BENZOIC ACID (BLUE), EPHEDRINE (PINK), EPHEDRINE HEMIHYDRATE (BLACK) AND THE NEW PRODUCT FORMED BY EPHEDRINE AND BENZOIC ACID SEPARATED BY A SPACE OF 4 CM (RED).

8.2.2 FTIR

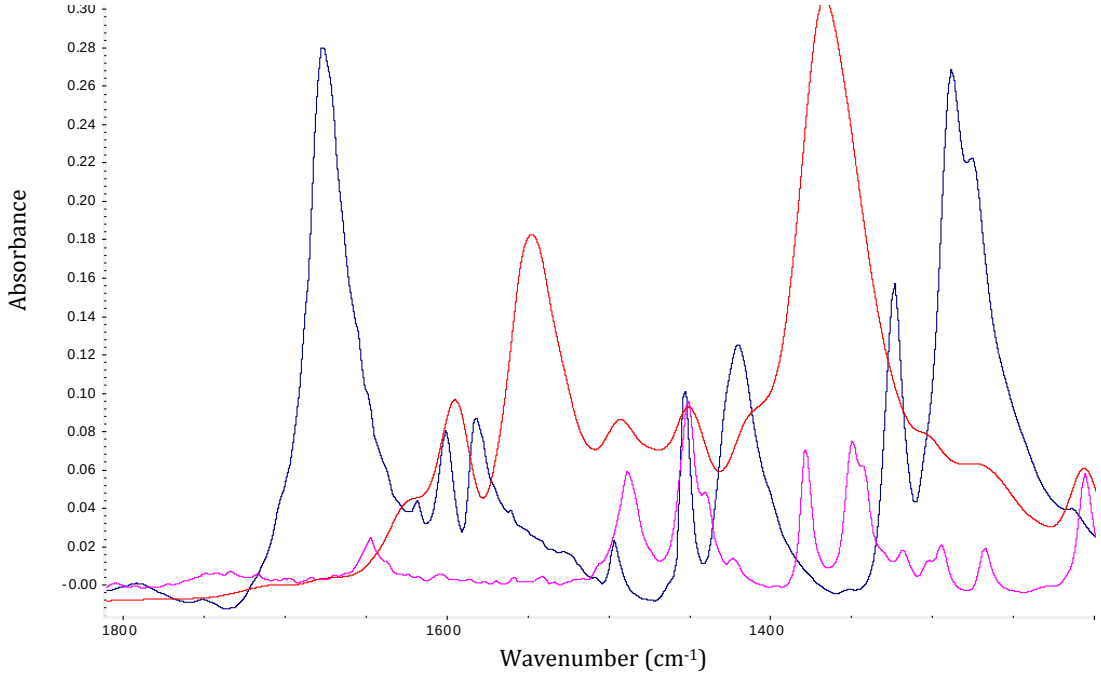

FIGURE 160- FTIR SPECTRA BETWEEN 1200 CM-1 AND 1800 CM-1 OF BENZOIC ACID (BLUE), EPHEDRINE (PINK) AND THE NEW PRODUCT FORMED BY EPHEDRINE AND BENZOIC ACID SEPARATED BY A SPACE OF 4 CM (RED).

8.3 IONISATION EQUATIONS

8.3.1 DERIVATION OF A^{2-} IN TERMS OF KNOWN CONSTANTS

$$c_1 - A^{2-} = HA^- + H_2A$$

$$HA^- = \frac{H^+A^{2-}}{Ka_2}$$

$$H_2A = \frac{H^+HA^-}{Ka_1}$$

$$c_1 - A^{2-} = \frac{H^+A^{2-}}{Ka_2} + \frac{H^+HA^-}{Ka_1}$$

$$Ka_1Ka_2\left(c_1 - A^{2-}\right) = H^+A^{2-}Ka_1 + H^+HA^-Ka_2$$

$$Ka_1Ka_2\left(c_1 - A^{2-}\right) = H^+A^{2-}Ka_1 + \frac{\left(H^+\right)^2A^{2-}Ka_2}{Ka_2}$$

$$Ka_1Ka_2\left(c_1 - A^{2-}\right) = H^+A^{2-}Ka_1 + \left(H^+\right)^2A^{2-}$$

$$Ka_1Ka_2c_1 - Ka_1Ka_2A^{2-} = H^+A^{2-}Ka_1 + \left(H^+\right)^2A^{2-}$$

$$Ka_1Ka_2c_1 = A^{2-}\left(Ka_1Ka_2 + \left(H^+\right)^2 + H^+Ka_1\right)$$

8.3.2 DERIVATION OF HA- IN TERMS OF KNOWN CONSTANTS

$$Ka_2 = H^+A^{2-} / HA^-$$

$$HA^- = \frac{H^+\left(\frac{Ka_1Ka_2c_1}{Ka_1Ka_2 + \left(H^+\right)^2 + H^+Ka_1}\right)}{Ka_2}$$

8.3.3 DERIVATION OF BH+ IN TERMS OF KNOWN CONSTANTS

$$BH^+ = c_2 - B$$

$$B = \frac{BH^+OH^-}{Kb}$$

$$BH^+ = c_2 - \frac{BH^+OH^-}{Kb}$$

$$KbBH^+ = c_2Kb - B^+OH^-$$

$$BH^+\left(Kb + OH^-\right) = c_2Kb$$

$$BH^+ = \frac{c_2Kb}{Kb + OH^-}$$

$$\frac{Kw}{H^+} = OH^-$$

$$BH^+ = \frac{c_2Kb}{Kb + \frac{Kw}{H^+}}$$

8.3.4 SUBSTITUTING DERIVED TERMS INTO THE FULL EQUATION

$$H^+ + BH^+ = HA^- + A^{2-} + OH^-$$

$$H^+ + \frac{c_2KbH^+}{H^+Kb + Kw} =$$

$$\left[\frac{H^+Ka_1\left(Ka_2\right)^2c_1}{H^+Ka_1 + \left(H^+\right)^2 + Ka_1Ka_2}\right] + \left[\frac{Ka_1Ka_2c_1}{Ka_1H^+ + \left(H^+\right)^2 + Ka_1Ka_2}\right] + \frac{Kw}{H^+}$$

$$\left(H^+\right)^2 + \frac{c_2Kb\left(H^+\right)^2}{H^+Kb + Kw} =$$

$$\left[\frac{\left(H^+\right)^2Ka_1\left(Ka_2\right)^2c_1}{H^+Ka_1 + \left(H^+\right)^2 + Ka_1Ka_2}\right] + \left[\frac{H^+Ka_1Ka_2c_1}{Ka_1H^+ + \left(H^+\right)^2 + Ka_1Ka_2}\right] + Kw$$

$$\left(H^+\right)^2\left(H^+Kb+Kw\right)+c_2Kb\left(H^+\right)^2=$$
$$\frac{\left(H^+\right)^2Ka_1c_1\left(H^+Kb+Kw\right)+2Ka_1Ka_2c_1H^+\left(H^+Kb+Kw\right)}{Ka_1Ka_2+\left(H^+\right)^2+H^+Ka_1}+Kw\left(H^+Kb+Kw\right)$$

$$\left(H^+\right)^2\left(H^+Kb+Kw\right)\left(Ka_1Ka_2+\left(H^+\right)^2+H^+Ka_1\right)+c_2Kb\left(H^+\right)^2\left(Ka_1Ka_2+\left(H^+\right)^2+H^+Ka_1\right)=$$
$$\left(H^+\right)^2Ka_1c_1\left(H^+Kb+Kw\right)+2Ka_1Ka_2c_1H^+\left(H^+Kb+Kw\right)+$$
$$Kw\left(H^+Kb+Kw\right)\left(Ka_1Ka_2+\left(H^+\right)^2+H^+Ka_1\right)$$

$$\left(H^+\right)^3KbKa_1Ka_2+\left(H^+\right)^5Kb+\left(H^+\right)^4KbKa_1+\left(H^+\right)^2KwKa_1Ka_2+$$
$$\left(H^+\right)^4Kw+\left(H^+\right)^3Ka_1Kw+c_2Kb\left(H^+\right)^2Ka_1Ka_2+c_2Kb\left(H^+\right)^4+c_2Kb\left(H^+\right)^3Ka_1=$$
$$\left(H^+\right)^3Ka_1c_1Kb+\left(H^+\right)^2Ka_1c_1Kw+2Ka_1Ka_2c_1\left(H^+\right)^2Kb+2Ka_1Ka_2c_1H^+Kw+$$
$$KwH^+KbKa_1Ka_2+Kw\left(H^+\right)^3Kb+Kw\left(H^+\right)^2KbKa_1+\left(Kw\right)^2Ka_1Ka_2+$$
$$\left(Kw\right)^2\left(H^+\right)^2+\left(Kw\right)^2H^+Ka_1$$

$$\left(H^+\right)^3KbKa_1Ka_2+\left(H^+\right)^5Kb+\left(H^+\right)^4KbKa_1+\left(H^+\right)^2KwKa_1Ka_2+\left(H^+\right)^4Kw+$$
$$\left(H^+\right)^3KwKa_1+\left(H^+\right)^2c_2KbKa_1Ka_2+\left(H^+\right)^4c_2Kb+\left(H^+\right)^3c_2KbKa_1=$$
$$\left(H^+\right)^3Ka_1c_1Kb+\left(H^+\right)^2Ka_1c_1Kw+2\left(H^+\right)^2KbKa_1Ka_2c_1+$$
$$2H^+KwKa_1Ka_2c_1+KwKa_1Ka_2H^+Kb+\left(H^+\right)^3KwKb+\left(H^+\right)^2KwKa_1Kb+$$
$$\left(Kw\right)^2Ka_1Ka_2+\left(Kw\right)^2\left(H^+\right)^2+\left(Kw\right)^2H^+Ka_1$$

$$\left(H^+\right)^5Kb+\left(H^+\right)^4KbKa_1+\left(H^+\right)^4Kw+\left(H^+\right)^4c_2Kb+\left(H^+\right)^3KbKa_1Ka_2+$$
$$\left(H^+\right)^3KwKa_1+\left(H^+\right)^3c_2KbKa_1-\left(H^+\right)^3Ka_1c_1Kb-\left(H^+\right)^3KwKb+$$
$$\left(H^+\right)^2KwKa_1Ka_2+\left(H^+\right)^2c_2KbKa_1Ka_2-\left(H^+\right)^2Ka_1c_1Kw-$$
$$2\left(H^+\right)^2KbKa_1Ka_2c_1-\left(H^+\right)^2KwKa_1Kb-\left(H^+\right)^2\left(Kw\right)^2-$$
$$2H^+KwKa_1Ka_2c_1-H^+KwKa_1Ka_2Kb-H^+\left(Kw\right)^2Ka_1-\left(Kw\right)^2Ka_1Ka_2=0$$

8.4 SOLUBILITY OF SALT VERSUS SOLUBILITY OF CONSTITUENT ACID

Initial work upon the commencement of this project focused on finding a correlation between the previously determined salt solubilities[1] and acid solubilities. The acid solubilities were determined by the method described in Section 2.2.2 and the comparison can be seen in Figure 161.

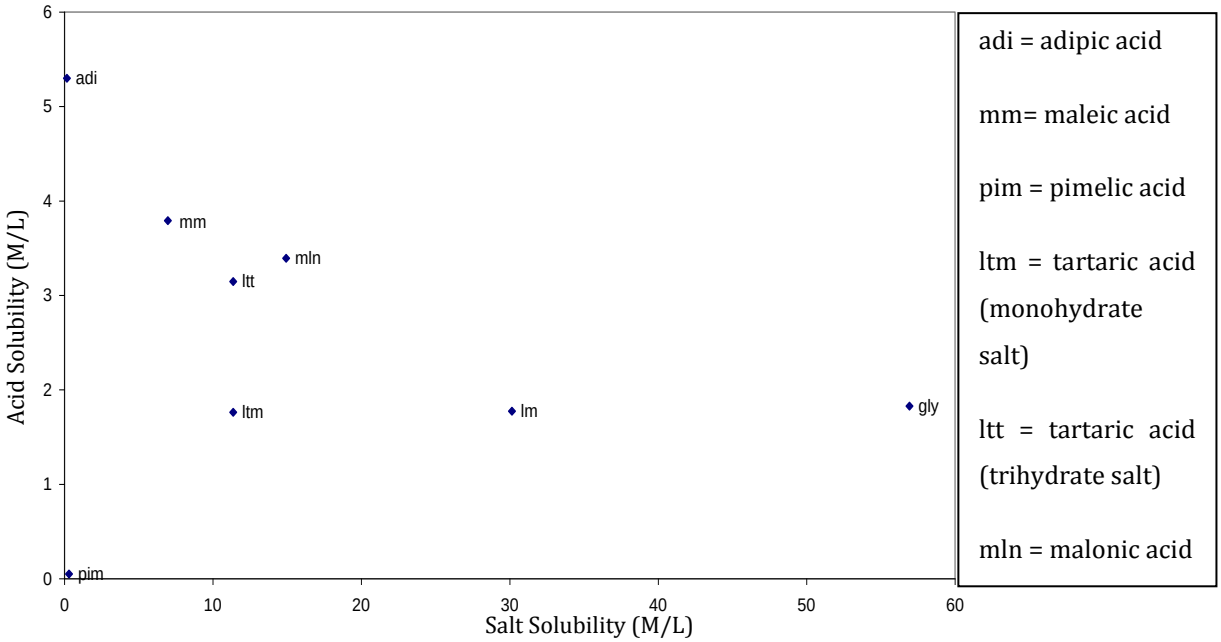

FIGURE 161- COMPARISON OF THE SOLUBILITIES OF EPHEDRINE SALTS AND THEIR CONSTITUENT ACIDS.

This work was not pursued further as there was deemed to be no correlation.

CRYSTAL GROWTH & DESIGN
2008
VOL. 8, NO. 10
3483–3485

Perspectives

On the Solubility of Saccharinate Salts and Cocrystals

Claire L. Cooke* and Roger J. Davey

The Department of Chemical Engineering and Analytical Science, The University of Manchester, Manchester, United Kingdom

Received June 13, 2008; Revised Manuscript Received July 18, 2008

ABSTRACT: A simple relationship allows pH versus solubility plots for molecular salts to be calculated from known pK's together with one measurement of solubility and the pH of the corresponding supersaturated solution. Using this methodology the solubility of a series of salts may be properly compared and judged against that of a cocrystal. One advantage of this method is that the equations also allow the calculation of an important thermodynamic parameter—the solubility product.

In the manufacture of pharmaceutical products, molecular salts of active ingredients are routinely used to improve certain solid form physical properties for production, processing, and formulation. Salt screening is, therefore, a major commercial research activity.[1−5] Salt formation is an acid−base reaction, involving the transfer of protons. The relative strengths (dissociation constants, pK_a) of the acid and the base concerned are thus of vital importance and determine whether or not salt formation occurs. This is reflected in the much quoted "rule" stating that the difference in pK_a between the acid and the base (ΔpK_a) must be >2 units for the salt to form.[6]

pH solubility relationships have been reported previously,[7,8] usually determined by titrimetry and spectrophotometric methods. These demonstrate that the pH of the saturated solution is a major factor in salt solubility, a feature of considerable importance in both salt isolation and in determining bioavailability of pharmaceutical products. While solubility data are not always accompanied by measurement of an associated pH,[9] Jones et al. [10] have recently shown how the simultaneous determination of the pH and solubility can be used to calculate the thermodynamic solubility product (K_{sp}). This method, which needs only one solubility value at a known pH together with the pK of each component, is employed in this paper. It offers an alternative to the more frequent[11−13] use of direct concentration measurements to calculate K_{sp} using the equation

$$K_{sp} = [A]^x[B]^y \quad (1)$$

for the dissociation of the salt A_xB_y according to

$$A_xB_y \leftrightarrows xA^{y+} + yB^{x-} \quad (2)$$

Here we apply this methodology to some recently reported data on saccharinates published by Bhatt et al.[14] and Banerjee et al.[15] Their interest was in comparing the solubility of saccharinate salts with saccharin cocrystals. A selection of pharmaceutical bases was crystallized with saccharin resulting in the isolation of 10 salts and one cocrystal. On the basis of their measured solubility it was concluded that, at least in the case of saccharin, salts are more soluble than cocrystals. This brief reexamination of their data serves two purposes. First, because they reported both the pH and the composition of the saturated solutions, we wish to emphasize how a simple calculation enables such data to be converted into a fundamental thermodynamic parameter, K_{sp}, the solubility product of the salts. Second, because solubility of salts and cocrystals depend on the ternary composition of the solution, comparison of solubilities can only be made with due attention paid to the pH. In the current examples, the pH of the saturated cocrystal solution was 3.27, much lower than those of the salts, which lay between 5.25 and 6.25. We were interested in the effect this pH difference might have on the relative solubilities.

Saccharin, with a pK_a of 2.2, acts as a weak acid to form a salt with a sufficiently basic molecule, or as a neutral molecule to form a cocrystal. Using the experimentally determined pH value and aqueous pK values given in these papers[14,15] (see Table 1), speciation diagrams were constructed. These showed that, at least in an aqueous environment, a salt could theoretically form for all the basic active pharmaceutical ingredients (APIs) with saccharin, including piroxicam (Figure 1). The latter in fact was isolated as a cocrystal, a consequence presumably of the shift in pK's in the mix of chloroform and ethanol used for crystallization. An illustrative example of a system that formed a salt, haloperidol saccharinate, is shown in Figure 2. In Figure 2 it is evident that between pHs 3 and 7 both former and active are nearly totally ionized, while this region is much smaller for the cocrystal system in Figure 1. In reality these materials were

* To whom correspondence should be addressed. Phone: 0161 3064362. E-mail: claire.cooke@postgrad.manchester.ac.uk.

10.1021/cg800621q CCC: $40.75
Published on Web 08/29/2008

Table 1. The Physical Properties of APIs and Their Saccharinate Salts

API			API saccharinate			
API	solubility[a](g/L)	pK	solubility (g/L)	pH	K_{sp} (mol^2/dm^6)	notes
haloperidol	<0.01	8.3[b]	6.08	5.44	1.18×10^{-4}	
mirtazapine	<0.05	7.7[c]	2.08	5.85	1.79×10^{-5}	
piroxicam	<0.10	6.3[b]	<0.10	3.27	0.01[e]	solubility data not accurate enough
quinine	<0.10	5.1[b]	5.40	5.55	2.96×10^{-5}	
pseudoephedrine	<0.50	9.8[b]	>300	6.25		solubility data not accurate enough
lamivudine	70.00	4.3[d]	10.56	3.35	6.12×10^{-4}	
risperidone	<0.10	8.2[b]	2.87	5.25	2.53×10^{-8}	
sertraline	<0.10	9.5[b]	6.45	5.85	1.74×10^{-4}	
venlaflaxine	<0.10	9.4[b]	30.06	5.95	4.26×10^{-3}	
zolpidem	<0.01	6.2[b]	11.90	6.05	3.44×10^{-4}	
amlopine	<0.01	8.6[b]				no solubility data

[a] API solubilities published without pH data. [b] pK values given by ref 14. [c] pK values given by ref 15. [d] pK values given by ref 16. [e] n.b. maximum possible solubility product for the cocrystal assuming K_{sp} = (solubility)^2; see ref 17.

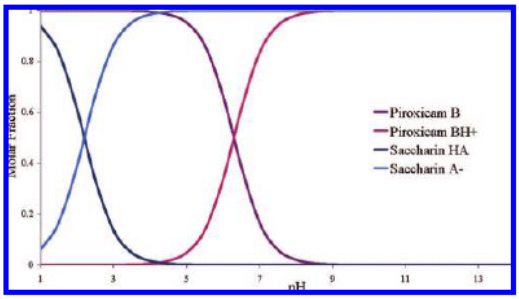

Figure 1. Speciation diagram of piroxicam and saccharin.

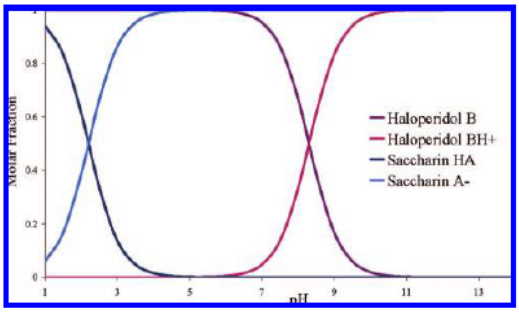

Figure 2. Speciation diagram of haloperidol and saccharin.

prepared by crystallization from nonaqueous media for which the pK's are unknown and for which the ΔpK rule may not be met.[2]

From the solubility data given in the refs 14 and 15 and using the pK_a values quoted in Table 1, a pH solubility relation can be determined using equations adapted from the work of Jones et al.[10] For the salt BHA of a weak acid, AH, and a monobasic base, B, the solubility will be the total of the concentrations of B in all of its forms, balanced with a stoichiometric amount of A. Using the acid−base equilibria and mass balance relationships, we can write

$$BH^+ \leftrightarrow B + H^+; K = [B][H^+]/[BH^+] \quad (3a)$$

$$AH \leftrightarrow A^- + H^+; K_a = [A^-][H^+]/[HA] \quad (3b)$$

with the overall solubility of the salt described by

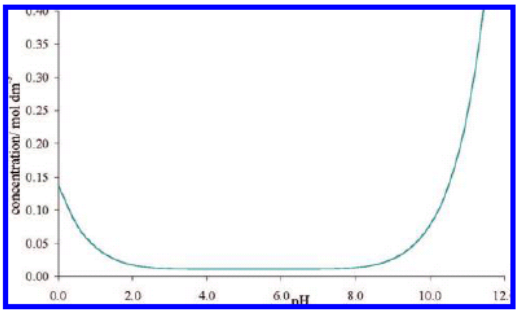

Figure 3. pH vs solubility relation for haloperidol saccharinate.

$$\text{solubility} = [BH^+] + [B] = [A^-] + [HA] \quad (4)$$

Equations 3a and 3b, which quantify the species in terms of the acid and base dissociation constants (K_a and K respectively), together with the solution pH, can be used to rearrange equation 4 to give

$$\text{solubility} = (K_{sp}(1 + [H^+]/K_a)(1 + K/[H^+]))^{1/2} \quad (5)$$

Examination of the pH vs solubility plots calculated using eq 5 revealed that, because of the large difference in pK's between the bases and saccharin, solubilities are rather insensitive to pH over the pH range 3−8. Thus, for example in the case of haloperidol saccharinate (Figure 3) the pH of the salt solution was given as 5.44 at which its solubility is 0.0108 mol/L. At a pH equivalent to that of the cocrystal solution, 3.27, the solubility would be slightly higher at 0.0113 mol/L. The general conclusion of the authors,[14,15] that their saccharinate salts are more soluble than the saccharin cocrystal, is therefore justified, despite the pH differences. The closer the pK's of the salt components the more sensitive the solubility will be to pH. Following the above arguments and given previous work,[17] it is evident that while there will be a pH dependence of cocrystal solubility, a full description (beyond the scope of this perspective) would need to take into account a revised definition of the solubility product as well as any possible complexation in solution. Examination of the speciation diagram, Figure 1, of the piroxicam-saccharin cocrystal indicates that at the reported pH the solubility will be affected by the ionization of the components. The underlying factors determining solubility relate, of course, to issues of both solid state and solution chemistry. Recent analysis of a series of ephedrine salts[2] suggests that at least for salts in aqueous solutions, ion solvation plays a pivotal role. This idea is certainly consistent with the

Appendix

data considered here given that solvation of the ions comprising the salts is likely to be increased compared to the uncharged molecules in the cocrystal.

In the calculations made to determine the pH vs solubility relation, the solubility product (K_{sp}) is also resolved by minimizing the difference between the experimental and theoretical solubilities at the experimental pH. The calculated solubility products (assuming solution ideality) for the salts are given in Table 1. One case, Lamivudine, reminds us that a salt is not necessarily more soluble than its free base, a point also made in the paper by Black et al.[2]

Acknowledgment. We thank AstraZeneca and the EPSRC for their continuing financial support. We also thank Dr. Helen P. Jones for her help with calculating pH vs solubility relations.

References

(1) Berge, S. M.; Bighley, L. D.; Monkhouse, D. C. *Pharm. Salts* **1977**, *66*, 1–19.
(2) Black, S. N.; Collier, E. A.; Davey, R. J.; Roberts, R. J. *J. Pharm. Sci.* **2007**, *96*, 1053–1068.
(3) Collier, E. A.; Davey, R. J.; Black, S. N.; Roberts, R. J. *Acta Crystallogr.* **2006**, *B62*, 498–505.
(4) Gould, P. L. *Int. J. Pharm.* **1986**, *33*, 201–217.
(5) Serajuddin, A. T. M. *Adv. Drug Delivery Rev.* **2007**, *59*, 603–616.
(6) Stahl, H. P.; Wermuth, C. G., *Handbook of Pharmaceutical Salts - Properties, Selection and Use*; Verlag Helvetica Chimica Acta: Zurich, 2002.
(7) Kramer, S. F.; Flynn, G. L. *J. Pharm. Sci.* **1972**, *61*, 1896–1904.
(8) Serajuddin, A. T. M.; Jarowski, C. I. *J. Pharm. Sci.* **1985**, *74*, 142–147.
(9) Srivijaya, R.; Vishweshwar, P.; Sreekanth, B. R.; Vyas, K. *CrystEngComm* **2008**, *10*, 283–287.
(10) Jones, H. P.; Davey, R. J.; Cox, B. G. *J. Phys. Chem.* **2005**, *109*, 5273–5278.
(11) He, N.; Zhan, X.; Li, C.; Lin, T.; Li, L. *J. Pharm. Sci.* **2005**, *94*, 540–546.
(12) Kahdu, J.; Harju, L.; Ivaska, A. *Anal. Chim. Acta* **1999**, *380*, 105–111.
(13) Zhan, X.; Li, C.; Li, Z.; Yang, X.; Zhong, S.; Yi, T. *J. Pharm. Sci.* **2004**, *93*, 441–448.
(14) Bhatt, P. M.; Ravindra, N. V.; Banerjee, R.; Desiraju, G. R. *Chem. Commun.* **2005**, 1073–1075.
(15) Banerjee, R.; Bhatt, P. M.; Ravindra, N. V.; Desiraju, G. R. *Cryst. Growth Des.* **2005**, *5*, 2299–2309.
(16) Product Monograph- Remeron, Organon Canada Ltd., Control Number 093844, 2004.
(17) Nehm, S. J.; Rodriguez-Spong, B.; Rodriguez-Hornedo, N. *Cryst. Growth Des.* **2006**, *6*, 592–600.
(18) Pereira, B. G.; Vianna-Soares, C. D.; Righi, A.; Pinheiro, M. V. B.; Flores, M. Z. S.; Bezerra, E. M.; Freire, V. N.; Lemos, V.; Caetano, E. W. S.; Cavada, B. S. *J. Pharm. Biomed. Anal.*, **2007**, *43*, 1885−1889.

CG800621Q

CRYSTAL GROWTH & DESIGN Article
XXXX, Vol. XXX
000–000

DOI: 10.1021/cg1011296

Binary and Ternary Phase Diagrams as Routes to Salt Discovery: Ephedrine and Pimelic Acid†

Claire L. Cooke,*,‡ Roger J. Davey,‡ Simon Black,§ Chris Muryn,⊥ and Robin G. Pritchard⊥

‡The Department of Chemical Engineering and Analytical Science, The University of Manchester, Manchester, United Kingdom, §Pharmaceutical Development, AstraZeneca, Silk Road, Macclesfield, United Kingdom, and ⊥The School of Chemistry, The University of Manchester, Manchester, United Kingdom

Received August 26, 2010; Revised Manuscript Received October 28, 2010

ABSTRACT: Despite the commercial importance of molecular salts in pharmaceutical applications, there are few previous studies of their phase behavior in binary and ternary systems. In this current study salt formation is explored in both the binary system (1*R*,2*S*)-(−)-ephedrine/pimelic acid and in the related ternary system using water as a solvent. The utility of the binary phase diagram as an aid to full exploration of phase space is demonstrated, and this investigation makes use of both dry techniques (grinding) and crystallization from solutions to access possible solid phases. Inherent problems of isolating a metastable phase in the ternary system are revealed.

Introduction

The control of the physical properties of active pharmaceutical ingredients (APIs) is vital in the production of safe and effective drugs for release to market. Typically, molecular salts are prepared[1] as a means of controlling physicochemical properties such as solubility, processability, bioavailability, and physical stability. However, despite this importance the selection of salt forms still remains a difficult and often semiempirical choice[2] with salt screening widely employed in order to determine the most appropriate salt form for the required function.[3,4] Such screens utilize a range of solvents and conditions with solvent-free routes[5,6] often not considered. While for bulk production solvent crystallization methods may be most effective and reliable, at the early screening stages all information can prove helpful in the quest to discover all possible salts and phases.

Despite this background there are apparently few publications detailing a complete study of a molecular salt system including preparation by dry grinding techniques, determination of the binary phase diagram to help guide discovery, and determination of the ternary phase diagrams to guide the development of robust processes. In recent years, publications in these areas have focused more closely upon cocrystals and their formation, with significant numbers of binary and ternary phase diagrams now available for such systems.[7−12] In the context of phase diagrams, the main difference between cocrystals and salts is the effect of ionization in salt systems causing greater potential for deviations from ideality, leading to pH-dependent effects.[10,13] General definitions of salts and cocrystals have been the subject of some dispute and details can be found in a number of publications.[14−16]

In 2007, Chiarella et al.[12] published work on the rationalization of cocrystal formation using both binary and ternary phase diagrams. This work provided scientific explanations for so-called serendipitous results involving dry and solvent drop grinding and highlighted how useful both types of phase diagrams can be. Recent work published by Guo et al.[11] shows complete binary and ternary phase diagrams for the caffeine/maleic acid cocrystal system, allowing full investigation of the formation of an elusive 2:1 cocrystal. However, this paper concludes that despite the extensive knowledge of this system they have gained, certain results are hard to rationalize.

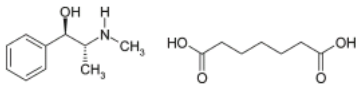

Figure 1. The molecular structures of (1*R*,2*S*)-(−)-ephedrine(left) and pimelic acid (right).

Table 1. Physical Properties of Pure Components

physical property	ephedrine	pimelic acid
melting point (K)	310	378
aqueous solubility (wt %)	5.39	4.65
aqueous pK_a	9.74	4.48, 5.42
enthalpy of fusion (kJ/mol)	11.96	31.78
polymorphs	no	3
hydrates	hemihydrate	no

The system chosen for study in this work is the salt formed between (1*R*,2*S*)-(−)-ephedrine (hereafter referred to only as "ephedrine") and pimelic acid (see Figure 1). A number of salts of ephedrine have previously been published and their crystal structures reported;[17] however no phase diagrams (binary or ternary) of these salts were fully determined,[10] nor are any salts of pimelic acid and ephedrine known. Physical property data is given for the two pure components in Table 1.

Pimelic acid exists in three different polymorphic forms, referred to as modifications I, II, and III[18] (III and I are often referred to as α and β,[19] respectively, with the crystal structure of modification II not known and rarely mentioned). According to the literature, the commercially available polymorph, III, transforms into II at around 330 K, and then to modification I between 370 and 370.6 K. The melting temperature discussed in this paper is that of polymorph I at 378 K. These polymorphic

†Claire L. Cooke thanks AstraZeneca and the EPSRC for funding.

*To whom correspondence should be addressed. Phone: 0161 3064362. E-mail: claire.cooke@postgrad.manchester.ac.uk.

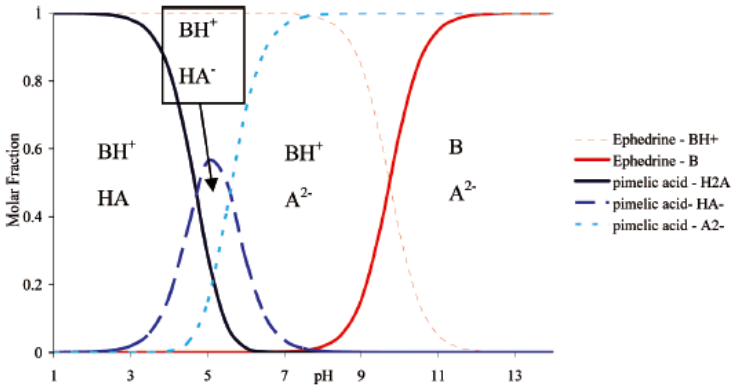

Figure 2. The speciation diagram for ephedrine and pimelic acid in water.

transformations can be seen in the DSC (Figure 11), with the transformation from III to II occurring at around 353 K; however this transformation is reported[18] to be hard to determine from DSC alone, perhaps explaining the difference with literature value (330 K).

Ephedrine readily hydrates in air, and consequently the behavior and properties of ephedrine previously reported[10,17] are often of the resulting hemihydrate. The work described here was completed using as-supplied (Sigma Aldrich) material, which is a mixture of hydrated and unhydrated phases. The properties of the two forms are evidently very similar with, for example, less that 1 °C difference in their melting points.

Evaluation of the data given in Table 1 suggests that this system is appropriate for salt formation. The two pK_a values of the acid are both greater than 2 pK_a units from that of the base (in water), thereby satisfying the general rule $\Delta pK_a > 2$ rule.[10] The speciation diagram is seen in Figure 2, and it is evident that at a pH of around 8, ephedrine is present exclusively as the anion and pimelate as the doubly deprotonated carboxylate suggesting that it will be easiest to nucleate a 2:1 salt at this pH. Upon lowering of the pH to 5, the maximum proportion of singly deprotonated carboxylate is present, meeting the requirements of a 1:1 salt. The aqueous solubilities of the acid and base are similar, suggesting that the ternary phase diagram will show two regions of salt formation occurring at 2:1 and equimolar ratios, the latter showing congruent dissolution. There is, therefore, the expectation of both a 1:1 and 2:1 salt present in the aqueous system.

Initially this prospect was tested by contacting the pure solids in both powder and single crystal forms to assess whether any salt formation occurs in the solid state. This was extended to dry grinding experiments where different stoichiometric ratios were coground to ascertain whether the pure components transformed fully to salt forms. It was considered that the low melting point of ephedrine would increase the likelihood of salt formation in the binary system due to the chance of a submerged eutectic.[7] To allow more certain identification of solid phases formed, the binary phase diagram was determined, allowing the solid phases attainable without the presence of a solvent to be assessed. Growth of single crystals and structure determination by single-crystal X-ray diffraction allowed definite identification of composition as well as the measurement of melting points and heats of melting and a subsequent assessment of the effect of crystal structure on salt properties. To understand the formation of these salts from aqueous solution, the solubilities of all the solid phases were determined leading to the construction of a ternary phase diagram.

Experimental Section

Materials. (1*R*,2*S*)-(−)-Ephedrine (99% chemical purity) and pimelic acid (99%) were obtained from Sigma-Aldrich (with the use of appropriate licenses in the case of ephedrine) and used as received. Distilled, deionized water was used with no further purification. The starting materials were initially characterized by powder X-ray diffraction (pXRD) and differential scanning calorimetry (DSC).

Single Crystals. Single crystals of the 1:1 and 2:1 salts were prepared from aqueous solutions. Single crystals and powders of the 1:1 salt were produced by slow evaporation of an aqueous solution prepared by stirring a mixture of ephedrine (0.010 mol), pimelic acid (0.010 mol), and 10 mL of water at 298 K for 1 day. Single crystals of the 2:1 salt were grown by adding ephedrine (0.100 mol) to pimelic acid (0.050 mol) in 0.5 mL of water at 298 K. More detail on how methods for salt formation were chosen is given in the Single Crystal Growth from Solution section of this paper. X-ray diffraction data for the 1:1 salt single crystal was collected on the Oxford XCaliber 2 diffractometer. X-ray diffraction data for the 2:1 salt single crystal was collected on the Bruker SMART CCD diffractometer. The selected crystals were mounted on glass fibers using Paratone-N oil and placed in a cryo-flow at 100 K.

X-ray Powder Diffraction (XRPD). Powders were characterized using a Rigaku Miniflex X-ray powder diffractometer (Cu Kα radiation, wavelength 1.5406 Å). Data were collected between 5° and 40° using a step size of 0.03°.

Differential Scanning Calorimetry (DSC). A Mettler DSC 30 was used to determine the melting temperatures and enthalpies of the pure components and the physical mixtures of components for the binary phase diagram. The samples were heated from 298 to 473 K at a rate of 10 K per min.

Infrared (IR) Spectrometry. FTIR spectra of the pure components and ground salts were collected using Thermo Nicolet Avatar 360 ESP with an attenuated total reflection (ATR) attachment, integrated with Nicolet's OMNIC software. All spectra were collected between 400 and 4000 cm^{-1}. The parameters used were 32 scans and a resolution of 16 cm^{-1}.

Gravimetric Vapor Sorption (GVS). GVS was completed on both the 2:1 and 1:1 salts to ascertain how they react to different levels of humidity using equipment supplied by Surface Measurement Systems and controlled using the *DVSWin software*, v.2.17. For the 2:1 salt, the relative humidity at 298 K was varied from 0 to 95% in 10% intervals and held at each level until the sample mass had stabilized. For the 1:1 salt the relative humidity at 298 K was varied from 0 to 70% in 10% intervals and held at each level until a stable sample mass had been obtained.

Solubility Determination. A gravimetric method was used to determine the solubility of the pure components and salts at 296 K. Samples were slurried in 10 mL of water for at least 2 days to ensure thats

Appendix

equilibrium had been reached, the pH of the solutions was recorded, and aliquots of saturated solution were taken and weighed. These samples were allowed to evaporate to dryness and reweighed; the compositions of these ternary saturated solution were determined using a method reported previously.[20]

Powder Samples of Salts. The 1:1 and 2:1 salts of ephedrine pimelate were prepared at room temperature by dry grinding in a pestle and mortar for 5 min continuously. Typically 6.05×10^{-3} mol (1 g) of ephedrine and 6.06×10^{-3} mol (0.97 g) of pimelic acid or 6.05×10^{-3} mol (1 g) of ephedrine and 3.03×10^{-3} mol (0.49 g) of pimelic acid were used to make the 1:1 and 2:1 salts, respectively.

Optical Microscopy. A polarizing Zeiss Axioplan 2 microscope was used together with a Linkam hot stage to both heat and cool samples. Single crystals were contacted on a microscope slide mounted on the hotstage and images were recorded every 10 s using an attached camera.

Results and Discussion

Screening for Salts in the Solid State. Two techniques were chosen for an initial screen with the aim of identifying both the existence and stoichiometry of potential salts. DSC experiments were used to determine the binary phase diagram, while dry grinding was performed on solid mixtures of known stoichiometry to test for the appearance of new solid phases.

To determine how the melting behavior of one component changes in contact with the other, different stoichiometric ratios were prepared, and their melting points were established using DSC. The usual method for determining the binary phase diagram of a system using DSC entails an initial melting cycle, followed by a recrystallization (cooling) cycle, and finally a second heating cycle. This is expected to give two well-defined peaks, the eutectic (from the first peak onset) and the melting point of the pure component (from the second peak position). However, for this system, no recrystallization ever occurred in the cooling cycle. This same result was also observed for pure ephedrine, suggesting the presence of ephedrine in the samples may be the cause of this issue. Consequently samples were prepared as uniformly as possible by extended grinding and heated only once to determine the various melting peaks. This method led to some irreproducibility in the peak positions of the DSC patterns, and therefore, the eutectic lines and liquidus curves on the binary phase diagram have some outlying points, as can be seen in Figure 3. However the general shape of the curves and position of the eutectic lines can be clearly observed, and sketched lines are used to guide the eye in Figure 3. The melting points determined agree with literature values for the pure single component solid phases.[10,18] As discussed in the Introduction the ephedrine used was approximately half anhydrous and half the hemihydrate form. In order too assess the effect of using this mixture; ephedrine was placed in a desiccator for a week to ensure all water had been removed. Three of the DSC experiments for the binary phase diagram were then repeated using the anhydrous sample, and no difference was seen in the results; therefore the presence of some hemihydrate in the ephedrine was not considered further.

Detailed examination of the binary phase diagram indicates the likely existence of a 1:1 salt, which dominates phase space over the wide acid composition range 0.3 to 0.9 mol fraction. In addition between 0.2 and 0.3 mol fraction of acid there is potentially a second liquidus peak appearing as a shoulder, hinting at the existence of a 2:1 salt in this system. The position of the eutectic lines agrees with this hypothesis with the eutectic for the ephedrine/2:1 salt at ~30 °C, the eutectic for the 2:1/1:1 salts at ~105 °C, and the eutectic for the 1:1 salt/pimelic acid at ~80 °C. The presence of a eutectic line at around 100 °C provides good evidence that a 2:1 salt does exist and is accessible by nonsolution methods. This region is included as a dotted line in Figure 3 in order to guide the eye and to imply uncertainty in the exact position of the region.

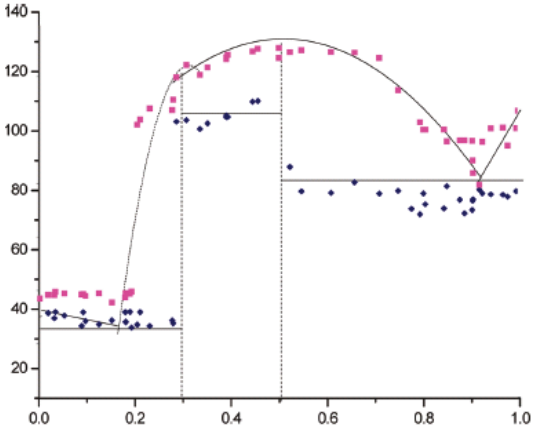

Figure 3. The binary phase diagram of ephedrine and pimelic acid showing experimentally determined points (pink = liquidus curves; blue = eutectic lines) and a schematic to guide the eye in which the solid horizontal lines show the eutectic and the curves show the melt temperatures of the components and salts in contact with one another. The dashed curved line is the suspected 2:1 salt region.

Previous work[7] has shown a relationship between cocrystal formation by grinding and the presence of a submerged eutectic liquid in the binary system, from which a multicomponent crystal can nucleate and grow. From the phase diagrams of Figure 3, it is uncertain whether a submerged eutectic might exist, since extension of the pure component liquidus lines suggests an intersection around room temperature (20−25 °C). Simple contacting of solid powders did produce a slight color change at the interface but microscopic examination of crystal−crystal contacts was inconclusive with no clear evidence of a liquid phase. Figure 4 shows the microscope images as a single crystal of pimelic acid is contacted with a small piece of ephedrine. It can be observed that the ephedrine decreases in size and seems to "melt into" the pimelic acid crystal. Analysis of this sample proved difficult due to the small scale; however with careful alignment, pXRD provided a pattern similar to that of the ground 1:1 ratio sample. Upon dry grinding of both 1:1 and 2:1 molar ratios however, significant visible changes occurred with products becoming slightly darker in color and of a more cohesive consistency. This was especially true for the 2:1 ratio. Subsequent analysis by pXRD, FTIR, and DSC showed that the pure components had yielded new crystalline phases. Figure 5, for example, compares the measured powder patterns of the final ground powders with those calculated for the starting materials. In agreement with the binary phase diagram, both the 1:1 (pattern second from top) and 2:1 (top pattern) ground samples showed highly crystalline patterns indicating the formation of new solid phases. Therefore in this system, grinding different salt stoichiometries is sufficient to determine the salts present without the need to define the binary phase diagram in full.

Analysis by DSC showed these new phases to have melting points of 123 and 132 °C, consistent with values (122 and 133 °C)

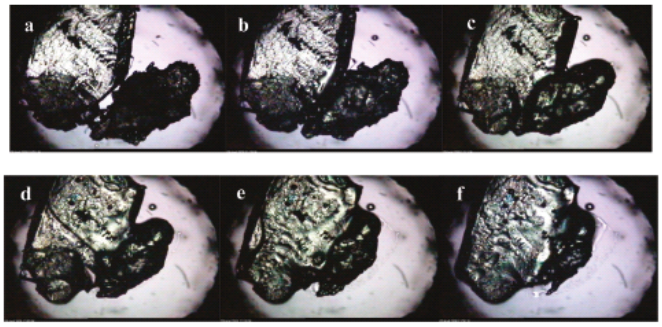

Figure 4. Microscope images of the contact of ephedrine (right) and pimelic acid (left). Images taken initially (a) and after 1 (b), 1.5 (c), 2.5 (d), 3.5 (e), and 4.5 h (f) using a 10× lens.

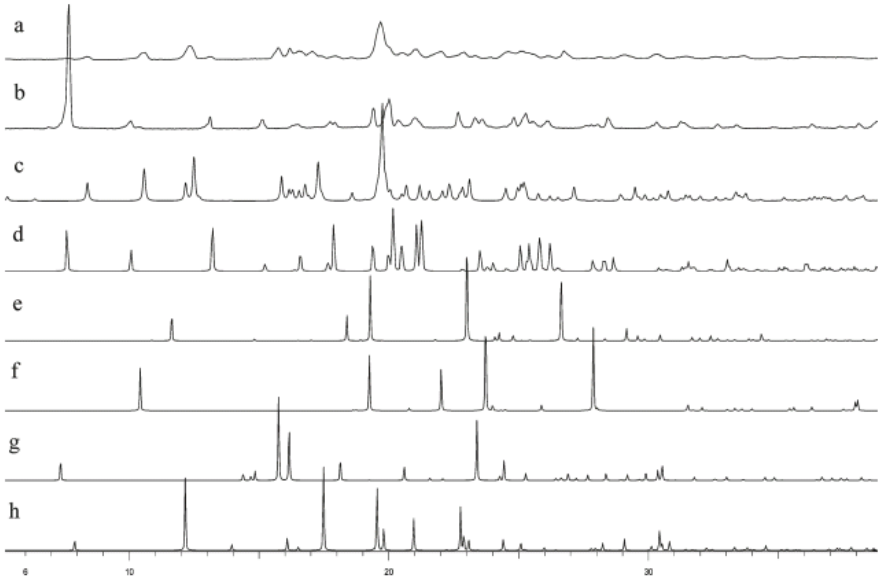

Figure 5. Powder XRD patterns: (a) experimental 2:1 (ephedrine/pimelic acid) ratio ground; (b) experimental 1:1 ratio ground; (c) 2:1 salt simulated; (d) 1:1 salt simulated; (e) α pimelic acid simulated; (f) β pimelic acid simulated; (g) ephedrine hemihydrate simulated; (h) ephedrine simulated.

deduced from the binary phase diagram, Figure 3. As a further check of salt formation, FTIR measurements of the new forms were compared with that of the pure acid. These data are seen in Figure 6 where the carbonyl band of pimelic acid clearly shifts from a single absorption at ~1681 cm^{-1} in its un-ionized form (blue) to three bands with values of 1694, 1624, and 1547 cm^{-1} in the 1:1 composition (red) and finally to a single peak at 1559 cm^{-1} in the 2:1 mixtures (green). These changes are consistent with the expected salt formation in which the acid adopts singly and doubly deprotonated forms. The three peaks at the 1:1 composition indicate the existence of two different carbonyl species, one hydrogen bonded and the other an ionized carboxylate (known to give two peaks), while the return to a broad absorption with a shoulder at the 2:1 stoichiometry is indicative of deprotonation of both acids to two carboxylate groups.[21]

Single-Crystal Growth from Solution. From the dry grinding experiments and the thermal, pXRD, and FTIR data, the presence of 1:1 and 2:1 salts in this system has been proven. In order to determine the structures of these salts and assess their physical properties, single crystals of both salts were grown from solution. Single crystals and powders of the 1:1 salt were easily produced by slow evaporation of an aqueous solution. Typically, a solution was prepared by stirring a mixture of ephedrine, pimelic acid, and water at 298 K for one day to give a solution 1 M in both components. This solution was then left to evaporate slowly until crystals had formed after around 3 days.

In applying a similar approach to the preparation of single crystals of the 2:1 salt (by adding 0.02 mol (3.304 g) of ephedrine to 0.01 mol (1.602 g) of pimelic acid at 298 K and adding 10 drops of water from a pipet), it was found that the resulting solutions are highly viscous, becoming more so upon evaporation, eventually solidifying as a clear mass rather than forming single crystals. pXRD and FTIR of this product showed it to be crystalline and identical to material produced

Appendix

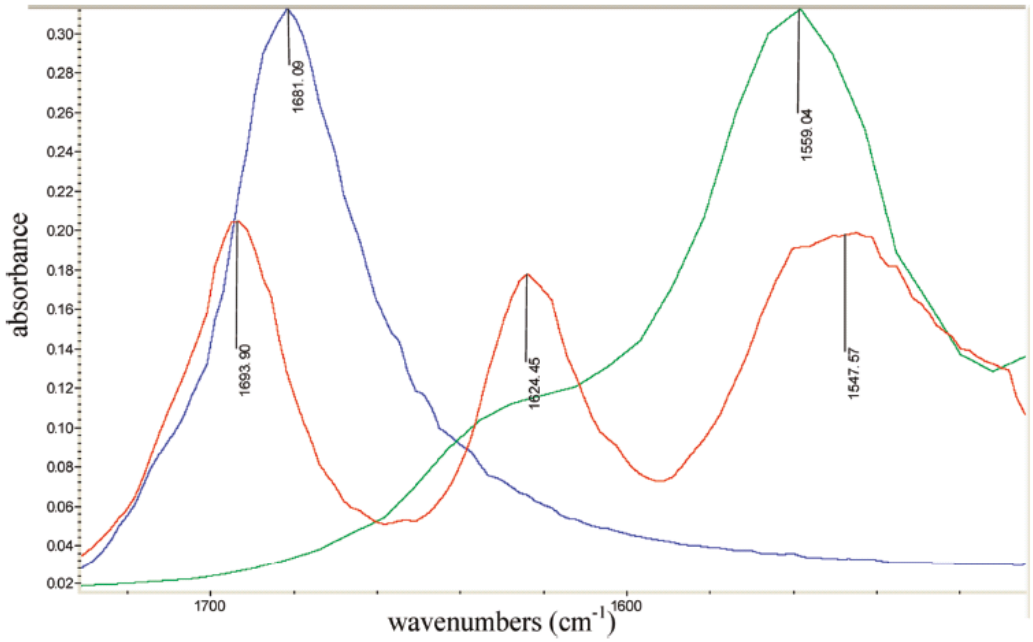

Figure 6. IR spectra of the pure acid (blue), 1:1 salt (red), and 2:1 salt (green) showing that the carbonyl peaks shift upon ionization from 1681 to 1559 cm^{-1}.

Table 2. Crystallographic Data Table for 1:1 and 2:1 Ephedrine Pimelate

system	1:1 ephedrine pimelate	2:1 diephedrine pimelate
empirical formula	$C_{10}H_{16}NO \cdot C_7H_{11}O_4$	$2(C_{10}H_{16}NO) \cdot C_7H_{10}O_4$
M_r (g/mol)	325.40	490.63
temp (K)	100	100
radiation type, wavelength	Mo Kα, 0.71073	Mo Kα, 0.71073
crystal system, space group	monoclinic, $P2_1$	monoclinic, $P2_1$
a, b, c (Å)	5.5353(5), 13.4324(13), 11.9231(11)	13.9597(10), 5.8075(4), 16.7716(15)
α, β, γ (deg)	90, 101.574(9), 90	90, 91.690(3), 90
vol (Å^3)	868.48(14)	1359.10(18)
Z, density (mg·m^{-3})	2, 1.244	2, 1.199
abs coeff (mm^{-1})	0.09	0.08
crystal size (mm^3)	1.00 × 0.4 × 0.25	0.3 × 0.1 × 0.05
$\theta_{min}/\theta_{max}$	3.8°/26.4°	3.1°/26.0°
reflns collected/unique (R_{int})	0.034	0.096
data/restraints/params	2887/1/316	2658/1/324
GOF on F^2	0.93	1.05
residual electron density	0.037	0.067
final R indices [$I > 2\sigma(I)$] R1/wR2	0.037/0.079	0.067/0.176

by grinding. As an alternative crystallization method, cooling of identical solutions was attempted, leaving the solutions to crystallize in a temperature controlled vessel at 283 K. After a period of 3 weeks, large needle-like crystals had grown and were extracted for structural analysis by single-crystal XRD.

Attempts to prepare bulk samples of the 2:1 salt proved equally difficult. The results described above suggested that evaporative crystallization would not be an effective means of preparing powder samples. The cooling method only worked at low temperatures for an extended time and large product yields were never obtained; therefore a drown-out method was tested. Addition of 50 mL of acetone to 100 mL of the 2:1 salt solution caused solids to precipitate, suggesting that acetone acts as an antisolvent for this system. However, these solid samples were found not to be phase pure but a mixture of the 2:1 salt with solid ephedrine. It has therefore not been possible to determine a reliable process for the formation of larger samples of the 2:1 salt.

A summary of the crystallographic data is given in Table 2 with structure projections shown in Figures 7 and 8. The structures are available on the CSD with deposition numbers CCDC 789638 and CCDC 789639 for the 1:1 and 2:1 salts, respectively.

In the 1:1 salt, the pimelic acid molecules utilize hydrogen-bonding interactions (O···O distance 2.61 Å) between protonated and deprotonated carboxylic acids groups on adjacent molecules to create an infinite chain running along the b axis. To this acid chain are bound ephedrine molecules. One is held via two hydrogen bonds in which the protonated amine nitrogen interacts with the carbonyl (O···N distance 2. 84 Å) of one acid and the carboxylate of a second (O···N

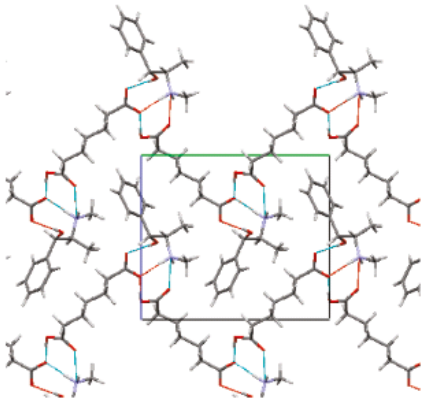

Figure 7. Structure of 1:1 salt viewed down the *a* axis.

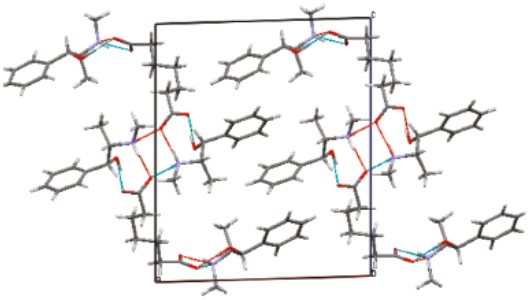

Figure 8. Structure of the 2:1 salt viewed down the *b* axis.

distance 2.695 Å). The second ephedrine is held through a hydroxyl−carboxylate hydrogen bond (O···O distance 2.66 Å). These ephedrine molecules then interact again with the adjacent chain through identical hydrogen bonds such that they form π stacks with a C···H distance of 3.29 Å. There are no inter-ephedrine hydrogen bonds in this structure, and it is noted that none of the structures previously determined by Collier et al.[17] had this packing motif.

The 2:1 salt is quite different in that both ends of the deprotonated acid chain bind separate ephedrine molecules, and there are no acid−acid interactions. In one carboxylate group, one oxygen forms a bifurcated hydrogen bond to amines on two separate ephedrine molecules (O···N 2.75 and 2.80 Å) while the second interacts with the hydroxyl of a third ephedrine molecule. The other carboxylate binds only two ephedrine molecules through O···N and O···O interactions (2.63 Å) to one molecule and O···N (2.77 Å) to the second. Four ephedrine molecules and two pimelic acid molecules bond in this manner to form tetramer units as shown in Figure 9 which are then interlinked via $\pi-\pi$ bonding (3.45 Å). The tetramer motif is similar to that seen in the adipate, glycolate, and malonate (1:1 ratio salts) reported by Collier et al.[17] and the (−)-(1*R*,2*S*)-ephedrine ent-2-methoxycarbonyl-cyclohex-4-ene-1-carboxylate.[22] Interestingly all of the salts subjected to GVS (adipate, glycolate, and malonate) proved to be deliquescent, as is the 2:1 salt (discussed in The Ternary Phase Diagram: Ephedrine/Pimelic Acid/Water).

The conformations of the pimelic acid ions in these two salts differ from those in polymorphs I and III of the pure

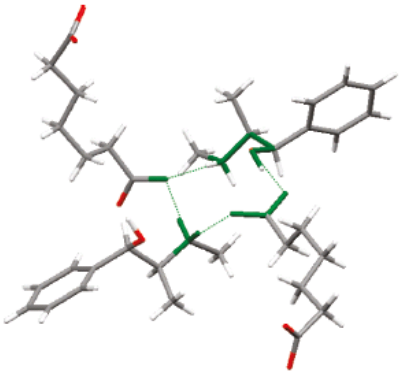

Figure 9. Structure of the 2:1 salt showing hydrogen bonding motif (highlighted in green) common to a number of ephedrine salts.

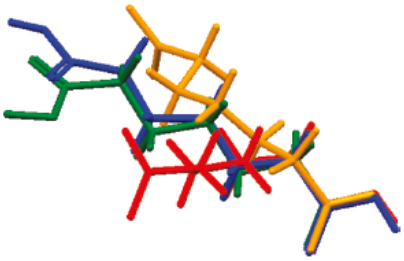

Figure 10. An overlay of conformations of pimelic acid found in III pimelic acid (green), I pimelic acid (blue), 1:1 salt (red), and 2:1 salt (yellow).

acid and from those found in four other pimelate salts in the CSD. Figure 10 shows an overlay of the two pimelic acid polymorph conformers and the pimelic acid conformations in the two ephedrine salts. The 1:1 salt shows rotation at the sixth carbon in the chain, and the 2:1 salt shows a twist at the fifth carbon. Of the other known salts, all but one contain pimelic acid in straight chain conformations identical to the pure acid polymorphs (blue and green in Figure 10). Only bis(DL-arginium) pimelate dihydrate shows another conformation with the twist at carbon four. Because the 2:1 salt has a very high solubility, it was suspected that the chain may be in an especially unfavorable, high-energy conformation; however by visual inspection, this does not seem to be the case, as is shown in Figure 10.

Ephedrine can exist in two conformations, folded or extended.[17] The extended conformation is the most common and lower energy state[23,24] and is displayed in the pure ephedrine, ephedrine hemihydrate, and both salt structures discussed in this paper. Salts of ephedrine previously formed, including the majority published by Collier et al.,[17] appear to favor the extended conformation. Therefore, the high solubility of the 2:1 salt cannot be assigned to the conformation of the ephedrine molecules.

It was confirmed that these single-crystal forms of the salts had properties matching those formed by grinding. The DSC results for the acid, the base, and both salts are given in Figure 11, with the corresponding data in Table 3. The pXRD patterns given in Figure 5 show that the simulated powder patterns from the crystal structures match the powder patterns

Appendix

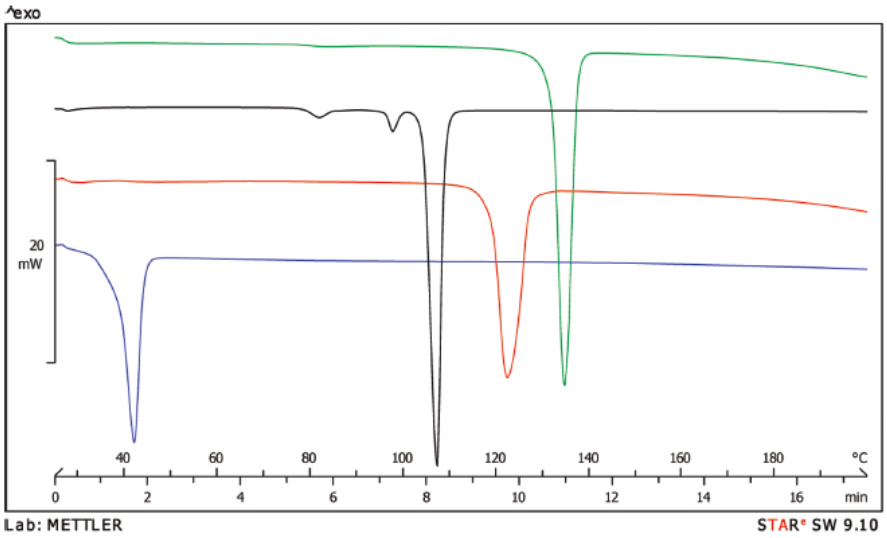

Figure 11. DSC traces of solid phases used to determine melting points and enthalpies of fusion. Ephedrine (blue), pimelic acid (black), 1:1 salt (green), and 2:1 salt (red).

Table 3. Melting Points and Enthalpies of Melting for Solid Phases

compound	melting temperature (K)	enthalpy of fusion (kJ/mol)	enthalpy of fusion per mole of ions (kJ/mol)
ephedrine	310	11.97	11.97
pimelic acid	378	31.78	31.78
1:1 salt	403	44.66	22.33
2:1 salt	393	45.54	15.18

collected from the ground powder samples. The IR spectra also agree with those formed by grinding. We can therefore confirm that the samples formed by grinding are the pure salt forms.

The molar enthalpy of fusion given in Table 3 is divided by the number of ions present in a molecule (two for the 1:1 salt and three for the 2:1 salt) in order to determine the enthalpy of fusion per mole of ions. The difference in enthalpy of fusion per mole of ions between the two salts is significant. The 1:1 salt has the greater value. This is consistent with the much larger region of stability of the 1:1 salt in the binary phase diagram (Figure 3).

The Ternary Phase Diagram: Ephedrine/Pimelic Acid/Water. Figure 12 shows the ephedrine−pimelic acid−water phase diagram measured at 296 K in which there are seven regions and two eutectic points. Region 1 is the undersaturated liquid region in which all compositions are single-phase liquids. In all other regions (2−8), solid phases exist in equilibrium with solutions. Regions 2, 4, 5, and 7 are pure solid phases of either starting materials (ephedrine or pimelic acid) or salts (either 1:1 or 2:1) in contact with their saturated solutions. Regions 3 and 6 are areas where mixtures of solid phases exist (ephedrine and 1:1 salt and 1:1 salt and pimelic acid, respectively) and are in equilibrium with solutions of different invariant compositions (exact compositions only estimated in this ternary phase diagram due to issues with the solubility determination discussed below).

The complementary effects of pimelic acid and ephedrine on their solubilities in water are clearly highly nonideal with both components significantly increasing the solubility of the

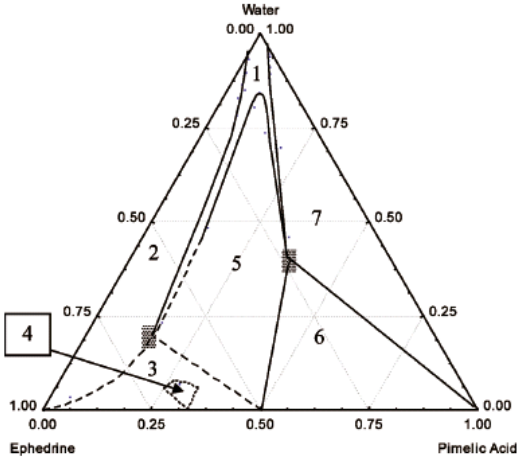

Figure 12. The ternary phase diagram of ephedrine−pimelic acid−water at 23 °C in mole fraction: (1) liquidus; (2) ephedrine + liquid; (3) ephedrine + 1:1 salt + liquid; (4) 2:1 salt; (5) 1:1 salt + liquid; (6) 1:1 salt + pimelic acid + liquid; (7) pimelic acid + liquid. Gray shading indicates uncertainty of the eutectic positions. The dashed lines indicate uncertainty of the liquidus lines due to very high solubilities. Note: the liquidus compositions are determined gravimetrically and hence refer to anhydrous ephedrine materials. The starting compositions utilize ephedrine that is partially hemihydrate. Assuming 50% by mass of the ephedrine to be hemihydrate leads to a maximum error of less than 1%.

other. Similar effects were reported by Lorenz et al. in aqueous racemic mandelic acid[25] and by Chadwick et al. in the benzophenone/diphenylamine/methanol system.[26] In the present case, the solubility of the pimelic acid increases to over 50 wt % in the presence of ephedrine, due to the ionization of the components. On the ephedrine-rich side of the

Table 4. pH and Solubilities of the Pure Phases

compound	solubility (wt %)	pH of solution
ephedrine	5.39	11.20
pimelic acid	4.65	2.25
1:1 salt	16.00	5.36
2:1 salt	~80	~9

phase diagram however, regions 2, 3, 4, and 5 could not be fully determined, as indicated by the dashed lines. This was due to the extremely high aqueous solubility of both ephedrine and the 2:1 salt leading to inherent problems of stirring and filtering solutions of high viscosity, which hampered both equilibration and effective gravimetric analysis. The solubility of ephedrine rose to over 90% by weight suggesting significant ionization, and potentially also complexation, of the two components but could not be determined with accuracy.

The pH values of the salt solutions, Table 4, are naturally within the pH regions required for salt formation at the given stoichiometries.

It is worth noting that Figure 12 shows a markedly different shape from those ternary phase diagrams hypothesized in the 2007 paper by Black et al.,[10] where the ternary phase diagram showing the congruent dissolution of adipic acid and ephedrine shows a much more "orthodox" shape. Because both adipic and pimelic acids are dicarboxylic acids, it would be a reasonable assumption that the phase diagrams may look similar. Therefore, this highlights the need to determine fully a phase diagram for quantitative process design, rather than predicting its shape from the solubilities of the salt/cocrystal and the two pure components.

After determination of the ternary phase diagram, it also became apparent that the 2:1 salt was metastable with respect to the 1:1 salt in aqueous solutions. Evidence for this came from GVS studies, which showed the 2:1 salt to be deliquescent, undergoing a change of mass of ca. 70% at a humidity level of 95%. Recrystallization of such a sample at ambient humidity was found to yield a mixture of the 2:1 and 1:1 salts, presumably due to higher stability of the latter. The complete conversion of this sample to the pure 1:1 salt occurred gradusally over a period of a month. For the 1:1 salt, a mass increase of 1.8% was observed at humidity levels up to 80% with all water being lost on the reduction of humidity levels back to zero.

Overall it is evident that because the solubilities of ephedrine and pimelic acid are very similar in water (see Table 4), the ternary phase diagram is rather symmetrical ensuring that congruent dissolution of the 1:1 salt should occur and that it may be easily crystallized by solvent evaporation. As discussed earlier by Chiarella et al. (2007), the utility of preparation by solid grinding may be understood since, in such experiments, the phase diagram is approached from the solid side and issues of metastability and solution viscosity are clearly avoided. In terms of defining a solution-based process for crystallizing the 2:1 salt, the ternary phase diagram is also useful, in this case highlighting potential processing problems with this form. Alternative solvents may present another easier route to accessing this salt; however this method has not been pursued.

Conclusions

From work completed in this paper, it can be seen that to understand a salt system fully, a range of different analyses should be used and appropriate phase diagrams determined. In this system, determination of the binary phase diagram gave useful support to the grinding experiments providing evidence for the existence of both salts. Without this evidence from the nonsolution methods, the presence of the 2:1 salt may not have been discovered due to exploration of the ternary aqueous system being considerably complicated by the high solubility of the 2:1 salt and its metastability. A consistent preparative route for bulk samples of the 1:1 salt has been developed from aqueous solutions, with this method reinforced by the determined ternary phase diagram. It is also clear from the ternary diagram that searching for a bulk method to prepare the 2:1 salt from water will be difficult and probably is not worth attempting.

References

(1) Stahl, H. P., Wermuth, C. G., Eds. *Handbook of Pharmaceutical Salts-Properties, Selection, and Use*; Wiley-VCH: Weinheim, Germany, 2002.

(2) Gould, P. L. Salt Selection for Basic Drugs. *Int. J. Pharm.* **1986**, *33*, 201–217.

(3) Tong, W.-Q.; Whitesell, G. In Situ Salt Screening-A Useful Technique for Discovery Support and Preformulation Studies. *Pharm. Dev. Technol.* **1998**, *3*, 215–223.

(4) Berge, S. M.; Bighley, L. D.; Monkhouse, D. C. Pharmaceutical Salts. *J. Pharm. Sci.* **1977**, *66*, 1–19.

(5) Braga, D. et al. Intra-Solid and Inter-Solid Reactions of Molecular Crystals: a Green Route to Crystal Engineering. In *Organic Solid State Reactions*; Toda, F., Ed.; Topics in Current Chemistry, Vol. 254; Springer: Berlin, 2005.

(6) Boldyrev, V. V.; Tkacova, K. Mechanochemistry of Solids: Past, Present and Prospects. *J. Mater. Synth. Processing* **2000**, *8*, 121–132.

(7) Chadwick, K.; Davey, R. J.; Cross, W. How Does Grinding Produce Co-crystals? Insights from the Case of Benzophenone and Diphenylamine. *Chem. Commun.* **2007**, *9*, 732–734.

(8) Habgood, M.; Deij, M. A.; Mazurek, J.; Price, S. L.; ter Horst, J. H. Carbamazepine Co-crystallization with Pyridine Carboxamides: Rationalization by Complementary Phase Diagrams and Crystal energy Landscapes. *Cryst. Growth Des.* **2010**, *10*, 903–912.

(9) Jayasankar, A.; Sreenivas Reddy, L.; Bethune, S. J.; Rodriguez-Hornedo, N. Role of Cocrystal and Solution Chemistry on the Formation and Stability of Cocrystals with Different Stoichiometry. *Cryst. Growth Des.* **2009**, *9*, 889–897.

(10) Black, S. N.; Collier, E. A.; Davey, R. J.; Roberts, R. J. Structure, Solubility, Screening, and Synthesis of Molecular Salts. *J. Pharm. Sci.* **2007**, *96*, 1053–1068.

(11) Guo, K.; Sadiq, G.; Seaton, C.; Davey, R.; Yin, Q. Co-Crystallisation in the Caffeine/Maleic Acid System: Lessons from Phase Equilibria. *Cryst. Growth Des.* **2010**, *10*, 268–273.

(12) Chiarella, R. A.; Davey, R. J.; Peterson, M. L. Making Co-crystals-The Utility of Ternary Phase Diagrams. *Cryst. Growth Des.* **2007**, *7*, 1223–1225.

(13) Jones, H. P.; Davey, R. J.; Cox, B. G. Crystallization of a Salt of a Weak Organic Acid and Base: Solubility Relations, Supersaturation Control and Polymorphic Behaviour. *J. Phys. Chem. B* **2005**, *109*, 5273–5278.

(14) Aakeroy, C. B.; Fasulo, M. E.; Desper, J. Cocrystal or Salt: Does It Really Matter? *Mol. Pharmaceutics* **2007**, *4*, 317–322.

(15) Childs, S. L.; Stahly, G. P.; Park, A. The Salt-Cocrystal Continuum: The Influence of Crystal Structure on Ionization State. *Mol. Pharmaceutics* **2007**, *4*, 323–338.

(16) Lara-Ochoa, F.; Espinosa-Perez, G. Cocrystal Definitions. *Supramol. Chem.* **2007**, *19*, 553–557.

(17) Collier, E. A.; Davey, R. J.; Black, S. N.; Roberts, R. J. 17 Salts of Ephedrine: Crystal Structures and Packing Analysis. *Acta Crystallogr.* **2006**, *B62*, 498–505.

(18) Burger, A.; Henck, J.-O.; Dunser, M. N. On the Polymorphism of Dicarboxylic Acids: 1 Pimelic Acid. *Mikrochim. Acta* **1996**, *122*, 247–257.

(19) Roux, M. V.; Temprado, M.; Chickos, J. S. Vaporization, Fusion and Sublimation Enthalpies of the Dicarboxylic Acids from C4 to C14 and C16. *J. Chem. Thermodyn.* **2005**, *37*, 941–953.

(20) Chadwick, K.; Davey, R.; Sadiq, G.; Cross, W.; Pritchard, R. G. The Utility of a Ternary Phase Diagram in the Discovery of New Co-crystal Forms. *CrystEngComm* **2009**, *11*, 412–414.

(21) Bellamy, L. J. *The Infrared Spectra of Complex Molecules*; Chapman and Hall: London and New York, 1980.
(22) Gais, H.-J.; Lukas, K. L. Enantioselective and Enantioconvergent Syntheses of Building-Blocks for the Total Synthesis of Cyclopentanoid Natural-Products. *Angewandte Chemie. International edition in English* **1984**, *23*, 142–143.
(23) Leusen, F. J. J.; et al. Towards a Rational Design of Resolving Agents. Part III. Structural Study of Two Pairs of Diastereomeric salts of Ephedrine and a Cyclic Phosphoric Acid. *Recl. Trav. Chim. Pays-Bas* **1991**, *110*, 13–18.
(24) Leusen, F. J. J.; Noordik, J. H.; Karfunkel, H. R. Racemate Resolution via Crystallization of Diastereomeric Salts: Thermodynamic Considerations and Molecular Mechanics Calculations. *Tetrahedron* **1993**, *49*, 5377–5396.
(25) Lorenz, H.; Seidel-Morgenstern, A. A Contribution to the Mandelic Acid Phase Diagram. *Thermochim. Acta* **2004**, *415*, 55–61.
(26) Chadwick, K.; Davey, R.; Dent, G.; Pritchard, R. G. Cocrystallization: A Solution Chemistry Perspective and the Case of Benzophenone and Diphenylamine. *Cryst. Growth Des.* **2009**, *9*, 1990–1999.

8.6 REFERENCES

1. Black, S. N., Collier, E. A., Davey, R. J. & Roberts, R. J. Structure, Solubility, Screening, and Synthesis of Molecular Salts. Journal of Pharmaceutical Sciences 96, 1053-1068 (2007).

Appendix